University of Glasgow

Malik, Natasha (2019) *Elucidating the role of mTOR complexes (mTORC1 and mTORC2) in normal haemopoiesis and in Chronic Lymphocytic Leukaemia.* PhD thesis.

Elucidating the Role of mTOR Complexes (mTORC1 and mTORC2) in Normal Haemopoiesis and in Chronic Lymphocytic Leukaemia

Natasha Malik, BSc

Thesis submitted for the Doctor of Philosophy at the

University of Glasgow

Institute of Cancer Sciences

School of Medicine, Veterinary and Life Sciences

Submitted: August 2019

Word count: 65289

Abstract

Mechanistic target of rapamycin (mTOR) functions within a complex signalling cascade, through its activity in two unique complexes mTORC1 and mTORC2, to promote a multitude of different cellular functions including autophagy, protein synthesis and survival. The exact role of these complexes during leukaemia initiation/maintenance remains to be elucidated. Here, using transgenic knockout (KO) mouse models, we determine the individual roles of mTORC1 (targeting *Raptor*) and mTORC2 (targeting *Rictor*) in normal haemopoiesis and in CLL initiation/maintenance.

Our results demonstrate that mice carrying a targeted KO of *Raptor* at the haemopoietic stem cell (HSC) stage (*Vav-Raptor* KO) do not survive post birth. This is due to anaemia resulting from a significant decrease in Ter119$^+$ population, a significant decrease in *Klf1* and *Klf2* gene expression, and a significant increase in the megakaryocyte-erythroid progenitor (MEP) population, suggesting a block at the MEP stage in *Vav-Raptor* KO foetal liver (FL). While mTORC1 plays a fundamental role in RBC development, we show that mTORC2 plays a potential role in RBC regulation, as *Rictor*-deficient HSPCs exhibit an increase in RBC colony formation *ex vivo*. Conditional KO (cKO) of *Raptor* (*Mx1-Raptor* cKO) in adult mice results in splenomegaly accompanied by increased spleen organ cellularity. Furthermore, there is a significant decrease in B cell lineage commitment, with a block in B cell development at the Lin$^-$Sca-1$^+$CD117$^+$ (LSK) stage in the BM. mTORC2, on the other hand regulates late B cell maintenance as indicated by a significant decrease in transitional B cells (T1/T2), marginal zone progenitor (MZP), and follicular 1 (fol1) cells in *Vav-Rictor* KO mice compared to controls.

To address the role of mTORC1 and mTORC2 in CLL initiation/maintenance *in vitro*, BM-derived haemopoietic progenitor cells (HPCs) isolated from control (cre-), *Raptor*-deficient (*Mx1-Raptor* cKO) or *Rictor*-deficient (*Vav-Rictor* KO) mice were retrovirally-transduced with a kinase dead PKCα (PKCαKR) construct to induce an aggressive CLL-like disease. *Raptor*-deficient BM progenitors exhibited reduced proliferation and failed to generate a CLL-like disease, due to

a block in B cell lineage commitment *in vitro*. However, there was an increase in cell cycling and migration in PKCαKR CLL-like cells with *Rictor*-deficiency suggesting a role of mTORC2 in disease maintenance.

To determine a role for mTORC1 in disease maintenance *in vivo*, NSG mice were transplanted with *Mx1-Raptor* control or *Mx1-Raptor* cKO PKCαKR transduced BM cells. Once disease was established *in vivo*, cKO was induced and disease load and progression was monitored. Our data demonstrate a decrease in disease load with *Raptor* cKO, together with a significant increase in survival. Additionally, host mice transplanted with *CD19-Raptor* KO PKCαKR cells exhibited a significant increase in survival. However, these mice eventually died of disease due to limitations of the KO model.

Lastly, to test the translational capacity of mTOR inhibitors, efficiency of AZD2014 (dual mTOR inhibitor), ibrutinib and a combination of the two drugs was assessed in reducing PKCαKR CLL-like disease load in host mice. AZD2014 was as efficient at reducing disease load as ibrutinib, however combination therapy of these drugs was not as efficient compared to single agents. Interestingly, we demonstrate that a more aggressive PKCαKR CLL-like disease (in secondary transplants) is more mTORC1 dependent than in primary transplants, as indicated by the superiority of rapamycin (allosteric mTORC1 inhibitor) in markedly decreasing disease load as compared to AZD2014 in host mice.

Taken together, mTORC1 plays an essential role in haemopoiesis, with *Raptor*-deficiency causing a block in RBC and B cell development at the MEP and LSK stage respectively. In comparison, *Rictor*-deficiency regulates later B cell lineages and promotes RBC colony formation, potentially through mTORC1 activation. Importantly, CLL-like cells lacking mTORC2 have increased cell cycling and migration whereas mTORC1 deficiency causes a decrease in disease load. Therefore, mTORC1 and mTORC2 play distinct/complementary roles in haemopoietic development and leukaemia initiation/progression. These studies provide a strong foundation for further studies testing novel mTOR inhibitors for CLL in our models.

Declaration

The work presented in this thesis represents the original work carried out by the author and has not been submitted, in any form, to any other university.

Natasha Malik

March 2019

Acknowledgements

Det har ingen betydelse hur sakta du går bara du inte stannar.

काल करे सो आज कर, आज करै सो अब |
पल में परलय होयगी, बहुरी करेगा कब ||

I would first and foremost like to thank Dr. Alison Michie for her endless support throughout my PhD. You are kind, generous, funny and a loving person and I am grateful to have you by my side as a friend and as the best mentor I could ever ask for. Thank you for always believing in me and in listening to anything and everything I have to say, no matter the situation. I don't think I can thank you enough for all that you do.

I would also like to thank Prof. Owen Sansom for all his time and effort throughout my PhD. I am grateful for all the opportunities and skills I have gained by being under your umbrella. Thank you.

A special thank you to Prof. Tessa Holyoake. No matter where you are, you always give us motivation to strive for the best and be the best version of ourselves.

Dr. Anuradha Tarafdar taught me basic laboratory skills when I first was a student and that helped me think as an independent scientist and strengthened my scientific platform. For that I thank you and am very grateful. Thank you, Dr. Emilio, Jennifer, Dr. Jodie, Dr. Ailsa, and Michael for helping me out in the lab and listening to my rants when I needed to vent. You all are wonderful people and have become great friends of mine. Big thank you to Karen Dunn, without you all the *in vivo* work would be a disaster. Thank you for always being there and helping me even when you have been very busy. A huge thank you to Colin Nixon from the IHC department for helping me with all the IHC and being so accommodating.

The Swedish quote translates: It does not matter how slow you go, just that you don't stop. The Indian 'doha' teaches to fight procrastination and to finish all work as soon as you can. My family and friends have given me constant

Table of Contents

Table of Figures

Table of Tables

List of Abbreviations

4EBP1	4E binding protein 1
AA	amino acids
ABC	avidin-biotin-complex
AGM	aorta-gonad-mesonenphros
AML	acute myeloid leukaemia
AMPK	AMP-protein kinase
APC	Antigen-presenting cells
APRIL	a proliferation-inducing ligand
ATF4	activating transcription factor 4
BAFF	B cell activating factor
BCAP	B-cell adaptor for PI3K
BCR	B-cell receptor
BCL-2	B cell CLL/lymphoma 2
BEL-A	Bristol Erythroid Line Adult
BFU-E	burst forming unit-erythroid
BLNK	B cell linker protein
BM	bone marrow
BMDM	bone marrow derived macrophages
BMSCs	Bone marrow stromal cells
ßME	ß-mercaptoethanol
BMSCs	BM stromal cells
bp	base pairs
BRU	Beatson Research Unit
BSA	bovine serum albumin
BTK	Bruton's tyrosine kinase
CAR-T cells	chimeric antigen receptor T cells
c-myc	c-myelocytomatosis viral oncogene
CD19-Raptor control	*CD19*-cre$^{-/-}$*Raptor$^{fl/fl}$*
CD19-cre$^{+/-}$*Raptor* KO	*CD19*-cre$^{+/-}$*Raptor$^{fl/fl}$*
CD19-cre$^{+/+}$*Raptor* KO	*CD19*-cre$^{+/+}$*Raptor$^{fl/fl}$*

CD19-Rictor control	*CD19*-cre$^{-/-}$*Rictor$^{fl/fl}$*
CD19-Rictor KO	*CD19*-cre$^{+/-}$*Rictor$^{fl/fl}$*
CDK	cyclin-dependent kinase
CFC	colony forming cell assay
CFU	colony forming unit
CFU-E	colony forming unit-erythroid
CFU-G	colony forming unit-granulocyte
CFU-GEMM	colony formation unit-granulocyte-erythroid-megakaryocyte-macrophage
CFU-GM	colony forming unit-granulocyte macrophage
CFU-M	colony forming unit-macrophage
CIRS	Co-morbidity illness Rating scale
cKO	conditional knockout
CLL	chronic lymphocytic leukaemia
CLP	common lymphoid progenitor
CML	chronic myeloid leukaemia
CMP	common myeloid progenitor
cre	causes recombination recombinase
D	day
DAB	diaminobenzidine tetrahydrochloride
dH$_2$O	deionised water
DLBL	diffuse large B-cell lymphoma
DN	double negative
DNMTs	DNA methyltransferases
DP	double positive
DPX	distyrene, polystyrene, xylene
e-KLF	erythroid Krüppel-like factor
E10	embryonic day 10
EBF1	early B cell factor 1
elF-4E	eukaryotic initiation factor
EF2K	elongation factor 2 kinase
ERK	extracellular regulated mitogen activated protein kinase
EryD	definitive erythroblasts

ES cells	Embryonic stem cells
ETC	electron transport chain
Exosc8	Exosome complex 8
FACS	fluorescent assorted cell sorting
FBS	foetal bovine serum
FCR	fludarabine, cyclophosphamide and rituximab
FL	foetal liver
FLT3-ITD	internal tandem repeats of FLT3
fol	follicular
FOXO1	Forkhead Box O1
FRB	FKBP-Rapamycin Binding
FSC-A	forward scatter-area
GC	germinal centre
GF	growth factor
GlyA	GlycophorinA
GMP	granulocyte-macrophage progenitor
GSK3	glycogen synthase kinase-3
H&E	haematoxylin and eosin
HBSS	Hank's balanced salt solution
HPCs	Haemopoietic progenitor cells
HRI	heme-regulated eIF2α kinase
HRP	horseradish-peroxidase
HSC	haemopoietic stem cell
HSCT	haemopoietic stem cell transplant
HSPC	haemopoietic stem progenitor cell
IFNß	interferon ß
IFNγ	interferon γ
Ig	immunoglobulin
IGF	insulin growth factor
IgV$_H$	Immunoglobin variable heavy chain
IHC	immunohistochemistry
IL2Rγ	interleukin 2 receptor common chain gamma

IMLECs	innate myelo-lymphoblastoid effector cells	
ip	intra peritoneal	
IRS	insulin receptor substrate	
ITAM	immunoreceptor tyrosine-based activation motifs	
KD	knockdown	
KI	knock-in	
KLF	Krüppel-like factor	
KO	knockout	
LCMV	lymphocytic choriomeningitis virus	
LN	lymph node	
loxP	locus of crossover in P1	
LPS	lipopolysaccharide	
LSCs	Leukaemic stem cells	
LSK	Lin-Sca1+cKit+	
LMPP	lymphoid-primed multipotent progenitors	
LT-HSC	long-term haemopoietic stem cell	
M-CSF	macrophage-colony stimulating factor	
MACS	Magnetic assorted cell sorting	
MAM	mitochondria-associated endoplasmic reticulum membranes	
MAPK	mitogen-activated kinases	
MCL	mantle cell lymphoma	
MCL-1	myeloid cell leukaemia 1	
MEP	megakaryocyte-erythrocyte progenitor	
MFI	mean fluorescent intensity	
MHC	major histocompatibility complex	
miR	microRNA	
MOPS	mM 3-(N-morpholino) propane sulfonic acid	
MPECs	memory precursor effector cells	
MPN	myeloproliferative neoplasm	
MPPs	multipotent progenitor cells	
mRNA	messenger RNA	
mTOR	mechanistic target of rapamycin	

mTORC	mechanistic target of rapamycin complex
Mx-Raptor cKO	*Mx1*-cre$^{-/+}$*Raptor*$^{fl/fl}$
Mx-Raptor control	*Mx1*-cre$^{-/-}$*Raptor*$^{fl/fl}$
Mx-Rictor cKO	*Mx1*-cre$^{-/+}$*Rictor*$^{fl/fl}$
Mx-Rictor control	*Mx1*-cre$^{-/-}$*Rictor*$^{fl/fl}$
MZ	marginal zone
MZP	marginal zone progenitor
NBF	neutral buffered formalin
NEAA	neutral essential amino acids
NFκB	nuclear factor kappa B
NICE	National Institute for Heath and Care excellence
NK cells	natural killer cells
NLCs	nurse-like cells
NOD	non-obese-diabetic
NRG	NOD-Rag-IL2Rγ
NSG	NOD-SCID-IL2Rγ
OG	Oral gavage
OS	Overall survival
PAMPs	pattern-associated molecular patterns
PAX5	paired-box-protein-5
PBMCs	peripheral blood mononuclear cells
PBS	Phosphate buffer saline
PD-1	programmed death 1
PDCD4	programmed cell death 4
PDK1	3-phosphoinositide-dependent kinase 1
PE	paired end sequencing
PFS	Progression free survival
PI	propidium iodide
PI3K	phosphoinositide 3-kinase
PIP2	phosphatidylinositol-4,5-phosphate
PIP3	phosphatidylinositol-3,4,5-phosphate
PKC	protein kinase C

PKCαKR	Kinase-dead PKCα
PLC	phospholipase C
poly(I:C)	polyionosinic:polycytidylic acid
polybrene	hexadimethrine bromide
POMC	Proopiomelanocortin
PP2A	protein phosphatase
PP2A	protein serine/threonine phosphatase A
proE	pro-erythroblast
PTEN	Phosphatase and tensin homolog
PVDF	polyvinylidene difluoride
QC	quality check
Rag	recombination activation genes
rapa	rapamycin
RBC	red blood cell
RCN	relative cell number
RIC	reduced intensity conditioning
RIN	RNA intergrinty value
RNAseq	RNA sequencing
ROR1	receptor tyrosine kinase-like orphan receptor-1
ROS	reactive oxygen species
RT	room temperature
RT-PCR	real time-polymerase chain reaction
S6K	S6 kinase
SA	streptavidin
SCF	stem-cell factor
SCID	severe combined immunodeficiency
SD	standard deviation
SDF-1	stromal cell-derived factor 1
SDS-PAGE	sodium dodecyl sulfate polyacrylamide gel electrophoresis
SEM	standard error of mean
SFK	Src family kinases
SGK1	serum and glucocorticoid-induced protein kinase 1

SIRPα	signal regulatory protein alpha
SLCs	surrogate light chains
SLECs	short lived effector cells
SSC-A	side scatter-area
SYK	spleen tyrosine kinase
T1	transitional 1
T2	transitional 2
T3	transitional 3
T-ALL	T cell-acute lymphocytic leukaemia
TAE buffer	Tris-acetate-EDTA buffer
TAM	tumour associated macrophages
TBP	TATA-box binding protein
TBS	Tris-buffer saline
TBST	Tris-buffer saline-Tween
TCL1	T cell leukaemia 1
TCR	T cell receptor
TE buffer	Tris-EDTA buffer
TECs	thymic epithelial cells
TF	transcription factor
Th	T helper cells
TLR	Toll-like receptor
TNF	tumour necrosis factor
T-reg	T-regulatory
TSC	tuberous sclerosis complex
Vav-Raptor control	*Vav*-cre$^{-/-}$*Raptor*$^{fl/fl}$
Vav-Raptor KO	*Vav*-cre$^{+/-}$*Raptor*$^{fl/fl}$
Vav-Rictor control	*Vav*-cre$^{-/-}$*Rictor*$^{fl/fl}$
Vav-Rictor KO	*Vav*-cre$^{+/-}$*Rictor*$^{fl/fl}$
VEGF	vascular endothelial growth factor
VRF	Veterinary Research Facility
WT	wildtype
YY1	yin-yang1

ZAP-70   70 kDA zeta associated protein

Chapter 1

Introduction

1 Introduction

1.1 Early Haemopoiesis:

Murine haemopoiesis initially occurs in the yolk sac and in two waves, the first of which is known as 'primitive' haemopoiesis. At this stage *de novo* haemangioblasts are generated and produce large quantities of erythrocytes to promote increased oxygenation, accommodating rapid growth. During the second wave of haemopoiesis or 'definitive' haemopoiesis, haemopoietic stem cells (HSCs) appear in the aorta-gonad-mesonenphros (AGM) region around embryonic day 10 (E10)(1). From E11, HSCs migrate to and colonise the foetal liver (FL) and subsequently the bone marrow (BM) with waves of repopulating HSCs that provide a continuous source of mature haemopoietic lineage cells during the adult life span. The nature of the HSCs differ depending on the microenvironmental niche, with HSCs in the BM being more quiescent than those in the FL(2,3). HSC differentiation into multipotent progenitor (MPP) cells occurs mainly in the FL prior to migration into specific haemopoietic organs, such as the thymus, for further lineage differentiation. Conventionally, MPPs give rise to oligopotent common myeloid or lymphoid progenitors (CMPs or CLPs). CMPs further give rise to megakaryocyte-erythroid progenitors (MEP) and granulocyte-macrophage progenitors (GMP), while CLPs give rise to lymphoid lineage cells(4). Nevertheless, there exists an alternate hierarchical model of haemopoiesis where MPPs give rise to lymphoid-primed multipotent progenitors (LMPPs) which have also been shown to develop into GMP myeloid progenitors but carry a lymphoid generation bias(5,6). It has previously been demonstrated, that the Lin$^-$Sca1$^+$cKit$^+$ (LSK) HSC compartment of cells express high levels of CD34, Flt3 and IL7, are able to sustain the granulocyte, monocyte, B and T cell lineages. However, they lose megakaryocyte and erythrocyte potential (7,8). It is the further expression of C/EBPα and EBF1 which supports a myeloid and B cell lineage fate respectively (9).

As they get primed towards a lymphoid lineage, they lose the myeloid lineage generation capacity and develop into CLPs (Figure 1.1).
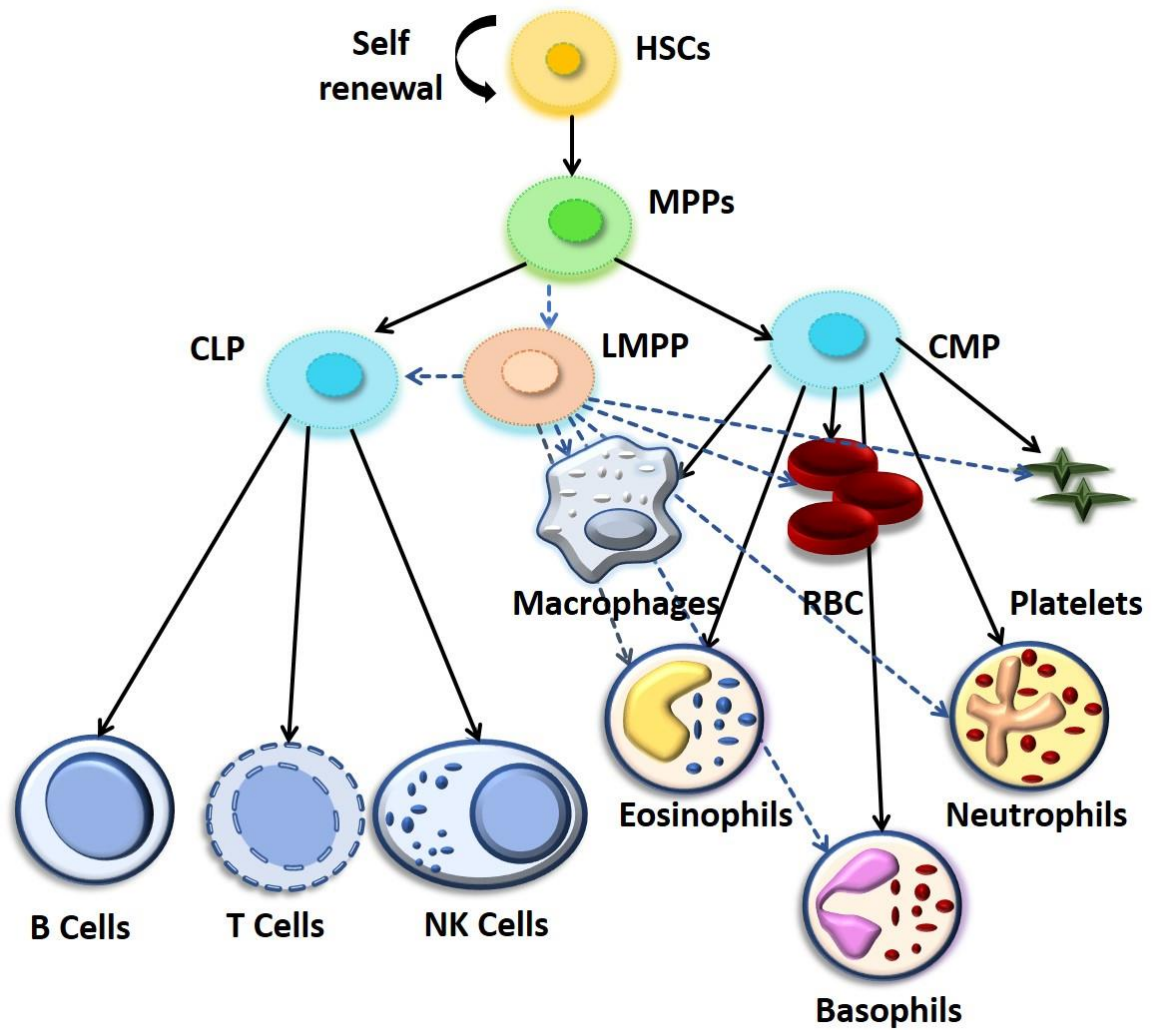
Figure 1.1 Diagram showing the hierarchy of haemopoietic cell differentiation.
Haemopoietic stem cells (HSCs) give rise to multipotent progenitors (MPPs) which either develop into common lymphoid progenitors (CLPs) or common myeloid progenitors (CMPs). Literature also alludes to a lymphoid-primed multipotent progenitor (LMPP) population which is lymphoid primed (gives rise to CLPs) but capable of generating megakaryocyte-erythrocyte progenitors (MEPs) and granulocyte-macrophage progenitors (GMPs) giving rise to myeloid and erythroid lineages. CMPs further give rise to MEPs and GMPs whereas CLPs give rise to lymphoid lineages including B, T, and NK cells. Dashed arrows suggest alternative routes of haemopoietic differentiation.

1.2 Erythropoiesis

Erythropoiesis is governed by the complex regulation of key transcription factors (TFs), which enable a balance between erythrocyte progenitors and erythroblasts enabling self-renewal and differentiation. The zinc-finger TFs(4) *Gata1* and *Gata2* play critical and non-redundant roles during erythroid maturation. *Gata2* is expressed in HSCs and early progenitor populations regulating the expression of self-renewal genes, in addition to genes responsible for initiating *Gata1* expression. GATA1 plays a vital role in erythroid differentiation, sustaining its own expression and suppressing GATA2 expression, a process known as GATA factor switching(10). *Gata1*-deficient (*Gata1*$^{-/-}$) mice in murine embryos gave rise to lymphoid cells and non-haemopoietic tissues but failed to give rise to a mature erythroid population, resulting from a block at the pro-erythroblast stage due to increased apoptosis. McIver *et al.,* have demonstrated that *Foxo3* and *Gata1* co-operativity represses exosome complex 8 (*Exosc8*) expression thereby promoting erythroid maturation. *Exosc8* is a vital component of the exosome machinery responsible for epigenetic regulation and RNA surveillance(11). Recently, IKAROS, a zinc-finger protein has been shown to play a role in foetal and adult erythropoiesis and erythroid lineage commitment as *Ikaros* gene silencing leads to an irreversible switch to myeloid lineage(12). *Pu.1* TF is an established master regulator in haemopoiesis as it is one of the key genes involved in primitive cell fate decisions. *Pu.1* expression levels determine myeloid and lymphoid cell fates where higher expression of *Pu.1* leads to myeloid cell fate whereas a lower expression to a lymphoid fate(13). Additionally, a myeloid cell fate is not solely regulated by *Pu.1* expression but also the inhibition of *Gata1*(14) and the expression of *Cebpa* (15). *Cebpa* is considered essential for myeloid fate by binding and transcribing genes associated with myelopoiesis at the long-term haemopoietic stem cell stage (LT-HSC) stage(16).

PU.1 and GATA1 interact to regulate lineage fate where upregulation of *Gata1* inhibits *Pu.1* transcription and promotes erythroid lineage(17) differentiation whereas expression of *Pu.1* inhibits *Gata1* expression promoting myeloid lineage fate(18). *Gata1* is known to be a very potent TF as it binds to the promoter region of erythroid-Krüppel like factor/ Krüppel like factor 1 (*e-Klf/Klf1*)(19). *Klf1* TF is vital for erythropoiesis as it regulates MEP lineage fate during

erythrocyte development. *Klf1* expression has been shown to promote CD71 surface expression, which leads to the development of the earliest pro-erythroblasts (proE). These cells are nucleated and have oxygen carrying capacity and circulate in the embryo. These cells then develop into definitive erythroblasts (EryD) which is marked by enucleation. CD71, a transferrin receptor, is known to be expressed at all embryonic stem (ES) cells and proE cells[20]. Nevertheless, during maturation, proE cells undergo 'maturational globin switching' leading to reduced CD71 expression and erythrocyte maturation. TER119, on the other hand is associated with glycophorinA (GlyA) and is correlated with maturing erythrocytes[21]. Together, CD71 and TER119 are widely used in flow cytometry to determine the developing stages of erythrocytes: EryA, EryB and EryC stages. TER119^{lo}CD71^{hi} population is considered as the proE stage. Subsequent populations which express TER119$^+$CD71$^+$FSC-A^{hi} are considered to be in the EryA stage as these populations are larger as they are nucleated. Subsequent enucleation reduces the size and therefore the forward scatter-area (FSC-A) in flow cytometry and EryB populations are CD71$^+$TER119$^+$. Lastly, maturation of erythrocytes is marked by a reduction in CD71 expression which are considered TER119$^+$ EryC cells[22].

'Maturational globin switching' also involves the 'globin switching' from *γ*- to *β-Globin* for the maturation of erythrocytes via *Klf1* activity[23]. In human haemopoietic development, β-GLOBIN is expressed when erythropoiesis moves to the BM. Initially, the yolk-sac expresses *ε*-GLOBIN, followed by the expression of *γ*-GLOBIN in the FL and spleen. Therefore, *Klf1* mediated β-GLOBIN expression is vital for the development of mature erythrocytes[24]. Whilst *Klf1* plays a major role in erythropoiesis, *Klf2* plays a role in endothelial growth, vascular remodelling and inflammation responses[25], which is vital for embryonic development.

1.3 B1 B cells and B2 B cells

B1 B cells were originally given this name as they were thought to appear earlier in ontogeny compared to B2 B cells. B1 B cells secrete majority of the IgM and play a vital role in pathogen-induced immunity. B1-a B cells express surface CD5$^+$ whereas B2 cells lack CD5, a marker initially only thought to be specific for T cells[26]. Nevertheless, there also exist CD5$^-$ B1 cells termed B1-b cells which

have similar phenotypes to B1-a cells. B1 B cells are thought to be 'rarer' and are not considered the 'conventional' B cells. B1 B cell heterogeneity is not restricted to CD5 expression, and different populations within B1 B cells have been identified, wherein increased levels of B cell receptor (BCR) signalling induced antigen-presenting cells (APCs) whereas other subtypes had a diminished BCR signalling alluding to cell quiescence(27).

B1 B cell precursors are considered to originate in the FL, whereas B2 precursor cells are said to originate in FL which later moves onto the BM after birth. However, B1 B cell generation has been shown in other-haemopoietic regions such as the blood island yolk sacs in the embryo, in the FL and in the BM after birth. Nevertheless, these B1 B cell pools in the BM do not contribute to B1 B cell development after 3-6 wk of birth(28) supporting previous work highlighting B1 B cell lineage to be a foetal/neonatal developed population. It also suggests that this population is maintained by self-renewal in the BM and not by *de novo* development.

Therefore, from hereon, B cell development and other aspects of B cells presented will refer to the 'conventional' B cell population – B2 B cells.

1.4 B cell development

B cells are a subtype of lymphocytes involved in the humoral immunity in the adaptive immune response of the body. B cell development comprises several phenotypic stages enabling B cell lineage commitment/maturation from HSCs initially in the FL during embryogenesis and then in the BM.

1.4.1 TFs involved in B cell development

Pu.1 is a vital TF most likely expressed during the MPP stage and is vital for determining lineage fate. Playing a role in lineage fate decisions between erythroid and myeloid lineages as seen in section 1.2, the graded expression of this TF has shown to determine B cell fate as high expression of *Pu.1* has shown to bias a myeloid lineage and lower expression of *Pu.1* has shown to bias to a B cell lineage(29).

Flt3 expression is present at the MPP stage and plays an important role in deciding B cell fate. Nevertheless, constitutive *Flt3* expression at later stages abrogates B cell development alluding to the importance of paired-box-protein 5 (*Pax5*) mediated repression of *Flt3*. Indeed expression of *Flt3, IL7* is essential for B cell development, mediated by *Ikaros* TF(30). Additionally, transition from the LMPP to the CLP phase is associated with an increase in IL7-receptor α (*Il7Ra*) expression as *Il7R*-deficient mice have a block in B cell development at the pre-proB cell stage suggesting *Il7R* expression is vital in initiating immunoglobulin (Ig) rearrangement(31,32).

IKAROS has shown vital roles for B cell development as *Ikaros*-deficiency has shown to block B cell development at the pre-proB cell stage. *Ikaros*-deficiency has also shown to regulate *Il7-Ra* and *Flt-3* expression as *Ikaros* knockout (KO) leads to a decreased expression of these proteins suggesting the expression of both these proteins is vital for B cell development(33). *Il7Ra* has been shown to promote the expression of early B-cell factor 1 (*Ebf1*) further highlighting the importance of IKAROS in normal B cell development(34).

E12 and E47 are helix-loop-helix proteins which comprise E2A. *E2A* TF is essential for lymphoid lineage development as it promotes the expression of *Ebf1*. Indeed, mice lacking *Ebf1* did not undergo Ig recombination suggesting the importance of the expression of this gene to induce the transition from the pre-proB to proB cell stage (35). E2A interactions with EBF1 induce *Pax5* expression, which positively regulates *Ebf1* expression along with *E2A*(32). Interestingly, it has also been shown that *E2A* interactions with Forkhead box O1 (*Foxo1*) (via the mTOR-AKT signalling pathway) together with *E2A-Ebf1* interactions induce *Pax5* expression (36). *Pax5* expression encodes various components responsible for the transition from pre-proB to preB cells by aiding pre-BCR expression. It also promotes expression of co-receptors CD19 and CD21(30). *Pax5* has shown to negatively regulate *Flt3* expression, as constitutive expression of *Flt3* is associated with impaired B lymphopoiesis, highlighting internal mechanisms of regulating B cell development(37). E2A-FOXO1 interactions have been shown to activate *Rag1* and *Rag2*, the main drivers of VDJ recombination and therefore Ig rearrangement and transition from the preB cell stage to the immature B cell stage(38).
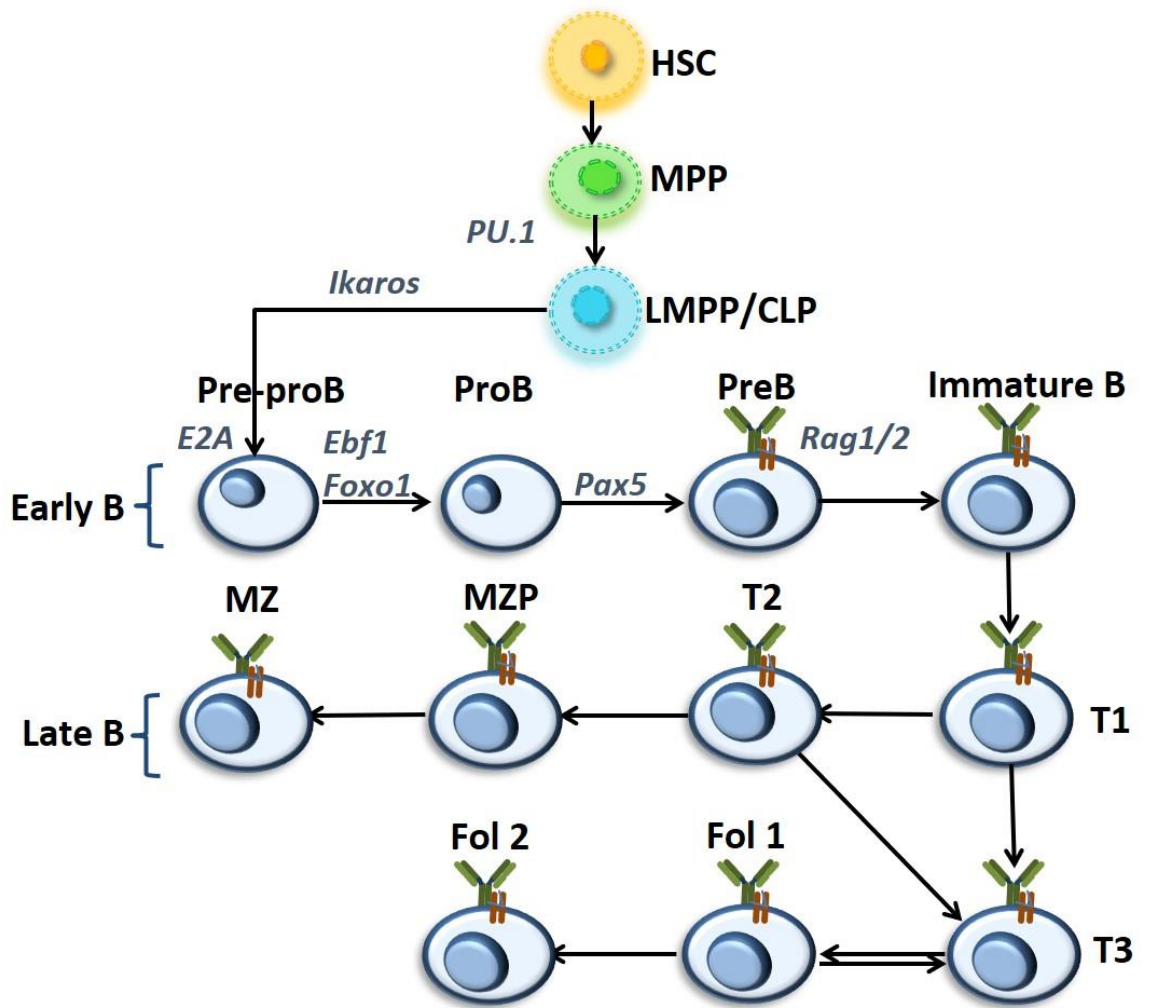
Figure 1.2 Diagram showing the summary of B cell development.
HSCs develop into MPPs which give rise to LMPPs which, under the appropriate signals, develop into CLPs, enabling B cell development. Pre-proB cells give rise to proB cells due to the interactions of *E2A* and *Ebf1* and *E2A* and *Foxo1*. These TFs induce *Pax5* expression, promoting CD19 expression and RAG1/2 expression, and subsequent IgV$_H$ re-arrangement. Functional VDJ re-arrangement leads to the maturation of the pre-BCR complex to a BCR complex and the development of preB cells into immature B cells. These cells then migrate into secondary lymphoid organs to further mature into different B cell subtypes via transitional 1, 2, and 3 stages (T1-3). These give rise to mature B cells subtypes including marginal zone (MZ) follicular 1 (fol1), fol2 B cells.

1.4.2 Developmental stages

At the CLP stage, stem cell factor (SCF) is released from the stromal cells in the microenvironment, binding to its receptor CD117 on early B cell precursors (39). Lymphoid precursors express CD117 and IL7Rα and are capable of developing into B, T or natural killer (NK) cells, but not erythrocytes/myeloid lineages. After the CLP stage, the earliest B cell precursors express B220, along with early NK cells. However, these lineages can be separated using other surface markers such as AA4.1, which is expressed on B cells up to the immature stage (31,40).

1.4.2.1 Early B cell development

It is after *Pax5* expression which promotes sequential recombination of the Ig gene segments of the heavy and light chains, forming the platform for B cell development. This functional rearrangement comprises the VDJ gene segments of the heavy chain (μ locus) and the VJ segments of the light chain (κ locus) initiated by recombination-activating genes 1 and 2 (*Rag1* and *Rag2*). Functional rearrangement of these genes enables the cell to generate antibodies which recognise various cell specific antigens. The rearrangement pattern of the Ig heavy chain (IgH) gene segments is associated with distinct stages of B cell development – pre-proB cell, proB, preB cells (Figure 1.2, Figure 1.3). B precursors with no rearrangement are in the pre-proB cell stage. The

Early B cell subsets

Develop-ment Stage	Pre-proB cells	ProB cells	PreB cells	Immature B cells
Events	No Ig re-arrangement *Ikaros* expression and start of B220 expression	Heavy Chain rearrangement: V_H and $D_H J_H$ rearrangement	Surrogate Light chain $V_{Pre}B$, Vλ5 and CD79a, CD79b for cell surface expression	Complete rearrangement of D_L-J_L
Phenotype	CD11b$^-$ CD19$^-$ B220$^+$ CD43$^+$ Lin$^-$	CD11b$^-$ CD19$^+$ B220$^+$ CD43$^+$ Lin$^-$	CD11b$^-$ CD19$^+$ B220$^+$ CD43$^-$ IgM$^-$ CD24$^+$ Lin$^-$	CD19$^+$ B220$^+$ IgM$^+$ IgD$^-$ CD24$^+$ CD25$^+$ Lin$^-$

Figure 1.3 Diagram showing stages of early B cell development in the bone marrow along with table summarizing various stages of early B cell development including phenotype (surface markers) and events in the pre-proB cell, proB cell, preB cell and immature B cell stages.

rearrangement of DJ segments in the H chain is correlated with the proB cell stage. *Mb1* expression at the proB cell stage is vital for Ig rearrangement as *Mb-1* encodes the Ig-α subunit, deficiency of which leads to BCR deficiency(41). *CD19* expression is also expressed at the proB cell stage, under the regulation of *Pax5*. V chain addition to the DJ segment(42) marks the large preB cell stage. *CD19* expression is marked by BCR dependent and independent events. CD19 interacts with the BCR to enhance BCR activity.

1.4.2.2 Late B cell development

Late B cell subsets
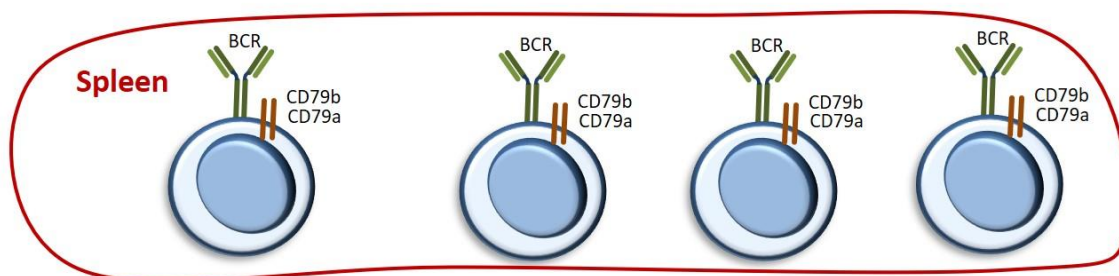
Develop-ment Stage	Transitional B			MZP/MZ		Follicular B		B1 B cells
Events	Immature B cells undergo transitional phases T1, T2, T3. T1 can transition into T2, T3, MZP. T3 can reversibly convert to Follicular 1. T2 transitions into MZ cells.			T1/2 transition into MZP and ultimately into MZ cells. These cells mature in the germinal centre (GC) of the secondary lymphoid organ (Spleen or LN)		T3 cells transition into fol1 and T2 to fol1/2. Play a role in T cell dependent and independent responses.		Generated during foetal and neonatal development. Self renew and localize in the pleural and peritoneal cavities. APC, Humoral response
Phenotype	T1 CD19$^+$ CD23$^-$ IgM^{hi} CD21^{int}	T2 CD19$^+$ CD23$^+$ CD1d^{int} CD21^{int} IgD^{hi} IgM^{hi} AA4.1$^+$	T3 CD19$^+$ CD23$^+$ CD1d^{int} CD21^{int} IgD^{hi} IgM^{lo} AA4.1$^+$	MZP CD19$^+$ CD23$^+$ CD21^{hi} CD1d^{hi}	MZ CD19$^+$ CD23$^-$ CD21^{hi} IgM^{hi}	Fol1 CD19$^+$ CD23$^+$ CD1d^{int} CD21^{lo} AA4.1$^-$ IgD^{hi} IgM^{lo}	Fol2 CD19$^+$ CD23$^+$ CD1d^{int} CD21^{lo} AA4.1$^-$ IgD^{hi} IgM^{hi}	CD19$^+$ CD11b- CD5$^+$(a) CD5$^-$(b) CD43$^+$ B220$^+$ IgD- IgM$^+$ Ag B7 CD23$^-$

Figure 1.4 Diagram showing stages of late B cell development in the spleen along with table summarizing various stages of early B cell development including phenotype (surface markers) and events in the transitional (T-3), marginal zone progenitor (MZP)/MZ, follicular 1 (fol1) and fol2 B cell and B1 B cell stages. APC – antigen-presenting cells.

After immature B cell development, the cells undergo one of three processes dependent on Ig interactions. Cells which undergo cross-linking of the BCR leading to high affinity interactions are associated with elimination via clonal deletion (negative selection). Low affinity interactions lead to non-responsive anergic cells which are short lived, or it could also lead to cells editing their BCR to become non-reactive(43). All other immature B cells, expressing surface bound IgM, migrate into the spleen where they mature into naïve, follicular (fol) or marginal zone (MZ; CD19$^+$CD21^{hi}CD23$^-$IgM^{hi}) B cells via transitional phases (T1-T3). Cariappa *et al.,* have shown there to be a transition from T1 (CD19$^+$CD21^{int}CD23$^-$IgM^{hi}) to T2 (CD19$^+$AA4.1$^+$CD21^{int}CD23$^+$CD1d^{int}IgD^{hi}IgM^{hi}) cells

which develop into fol2 B cell populations. Fol2 B cells give rise to MZ progenitors (MZP; CD19$^+$CD21^{hi}CD23$^+$CD1d^{hi}) and ultimately MZ B cells together with fol1 cells. Nevertheless, T1 cells also transition to T3 cells to give rise to fol1 cells (44). Association of Toll-like receptor (TLR) signalling together with pattern-associated molecular patterns (PAMPs) leads to MZ B cell development into IgM plasma cells forming the first line of innate immunity against pathogens(45). Fol1 B cells (CD19$^+$AA4.1$^-$CD21^{lo}CD23$^+$CD1d^{int}IgD^{hi}IgM^{lo}) form the bulk of the circulating population whereas fol2 cells (CD19$^+$AA4.1$^-$CD21^{lo}CD23$^+$CD1d^{int}IgD^{hi}IgM^{hi}) form one-third of the circulating population, being more quiescent and considered to be more primitive(44) residing in B cell follicles (Figure 1.2, Figure 1.4). It is the interaction of T helper (Th) cells with these fol B cells which leads to the expansion of B cells comprising the germinal centres (GCs) in secondary lymphoid organs(45). *CD19* expression is vital for the maintenance of peripheral B cells as *CD19*-null mice have shown to have decreased survival compared to normal B cells. This maintenance is partially via the BCR/B cell lymphoma-2 (Bcl-2) axis, as increasing *Bcl-2* expression in *CD19*-null mice rescued MZ and fol B cell generation(46). Phosphoinositide 3-kinase-delta (PI3Kδ) expression is restricted to B and T cells and has shown to play a role in late B cell development. PI3Kδ-null mice show block in B cell development at the preB cell stage. It has been shown that PI3K expression is regulated by pre-BCR signalling, and PI3K isoforms, p110α and p110δ, modulate *Pax5* expression, absence of which arrests B cell development at the preB cell stage(47), making PI3Kα and PI3Kδ redundant for early B cell development. PI3Kδ has shown to be vital for late B cell development, particularly for MZ cells(48,49). There is a significant reduction in MZ B cells with PI3Kδ-deficiency due to reduced CXCR5 mediated migration(50) as PI3Kδ-deficient mice have a reduction in MZ B cell homing into proliferative centres suggesting a role of PI3Kδ in MZ B cell maturation and homing capacity.

1.5 mTOR signalling pathway

The BCR signalling pathway regulated B-cell proliferation and survival and it is known for its crosstalk between other signalling pathways including MAPK, NFκB and mTOR signalling pathways. BCR engagement leads to the phosphorylation of tyrosine residues located on immunoreceptor tyrosine-based activation motifs (ITAMs) of CD79a and CD79b by protein tyrosine kinases including Lyn, Syk.

Through this, downstream proteins including BCAP and BLNK are activated[51]. Additionally, CD19 engagment is vital for BCAP binding pf p85 which is essential for the PI3K phosphorylation[52]. Moreover, CD19 is a surface protein, co-ligation of which to the BCR, is known to modulate BCR signalling positively and negatively by attenuating PI3K activity[53]. BLNK is responsible for PLCy1, VAV and BTK, whereas BCAP is responsible for the activation of PI3K, downstream which, is the mechanistic target of rapamycin (mTOR) signalling pathway.

mTOR is a serine/threonine kinase, which is involved in various signalling pathways regulating metabolism. mTOR, as the name suggests, is targeted by rapamycin which is an anti-fungal macrolide first characterised in *Streptomyces hyroscopicus*. Due to the anti-proliferative properties of rapamycin, extensive research was carried out on this and TOR was then discovered. Its consequent purification in mammals also showed the vast application of TOR in mammals, known as the mTOR signalling pathway[54]. It is involved in protein synthesis, mitochondrial function, autophagy, cytoskeleton organisation, and cell survival mechanisms. However, how mTOR signalling is regulated is not fully understood.

The mTOR pathway is activated by a variety of signals including insulin/insulin growth factors (IGF), glucose, amino acid, tumour necrosis factor (TNF) and BCR signalling (Figure **1.5**). mTOR belongs to the PI3K family and it forms two different complexes – mTORC1 and mTORC2. mTORC1 comprises of 6 proteins and mTORC2 of 7 proteins. Of these, they share the common mTOR subunit, along with GßL, DEPTOR, TTI1/TEL2 complex. The subunits which make the respective complexes unique are RAPTOR (rapamycin TOR sensitive), PRAS40 which are specific to mTORC1 and RICTOR (rapamycin TOR insensitive), mSIN1, and PROTOR1/2 specific to mTORC2[55]. The complexes, RAPTOR and RICTOR are what make mTORC1 and mTORC2 sensitive or insensitive to rapamycin respectively[56]. Rapamycin is an allosteric inhibitor of mTORC1, as recent co-crystal structures of mTOR-mLST8 show that rapamycin binds to the FKBP-Rapamycin binding (FRB) domain thereby highly recessing the active site[57]. Therefore, it is responsible for partial, not full mTORC1 inhibition.
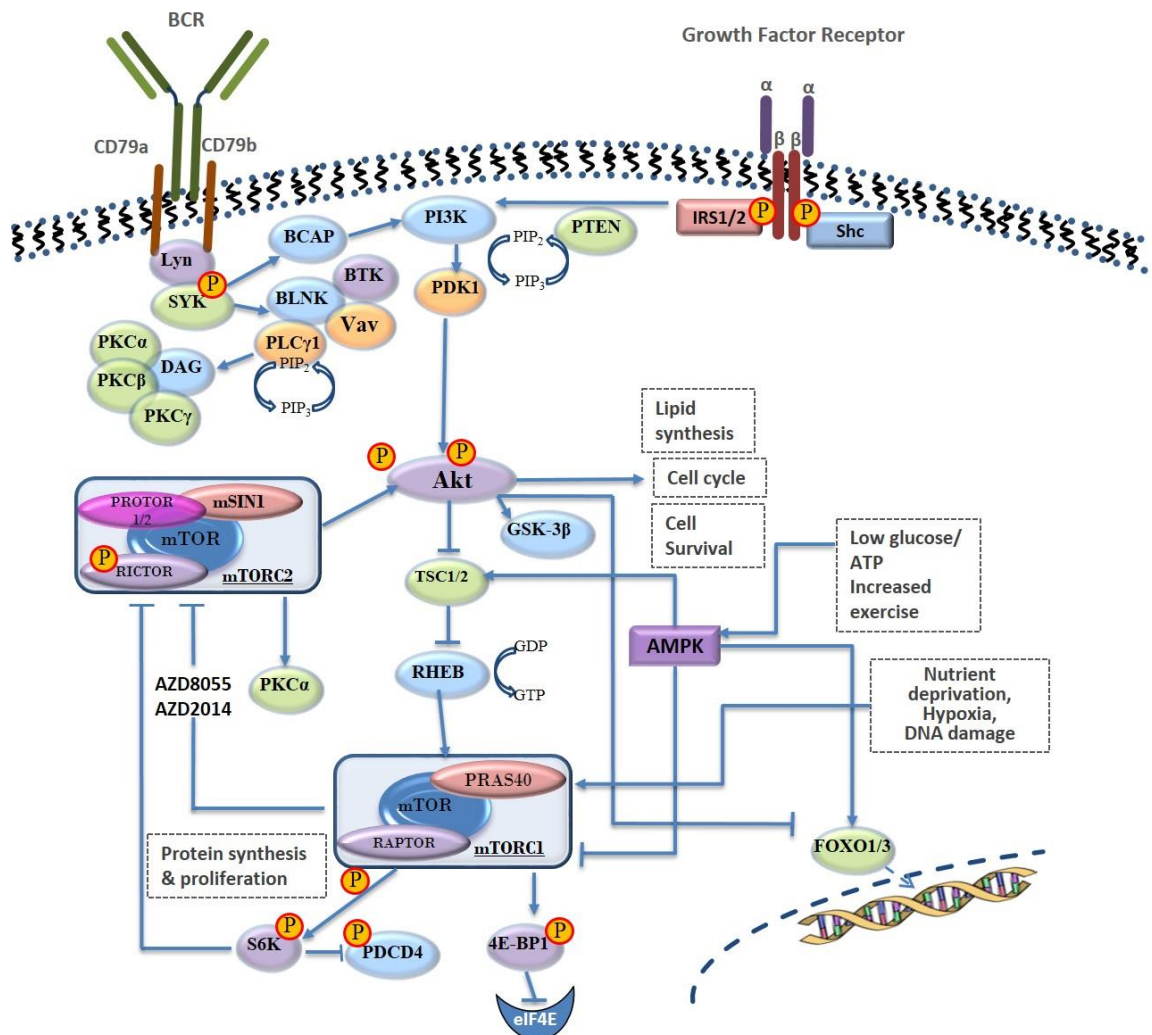
Figure 1.5 Diagram of the AKT/mTOR signalling pathway.

Downstream signalling from the B cell receptor (BCR) and growth factor receptors is shown. Activation of these receptors results in phosphorylation and activation of AKT, which leads to the activation of mTORC1 (PRAS40, RAPTOR), thereby initiating cell processes such as protein synthesis and proliferation. The downstream target of mTORC1, S6K negatively regulates mTORC2 (PROTOR1/2, mSIN1, RICTOR), which is responsible for the activation of AKT. This creates a negative feedback loop, which regulates this pathway. mTORC1 and mTORC2 share the subunits mTOR, GβL, DEPTOR and TTI1/TEL2 (not shown). AKT negatively phosphorylates FOXO1/3, which regulates cell cycle. Kinases such as AMPK are activated in stress responses and inhibit the mTORC1 pathway. Allosteric inhibitors such as rapamycin and other rapalogs partially inhibit mTORC1 activity whereas ATP competitive inhibitors such as AZD2014 are pan mTOR inhibitors. Abbreviations: PLC (Phospholipase C), BLNK (B-cell linker protein), BTK (Bruton's tyrosine kinase), BCAP (B-cell adaptor for PI3K).

Rapamycin has similar structure to FK506 which blocks Ca^{2+}/calcineurin dependent signalling in T cells required for growth and proliferation. Rapamycin on the other hand binds to FKBP12 and inhibits mTORC1 activity by blocking the cytokine signalling required for growth.

The upstream mediator of mTOR is PI3K (Figure 1.5). PI3K can bind to Insulin receptor substrate proteins (IRS) and converts phosphatidylinositol-4,5-

phosphate (PIP$_2$) to phosphatidylinositol-3,4,5-phosphate (PIP$_3$). Phosphatase and tensin homolog (PTEN), a tumour suppressor, blocks PIP$_3$ accumulation and PIP$_3$ phosphorylates and activates 3-phosphoinositide-dependent protein kinase 1 (PDK1) and AKT. AKT then activates mTORC1 via the inhibition of the tuberous sclerosis proteins TSC1 and TSC2. They form a heterodimer and inhibit RHEB which then binds to mTORC1 causing conformational changes in the protein and activation(58). However, whether RHEB binds and activates mTORC2 has not been determined.

1.5.1 mTOR signalling and its functions

1.5.1.1 mTORC1 signalling:

RAPTOR binds mTOR to enhance its' activity, as indicated by the finding that RAPTOR inhibition using RNAi, leads to decreased mTOR activity(59). In a low-energy state (low ATP:AMP ratio), AMPK, a conserved energy sensor, is activated leading to TSC2 phosphorylation and the subsequent inhibition of mTORC1 activity(60). However, in a high-energy state, the mTORC1 pathway is activated, promoting protein synthesis, lipogenesis and mitochondrial biogenesis and function(8-11). Indeed, mTORC1 plays a pivotal role in mitochondrial oxidative function through regulation of the transcription factor yin-yang1 (YY1), which subsequently controls gene expression of mitochondrial transcriptional regulators including PGC-1α(10). Additionally, mTORC1 controls mitochondrial biogenesis and respiration through phosphorylation/inhibition of the eukaryotic initiation factor 4E (eIF-4E) binding proteins (4EBPs) and regulation of the translation of nucleus-encoded mitochondrial-related mRNAs, which in turn increases ATP generation in the cell(11) (Figure 1.5). In the absence of mTORC1 activity, 4EBP1 is hypo-phosphorylated and interacts with the mRNA cap binding protein eIF-4E, inhibiting translation of cap-dependent proteins. Upon mTOR activation, hyper-phosphorylation of 4EBP1 releases eIF-4E, enabling its association with eIF-4A (RNA helicase) and the scaffolding protein eIF-4G to form the eIF-4F complex. The mTORC1-eIF-4E pathway is upregulated in most cancers and thus represents an attractive therapeutic target(61).

mTORC1 also phosphorylates/activates S6 Kinase 1 (S6K1) at T389, which was initially thought to play a role in protein/ribosomal biogenesis by activating 40S

ribosomal protein. However, it is now appreciated that S6K1 is important in a number of mechanisms, together with S6K2, including transcription, cell proliferation, apoptosis and potential mRNA splicing(62). S6K phosphorylates programmed cell death 4 protein (PDCD4) at S67 targeting it for proteosomal degradation(63). PDCD4 is a tumour suppressor responsible for inhibiting eIF-4E. Moreover, a recent study in a colorectal cancer model shows that S6K phosphorylates and inhibits elongation factor-2 kinase (EF2K), in turn relieving EF2K inhibition of EF2 and thus elongation of nascent polypeptide chains(15). S6K also plays a role in actin organisation by the direct binding to F-actin. A role in cytoskeletal rearrangement is also seen as S6K activates Rho family members regulating this - CDC42 and RAC1 and their downstream target PAK1. As deletion of S6K leads to a decrease in activation of the Rho family members, cytoskeletal organisation and migration in ovarian cancer cells, S6K is a promising target for enabling reduction of tumour progression(64). An additional target of S6K1 is RICTOR(65), which when phosphorylated at T1135, leads to mTORC2 inhibition, establishing a negative feedback loop between mTORC1 and mTORC2(66).

1.5.1.2 mTORC2 signalling

AKT can be considered the hub of the PI3K pathway as its downstream signalling leads to mechanisms controlling a multitude of diverse functions within the cell. AKT is only activated in response to receptor signalling via phosphorylation of two key sites, T308 by PDK1 and S473 by mTORC2, via growth factor (GF) receptor activation(67). The majority of mTORC2 functions occur through AKT regulation, including activation of mTORC1, placing AKT both upstream and downstream of mTOR regulation. During low-energy conditions, AMPK activation leads to an upregulation of mTORC2 and its downstream targets(68). Such downstream targets include the FOXO family of transcription factors, which are phosphorylated by AKT leading to an inhibition of their function. FOXOs play an important role in the repression of cell proliferation and survival, but in certain cell contexts are considered to play a role in tumorigenesis(69). FOXOs regulate apoptosis in distinct ways, repressing apoptosis through the downregulation of the pro-apoptotic BCL-2 family member BIM, or promoting apoptosis through transcriptional upregulation of FAS ligand(70). mTORC2-FOXO1 signalling also regulates innate immune responses as RICTOR deletion leads to attenuated AKT signalling, thereby increasing nuclear FOXO1, resulting in hyper-inflammatory

responses via TLR4(71). mTORC2 has been shown to localise at the mitochondria-associated endoplasmic reticulum membranes (MAM) in a GF-dependent manner, and *RICTOR* deletion disrupts AKT-dependent phosphorylation of mitochondria associated proteins. These events lead to a reduction in mitochondrial function, increasing mitochondrial membrane potential and effecting energy metabolism and cell survival, thereby demonstrating a vital role of mTORC2 signalling in mitochondrial physiology(25). The importance of mTORC2 in AKT activation was highlighted by a recent study demonstrating that deletion of the AKT binding site within the mTORC2 component mSIN1 greatly reduced AKT^{S473} phosphorylation, rendering it unable to phosphorylate FOXO1/3a, while other targets such as glycogen synthase kinase 3 (GSK3) and mTORC1 were unaffected(72) (73). These findings suggest that mTORC2 activation is important for AKT-mediated cell survival mechanisms.

Further downstream targets of mTORC2 include protein kinase C-alpha (PKCα) as mTORC2 inactivation reduced PKCα phosphorylation(74), which is responsible for functions including cell proliferation, differentiation, motility, apoptosis and inflammation(75). mTORC2 also regulates growth and ion transport by phosphorylating the hydrophobic motif of serum and glucocorticoid-induced protein kinase 1 (SGK1)(76). SGK1 inhibition induces autophagy, apoptosis and cell cycle arrest in the G$_2$/M phase in prostate cancer cell lines, at least in part through an mTOR-FOXO3a-mediated pathway(31). SGK1 regulates Th2 differentiation and negatively regulates interferon gamma (IFNγ) production, thereby highlighting the importance of mTORC2 in T cell effector function(77). mTORC2 has also shown to play a role in cytoskeletal organisation by activating RhoA GTPases(78).

1.5.2 mTOR in embryogenesis

The mTOR complexes are essential for cell survival and growth, and studies generating KO mice established that mTOR kinase and individual complexes mTORC1/2 were essential for normal embryogenesis(79,80). A homozygous KO of *mTOR* (*mTOR$^{-/-}$*) resulted in the death of mouse embryos soon after implantation (E5.5-6.5). Despite normal blastocyst development, the embryo did not develop further due to limited cell proliferation and survival signalling. Nevertheless, *mTOR$^{+/-}$* mice developed fertile and normal embryos. Similarly, *Raptor$^{-/-}$*

embryos die during early development (E7) whereas the *Rictor*^{-/-} mice survived slightly longer (E10.5)(80). These studies indicate mTOR function is mediated mainly through mTORC1 during early embryogenesis, but both mTORC1/2 play critical roles.

1.5.3 mTORC1 and mTORC2 signalling in HSCs/HSPCs

Targeted deletion of mTORC1 and/or mTORC2 in mouse models demonstrate a critical role for the mTOR pathway in haemopoiesis and highlight the importance of the individual mTOR-containing complexes at specific stages of HSC homeostasis and haemopoietic lineage commitment and maturation, as discussed below.

1.5.3.1 HSCs

Conditional knockout (cKO) mouse models of PTEN and TSC1, upstream negative regulators of mTORC1 in HSCs, revealed an increase in short-term HSC cycling and a concomitant decline in LT-HSC quiescence and self-renewal through constitutive activation of mTORC1(81,82). TSC1^{-/-} in HSCs led to an elevation in mitochondrial biogenesis, resulting in increased reactive oxygen species (ROS) production, driving HSCs from quiescence to rapid cell cycling thereby reducing self-renewal capacity(83). These studies identify the importance of mTOR regulation in HSC quiescence through ROS regulation. Interestingly, similar findings were reported in mTOR cKO mice, in which BrdU labelling revealed rapid cell cycling in HSC leading to a loss of quiescence and defective HSC engraftment and repopulation upon transplantation into NSG mice(84). Recent studies establish crosstalk between the extracellular regulated mitogen activated protein kinase (ERK) and mTOR signalling pathways, with ERK activity regulating mTORC1 activation, thus limiting its strength to promote HSC cycling in favour of quiescence. Indeed, HSCs derived from MEK1 cKO mice exhibit exhaustion due to increased mTORC1-mediated ROS production resulting in increased mitochondrial damage(85). These studies identify the importance of precise mTOR regulation during HSC maintenance and haemopoiesis.

The WNT signalling pathway can activate the mTOR pathway by inhibiting GSK3-mediated phosphorylation of TSC2 independently of *β-catenin* transcription.

GSK3 inhibits mTOR activation by phosphorylating TSC2 in a manner coordinated by AMPK (86). Knockdown (KD) of *Gsk-3* disruption initially resulted in an increase in LSK populations due to an activation of both WNT-signalling (β-catenin dependent) and mTOR pathways. However, long-term disruption of GSK3 expression/activity led to a depletion of HSC populations due to mTOR activation, which could be reversed through inhibition of mTORC1 and β-catenin(87). Inhibition of the mTOR pathway together with activation of the WNT-β-catenin pathway led to increased LT-HSC numbers and the potential to culture HSCs *ex vivo* in a cytokine free environment, highlighting the importance of appropriate regulation the WNT and mTOR signalling pathways in stem cell renewal(88).

Reduction in signalling downstream of mTOR enhances HSC self-renewal and repopulating properties: mice lacking S6K1(89) or mice treated with rapamycin, a partial mTORC1 inhibitor(90), exhibit increased life- and health-span compared to controls due to an increase in repopulating LT-HSCs. Collectively, these findings suggest that the loss in mTOR function during haemopoiesis primarily represents a loss of mTORC1 activity, with mTORC2 not playing a key role in HSCs.

1.5.3.2 Haemopoietic stem/progenitor cell (HSPCs):

Assessing the role of mTOR on haemopoietic lineage commitment using an *mTOR* cKO model in adult mice revealed significant aberrations in the development of haemopoietic lineage populations, resulting in a reduction of splenic weight and size. Closer analysis revealed that mTOR disruption led to pancytopenia, including a block in erythrocyte development at the pro-erythroblast stage, and anaemia(84). The decline in haemopoietic lineage commitment was accompanied by increased apoptosis and decreased myeloid cell leukaemia 1 (MCL-1) expression. Within BM HPC populations, there was a skew towards CMPs and a decrease in CLPs in *mTOR*-deficient mice. While there was an increase in the LSK population, the colony forming ability of these LSKs was impaired. There was also an attenuation in S6K and 4EBP1 phosphorylation/ activation and increased phosphorylation of AKT, implicating an aberration in the S6K-mediated negative feedback loop regulation of mTORC2 activity(66,84).

The mTORC1 cKO model (*Mx1*-cre$^+$*Raptor$^{fl/fl}$*; *Mx1-Raptor* cKO) exhibited an increased LSK population in the spleen in addition to the BM, suggesting extramedullary haemopoiesis. The LSKs were arrested at the G$_1$ phase of cell cycle compared to controls, suggesting a reduction in cell division(91). Metabolite analysis of LSKs revealed an increase in intermediates used in lipid metabolism, and in AMP and NADP$^+$ involved in redox homeostasis, and a decrease in nitrogen metabolism(91). LSK$^-$CD48$^-$CD150$^+$ cells derived from the *Mx1-Raptor* cKO BM failed to engraft into recipient mice. While these cells were able to home to the BM, they localized further from osteoblast cells, indicating a role for mTORC1 in the integration of niche signals. *Mx1-Raptor* cKO HSCs also possessed regenerative and self-renewal aberrations compared to controls and those cells that 'escaped deletion'. A compound *Rictor*/*Raptor* cKO in adult mice exhibited similar results as *Mx1-Raptor* cKO mice in haemopoiesis, however this mouse model did not develop BM failure and retained the deletion of alleles of *Raptor* and *Rictor* for almost one year after KO induction(91). These results suggest that the mTOR pathway is not essential for survival and haemopoietic maintenance in adult mice but is essential for haemopoiesis initiation during embryonic development.

Genetic targeting studies to ablate mTORC2 function in haemopoiesis revealed a more subtle role compared to mTORC1. Studies in *Mx1-Rictor* cKO (*Mx1*-cre$^+$ *Rictor$^{fl/fl}$*) mice indicated that mTORC2 does not play a significant role in HSCs and progenitor populations(92). However, Magee *et al.*, elegantly demonstrated that after *Pten*-deletion, which activates the mTOR-signalling pathway, deletion of *Rictor* abrogates leukemogenesis and HSC depletion in adult, but not neonatal mice(93), highlighting that the PTEN-mTORC2 signalling axis has a role in activating these processes in a temporally-dependent manner.

1.5.4 mTORC1 and mTORC2 signalling in Erythrocytes

The *mTOR* cKO model revealed a block in erythropoiesis at the proE stage, highlighting the importance of mTOR signalling in red blood cell (RBC) development(84). Interestingly, results from this model are similar to that observed in the *Tsc1* cKO mouse, which exhibited a reduction in erythrocytes in the BM(82), through activation of mTORC1-mediated signalling. These studies indicate that a complex regulation of mTOR signalling is required for appropriate

RBC development. Analysis of the importance of mTOR function in erythropoiesis revealed that loss of FOXO3 in erythroblasts results in an overactivation of the mTOR pathway thereby compromising erythroid maturation(94). FOXO3 regulates *Gata1* expression and represses *Exosc8* expression which are both involved in erythroid maturation(95). Additionally, ectopic expression of microRNA9 (miR9) disrupts erythropoiesis via the suppression of FOXO3-mediated pathways, causing an increase in ROS due to the downregulation in ROS scavenging enzymes(96).

Recent studies show that mTORC1 plays a critical role in RBC commitment, growth, proliferation and homeostasis. Knight *et al.*, demonstrated that mTORC1 activity is regulated by dietary iron, and a loss or overexpression of mTORC1 in HSCs leads to microcytic or macrocytic anaemia respectively with a loss of proliferation in RBC progenitors(97). Furthermore, mice treated with the ATP competitive mTOR inhibitor MLN0128, and subsequently treated with phenylhydrazine to induce haemolysis, was shown to be lethal, demonstrating the reliance of the mTOR pathway in RBC development(97). Zhang *et al.*, have shown that the heme-regulated eIF2α kinase (HRI)-activating transcription factor 4 (ATF4) pathway, which regulates heme uptake for haemoglobin production and stress response genes, suppresses mTORC1 activity in iron deficiency anaemia. The HRI-ATF4 pathway promoted RBC progenitor differentiation, and pharmacological inhibition of mTORC1 rescued RBC counts and haemoglobin content in the blood(98). mTOR also plays a role in microenvironmental homeostasis associated with RBC development through regulation of neutral essential amino acids (NEAA) uptake into cells during erythropoiesis for haemoglobin production. mTORC1/4EBP1 signalling regulates Lat3, a transporter of NEAA in RBCs(99).

1.5.5 mTORC1 and mTORC2 signalling in Myeloid cells

cKOs of *Mtor* or *Raptor* in HSCs lead to a significant accumulation of CD11b$^+$Gr1$^-$ population(84,100). *Mtor* cKO mice on a severe combined immunodeficiency (SCID) background exhibited reduced monocyte/macrophage populations in *in vitro* and *in vivo* assays. However, removal of *mTOR* expression specifically in myeloid cells (*Mtor-Lyzs*-cre), revealed normal levels of monocyte/macrophage populations, suggesting that mTOR plays a role during lineage commitment, but not during survival and maturation(101). Following *mTOR* deficiency, a decrease

in the expression of macrophage-colony stimulating factor (M-CSF) receptor CD115 was noted, which may result in decreased monocyte/macrophage populations due to overactive STAT5 and downregulation of IRF8(101). M-CSF promotes mTORC1 activation which further promotes CD115 expression, and expression of *Pu.1* and *Irf8* to promote myelopoiesis. In the absence of mTORC1 activity there is a block in glucose uptake and lipid metabolism thereby abrogating myeloid differentiation along with an impaired immune response to bacterial infection(102). Constitutive activation of mTORC1 in *Tsc* KO BM-derived macrophages (BMDMs) attenuated AKT signalling through the negative feedback loop via mTORC2 leading to a defect in IL4-induced M2 polarisation. These BMDMs produce more pro-inflammatory responses compared to controls suggesting an important role of mTORC1 in the regulation of inflammation(103). Additionally, it has recently been shown that *Raptor* cKO, but not granulocyte-specific KO (*Raptor-Lyz2*-cre) mice lead to a significant increase and accumulation of innate myelo-lymphoblastoid effector cells (IMLECs). This suggests that IMLEC accumulation driven by *Raptor*-deficiency occurs earlier in development, caused by reduced expression of *Myb* in CMPs(104).

A myeloid lineage specific KO model of *Rictor* (*LysM*-cre) revealed a significant decrease in monocytes, while the neutrophil population was unaffected. BM monocytes and peritoneal macrophages displayed decreased proliferation and increased susceptibility to pro-apoptotic stimuli. Furthermore, stimulation of TLR4 on $Rictor^{-/-}$ macrophages with lipopolysaccharide (LPS) potentiated a pro-inflammatory response, with cells skewing towards an M1 phenotype and downregulating IL10 expression, suggesting that mTORC2 signalling is a negative regulator of TLR signalling in macrophages(105,106). Interestingly, the inflammatory response observed in $Rictor^{-/-}$ cells was reversed by the inactivation of *Raptor*, indicating that mTORC1 regulates inflammatory responses in macrophages(105).

1.5.6 mTORC1 and mTORC2 signalling in B cells

The importance of mTOR signalling during B cell development is evident from a study analysing mice in which mTOR expression is reduced. Reduced expression was achieved by the neomycin insertion at exon 12 of *mTOR* thereby creating a *mTOR*-knock-in (KI) model partially disrupting *mTOR* transcription(107). A

reduction in progenitors B cells was observed in these *mTOR*-KI mice, with a block between large preB cells (B220$^+$CD24$^+$CD43$^+$) and small preB cells (B220$^+$CD24$^+$CD43$^-$). Within the spleen, an increased number of mature B cells (B220$^+$IgD^{high}CD21$^+$IgM$^-$) and decreased T1 and T2 transitional B cells were observed compared to wildtype (WT) mice(107). Deletion of the TSC1 complex in B cells (*CD19*-cre) renders mTOR constitutively active, resulting in a partial block in B cell maturation as indicated by an elevation in T1 and T2 transitional B cells, and a depletion of MZ B cells(108).

Assessing mTORC1 signals more directly, *Raptor* cKO mice exhibit a significant decrease in B cell generation, due to an early block in lineage commitment(100,109). For this reason, the effect of *Raptor* ablation on B cells was analysed using B cell specific models (*Mb1*-Cre), which resulted in a profound block at the preB cell stage abrogating B cell maturation, proliferation, GC reaction and antibody production(109). Additionally, a cKO of *Raptor* specifically in B cells (hCD20$^-$*Tam*$^-$Cre) resulted in a decrease in GC B cells and nascent antibody secreting plasma cells, and the elimination of GCs resulting in a decline in serum-antibodies(110). These studies illustrate the importance of mTORC1 at multiple stages of B cell maturation, and highlights the critical role played by mTOR in mounting an appropriate humoral immune response.

Rictor KO models revealed a role for mTORC2 during B cell maturation, resulting in a decrease in mature B cells(111). Studies demonstrate an increase in early B cell populations including the proB, preB and immature B cells in *Rictor* cKO mice, characterised by elevated FOXO1 and RAG1 expression and a subsequent reduction in mature splenic B cells(92). However, HSCs isolated from *Sin1*$^{-/-}$ mice reconstituted haemopoietic lineages suggesting a minimal role for mTORC2 in B cell development during early stages. However, these mice exhibited increased IL7 production and RAG1/2 expression at the proB stage and fewer IgM$^+$ immature B cells suggesting a role for mTORC2 after B lineage commitment(112). mTORC2 has also been shown to play an important role in B cell survival, as *Rictor*-null mice display increased caspase-3 and PARP expression, together with increased cell death and a decrease in B-cell activating factor (BAFF) expression in mature B cells(111). Lee *et al*., proposed that mTORC2 regulates canonical and non-canonical nuclear factor kappa B (NFκB) signalling pathways responsible for mature B cell maintenance and

survival(111). Interestingly, *Rictor*-null mice possess increased CIP2A binding to protein serine/threonine phosphatase A (PP2A) leading to increased c-myelocytomatosis viral oncogene (C-MYC) phosphorylation and expression, and decreased E2F1 expression, which leads to apoptosis(113).

1.5.7 mTORC1 and mTORC2 signalling in T cells

T cells develop in the thymus, undergoing rigorous positive and negative selection processes at the $CD4^+CD8^+$ double positive (DP) stage of development, to generate a pool of T cells that recognise foreign peptides in the context of self-major histocompatibility complex 1 (MHC-I) ($CD8^+$-cytotoxic T cells) or MHC-II ($CD4^+$-helper T cells). Analysis of mTORC1 signalling inhibition during T cell development showed that rapamycin treatment and *Raptor*-deletion in cKO mice resulted in reduced thymic cellularity and a decrease in the proportion of DP cells, coupled with a concomitant increase in $CD4^-CD8^-$ double negative (DN) cells(114). Within the DN population, rapamycin blocked T cell development at the DN3 stage, likely prior to the proliferative burst associated with β-selection, while development was arrested at the DN1-DN2 transition in *Raptor*-null mice both *in vitro* and *in vivo*. This block was associated with a reduction in proliferation due to an instability of cyclinD/cyclin-dependent kinase 6 (CDK6) complexes. Similar results were noted with an *Mtor* cKO mouse model, while *Rictor* cKO mice exhibited a block in proliferation at the DN3 stage of development (115,116), suggesting that mTORC1 plays a critical role, which is distinct from mTORC2, during the early stages of T cell development.

The thymic microenvironment plays a critical role in enabling the appropriate development of nascent T cells, particularly thymic epithelial cells (TECs). Selective $Rictor^{-/-}$ in TECs results in a reduction in thymic mass and cellularity of TECs, and decreased generation of specific T cell lineages: T-cell receptor $\alpha\beta$ (TCR$\alpha\beta$), TCR$\gamma\delta$, invariant NK-T(117) and regulatory T cells thereby revealing an important role of mTORC2 in thymopoiesis and T cell lineage generation(118).

In the periphery, reduced mTOR expression/activity decreased T cell numbers, T cell activation and proliferation(107). Furthermore, TSC1 ablation drove naïve T cells from quiescence to a poor immune response, altering the cell size and cycling(119). mTORC1 activation, through TSC2 deletion, led to increased,

terminally-differentiated effector CD8^{+} T cell formation not capable of conforming to a memory T cell phenotype. However, mice deficient in mTORC1 activity, through deletion of RHEB, led to loss of effector CD8^{+} T cell formation with no change in memory T cell expression, suggesting a role of mTORC1 in the differentiation of specific T cell subsets(120). Indeed, mTORC1 is involved in Th1 and Th17 differentiation from naïve CD4^{+} T cells, as deletion of RHEB blocks Th1 and Th17 differentiation, but not Th2 differentiation *in vivo* and *in vitro*(121). Moreover, mTORC1-mediated signalling plays a critical role in CD4^{+} T cell proliferation, by enhancing PPARγ activity, which in turn activates fatty acid metabolism, thus enabling the metabolic reprogramming required to activate CD4^{+} T cells(122).

Th cells require mTORC2 for T cell differentiation as ablation of mTORC2 in T cells led to impaired Th1 and Th2 differentiation, which could be reversed by activating AKT and PKCθ respectively(123). However, mTORC2 is mainly considered to regulate Th2 differentiation, as *Rictor* KO in CD4^{+} T cells specifically led to the generation of Th1 and Th17 cells but not Th2 cells(124). mTORC2 controls CD8^{+} T cell differentiation in a FOXO1-dependent manner as ablation of mTORC2 led to an increase in memory precursor effector cells (MPEC) and not in the short lived effector cells (SLEC) driven due to *Eomes* and *Tcf-1* upregulation caused by FOXO1(120,125). Recently, Velde and Murray demonstrated that mTORC2 plays an important role in microenvironment sensing in CD4^{+} T cells. In a normal setting, CD4^{+} T cells require essential and non-essential amino acids (AAs) to undergo cell division. Limiting arginine and leucine resulted in cell cycle disruption, which could be bypassed in the absence of *Rictor*. This resulted in cells initiating cell cycle regardless of limiting AA, thus bypassing micro-environmental sensing(126).

1.5.8 mTOR signalling in leukaemogenesis

The PI3K/AKT/mTOR pathway plays a major role in the haematopoiesis as constitutive activation of the mTOR pathway led to impairment of HSC function. Additionally, deletion of mTORC1 leads to pancytopenia and is vital for HSC regeneration. The AKT/mTOR axis has shown to play a role in leukaemogenesis as in a mouse model of leukaemia evoked by *Pten*-loss, mTORC1 deletion resulted in a significant increase in survival(91). mTOR signalling is not only

involved in leukaemia, but lymphoma too. For instance, mantle cell lymphoma (MCL) has activated BCR signalling with increased activation of Src family kinases (SFKs) including Lyn. Consequently, treatment of MCL murine models with dasatinib (SFK inhibitor) leads to reduction in tumour size(127). Recent research shows that this pathway is upregulated in CLL patients from distinct cohorts and this can also be seen in CLL murine models. Inhibition of this pathway with AZD8055 (dual mTORC1/2 inhibitor) led to a greater level of apoptosis when compared to rapamycin in primary CLL patient samples(128) .

Rapamycin, along with its analogues, 'rapalogs' have shown promise in targeting CLL. Rapamycin has shown to induce cell cycle arrest by modulating the mTOR/S6K pathway and abrogating cyclin E, cyclin D3 and cyclin A expression. Additionally, survivin a protein upregulated in CLL along with other cancers, is associated with disease survival. Survivin has also become a therapeutic target for many cancers. Rapamycin has shown the potent inhibition of this protein suggesting a potent role in CLL abrogation(129). Moreover, due to the known role of the microenvironment in CLL maintenance, rapamycin could play a potent role in abrogating microenvironmental signals. Rapamycin was first identified as an immunosuppressant of T cell mediated signals including IL2 and IL4 signalling(130). These signalling pathways are upregulated in CLL and have shown to mediate CLL survival highlighting the importance of rapalogs in CLL maintenance. Indeed, Decker *et al.* have demonstrated a block in proliferating CLL cells with rapamycin treatment. Rapamycin treatment led to a decrease in cyclin D3 and a decrease in CDK2 via the suppression of cyclinE and cyclinA leading to cell cycle arrest. Although rapamycin did not induce apoptosis, impairment of cell cycle regulating proteins blocked proliferation of CLL cells(131).

FOXO1 is the main isotype observed in CLL patients responsible for cell cycle arrest. AKT activation phosphorylates FOXO1 to inactivate it thus halting its translocation into the nucleus. However, AZD8055 (but not rapamycin) treatment led to an increased translocation of FOXO1 into the nucleus thus inducing apoptosis in cells. Cosimo *et al.,* have recently shown that microenvironment signals enable constitutive activation of PI3K/AKT/mTOR signalling in chronic lymphocytic leukaemia cells, which inactivates FOXO1. This may assist in disease progression. Moreover, dual mTOR complex inhibitors

AZD8055/2014 enable a reduction in disease progression and an activation of FOXO transcriptional program which was enhanced by combination with ibrutinib(128).

1.6 Chronic Lymphocytic Leukaemia

Chronic lymphocytic leukaemia (CLL) is the most common leukaemia in the Western world, which exhibits a monoclonal expansion of B cells. CLL-B cells are characterised by $CD19^+CD23^+CD5^+IgM^+IgD^{lo}$ surface expression, a phenotype of mature B cells(132). It is known to mainly affect the elderly, displaying a median age of 70 years and is 1.5 times as prevalent in males as in females, with about 3,200 patients diagnosed with CLL in the UK in 2011(133). Current diagnosis of the disease is based upon the morphology of lymphocytes, $>5X10^9$ circulating B cells for more than 3 months, and a characteristic immunophenotype(134). This scoring system is the CLL scoring system based on the immunophenotypic characteristics. Immunophenotype of CLL patients are mostly positive for CD5, with dim expression for CD20, along with dim or no expression of surface Ig, CD79b, CD22, MFC7. CD38 has shown to be overexpressed in some cases along with increased 70 kDa zeta associated protein (ZAP-70) which are correlated with patients having a poorer prognosis with unmutated IgV_H gene. For instance patients are scored depending in the immunophenotype the present, if the scoring reaches or exceeds 3, they present true CLL (135). Typically, the Rai and Binet staging system is used for assessing the prognosis of the disease. Rai staging is mostly used in the USA and the system is divided into 5 stages where lymphadenopathy, lymphocytosis and anaemia are taken into account. Binet staging system is mostly followed in the UK and Europe and is divided into three stages, A-C, which is dependent upon the levels of anaemia and white blood cell count (136). Regardless of the staging system, patients with a more advanced disease have a median survival of 1-2 yr as opposed to patients with a more benign disease with a median survival of more than 10 yr(137,138). Despite extensive research on CLL in the past decade, it remains incurable with standard therapy, demonstrating the need to develop novel strategies for CLL therapeutic research.

1.6.1 Mutational status and prognosis

The differential clinical behaviour of the disease has been associated with the somatic mutational status of the IgV_H regions of the BCR. It has been shown that patients with CLL cells carrying unmutated IgV_H regions display a poorer prognosis with a diminished survival time (median survival time of ~8 yrs) as compared to those patients with somatic IgV_H mutations with a median survival time of ~24 yrs (139). Patients with poorer prognosis have also been shown to express upregulated levels of CD38 (140) and ZAP-70 and activate key signal transduction pathways more readily in response to BCR signalling(141).

While chromosomal abnormalities are not required for the development of CLL, 80 percent of patients with CLL have chromosomal deletions/gene mutations at diagnosis. With the progression of the disease, the cells can acquire increasing deletions showing a poorer prognosis of the disease. The most common chromosomal deletion, occurring in about 55% of cases, is the 13q band deletion which displays a benign phenotype. This region (13q14) encodes for the *miR16-1* and *miR15a* which have shown to play a role in leukemogenesis and the *miRs* regulate BCL proteins. However, patients with deletions in the 11q chromosomal band (in 10% patients with early stage and 25% with advanced disease stage) have a more aggressive phenotype with rapid progression and reduced survival. The 11q23 region harbours the *ATM* gene, which encodes a DNA damage response kinase, the lack of which leads to a progression of the disease. Another chromosomal deletion (found in about 5-7% patients) is deletion in the 17p band which deletes the *TP53* tumour suppressor gene and displays the most aggressive form of the disease(142). Of note, in patients carrying a 17p deletion, the accompanying allele has a mutated copy of *TP53* in 60% of cases, therefore rendering the CLL cells with no functional p53. This makes p53 mutated CLL cells highly chemorefractory.

1.6.2 Role of microenvironment

Although, CLL was initially classified as a disease of accumulation of B-lymphocytes(143), since the identification of CLL as a dynamic(144), and not a static disease, cross-talk between the microenvironment and malignant B cells have shown to further cause clonal expansion of the disease. CLL cells have been

shown to migrate to lymphoid organs and proliferate in centres through signals further enhanced by the microenvironment. $CD4^+CD40L^+$ T cells have shown to interact with CD40 receptors on malignant cells in the proliferation centres to increase survival by increasing expression of anti-apoptotic proteins BCL_{XL} and MCL-1. $CD40^+$ stimulated CLL cells were resistant to drug induced apoptosis[145] suggesting that the microenvironment interactions enhances disease progression. Furthermore, activated BCR signalling in CLL is responsible for upregulating MCL-1 via PI3K/AKT signalling[146].

T cells are known to play a critical role in CLL progression. CLL is associated with an increase in $CD8^+$ and $CD4^+$ T cells along with their exhaustion linked with an increase in programmed death 1 (PD-1) expression[147]. CLL cells have an increased expression of PDL1/PD1 with increased CD40 stimulation[148] PD/ suggesting a potential role of PD-1/PDL1 in CLL therapy. Indeed, PDL1 inhibitors are in clinical trials for other Hodgkin and non-Hodgkin lymphomas[149,150] showing promising results which could also prove to be effective in CLL. Additionally levels of CCL3 and CCL4 have also shown to be upregulated in CLL[151], behaving as chemoattractants for monocyte derived nurse-like cells (NLCs), enhancing CLL survival and homing in secondary lymphoid organs. In CLL, these chemokines may help to enhance microenvironment to induce anti-apoptotic signals thereby further protecting the disease. CCL3 has also been associated with a poor prognosis of CLL.

BM stromal cells (BMSCs) have also shown to protect CLL cells due to an increase in anti-apoptotic signals [152] with increasing CLL cell affinity towards BMSCs. Increased migration towards stromal cell-derived factor 1 (SDF-1)/ CXCL12 (released by BMSCs) is due to the increased expression of CXCR4 [153]. In normal B cells, CXCR5 is responsible for the homing of B cells into the GCs of secondary lymphoid organs via the affinity of CXCL13 released by NLCs in these organs. In leukaemic B cells, there is an increase in CXCR5 expression, leading to increased homing towards CXCL13 leading to changes in actin polymerisation and chemotaxis[154]. NLC released BAFF and a proliferation-inducing ligand (APRIL) have also shown to bind to their receptors on malignant B cells and protect the disease in a NFκB dependent manner[155].

Calissano *et al.,* have shown heterogeneity within a CLL disease where there exist two subpopulations with varying phenotypes. One population comprises a CD5^{dim}CXCR4^{hi} resting-cell like population whereas the second subtype has a CD5^{hi}CXCR4^{dim} phenotype with a proliferative characteristic with increased Ki67 suggesting increased cell cycling and an increase in anti-apoptotic genes[156]. This is termed the Calissano model which highlights the spectrum of CLL cells within the same disease. Interestingly, ibrutinib and idelalisib have been shown to target the CXCR4-SDF-1 axis and potentially disrupt the 'resting CLL cells' leading to an increase of these cells from the lymphoid organs into the peripheral circulation (lymphocytosis) post ibrutinib treatment[157,158]. These findings suggest a targeting of a CLL subset with current drugs in clinics.

1.6.3 Current therapy

Current therapy has evolved drastically over the past few years and has become increasingly heterogeneous depening on the aggressiveness of the disease and the fitness level of the patients. How 'fit' a patient is depends on other diseases and co-morbidities such as cardiac issues, etc. Some clinical trials use the Co-morbidity illness Rating scale (CIRS) to assesses fitness objectively. According to current guidelines, all CLL patients are tested for both *TP53* mutations and deletions as recent research has shown that attenuated *TP53* affects therapy[159]. This brings in into question the use of the scoring system altogether in an age of molecular testing. Currently, the use of the scoring system is reassuring with the novelty of molecular testing, in the future, perhaps the scoring system will be redundant.

First line therapy differs between ptients depending on patient fitness and *TP53* mutations. How 'fit' they are which alludes to other diseases and co-morbidities such as cardiac issues, etc. In the pivotal CLL8 study, Hallek *et al.,* demonstrated that the addition of Rituximab (R) (anti-CD20 antibody that specifically targets B cells) to the backbone of chemoimmunotherapy comprising cyclophosphamide (C) which is an alkylating agent interfering with DNA synthesis, and fludarabine (F) which is a purine analogue interfering with DNA synthesis improved the progression-free survival (PFS) and overall survival (OS) of fit CLL patients without *TP53* alterations [134,160]. Therefore, FCR is approved for first line therapy for fit CLL patients without TP53 alterations and

is approved by the National Institute for Health and Care Excellence (NICE). Indeed, the mechanism of action of FC drugs require p53 activity, therefore patients with 17p deletions or *TP53* mutations require different treatments(161).

Less fit patients, two major clinical trials CLL11 by the German CLL study Group and COMPLEMENT-1 led to the introduction of chlorambucil in combination with Obinutuzumab or Ofatumumab for less fit CLL patientsa and are NICE approved. CLL11 demonstrated superiority of chlorabucil-obinutuzumab over chloambucil-R or chlorambucil alone (162). COMPLEMENT-1 study demonstrated superiority of chlorambucil-ofatumumab over chlorambucil alone(163). Moreover, ibrutinib is licensed for front-line use in CLL patients without TP53 abberations as patient showed increased OS with ibrutibin over chlorambucil alone in the RESONATE-2 trial but has not received approval from NICE as of now(164).

Recent therapeutic strategies for CLL patients with TP53 abberations have focused on inhibiting signalling and survival pathways which are important in CLL initiation and development. Indeed, BCR signalling plays a central role in the survival of CLL, and in the prognostic outcome of patients, therefore making this signalling pathway an attractive therapeutic target(165). Furthermore, recent findings demonstrating that autonomous BCR signalling is evident independent of cell-antigen interactions makes this pathway an important therapeutic target(166). Two major drugs, ibrutinib and idelalisib, which have been introduced in clinics are inhibitors of the downstream kinases, Bruton's tyrosine kinase (BTK) and PI3Kδ respectively of the BCR signalling pathway.

PI3Kδ expression is limited to leukocytes where it plays a role in B cell development(167) and in T-regulatory (T-reg) cell function(168). The constitutive activation of the BCR in CLL makes PI3Kδ an ideal therapeutic target. Indeed, Hoellenriegel *et al.,* have demonstrated an aberration in CLL migration and homing (via CXCL12 and CXCL13 impairment) with idelalisib treatment(169). Although idelalisib had been approved in by NICE for its efficacy and safety profile for patients with TP53 abberations, major side effects of this drug included fatal or severe diarrhoea, colitis and hepatoxicity(170). Similar side effects were observed in PI3K-deficient mouse model developed by Okkenhaug *et al.*, where the mice developed inflammatory bowel disease together with impaired B and T cell function(171). These results highlight the

need to identify novel therapeutic targets for CLL. This drug was reviewed and has been set as first line therapy with rituximab for CLL apatients with TP53 abberations which are not for for alternative therapy(172). Although BTK was not found to be constitutively active, BTK protein levels were upregulated with increased BCR activity suggesting increased downstream PI3K/mTOR activity in mediating survival signals in CLL(173). Ibrutinib, an irreversible inhibitor of BTK, has shown promise in murine models of CLL, as ibrutinib treatment of Eµ-TCL1 mice (CLL mouse model) leads to a significant increase in survival via a delay in disease development by promoting apoptosis(174). Ibrutinib is now increasingly being prescribed as to patients with poor prognosis and is NICE approved for patients with TP53 abberations after the RESONATE-17 clinical trial(175). Nonetheless, side effects such as atrial fibrillation and haemorrhage can lead to discontinuation of treatment in some patients with resistant mutations due to clonal evolution(176) indicating the need for novel agents/therapeutic targets. Recently, ABT-199 (venetoclax), a BH3 mimetic has also entered clinical trials and shown promise in patients with 17p deletions(177).

Currently, ibrutinib synergy with venetoclax, a BH3 mimetic is being tested for alternative therapy for CLL in the CLARITY clinical trial(178). Recently, ARQ-531, a reversible and less potent target of BTK is was assessed for its efficiency in targeting CLL. Despite partial inhibition of BTK, ARQ-531 targeted SFK kinases and ERK signalling thereby targeting multiple pathways involved in CLL. Indeed, ARQ-531 treatment of Eµ-TCL1 mice resulted in increased survival compared to ibrutinib treated mice suggesting global inhibition of signalling pathways leads to more robust results(179).

The BCL family, including anti-apoptotic proteins BCL-2, MCL-1, and the counterbalancing pro-apoptotic proteins (eg. BID, BAX), contain BH3 domains in their structure. BH3 mimetics such as venetoclax that inhibit the function of BCL-2, has recently been approved as second line therapy for relapsed patients treated with ibrutinib(180). BCR inhibitors and BH3 mimetics improve outcome in patients with a more aggressive disease and improve disease conditions in poor prognostic patients, particularly in patients with 17p deletions(181). However, resistance mutations are already evident in patients treated with venetoclax due recurrent Gly101Val mutations(182), suggesting the need for additional therapeutic targets or combination therapies.

Haematopoietic stem cell transplantation (HSCT) is another CLL therapy procedure. However, it can only be considered for the younger/fitter patients with an aggressive form of the disease as the older populations with the disease cannot undergo such harsh treatments. It is known to decrease treatment-related mortality but has known to have relapses(183). However, more emphasis has been put on the reduced intensity conditioning (RIC) HSCT which can also be given to the elderly population(184). RIC-HSCT has led to a decreased relapse mortality rate by 16-23% and seems to be a powerful therapeutic regime(183). According to NICE recommendations, transplants are only recommenbed to pateints who have failed chemoimmunotherapy and therapy using BCR inhibitors.

Chimeric antigen receptor-T (CAR-T) cells have recently shown promising results in treating various Hodgkin and non-Hodgkin lymphomas. CAR-T cell therapy involves the re-engineering of self T cells to recognise specific tumour associated antigens including targets such as CD19, CD20(185). Recently, a small cohort of patients (18 patients) with relapsed CLL who had been treated with ibrutinib, were treated with CD19 CAR-T cells. Results were very promising which showed high CAR-T CD4:CD8 ratio with complete responses in patients. However, this treatment was only introduced to the clinic in 2016 and thus is in an early phase and needs to be monitored for a longer duration(186).

1.7 Mouse models commonly used in haemopoiesis

1.7.1 Cre-loxP KO system

Naturally present in bacteriophage P1, the cre-loxP system is extracted from this virus and is now widely used in murine studies and in other mammals for genome editing/omitting. Cre (causes recombination) recombinase (cre) re-combines two loxP (locus of crossover in P1) sites in the genome, the gene is then considered to be 'floxed', leading to genome editing depending on loxP orientation.

Embryonic stem (ES) cells are conventionally used to incorporate cre gene. P1 encodes Cre, which is a 38 kDa enzyme and it recognises DNA-base pair (bp) repeats and recombines them by covalent-linking of protein between the two DNA-repeat sites. The expression of cre is usually controlled by a specific

promoter, thereby ensuring a controlled expression. It also allows cre expression in specific tissues, depending on the promoter of choice. Cre can be expressed in the coding sequence of the promoter thereby silencing the gene itself, or it could be present at the flanking end. Cre construct is cloned into ES cells via conventional methods and is subsequently microinjected into the pronucleus of mouse embryos, which can then be injected into mouse oviduct(187).

LoxP are 34-bp long DNA of which there is an 8 bp long core with 13-bp long palindromic DNA repeats at either side. These sites are inserted around a gene of choice, usually target gene of excision. The sites of insertion of these genes are important: loxP sites should not be inserted at important coding regions, thereby ensuring proper functioning of the gene in the absence of cre(187).

There can be various functions of this system. One of the most straightforward uses is gene deletion. Here the gene of interest will be floxed and cre-expression will be regulated by a promoter of choice. This can be done both *in vivo* and *in vitro*. Mice harbouring either loxP sites or cre are bred together to obtain either WT mice, mice containing only loxP or cre sites or both, which is the desired model(187). Subtle modifications have also been made within the genome by the insertion of point mutations utilising the cre-loxP system. This is done by the addition of a vector which harbours the mutation along with the flanked loxP site around the target gene. Therefore, when cre expression is induced, insertion occurs of the point mutation and loxP sites remain. Gene/exon replacement is also possible using this model whereby a replacement vector is added to one loxP site, where both loxP sites are flanked around the gene/exon to be replaced. Cre expression excises the original gene/exon leaving the loxP sites together with the replaced vector. Similarly, chromosomal translocations, insertions, inversions and conditional deletion of genes have successfully been demonstrated using the cre/loxP system(188). There are a variety of cre-loxP systems which have been used to assess the role of mTORC1 (via exision of *Raptor*) and mTORC2 (via exision of *Rictor*) in haemopoiesis. The most commonly systems used for haemopoietic cells and B cells are summarised in Table 1.1 below:

Promoter	Stage	fl/fl	Reference
ROSA26-Cre	All cells except brain cells	*Raptor/Rictor*	(111,114)
MX1-Cre	All cells except skeletal muscle	*Raptor/Rictor*	(93,104)
VAV-Cre	All haemopoietic, embryonic, germ cells	*Raptor/Rictor*	(93,97)
CD2-Cre	Common Lymphoid progenitors (CLPs)	*Raptor/Rictor*	(189)
MB1-Cre	Pre-proB cell stage	*Raptor*	(109)
CD19-Cre	Mature B cells	*mTOR, TSC1*	(190)
CD20-Cre	Mature B cells, more specific than CD19	*Raptor*	(110)
Aicda-Cre	GC B cell development	Raptor	(191)

Table 1.1 Summary of various promoters used in the cre-loxP system to excise mTORC1 (*Raptor*) or mTORC2 (*Rictor*) in haemopoietic cells and in B lymphocytes.

In this thesis, three different promoters have been used which control expression of cre at different stages of development thereby excising mTORC1 (*Raptor*) or mTORC2 (*Rictor*) at different stages. These are explained and summarised in Table 1.2 below:

Promoter	Cre expression
Vav	In all haemopoietic cells. Also expressed in embryonic stem cells and germ cells (192).
Mx1	Expressed ubiquitously in all tissues. Minimal expression in the skeletal muscle.
CD19	Only expressed in mature B cells.

Table 1.2 Summary of promoters used to control cre expression. Table also describes all the organs/cells the cre transgenes will be active.

1.7.1.1 *Vav*-cre model

Vav1 gene has previously shown to be expressed in all haemopoietic organs whereas *Vav2* and *Vav3* have a broader gene expression pattern(193). Besides haemopoietic organs, its expression is restricted to developing teeth, ES cells, testicular germ cells(192). The ubiquitous expression of *Vav1* in haemopoietic lineages occurs regardless of their developmental stage. Nevertheless, *Vav* expression is not fundamental for haemopoietic development as *Vav*-null mice still had functional B and T cells but had an aberration in proliferative capacity suggesting a redundant role of *Vav* in haemopoiesis(194). Additionally, *Vav* has shown to play a role in cytoskeletal organisation and proliferation, and has shown to activate the Rac/Jun signalling pathway(195). *Vav* expression also had sporadic reductions at later haematopoietic lineages suggesting a potent expression at developmental stages(192).

Vav mediated cre expression has shown to be a very effective method of mutagenesis using the cre-loxP system with a complete KO of floxed gene(196). However, there have been off-target homologous recombination in endothelial cells observed in some laboratories whilst not in others (197). Additionally, there have been rare off-target excisions in BM cells lacking haemopoietic markers suggesting excisions in stromal cells with *Vav*-mediated cre expression(198).

Nonetheless, the high efficiency of this model is well recognised, and it is widely used.

1.7.1.2 *Mx1*-cre model

MX1 is expressed in most organs (besides skeletal muscle), including all haemopoietic organs(199), and is widely expressed from very early stages of development. It is involved in innate immunity, activated post viral infections, with expression of MX1 being effective against influenza virus(200). It is activated by STAT-1 activation of TLR3 receptors(201). TLR3 activation has been associated with response to virus infiltration within the body. In research, polyinosinic-polycytidylic acid (poly(I:C)) mimics the double stranded RNA structure of some viruses, and activates the TLR3 thereby activating *Mx1* expression(202).

Mx1 is widely used in the cre-loxP system to induce a cKO (via poly(I:C) inoculation) thereby controlling time of KO induction which is a beneficial tool in research. Although this model has been shown to induce almost a complete KO in lymphocytes after a few days with complete KO in other haemopoietic lineages, there remain some limitations in using this model. One very important limitation is the spontaneous recombination caused in the *Mx1*-cre model prior to the inoculation of poly(I:C). This spontaneous recombination has previously been demonstrated to occur due to the constitutive activation of internal tandem duplications of FLT3 (FLT3-ITD) in acute myeloid leukaemia (AML) in mice. This increased the observed recombination prior to poly(I:C) inoculation from 2-3% to 30-50%(203). Therefore, it is very important to have appropriate controls when using this model to determine affects of spontaneous recombination. Another limitation is the phenotype of HSPCs, which is perturbed for a short time following poly(I:C) inoculation in mice. Following poly(I:C) inoculation, there is a transient change in the expression of HSPCs where there is an increase in Sca1$^+$ populations for a short duration (D8), which could disrupt the 'normal' HSPC phenotype in short-term studies(204). It is important to consider this if the timepoint of the experiment comprising this model is very short, as it might alter the results.

1.7.1.3 *CD19*-cre model

CD19 is a surface expressed at the proB cells stage and usually referred to as a marker for mature B cells which is responsible intrinsic signalling mediated via BCR signalling. *CD19* is responsible for the Ig-mediated activation of B cells and downstream activation of PI3K and AKT signalling which modulate proliferation and expansion of B cells(205).

CD19-mediated cre excision has also been used in the cre-loxP system. In mice, this system has shown to have a good excision in the spleen (90-95% excision), however a lower deletion efficiency in the BM: 75-80%(206). The *Mb1*-cre (expressed at the pre-proB cell stage) is the pan-B cell specific KO model for the cre-loxP system with a higher deletion efficiency(41).

1.7.2 Limitations of the cre/loxP system

Although the cre/loxP system is used widely in research, there remain some limitations to this system which should be considered whilst designing the experiments depending on the nature experiment.

The cre/loxP system has shown to have off-target cre-mediated excisions in mammals making the model 'leaky'. There exist pseudo-loxP sites in human and murine genome leading to various off target excisions(207). Therefore, it is important to determine the level of non-specific excisions ensuring that the off-target excisions (if any) do not hinder or significantly alter the results. Additionally, off-target excisions could occur in cre induced expression in germ-line due to the presence of many lineages in embryogenesis(208).

Cre toxicity is another limitation of the system. Increased cre expression has been associated with tissue/cell specific cre mediated toxicity. Research has shown that increased cre expression is associated with decreased proliferation and chromosomal aberrations in certain cell types(209). Additionally Li *et al.*, have shown complete tumour regression due to cre expression suggesting cell toxicity due to expression of cre(210). Conversely, it has been shown that cre excision of target floxed genes may not be completely efficient. This is usually due to cre-loxP models with induced expression of cre. As such, the method of cre induction could affect cre expression and therefore the deletion-efficiency.

For instance, tamoxifen induced inefficient cre-expression could depend on the frequency and volume of the inoculation of tamoxifen(211).

1.7.3 NSG/NRG mouse models

Several lymphoid mouse models have been generated for transplantation of cancer cells or human haemopoietic cells into mice in *in vivo* studies, with efficient models being NOD-SCID-IL2Rγ$^{-/-}$ (NSG) and NOD-Rag$^{-/-}$-IL2Rγ$^{-/-}$ (NRG) mouse models.

In 1983, the severe combined immunodeficiency (SCID) mouse model was defined wherein the autosomal recessive mutation of the *Prkcd* gene led to impaired rearrangement of the BCR and the TCR resulting in impaired B and T cell signalling. This is because the *Prkdc* gene encodes a DNA-dependent protein kinase catalytic subunit which is vital for VDJ recombination in developing B and T cells. In fact, there was almost a complete loss of B and T cells with impaired lymph node (LN) development(212). Although the SCID model is efficient at engrafting xenografts, the generation of a mouse model where the 'eat me not' signal was constitutively active, led to the efficient binding of signal regulatory protein alpha (SIRPα), ubiquitously expressed, with the human CD47L leading to the inhibition of phagocytosis by macrophages(213). These mouse models were termed non-obese-diabetic (NOD) mice. Backcrossing this strain with SCID mice led to a more effective and efficient xenograft model than SCID mice alone(214). Although these mice lacked functional B and T cells, NK cells were still present in the mouse models. The depletion of NK cells proved to enhance human CD34$^+$ HSC engraftment in NOD-SCID mice without compromising the ability of HSC cells to differentiate into haemopoietic lineages(215). Consequently, deletion of interleukin 2 receptor common chain gamma (IL2Rγ$^{-/-}$) led to impaired IL2, IL4, IL7, IL9 and IL15 signalling,(216) which are vital for T and NK cell development leading to a drastic decrease in NK cells. This model was incorporated into the NOD-SCID model as the NOD-SCID-IL2Rγ$^{-/-}$ model (NSG) model and has shown to be more effective at xenotransplant engraftment compared to NOD-SCID model alone(217).

Another model that has been shown to have a similar engraftment efficiency as NSG mice is the NOD-Rag$^{-/-}$-IL2Rγ$^{-/-}$ (NRG) mouse. This model is similar to that of

the NSG mouse model. Nevertheless, NRG mice have a deficiency of *Rag1* or *Rag2* genes as opposed to the *Prkcd* gene in NSG mice. Recombination-activating genes (*Rag*), as the name suggests are responsible for the initiation of Ig recombination in B and T cells. *Rag1/2*-null mice also have abberations/deletions in IL2Rγ chain(218) leading to a similar phenotype leading to concomitant decline in B and T cells altogether. Human HSC engraftment in NSG and NRG mice are equivalent(218).

1.8 Mouse models in CLL

1.8.1 TCL1 mouse model

T-cell leukaemia 1 (TCL1) was first identified in T-prolymphocytic leukaemia (T-PLL) as it was overexpressed in almost all cases. TCL1 has shown to affect B and T cell differentiation and *Tcl1*-KO mice have slight effects on B and T cell differentiation. It plays a more potent role in modulating embryonic development, stem cell differentiation and hair follicle generation(219). It has been shown to interact with AKT1/2 downstream of the PI3K signalling pathway and modulate cell proliferation and survival via interactions with DNA methyltransferases (DNMTs), NFκB inhibitor α (NFκBα) and receptor tyrosine kinase-like orphan receptor-1 (ROR1)(219).

Tcl1-overexpression (OE) studies showed roles of TCL1 in development and a slight role in leukocytes. *Tcl1*-KI led to the development of T and B cell leukaemia in mice depending on the promoter of choice. *Lck* promoter led to the development of T-PLL in mice(220) whereas *Tcl1*-tg OE under the V_H-promoter Ig_H-*Eμ*-enhancer led to the generation of a CLL mouse model(221) (Eμ-TCL1 CLL mouse model) which is the most commonly used CLL-mouse model in research.

It has been shown that this mouse model represents a poor prognostic model of CLL. Disease development is associated with increased surface expression of $CD23^+IgM^+CD19^+$ together with increased levels of ZAP-70. There was also an increase in unmutated IgV_H status with increased BCR signalling. Nevertheless, aggressive disease development has shown to take considerable time as disease proliferation becomes visible in the peritoneal cavity at 2 months with visible disease homing ~4 and ~6 months in the spleen and BM respectively. Monoclonal

expansion was evident at ~8 months and was detectable in the blood after 13-18 months alluding to an aggressive disease(222).

Leukemic survival is caused by the interactions in the microenvironment which involves BCR signalling along with other co-interactions between cytokines and CD40L-CD40 signalling(223). The more aggressive CLL phenotype (unmutated IgV_H) is associated with sustained BCR signalling which leads to the survival and proliferation of B cells. Recently Hayakawa *et al.,* showed that early B1 B cells taken from an Eµ-T cell leukaemia 1 (Eµ-TCL1; CLL mouse model), develop into CLL with an upregulation in C-MYC, suggesting that the BCR repertoire within B1 B cells is essential for the generation of CLL(224). Other B cell subpopulations were not able to develop into disease alluding to B1 B cells as the cell of origin in CLL in this mouse model.

1.8.2 PKCαKR model *in vivo*

Protein kinase C (PKC) proteins are serine/threonine kinases which are involved in functions including proliferation, apoptosis, cell differentiation(75). There exist Ca^{2+}-dependent isoforms (α,β,γ), Ca^{2+}-independent isoforms (δ,ε,η,θ), and atypical isoforms (ζ,λ)(225). These kinases modulate B cell functions via well-known signalling pathways such as the PI3K/AKT, NFκB signalling pathways(226,227). PKCs have also shown to play a role in CLL as activation of PKCs in CLL cells leads to protection of the disease from apoptosis due to the induction of differentiation(228). Moreover, it has been shown that the retroviral transduction of a kinase-dead PKCα isoform (PKCαKR), and not the PKCδ or PKCζ isoform, lead to the subversion of B cells into $CD19^+CD23^+CD5^+IgM^{lo}$ CLL-like cells which are refractory to apoptosis(229). This suggests that PKCαKR isoform has this specific characteristic responsible for regulating vital processes involved in CLL. These retrovirally transduced PKCαKR HSPCs led to the generation of a poor-prognostic CLL mouse model. This model exhibited an upregulation of ZAP-70, together with an increase in ERK-MAPK-mTOR signalling and PKCβII expression, resembling a more aggressive disease phenotype(230).

1.8.3 PKCαKR model *in vitro:* OP9 co-culture

Nakagawa *et al.,* have previously shown that the retroviral transduction of HSPCs with PKCαKR leads to the generation of a poor prognostic disease *in vivo*. However, this disease can also be maintained by the co-culture on the OP9 cell line. OP9 cell line is derived from stromal cells from the calvaria of *op/op* mice which lack M-CSF. This cell line is capable of supporting mainly B lineage cells with the generation of myeloid and NK cells lineages early in the co-culture, together with the addition of the respective growth factors(231,232). This cell line was used in co-culture with the PKCαKR retrovirally HSPCs to promote a B cell lineage for the generation of a B-CLL-like disease. Cytokines IL7 and Flt3 have previously been demonstrated to play a vital role in B cell lineage commitment(33). Therefore, these cytokines were supplemented to the co-culture to generate a poor prognostic disease.

1.9 Aims of project

Although the mTOR/AKT signalling pathway has shown to be upregulated in CLL, the exact mechanism of this signalling pathway was not known. Additionally, the individual roles of the mTOR complexes have not been fully determined in normal and malignant CLL-like B cells. Therefore, the aim of my PhD was to:

i) delineate the individual roles of mTORC1 and mTORC2 in normal haemopoiesis utilising specific KO mouse models for *Raptor* (mTORC1) and *Rictor* (mTORC2) *in vivo*.

ii) determine the individual roles of mTORC1 and mTORC2 in leukaemogenesis *in vitro* and *in vivo* via the KO mouse models.

iii) utilise mTOR inhibitors in the presence and absence of current drugs in clinic to assess synergy in reducing CLL *in vivo*.

Chapter 2

Materials and Methods

2 Materials and Methods

Names of companies/suppliers and their address details from where all the reagents were purchased are listed in Table 2.1.

2.1 Mouse models

B6.SJL mice were used as a background for generating the desired KO mouse models using the cre-loxP system. For transplants of the CLL-like disease, NSG and NRG mice were used as host for the disease.

2.1.1 Cre-loxP System

Mice expressing the cre/loxP system with *Raptor* (*Raptor$^{fl/fl}$*) or *Rictor* (*Rictor$^{fl/fl}$*) were obtained from Prof. Michael N. Hall (University of Basel, Switzerland)(233) and maintained at the Beatson Research Unit (BRU; Glasgow, UK). Prof. Tessa L. Holyoake (University of Glasgow, UK) generously provided transgenic mice expressing *Mx1*-cre and *Vav*-cre. The *CD19*-cre transgenic mice were a gift from Dr. Dinis Calado (Francis Crick Institute, London, UK). The *Mx1* and *Vav*-cre mice were maintained at the Beatson Research Unit (BRU) while the *CD19*-cre mice were housed at the Veterinary Research Facility (VRF). We crossed *Mx1*-cre$^{+/-}$, *Vav*-cre$^{+/-}$ or *CD19*-cre$^{+/-}$ transgenic mice with *Rictor$^{fl/fl}$* or *Raptor$^{fl/fl}$* on a background of B6.SJL mice to obtain the desired KO models. The cre-loxP system excises the floxed gene of interest under the expression of cre by homologous recombination. Cre-recombinase expression can be controlled under a promotor to induce a genetic deletion or KO at a specific developmental stage or lineage (Figure 2.1). The *Mx1* promoter is activated upon TLR3 activation(234), by inoculating, for example, the cre^{+}-*Raptor$^{fl/fl}$* mice with 3,4, or 5 doses of 10 mg/kg TLR3 agonist poly(I:C) (GE Healthcare, WI, USA) to induce *Raptor* cKO in the mouse. *Vav* expression is activated at an early HSC stage, therefore the *Vav*-cre model will induce the KO in HSCs at an early stage thus inducing a KO in all haemopoietic lineages(235). Lastly, *CD19* is expressed at the proB cell stage of B lineage development. Thus, *CD19*-cre$^{+/-}$*Raptor$^{fl/fl}$* (*CD19*-cre$^{+/-}$ *Raptor* KO) mice lack *Raptor* only in B cells(206). Excessive cre expression has been demonstrated to be leaky by causing widespread recombination depending on tissue specificity(208). Furthermore, there exist pseudo-loxP sites

in the mouse genome, and when cre is highly expressed, it could cause toxicity due to off-target deletions(208). Therefore, we focused on mice carrying heterozygous (cre$^{+/-}$) and not homozygous (cre$^{+/+}$) mice for phenotyping and experimental models.

For *Vav*-cre *Raptor* mice, time matings were carried out where *Vav*-cre *Raptor*$^{wt/fl}$ were mated with *Vav*-cre *Raptor*$^{wt/fl}$ mice and if/when the female mouse was pregnant, the mouse was sacrificed at E13, E15, or E18. The mouse was dissected to obtain the FL from the litter.

2.1.2 Organ Processing

2.1.2.1 BM processing

The BM was obtained by either flushing or crushing the bones of the mouse. For BM obtained by flushing, BM was cut on either ends of the femur with a scissors and was then flushed using a 1 ml syringe and a needle with phosphate buffer saline (PBS). This was repeated 4-5 times to ensure maximum yield. The supernatant was then filtered through a 45 μM sieve. For BM obtained by crushing: ilium, femur, fibula, tibia, humerus and ulna from both limbs were removed from mice and crushed in 2% FBS in PBS using a pestle and mortar. The cells were filtered through a 45 μM sieve to obtain a single cell suspension. This was centrifuged for 10 min at 300g.

2.1.2.2 Spleen, LN Thymus, blood, FL processing

The spleen, LN, thymus and blood was removed from the transgenic mice. The spleen, thymus, LN and FL were crushed to obtain a single cell suspension and all the cells obtained were filtered through a 70 μm nylon mesh (CellMicroSieves™, Thermo Fisher Scientific, Renfrew, UK). All the cell suspensions (excluding blood and FL) were counted in thymus and LN using a haemocytometer chamber (Hawksley, Lancing, UK) and Trypan Blue (Merck Millipore, Livingston, UK) exclusion method.

2.1.2.3 Lymphocyte enrichment in BM and Spleen

 The cells collected from the BM and spleen were enriched for haemopoietic cells (excluding red blood cells and dead cells) by density centrifugation via a

gradient solution, Lympholyte-Mammal (Cedarlane, Ontario, Canada). Cells were pelleted for 5 min in 3 ml PBS at 325g. Then cell pellets were re-suspended in 3 ml PBS and 1 ml Lympholyte at room temperature (RT) was carefully added using the underlay method and centrifuged for 20 min at 625g at RT. The leukocytes collect at the interface and this layer was carefully isolated using Pasteur pipette. These cells were washed in 10 ml PBS and centrifuged at 500g for 10 min at RT. The cells were washed once more in 5 ml PBS for 5 min at 325g at RT and counted using a haemocytometer.

2.1.3 Transplants

2.1.3.1 Primary Transplants

BM was taken from either *Mx1*-cre *Raptor* mice (without poly(I:C) inoculation), *CD19*-cre *Raptor* mice or B6.SJL WT mice, and was processed by crushing the bones (Section 2.1.2.1), and was RV transduced with either PKCαKR vectors as described below (Section 2.1.6). BM cells were co-cultured with OP9-GFP stromal cells supplemented with IL7 and Flt-3 till day 7-9 (D7-9) and then counted. 5x10^5 cells/100µl cells were transplanted into NSG mice via tail vein injections to establish a CLL-like disease *in vivo*. Disease progression was monitored by sampling the blood of the mice weekly (20 µl/week) and the bloods were analysed for GFP$^+$ CLL-like cells, as described in section 2.3.2, by flow cytometry. Once the health was compromised, these NSG mice were sacrificed and the organs analysed for CLL-like cells.

2.1.3.2 Secondary Transplants

As NSG mice injected with PKCαKR CLL-like cells, retrovirally transduced from B6.SJL WT mice, were sacrificed, the spleens were processed in a sterile hood, and 3x10^5 splenic cells were further transplanted into NSG or NRG mice for secondary transplants.

2.1.3.3 Drug Treatments *in vivo*

After confirmation of CLL-like disease (≥0.4% GFP$^+$CD19$^+$ cells for primary transplants and ≥10% GFP$^+$CD19$^+$ cells for primary transplants in the blood), NSG or NRG mice (CLL-like disease generated from BM of B6.SJL WT mice) were

treated for 2 wk (primary transplants) and 3 wk (secondary transplants) with individual inhibitors, or combination or vehicle control and then sacrificed. BM, spleen, LN and blood were collected for analysis (as described in section 2.1.2). AZD2014 (a gift from AstraZeneca, Macclesfield, UK) was formulated at 3 mg/mL in 20% Captisol (Ligand Pharmaceuticals, Inc., La Jolla, CA) and administered daily at 15 mg/kg via oral gavage (OG). Ibrutinib (LC Laboratories, MA, USA) was prepared at a concentration of 2.4 mg/ml in 0.5% methyl cellulose (Sigma-Aldrich, Irvine, UK) and administered at a dose of 12 mg/kg. For vehicle controls, captisol and methylcellulose alone or in combination were administered. Rapamycin (rapa) was delivered once daily by intraperitoneal (ip) injection at a dose of 4 mg/kg dissolved in Tween-80 5.2% / PEG-400 5.2% (v/v).

2.1.4 OP9-GFP cell line

OP9 was derived from the new born calvaria of C57BL/6XC3H F2-*op/op* mice which lack the production of M-CSF due to a genetic mutation in the M-CSF gene(231). OP9 cell line supports the differentiation of HSCs into B cells when culture is supplemented with IL7 and β-mercaptoethanol (βME)(236). OP9 cell line was retrovirally-transduced with GFP and grown in culture in complete media: alpha-MEM (Gibco, Thermo Fisher Scientific) media supplemented with 10 mM HEPES, 1 mM sodium pyruvate, 10 µg/ml gentamycin, 50 µM βME, 100 µg/ml streptomycin, 100 U/ml penicillin, 2 mM L-glutamine, 20% foetal bovine serum (FBS). The cells were kept in culture at 37°C in a humidified incubator with 5% (v/v) CO_2 and passaged every 2 – 3 days.

2.1.5 Retroviral packaging lines

The cell line derived from mouse embryonic fibroblast cells, NIH-3T3 cells were transfected with *gag, pol* and *env* genes to produce GP+E.86 cells(237). These cells were retrovirally-transduced to express MIEV (empty vector control; GP+E.86-MIEV), or PKCαKR (GP+E.86-PKCKR)(238). These were cultured at 37°C in a humidified incubator with 5% (v/v) CO_2 in complete DMEM media containing 10 mM HEPES, 1 mM sodium pyruvate, 10 µg/ml gentamycin, 50 µM βME, 100 µg/ml streptomycin, 100 U/ml penicillin, 2 mM L-glutamine, 10% FBS.

2.1.6 Retroviral transduction

2.1.6.1 Mitomycin C preparation and treatment

Mitomycin C (2mg/ampule) (Sigma-Aldrich, Irvine) was prepared to a stock concentration of 200 µg/ml (20x) in serum free DMEM and was stored in 4°C for up to 6 wk in the dark.

GP+E.86-MIEV and GP+E.86-PKCαKR packaging lines were cultured in T75 flasks in DMEM complete media and when cells reached 70% confluence, they were treated with 10 µg/ml mitomycin C in DMEM complete media for 3 hr. Thereafter, mitomycin C was removed and 10 ml PBS was added to each flask. This was repeated 3-4 times until no residual media was visible and was replaced by complete DMEM media for recovery overnight in culture at 37°C in a humidified incubator with 5% (v/v) CO_2.

Three hours prior to retroviral transduction, mitomycin C treated GP+E.86-MIEV and GP+E.86-PKCαKR cells were trypsinised and plated in individual 6 well plates at 70-80% confluence. This enabled the GP+E.86 cells to adhere to the plates.

2.1.6.2 CD117 enrichment using magnetic assorted cell sorting (MACS)

BM was obtained by crushing as mentioned in section 2.1.2.1 and was enriched for lymphocytes as described in section 2.1.2.3. Post lymphocyte enrichment from BM, cell pellets were re-suspended in 80 µl MACS buffer (2% FBS, 2 mM EDTA in PBS) and 20 µl CD117 MicroBeads (MACS Miltenyi Biotec, Surrey, UK) were added and incubated for 15 min at 4°C in the dark. Post incubation, 2 ml MACS buffer was added to each sample and was centrifuged for 10 min at 500g.

MS columns (MACS Miltenyi Biotec) were used for CD117 enrichment as described in the manufacturer's protocol. Briefly, the plunger was removed, and the columns were placed on a MS column-holding magnet. The columns were first activated using 500 µl MACS buffer. Subsequently, each sample was re-suspended in 500 µl MACS buffer and pipetted onto the top of the MS columns. Once all the flow-through was collected, 500 µl MACS buffer was added onto each column to wash the column. This was repeated 3 times. Subsequently, the MS column was removed from the magnet and placed onto a 15 ml falcon tube. 1

ml MACS buffer was added onto the column and the plunger was immediately inserted into the column to elute CD117$^+$ cells within the column. The plunger was then removed and an additional 500 µl buffer was added and then plunged. The CD117$^+$-purified cells were then centrifuged at 500g for 10 min.

2.1.6.3 Retroviral transduction

HSC-enriched cell pellets of individual samples were re-suspended in 4 ml complete DMEM media containing IL7 and Flt3 (10 ng/ml of each; Peprotech, London, UK) and hexadimethrine bromide (Polybrene) (4 µg/ml) (Sigma-Aldrich).

The supernatants of GP+E.86-MIEV and GP+E.86-PKCαKR cells, when adhered to 6 well plates, were removed by pipetting and 2 ml of each sample of HSCs was added onto individual MIEV and PKCαKR wells. These were then cultured overnight at 37°C in a humidified incubator with 5% (v/v) CO$_2$ (Figure 2.2).

2.1.6.4 Post transduction and growth of MIEV and PKCαKR transfected cells

The retrovirally transduced HSC-enriched cells were removed from the plates and centrifuged at 400g for 10 min. The pellets were then re-suspended in complete alpha-MEM media supplemented with IL7 and Flt3 (10ng/ml of each) and plated onto OP9-GFP cells at 20% confluence. The day the BM samples were co-cultured with OP9-GFP stromal cells is D1 of culture. These cells were re-plated with fresh OP9-GFP cells every 3-4 days, and Flt3 was removed after D7 of culture.

2.1.7 *In vitro* KO induction

The *Mx1*-cre-*Raptor*/*Rictor$^{fl/fl}$* models were used to induce KO *in vitro* to assess disease maintenance. RV-transduced BM cells were cultured *in vitro* until D10 for *Raptor$^{fl/fl}$* or D20 for *Rictor$^{fl/fl}$*. Wells containing between 0.5-1x10^6 cells were treated with 50 units (U)/well interferon ß (IFNß) (Pbl Assay Science, NJ, USA) for 2 or 3 days, or 200 U/well IFNß for 24 hr, and harvested 4 days post treatment.

2.2 K562 cell lines

K562, a chronic myeloid leukaemia (CML) cell line which is derived from a CML patient in blast crisis by pleural effusion[239]. This cell line was used to induce erythroid differentiation. Differentiation was induced by hemin[240] treatment or by galactose supplementation[241] in media.

2.2.1 Hemin treatment induced erythroid differentiation

$2x10^5$ K562 cells were cultured in either K562 media comprising RPMI-1640 media, no glutamine, supplemented with 10% FBS, 50 U/ml penicillin, 50 µg/ml streptomycin and 2 mM L-Glutamine, in a 6 well plate. The cells were treated with 50 µM Hemin (or 20 mM NaOH as control) to the culture. Erythroid differentiation was confirmed by pellet colour (red).

2.2.2 Galactose supplemented erythroid differentiation

$2x10^5$ K562 cells were cultured till D7 in either K562 media, or with K562 media supplemented with galactose (Gal-media) comprising RPMI-1640, no glucose, supplemented with 10% FBS, 50 U/ml penicillin, 50 µg/ml streptomycin, 2 mM L-Glutamine and 11 mM galactose (Figure 2.3A).

2.2.3 Drug treatment

$2x10^5$ K562 cells were cultured with either K562 media or Gal-media to induce erythroid differentiation. Each was also treated with either DMSO, 10 nM rapamycin (LC Laboratories) or 100 nM AZD8055 (Stratech Scientific Ltd., Suffolk, UK). The cells were cultured till D7 and analysed by either qPCR or by flow cytometry (Figure 2.3B, C).

2.3 Flow cytometry

Data was acquired using the fluorescent assorted cell sorting (FACS) Canto II using the BD FACS DIVA software and analysed using the FlowJo software (Oregon, USA).

2.3.1 Assessing K562 differentiation

5×10^5 K562 cells were stained with 3 µl GlycophorinA (GlyA) (BD Biosciences, Clone: GAR2) and 10 µl CD71 (Miltenyi Biotec, Clone: AC102) and incubated on ice in the dark for 25-30 minutes. The cells were then washed twice with 1 ml PBS at 300g for 5 min and analysed.

2.3.2 CLL and lineage phenotyping

Single cell suspensions obtained by *in vivo* or *in vitro* experiments (sections 2.1.2, 2.1.7) were stained with cocktails of antibodies containing cell surface markers for either CLL disease comprising CD23, CD5, CD19, CD45, CD11b surface markers, lineage detection with CD19, CD4, CD8, CD11b, NK1.1, Gr1 as surface markers, early B and myeloid markers (CD45, B220, CD19, Lineage (Table 2.3), sca-1, CD117, CD16/32, CD34) (Figure 2.4), or late B cell markers (CD19, CD23, CD1d, IgD, IgM, CD21, AA4.1) (Figure 2.5) (Table 2.2). 5×10^5 cells obtained from cell suspensions were initially stained with FcγRII/III (CD16/32) antibody (except for the early B and myeloid staining cocktail) to block any non-specific staining for 2 min. Proceeding this, a cocktail of antibodies was added to the cells and incubated on ice, in dark for 25-30 min. The cells were washed once with 2 ml PBS, resuspended in 100µl and analysed using the flow cytometer (Canto II, BD Biosciences, Berkshire). For the early B and myeloid staining, cells were then stained with V450 streptavidin (SA, BD Biosciences) for 20 min in the dark on ice to bind the lineage biotin antibody mix. Cells were washed in 2 ml PBS, resuspended in 100µl and analysed.

2.3.3 Fixation and permeabilization

After cell culture/treatment or single cell suspensions obtained from tissues, $0.5\text{-}1 \times 10^6$ cells were harvested and washed twice in PBS by centrifugation at 325g for 5 min. Then 1 ml 80% ethanol was added dropwise to each sample while vortexing to minimise cell stress. Of note, 80% ethanol was added in order to make the final concentration of ethanol 70% with the residual supernatant in each sample after centrifugation. The cells were then stored in -20ºC overnight or for up to 2-3 wk.

2.3.4 Assessing intracellular markers

After fixing and permeabilization (section 2.3.3), each sample was stained with the recommended amount/Test (listed in Table 2.4) of either isotype control or phospho-AKT, phospho-4EBP1, phospho-S6 or Ki67 and stained for 30 min on ice in the dark. The samples were then washed with 2 ml PBS and centrifuged for 5 min at 325g. Cells were then analysed using flow cytometry.

2.3.5 Assessment of Apoptosis

5×10^5 cells were counted and were washed with 1x Hank's Balanced Salt Solution (HBSS) (Thermo Fisher Scientific) at 300g for 5 min at RT. 100 µl HBSS containing 2.5 µl AnnexinV and 2.5 µl 7AAD (BD Biosciences) was added into each ample and was incubated for 10 min at RT in the dark (Table 2.5). The samples were then analysed using the flow cytometer (Figure 2.6).

2.3.6 Assessment of Cell Cycle

After fixing and permeabilization (section 2.3.3), cells were pelleted by centrifugation at 350g for 5 min and were washed twice in PBS by centrifugation at 350g for 5 min to remove any excess ethanol. 350-500µl propidium iodide (PI)/RNAase Staining Buffer (BD Biosciences) was added to each sample and was incubated at RT in the dark for 15 min. The samples were then analysed using the flow cytometer (Figure 2.7).

2.3.7 Assessment of proliferation

A 5 mM stock concentration was prepared by adding 20 µl DMSO (component B) to one vial of CellTrace™ Violet reagent (Component A) and mixing (Invitrogen, Paisley, UK). Then, 1 µL 5 mM CellTrace™ Violet stock solution in DMSO was added to each mL of 1×10^6 cell suspension in PBS/2% FBS for a final working concentration of 5 µM. The cells were incubated for 20 min at 37˚C, protected from light. Five times the original staining volume of culture medium (containing at least 1% protein) was added to the cells and incubated for 5 min at 37˚C in the dark, to remove any free dye remaining in the solution. The cells were pelleted by centrifugation and were re-suspended in pre-warmed complete

medium and kept in culture for at least 20 min before analysis (d0 timepoint) to allow the CellTrace™ Violet reagent to undergo acetate hydrolysis.

300 μL of each sample was then transferred into FACS tubes and analysed with flow cytometry, where 10,000 events were collected on the machine for 3 consecutive days (every 24 hr) to assess proliferation levels (Figure 2.8).

2.4 Colony Forming Cell (CFC) Assay

MethoCult™ (Stem Cell, Cambridge, UK) was thawed and frozen at -20℃ in 4 ml aliquots. When needed, MethoCult was thawed at RT. Single cell suspensions of 1×10^5 HSC-enriched BM cells (Section 2.1.2.1) /100μl IMDM containing 20% FBS were added per ml of MethoCult into the falcon tube containing 4 ml of MethoCult aliquot. Tubes were then vortexed for 3-4 sec to homogenise the mixture. To set up colony formation units (CFUs), a 5 ml syringe attached to a 16-gauge blunt-end needle was used. Most of the MethoCult was taken up in the syringe, and the plunger was gently depressed completely (to remove air bubbles). This was repeated 3 times in 5 min intervals. More than 3.3 ml of MethoCult media (from a total of 4ml) was taken up in the syringe and 1.1 ml was gently expelled into a 35mm dish in a spiral motion. This was repeated twice to make three technical replicates. These dishes were rotated to evenly spread the solution across the total surface area. 3-6 dishes were kept in a 150mm petri dish along with 2 dishes (without a lid) filled with 3-5 ml sterile deionised water (dH$_2$O). The lid of the 150mm petri dish was added on top to maintain humidity and was incubated at 37°C, 5% CO$_2$ and ≥95% humidity till D7-10. Colonies were counted after D7 (Figure 2.9). Colonies included: CFU-GEMM (colony formation unit-granulocyte-erythroid-megakaryocyte-macrophage), CFU-GM (colony forming unit-granulocyte macrophage), CFU-G (colony forming unit-granulocyte), CFU-M (colony forming unit-macrophage), CFU-E (colony forming unit-erythroid), BFU-E (burst forming unit-erythroid).

2.5 Migration Assay

2.5.1 Cell Starvation

Between 2-5x10^5 cells/100 μl was prepared where each sample was counted and cultured for 2 hr at 37℃ in a 48 well plate in 250 μl in starvation media (DMEM

containing 0.5% bovine serum albumin (BSA), 10 mM HEPES, 1 mM sodium pyruvate, 10 µg/ml gentamycin, 50 µM ßME, 100 µg/ml streptomycin, 100 U/ml penicillin, 2 mM L-glutamine).

2.5.2 SDF-1 mediated Migration Set-up

During the starvation step, 150 ng/ml SDF-1 (Peprotech) was added to the starvation media to make up the migration media. Transwell® permeable support chambers (Corning Inc, ME, USA) were set up such that the bottom of each well contained 600 µl of migration media and 100 µl of the cells from the starvation step was carefully pipetted onto the chamber in duplicate. For the negative and positive controls, starvation media was used instead of the migration media where starved cells were either pipetted onto the chamber or directly into the bottom respectively. Cells were cultured at 37°C for 4 hr.

To assess migration after 4 hr, the chambers were removed from all wells, and 150 µl media was pipetted from every well into 3 FACS tubes. The cells were then acquired in the flow cytometer on low speed for exactly 30 sec. The live cells counted were then assessed using FlowJo software.

2.6 RNA extraction

Haemopoietic enriched cells removed from BM of *Vav*-cre *Rictor*$^{fl/fl}$ mice were retrovirally transduced with either MIEV or PKCαKR (section 2.1.6). These cells were co-cultured with OP9-GFP cells till D21 and were harvested for messenger RNA (mRNA) extraction. RNA was extracted from cells using the RNA mini kit columns (Qiagen, Manchester, UK) using the manufacturer's protocol and RNA (PolyA selection) was eluted in RNA-ase free H$_2$0.

2.7 cDNA Synthesis:

2.7.1 cDNA synthesis - RT-PCR

Up to 1 µg RNA was used per 20 µl reverse transcription reaction using the First Strand cDNA Synthesis Kit for real time-polymerase chain reaction (RT-PCR) (Roche, West Sussex, UK). Each sample was diluted in 1x Tris-EDTA (TE) buffer.

2 µl cDNA was used per 10 µl PCR reaction containing 2x PowerUp™ SYBR® Green Master Mix (Thermo Fisher Scientific) and 300 nM of forward and reverse primer for each gene (listed in Table 2.6). All reactions were performed in technical triplicates and at least three biological replicates using the 7900HT Fast Real-Time PCR system (Applied Biosystems, Warrington, UK) programmed to complete 40 cycles as follows: 50°C for 2 min, 95°C for 10 min, followed by 40 cycles of 95°C for 15 sec, and 60°C for 1 min. After normalization to the endogenous control gene, levels of gene mRNA expression in each sample were determined by the ΔΔCT method of relative quantification(242). TATA-Box binding protein (TBP) was used as the reference gene unless otherwise stated.

2.7.2 One-step cDNA synthesis:

2.7.2.1 Sample, master mix and primer mix preparation:

Retrovirally transduced cells (MIEV or PKCαKR) were stained with anti-CD45 antibody (Table 2.2) on ice for 30 min in the dark. Samples were then washed once with 2 ml PBS for 5 min at 300g and resuspended in 500µl PBS. From each sample, 300 cells GFP$^+$CD45$^+$ cells were sorted into the PCR tubes containing the master mix.

For the master mix, a 2x reaction mix of 5 µl was added to each PCR tube per sample containing: Cells direct 2x reaction (2.8 µl), 0.2x Primer mix (1.4 µl), RNAase out (0.056 µl), Superscript III RT/Platinum Taq Mix (0.112 µl), TE Buffer (0.672 µl) (part of SuperScript™ III Platinum™ One-Step qRT-PCR Kit, Invitrogen).

For the primer mix, all primers of interest were selected (Table 2.6) and each forward and reverse primer were added to a master mix with a final concentration of 0.125µM for each primer in a total volume of 200µl (made up with TE buffer).

2.7.2.2 FACS and PCR:

After sorting, the tubes were vortexed and centrifuged at 500g for 30 sec. The samples were then run on a PCR with the following conditions: 50ºC for 15 min, 95ºC for 2 min followed by 20 cycles of 95ºC for 15 sec and 65ºC for 4 min. After

these cycles, the samples were brought to a hold at 4ºC. After the completion of the PCR, the samples were diluted 10x with TE buffer (45 µl).

Quantitative PCR was performed to assess gene expression of genes included in the primer mix (Table 2.6).

2.8 DNA extraction and Gel electrophoresis

DNA was extracted for samples using the Qiagen DNA blood/tissue extraction kit and following the manufacturer's protocol (Qiagen). The DNA was quantified using a spectrophotometer (Nanodrop ND1000 Spectrophotometer; Labtech International Ltd, East Sussex, UK).

240 ng/ 25 µl of DNA was amplified in a PCR reaction with a hot start of 95ºC for 2 min followed by 35 cycles of: 30 sec denaturation at 95°C, 30 sec annealing at 59°C, 1 min extension at 72°C; and a final extension at 72°C for 5 min. The primers used are listed in Table 2.6. Products were separated by 1% agarose gel electrophoresis in 1x Tris-acetate-EDTA (TAE) buffer and visualised by the addition of SYBR Safe DNA (Invitrogen) in the agarose gel (1:10,000). Gel electrophoresis was performed at 100 volts (V) for 45 min and the gel was imaged using the Odyssey® Fc Imaging system (LI-COR Biosciences, Germany).

2.9 Western blotting

Single cell suspensions from organs were counted and $1x10^7$ cells were pelleted and were re-suspended in 100 µl lysis buffer (20 mM Tris pH 7.4, 2mM EDTA, 1% Triton, 1mM DTT) containing protease inhibitor cocktail (Roche) (Table 2.7) and phosphatase inhibitor cocktail (Roche) on ice for 30 min. Lysates were then spun at 21900g for 10 min at 4ºC and supernatant was collected. Quantification of protein concentration in the lysates was calculated using the Bradford assay(243). BSA standards with concentrations of 0, 2.5, 5, 7.5, 10, 15, 20 µg/ml were prepared in 1 ml Bradford dye in 1.5 ml eppendorfs. Following this, 1 µl of each unknown sample was added to 1 ml Bradford dye in 1.5 ml eppendorfs. These were then vortexed and then 100 µl from each standard and unknown sample was loaded on a flat bottomed 96 well plate in duplicate. Absorbance was read at 562 nM on a Spectramax M5 plate reader (MDS Analytical

Technologies, Berkshire, UK) and analysed with SoftMax Pro 5.2 software (MDS Analytical Technologies).

Equal amounts of protein (typically 10 μg/10 μl) were incubated with 4x NuPage LDS Sample buffer and 10x DTT used as a reducing agent at 70°C for 10 min. Proteins were separated by sodium dodecyl sulfate polyacrylamide gel electrophoresis (SDS-PAGE) in a 4-12% NuPAGE Novex BisTris precast gel (Invitrogen) (unless otherwise stated), using 1x solution of 20x 50 mM 3-(N-morpholino) propane sulfonic acid (MOPS) SDS Running Buffer (50 mM TrisBase,3.5 mM SDS and 1.0 mM EDTA (pH 7.7)) supplemented with NuPAGE antioxidant (Invitrogen). Samples were run alongside HyperPAGE pre-stained protein marker (Bioline, TN, USA) at 80 V for 45 min and then at 180 V for 1 hr. Gels were then transferred onto Immun-Blot polyvinyliden difluoride (PVDF) membranes (Bio-Rad Laboratories, Hertfordshire, UK) using a 1x solution of 20x NuPAGE transfer buffer (25 mM Bicine, 25 mM Bis-Tris, 1.0 mM EDTA, 50 μM Chlorobutanol (pH 7.2)) supplemented with 20% (v/v) methanol (Merck Millipore). Briefly, the PVDF membrane was soaked in 100% methanol for 1 min, rinsed in distilled water (dH$_2$0) and equilibrated in transfer buffer prior to assembly of gel/membrane sandwiches using 1.0 mm gel blotting paper (Whatman plc, Kent, UK) and sponges in an XCell IITM Blot Module (Invitrogen, Paisley). Transfer was performed at 30 V for 1 hr.

Blots were washed with 1x Tris-buffer saline (TBS) (20 mM Tris HCl pH 7.4, 150 mM NaCl), blocked in TBS containing 5% milk for 1 hr at RT, and incubated with primary antibody overnight at 4°C (Table 2.8). Thereafter, the blots were washed 2 times with TBS and 2 times with TBST (TBS+ 0.01% Tween 20) for 5-10 mins each and incubated with horseradish-peroxidase (HRP)-labelled secondary antibodies for 1 hr at RT. After 2 washes with TBST and 2 washed with TBS for 5-10 mins each, the blots were developed with Immobilon Forte Western HRP substrate (Merck Millipore) for 1 min and imaged with the Odyssey® Fc Imaging system (LI-COR Biosciences). Western blot antibodies were purchased from Cell Signalling Technology (Herts, UK) unless otherwise stated.

2.10 Immunohistochemistry

Immunohistochemistry (IHC) was performed by the Beatson Institute of Cancer Research. Organs were removed from the mouse and drop-fixed in 5ml 10% neutral buffered formalin (NBF) (Cellpath, Newtown, UK) prior to tissue infiltration, a process whereby the tissue is suspended in a series of graded ethanol baths (70-100% ethanol) to displace water in the tissue. Proceeding this, the tissue is paraffin-embedded onto a paraffin wax block. Once the wax has solidified and set (takes 1 hr), the block is then sectioned into 5 µM sections and placed onto clean glass slides and left for 20 min in a 65°C oven to just melt the paraffin into the glass slide. Slides are left overnight at RT to cool. To assess the expression levels of various proteins (Table 2.9), sectioned slides are immersed in 100% xylene for 5 min to remove paraffin and subsequently placed in 100% ethanol baths twice, 70% ethanol, and dH_2O bath for 1 min each to rehydrate the tissue.

2.10.1 Antigen retrieval:

Slides were kept in washing containers with 1x Citrate retrieval buffer (Thermo Fisher Scientific) and were kept in a water bath at 98°C for 30 min. Containers were then removed from the water bath and allowed to cool at RT. Slides were washed in dH_2O for 5 min.

Endogenous peroxidase quenching and blocking: slides were treated with 3% H_2O_2 solution for 10 min (Agilent Dako) followed by a 5 min wash with TBST. Sections were blocked with 5% normal goat serum in TBST for 30 min at RT.

2.10.2 Antibody staining:

$pAKT^{S473}$, $p4EBP1^{T37/T46}$, $pS6^{S235/S236}$ or Ki67 antibody was added to the sections in 5% NGS O/N at 4°C and left overnight (Primary Antibody diluent, Agilent Dako) (Table 2.9). The sections were then washed twice in TBST for 5 min. Biotinylated anti-rabbit secondary antibody (Table 2.9) was added to the sections for 30 min at RT (Vector Labs, Peterborough, UK). Sections were then washed twice in TBST for 5 min.

NB: Haematoxylin and eosin (H&E) staining was performed by the IHC department at the Beatson (Colin Nixon). This was done via standard procedures.

2.10.3 Amplification and Visualisation:

Sections were then incubated with pre-mixed avidin/biotin complex (ABC) (HRP tagged) (Vector ABC Kit, Vector Labs) for 30 min at RT followed by 2 washes in TBST for 5 min. For visualisation, sections were treated with 3,3'-Diaminobenzidine tetrahydrochloride (DAB), which forms a brown precipitate on oxidation by HRP, for 10 min followed by a wash in dH_2O for 1 min.

2.10.4 Counterstaining and dehydration:

The slides were counterstained by staining with haematoxylin Z for 7 min for nucleus visualisation, followed by dH_2O wash for 1 min. The slides were then dehydrated by placing the slides in 70% ethanol for 1 min twice and then in 100% ethanol for 5 min. The slide was then treated with one drop of distyrene, polystyrene, xylene (DPX) solution to mount and preserve the staining and left to dry for 5 min. The slides were visualised under an inverted microscope at x4 magnification (Olympus Life Sciences, Japan).

2.11 Statistics

Statistical analyses were carried out between the data sets by using GraphPad Prism 6 Software (San Diego, California, USA). The analysis carried out was, either paired or unpaired, student t-test or one-way ANOVA. Data is represented as mean±standard error of mean (SEM) or as mean±standard deviation (SD) where $p \geq 0.05$, as stated in the figure legends.

2.12 Tables and Figures

Supplier	Supplier Address
Applied Biosystems	Part of Thermo Fisher Sceintific Lingley House, 120 Birchwood Boulevard, Warrington, WA3 7QH, UK
Agilent Dako	5301 Stevens Creek Blvd, Santa Clara, CA 95051, United States
AstraZeneca	Charter Way, Macclesfield, SK10 2NA
BD Biosciences	1030 Eskdale Road, Winnersh Triangle Wokingham, Berkshire, RG41 5TS
Bioline, Meridian life sciences, Inc.	Meridian Life Science, Inc., 5171 Wilfong Rd., Memphis, TN 38134
Bio-Rad Laboratories Ltd.	Bio-Rad Laboratories Ltd. The Junction, Station Road, Watford, Hertfordshire, WD17 1ET
eBioScience	Part of Thermo Fisher Scientific 3 Fountain Dr, Inchinnan, Renfrew PA4 9RF, UK
Clarivate Analytics	1500 Spring Garden, Philadelphia, PA 19130, United States
Cedarlane	4410 Paletta Court, Burlington, Ontario L7L 5R2, Canada
Cellpath	Mochdre Enterprise Park, Mochdre, Newtown SY16 4LE
Cell Signaling Technology c/o New England Biolabs	75-77 Knowl Piece, Wilbury Way, Hitchin, Herts SG4 0TY, UK
Corning Incorporated	2 Alfred Road, Kennebunk, ME 04043 USA
GE Healthcare	3000 N Grandview Blvd Waukesha, WI 53188 United States
Greiner Bio-One Ltd.	Unit 5, Stroudwater Business Park, Gloucestershire, GL103SX, UK
Hawksley	25 Marlborough Rd, Lancing BN15 8TN
Illumina Inc.	5200 Illumina Way, San Diego, CA 92122, United States
Invitrogen, Paisley, UK Ltd.	Part of Thermo Fisher Scientific 3 Fountain Dr, Inchinnan, Renfrew PA4 9RF, UK
LC Laboratories	165 New Boston Street, Woburn, MA 01801, USA

LI-COR Biosciences	Siemensstraße 25, 61352 Bad Homburg vor der Höhe, Germany
Merck Millipore	Fleming Rd, Livingston EH54 7BN, UK
Miltenyi Biotech	Almac House, Church Lane, Bisley, Surrey, GU24 9DR, UK
Olympus Life Sciences	Shinjuku Monolith, 2-3-1 Nishi-Shinjuku, Shinjuku-ku, Tokyo 163-0914, Japan
Pbl Assay Science	131 Ethel Road West #6, Piscataway Township, NJ 08854, USA
PeproTech EC Ltd	PeproTech House, 29 Margravine Road, London, W6 8LL, UK
Polyomics, University of Glasgow	Switchback Road, Bearsden, Glasgow, G61 1BD, UK
Qiagen	Skelton House, Lloyd St N, Manchester M15 6SH, UK
R&D Systems	R&D Systems Europe Ltd., 19 Barton Lane, Abingdon Science Park, Abingdon, OX14 3NB, UK
Sigma-Aldrich Co Ltd	Second Ave, Heatherhouse Industrial Estate, Irvine, KA12 8NB
Stem Cell Technologies	Building 7100, Cambridge Research Park, Beach Drive, Waterbeach, Cambridge CB25 9TL
Stratech Scientific Ltd.	Cambridge House, St Thomas' Pl, Ely CB7 4EX
Thermo Fisher Scientific	3 Fountain Dr, Inchinnan, Renfrew PA4 9RF
Vector Labs	Bakewell Rd, Peterborough PE2 6XS

Table 2.1: List of companies and their addresses from where reagents and materials were purchased.

Name	Reactive Species	Clone	Format	Manufacturer	Dilution
CD19	Mouse	1D3	APC-Cy7	BDBiosciences	1:200
CD11b	Mouse	M1/7O	Pacific Blue	BDBiosciences	1:200
CD45	Mouse	30-F11	PerCP	BDBiosciences	1:200
CD5	Mouse	53-7.3	APC	BDBiosciences	1:200
CD23	Mouse	B3B4	PeCy7	BioLegend	1:200
Gr1	Mouse	RB6-8C5	PerCP-Cy5.5	eBiosciences	1:200
CD4	Mouse	RM4-5	PE	BDBiosciences	1:200
CD8a	Mouse	53-6.7	APC	BDBiosciences	1:200
NK1.1	Mouse	PK136	PECy7	BDBiosciences	1:200
Ter119	Mouse	TER-119	FITC	BioLegend	1:200
CD34	Mouse	RAM34	FITC	BDBiosciences	1:200
B220	Mouse	RA36B2	PE	BDBiosciences	1:400
CD117	Mouse	2B8	APC	BDBiosciences	1:200
Sca-1	Mouse	D7	Pe-Cy7	BDBiosciences	1:200
CD16/32	Mouse	2.4G2	BV510	BDBiosciences	1:200
Streptavidin			V450	BDBiosciences	1:200
IgD	Mouse	11-26c.2a	BV510	BioLegend	1:200
CD1d	Mouse	1B1	PerCP-Cy5.5	BioLegend	1:200
AA4.1	Mouse	AA4.1	PE	BDBiosciences	1:200
IgM	Mouse	II/41	APC	BDBiosciences	1:200
CD21	Mouse	7E9	Pacific Blue	BioLegend	1:200

Table 2.2: Antibodies used for flow cytometry. Master mixes (MM) made for phenotypic identification.

CLL disease MM: CD23, CD5, CD19, CD45, CD11b; Lineage MM: CD19, CD4, CD8a, CD11b, NK1.1, Gr1, Ter119; Early B and myeloid MM: CD45, B220, CD19, Lineage

Table 2.3), sca-1, CD117, CD16/32, CD34; Late B cell MM: CD19, CD23, CD1d, IgD, IgM, CD21, AA4.1.

Name	Reactive Species	Clone	Format	Manufacturer	Dilution
CD4	Mouse	GK1.5	Biotin	BDBiosciences	1:200
CD8a	Mouse	53-6.7	Biotin	BDBiosciences	1:200
CD3e	Mouse	145-2C11	Biotin	BDBiosciences	1:200
NK1.1	Mouse	PK136	Biotin	BDBiosciences	1:200
TCR	Mouse	H57-597	Biotin	BDBiosciences	1:200
Ter119	Mouse	Ter119	Biotin	BDBiosciences	1:200

Table 2.3: Biotinylated antibodies used to delineate early B and myeloid developmental stages and lineages for flow cytometry.

Name	Reactive Species	Clone	Format	Dilution
anti-4EBP1 (pT36/pT45)	Mouse	M31-16	PE	15μl/Test
anti-S6 (pS235/pS236)	Mouse	N7-548	V450	3μl/Test
anti-AKT (pS473)	Mouse, Human	M89-61	Alexa Fluor® 647	3μl/Test
anti-Ki67	Mouse, Human	B56	PE-Cy™7	3μl/Test
κ Isotype Control	Mouse	MOPC-21	V450	3μl/Test
IgG1 κ Isotype Control	Mouse	MOPC-21	Alexa Fluor® 647	3μl/Test

Table 2.4: List of antibodies used for phospho-flow cytometry. All antibodies were purchased from BD Biosciences, unless stated otherwise.

Name	Format	Manufacturer	Dilution
AnnexinV	APC	BDBiosciences	2.5µl/Test
7-AAD		BDBiosciences	2.5µl/Test

Table 2.5: Antibodies used for viability assays on the flow cytometer.

Gene	Forward	Reverse Complement	Species
Actb	ctcctcctga gcgcaagtac	gccatgccaat gttgtctct	Mouse
Bcl2	a tgactgagta cctgaaccg	tcaaacagaggtcgcatgct	Mouse
Bid	gccagattctg aaagtcagg	gctagctgtc tcaccagtgt	Mouse
Ccnd1	gtg ccacagatgt gaagttc	gt cacacttgat gactctgg	Mouse
Ccnd2	caagatcacc cacactgatg	gtt atgctgctct tgacgga	Mouse
Ccnd3	atg cggaagatgc tggcata	gaagct gcaattgcgc cttt	Mouse
Cdkn1a	cggtggaactttgacttcgt	agagtgcaagacagcgacaa	Mouse
Cdkn1b	gata cgagtggcag gaggtg	tctga cgagtcaggc atttg	Mouse
Cebpa	aaga acagcaacga gtaccg	ttctgtt gcgtctccac gtt	Mouse
Ebf1	tac agaaggtcat tcctcgg	atcccatacagggcttc aac	Mouse
Gata1	atgatt gtcagcaaac gggc	aggcattgcataccgga tct	Mouse
Gata2	gacgacaacc accaccttat	ggt cagtggcctg ttaacat	Mouse
Gusb	ta agacgctgat cacccaca	cagataacatccacgtacg g	Mouse
Hba-a1	aacttcaag ctcctgagcca	tgctca agaggcaaggaat	Mouse
Klf1	ctaagagg caggcggcacat	ctgagcgagcgaacctcc	Mouse
Klf2	ccaagagc tcgcacctaaag	gtggcactgaaa gggtctgt	Mouse
Pax5	acagga catggaggag tgaa	tgacaccttg atgggcaagt	Mouse
Prkcb	catcgacaga gaggttctca	g gatcagggat cagtttcag	Mouse
Pu.1	cagcgatgga gaaagccata	ctctgtgaagtggttctcag	Mouse
Rptor	atggtagcaggcacactcttcatg	gctaaacattcagtccctaatc	Mouse
Rptor-Del		ctcagagaactgcagtgctgaagg	Mouse
Rictor	ttattaact gtgtgtgggttg	cgtcttagt gttgctgtctag	Mouse
Rictor-Del		cagattcaagca tgtcctaagc	Mouse
Tbp	gtacccttcaccaatgact c	cagccaagattcacg gtaga	Mouse
HBB	gcaaggtga acgtgg atgaa	agcact ttcttg ccatgagc	Human
GATA1	tattcc tctccc aagcttcg	catctt gtgata gaggcc gca	Human
GATA2	gacgacaacc accaccttat	ggt cagtggcctg ttaacat	Human
RNF20	ggtgtc tcttca acggag gaa	tagtgaggc atcatc agtggc	Human

Table 2.6: List of primers used for PCR reactions.
The full sequence for each gene was obtained from PubMed website. Each primer was designed to have close to 10 C=G and 10 A=T bonds. The length between the forward and reverse primer is between 150-300 base pairs (bp). *Rptor*-Del and *Rictor*-Del are reverse primers designed to complement the gene of interest (*Raptor* and *Rictor* respectively) between the two loxP sites.

Inhibitor
Aprotinin
Bestatin
Calpain Inhibitor I
Calpain Inhibitor II
Chymostatin
E-64
Leupeptin
α_2-Macroglobulin
Pefabloc SC
Pepstatin
PMSF
TLCK-HCl
Trypsin Inhibitor (chicken, egg white)
Trypsin Inhibitor (soybean)

Table 2.7: List of protease inhibitors in the cOmplete mini, EDTA-free protease inhibitor cocktail from Roche.

Name	Reactive Species	Clone	Dilution	Secondary Ab
RAPTOR	Human, Mouse, Rat	24C12	1:1000	Rabbit
RICTOR	Human, Mouse	D16H9	1:1000	Rabbit
pAKT^{S473}	All	23C8D2	1:1000	Rabbit
AKT (pan)	Human, Mouse, Rat	C67E7	1:1000	Rabbit
pS6$^{S235/S236}$	Human, Mouse, Rat	D57.2.2E	1:1000	Rabbit
S6	Human, Mouse, Rat	54D2	1:1000	Mouse
p4EBP1$^{T37/T46}$	Human, Mouse, Rat		1:1000	Rabbit
4EBP1	Human, Mouse, Rat	53H11	1:1000	Rabbit
GAPDH	Human, Mouse, Rat	D16H11	1:1000	Rabbit
β-ACTIN	Human, Mouse, Rat		1:1000	Rabbit
Anti-mouse IgG, HRP-linked Antibody			1:10000	
Anti-rabbit IgG, HRP-linked Antibody			1:10000	

Table 2.8: List of antibodies used for western blotting.
List of antibodies and their dilutions in 5% BSA in TBST (except for S6 ribosomal protein, which was in 5% milk in TBST). All antibodies were purchased from Cell signalling (Herts, UK).

Name	Reactive Species	Clone	Dilution	Manufacturer	Isotype
pS6$^{S235/S236}$	Mouse	D57.2.2E	1:800	Cell signalling	Rabbit IgG
Ki67	Mouse	RM-9106-S	1:100	Thermo Fisher	Rabbit IgG
pAKT^{S473}	Mouse	9DE	1:25	Cell signalling	Rabbit IgG
p4EBP1$^{T37/T46}$	Mouse	236B4	1:500	Cell signalling	Rabbit IgG
Biotinylated goat anti-rabbit	Mouse			Vector Labs	Rabbit IgG

Table 2.9: List and details of antibodies used for IHC.
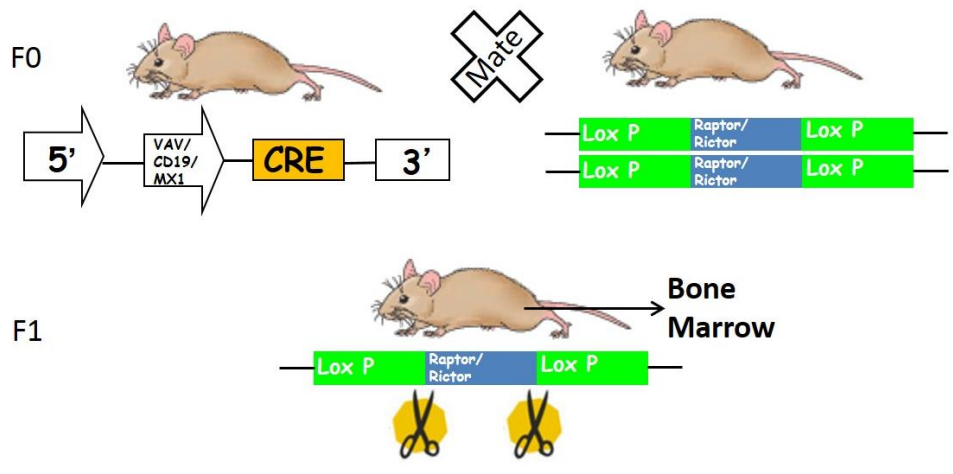
Figure 2.1: Cre-loxP system and excision of *Rictor/Raptor* under promoters including *Vav, Mx-1* and *CD19*.
Upon the expression of the promotors, cre is expressed and it excises the floxed gene flanked by loxP sites thereby generating a KO of the gene of interest (in this case gene of interest being *Raptor* and *Rictor*).
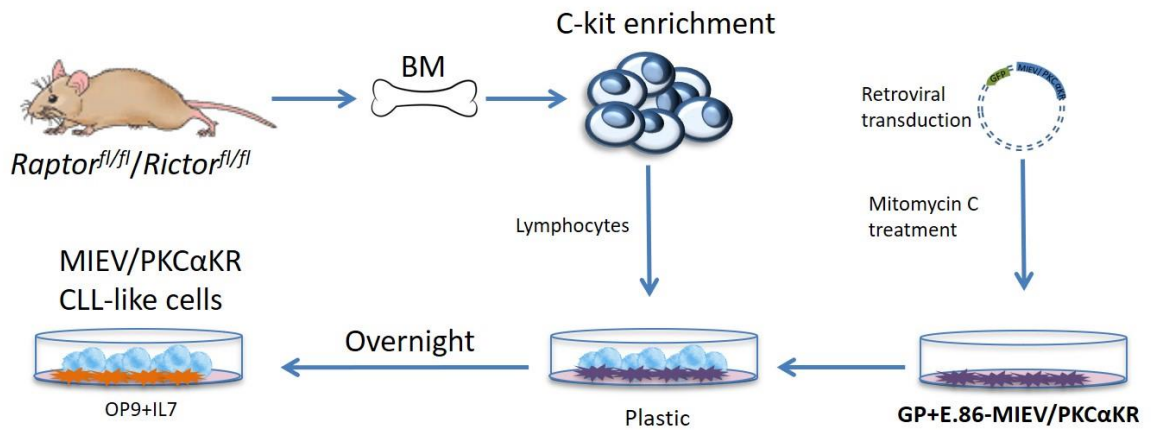
Figure 2.2 *In vitro* system for the retroviral transduction of BM removed from KO mouse models.
BM is enriched for CD117 by MACS, and co-cultured overnight with GFP tagged GP+E.86 MIEV/PKCαKR supplemented with IL7, Flt3, and polybrene in complete DMEM media to retrovirally transduce the enriched BM cells. Post transduction, cells are co-cultured on OP9-GFP^{+} stromal cells supplemented with IL7 and Flt3 cytokines to promote B cell lineage generation.
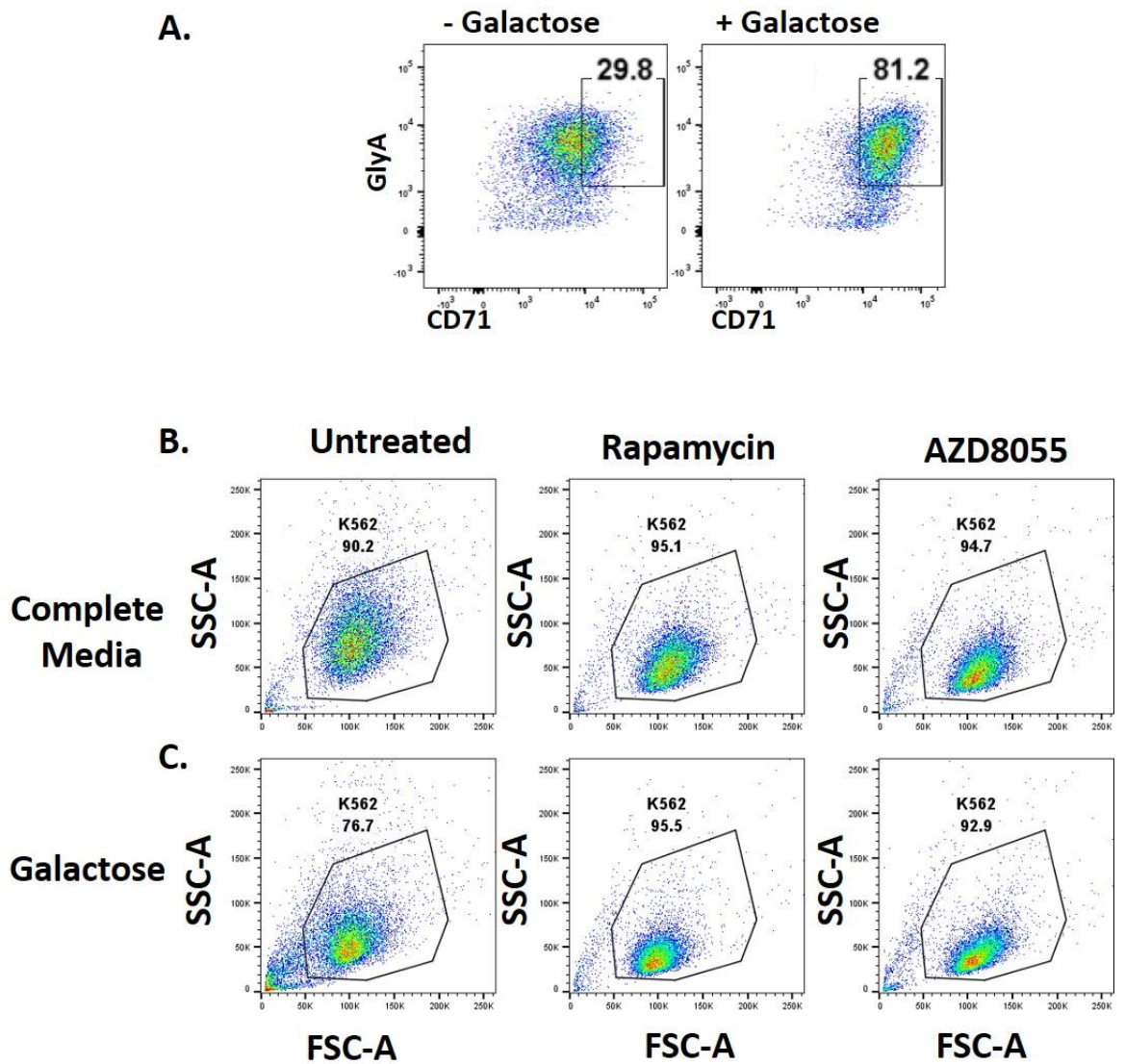
Figure 2.3 K562 cell line and its differentiation into an erythrocyte-like lineage.
A. Flow cytometry representative plot of K562 demonstrating the increase in CD71+GlyA+ surface expression with the substitution of glucose with galactose in media. Live cells were gated by looking at forward scatter and side scatter area (FSC-A and SSC-A). Doublet cells were excluded by FSC-A and forward scatter height (FSC-H). Representative flow cytometry plots showing the change in size and granularity through FSC-A and SSC-A plots of K562 cells (**B**) or K562 cells cultured with galactose (**C**) and treated with 10 nM rapamycin or 100 nM AZD8055.
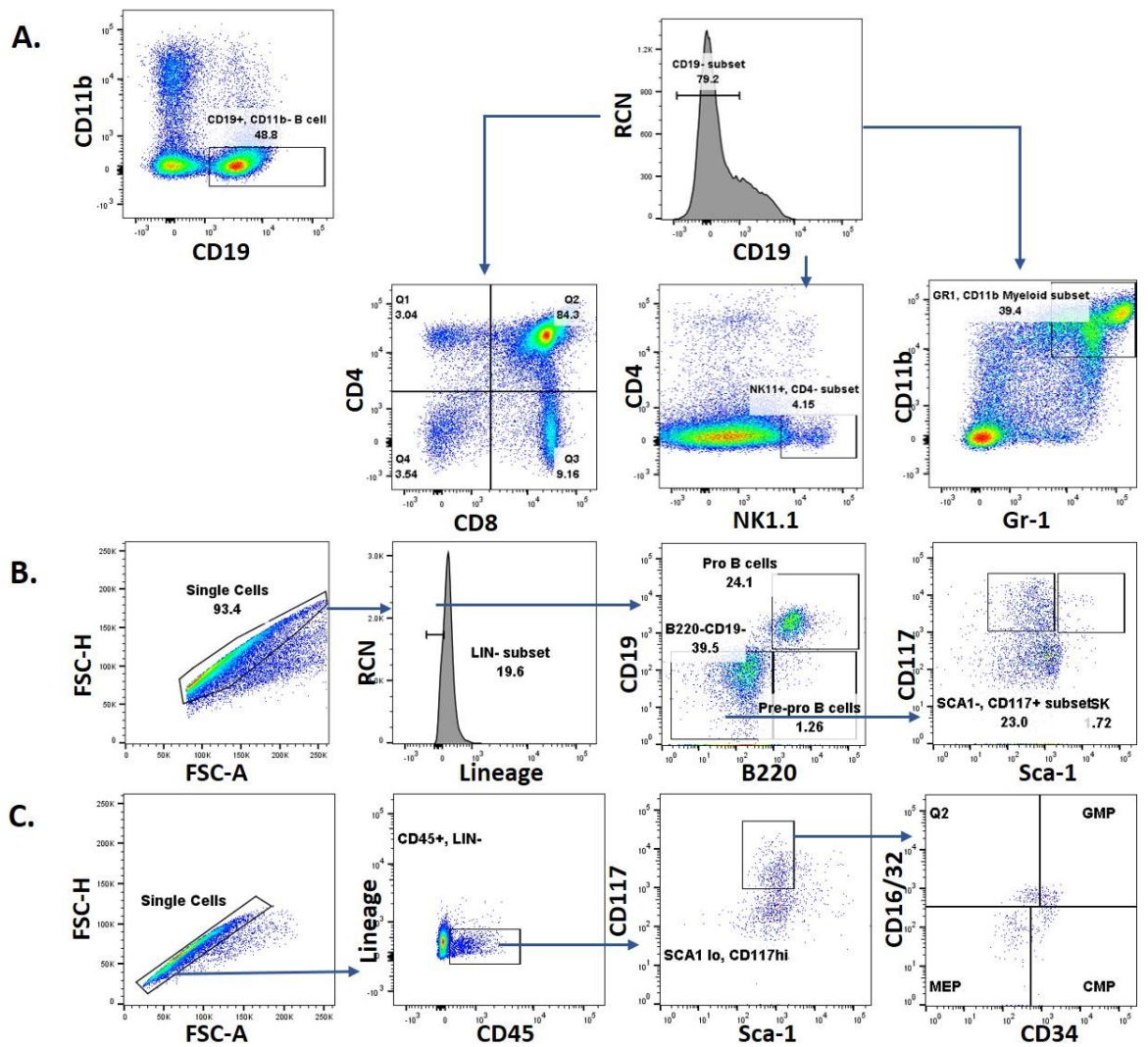
Figure 2.4 Representative flow cytometry graphs and gating strategy.
Flow cytometry graphs demonstrating gating strategy for various haematopoietic lineages (**A**), early B cells (**B**), early myeloid populations (**C**). Various organs obtained from *Mx1*-cre *Raptor$^{fl/fl}$* mice stained for lineage, and early B and myeloid surface markers. Live cells were gated by looking at FSC-A and SSC-A. Doublet cells were excluded by FSC-A and FSC-H. Mature B cells (CD11b$^-$CD19$^+$), CD4 T cells (CD19$^-$CD8a$^-$CD4$^+$), CD8 T cells (CD19$^-$CD4$^-$CD8a$^+$), NK cells (CD19$^-$CD4$^-$NK1.1$^+$), mature myeloid cells (CD19$^-$CD11b$^+$Gr1$^+$), pre-proB cells (lin$^-$CD19$^-$B220$^+$), proB cells (lin$^-$CD19$^+$B220$^+$), LSK (lin$^-$CD19$^-$B220$^-$Sca-1$^+$CD117$^+$), sca^{lo}CD117^{hi} (lin$^-$CD19$^-$B220$^-$sca-1^{lo}CD117^{hi}), CMP (lin$^-$CD45$^+$Sca^{lo}CD117^{hi}CD34$^+$CD16/32$^-$), GMP (lin$^-$CD45$^+$Sca^{lo}CD117^{hi}CD34$^+$CD16/32$^+$), MEP (lin$^-$CD45$^+$Sca^{lo}CD117^{hi}CD34$^+$CD16/32$^+$).
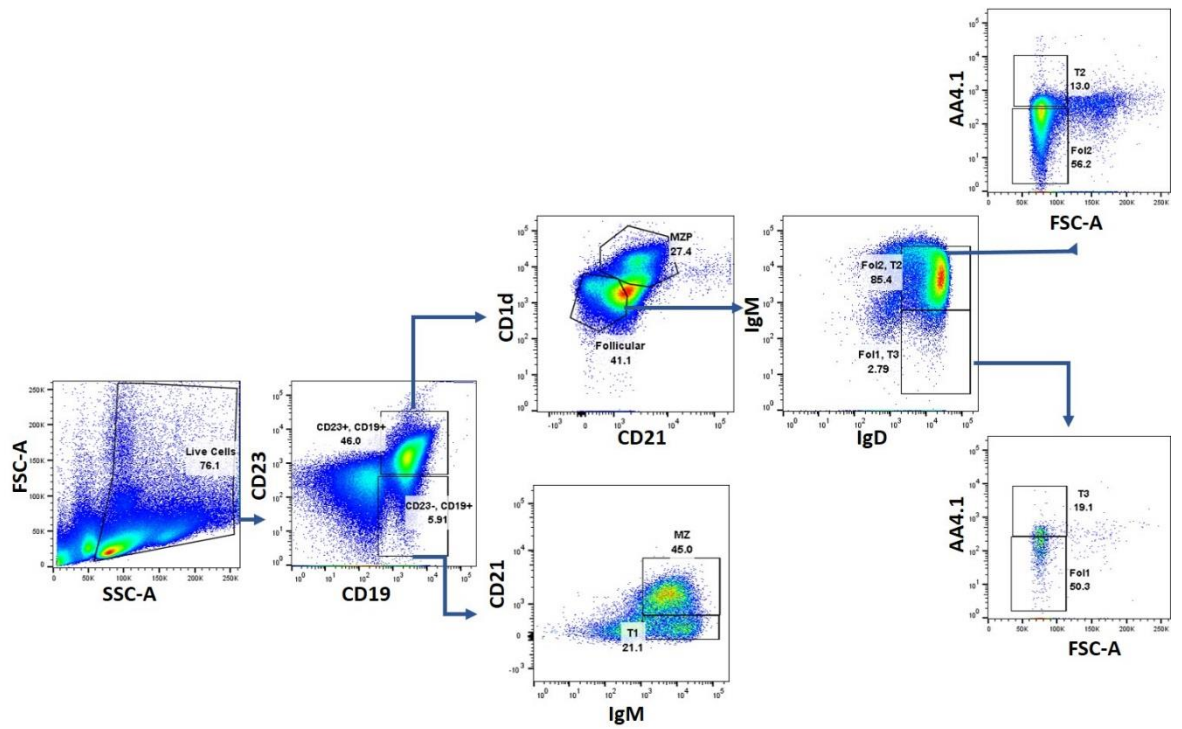
Figure 2.5 Representative flow cytometry plots showing the gating strategy for late B cell subsets.
Spleens obtained from *Mx1*-cre *Raptor*$^{fl/fl}$ mice stained for late B cell surface markers. Live cells were gated by looking at FSC-A and SSC-A. T1 cells (CD19$^+$CD23$^-$IgM$^+$CD21$^-$), T2 (CD19$^+$CD23$^+$CD21$^-$CD1d^{lo}IgD$^+$IgM$^+$AA4.1$^+$), T3 (CD19$^+$CD23$^+$CD21$^-$CD1d^{lo}IgD$^+$IgM$^-$AA4.1$^+$), MZP (CD19$^+$CD23$^+$CD21$^+$CD1d$^+$), MZ (CD19$^+$CD23$^-$IgM$^+$CD21$^+$), Fol1 (CD19$^+$CD23$^+$CD21$^-$CD1d^{lo}IgD$^+$IgM$^-$AA4.1$^-$), Fol2 (CD19$^+$CD23$^+$CD21$^-$CD1d^{lo}IgD$^+$IgM$^+$AA4.1$^-$). Abbreviations: T1-3 – Transitional cells, fol – follicular cells, MZP – marginal zone progenitors.
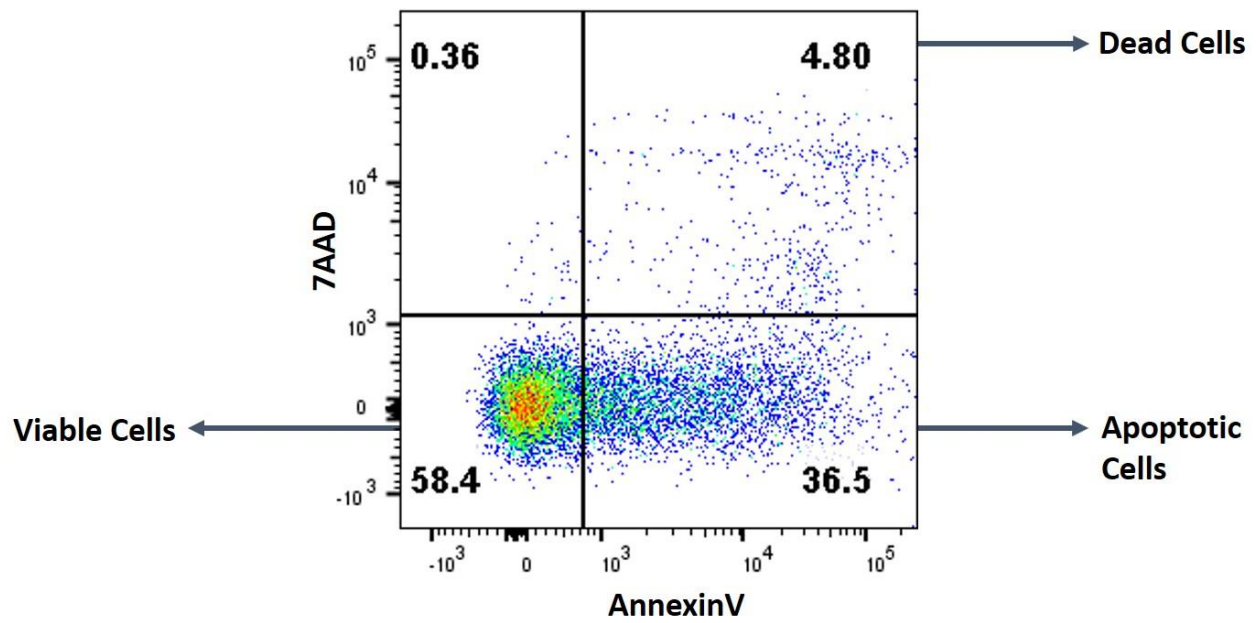
Figure 2.6 Representative flow cytometry plot showing AnnexinV and 7AAD staining.
AnnV⁻7AAD⁻ are viable cells, AnnV⁺7AAD⁻ are apoptosing cells, AnnV⁺7AAD⁺ are dead cells. BM cells obtained from *CD19*-cre *Raptor^{fl/fl}* mice.
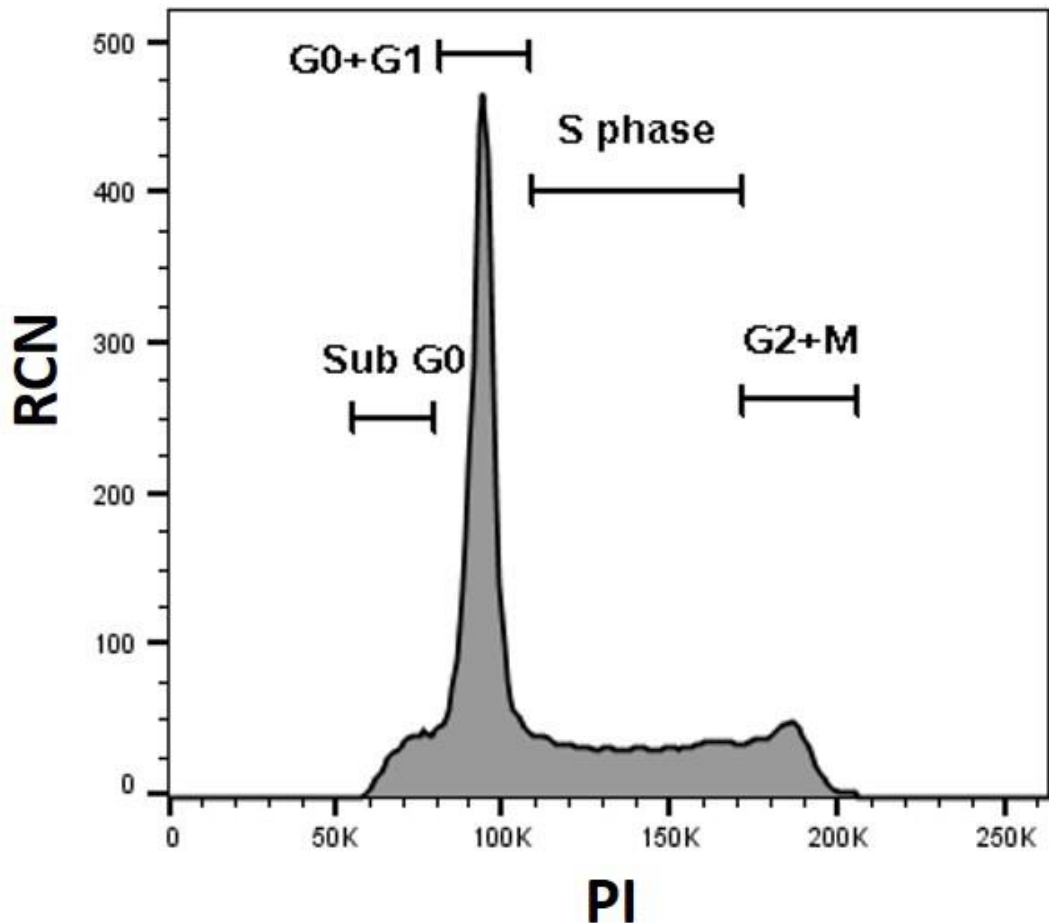
Figure 2.7: Flow cytometry representative plot showing the different phases of cell cycle by propidium iodide (PI) staining.
Retrovirally transduced PKCαKR cells, which were derived from BM of *Vav*-cre *Rictor^{fl/fl}* mice. PI assay was set up at D22 *in vitro*. Live cells were gated by looking at FSC-A and SSC-A. Doublet cells were excluded by FSC-A and FSC-H. GFP⁻ cells were excluded and then PI was observed in the graph above. Sub G_0 phase contains apoptotic cells, cells in G_0 phase are quiescent cells, cells in G_1 phase are in preparation for doubling the chromosomal levels for mitosis, cells in S phase indicate DNA synthesis, G_2 phase is where mitosis preparation occurs, and M phase is where mitosis occurs. RCN - Relative cell number.
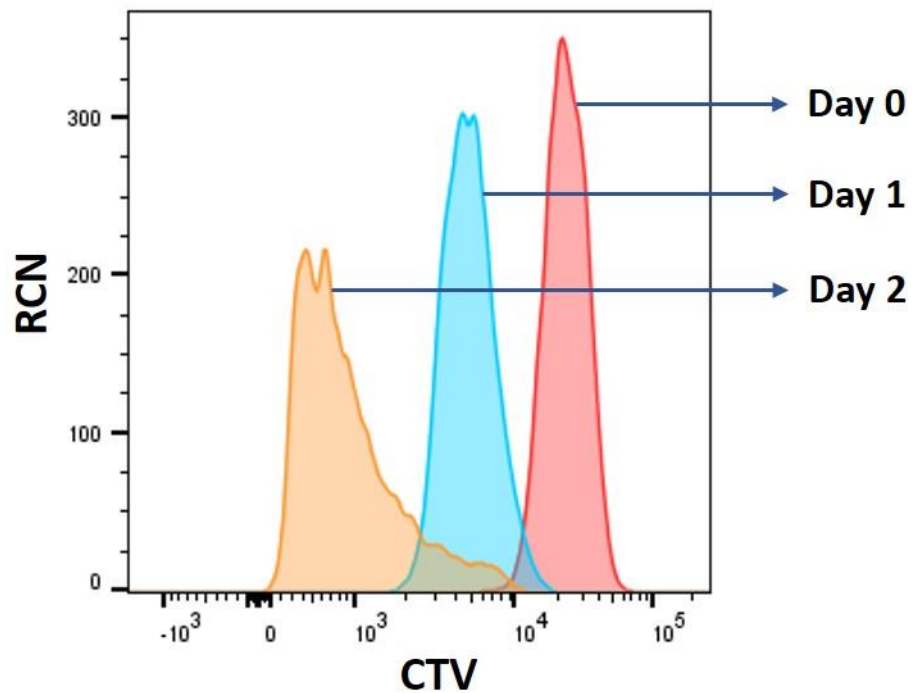
Figure 2.8 Representative plot showing cell trace violet (CTV) fluorescence over 3 days thereby measuring the proliferation of a population.
Retrovirally transduced PKCαKR cells, which were derived from BM of *Mx1*-cre *Raptor^{fl/fl}* mice. Cells were treated with 200 U/well interferonβ (IFNβ) for 24 hr *in vitro*. This proliferation assay was set up 3 days after treatment. Live cells were gated by looking at FSC-A and SSC-A. Doublet cells were excluded by FSC-A and FSC-H. GFP⁻ cells were excluded and then CTV fluorescence was observed in the graph. Red, blue and yellow peaks represent CTV fluorescence at D1, 2, and 3 respectively. RCN - Relative cell number.
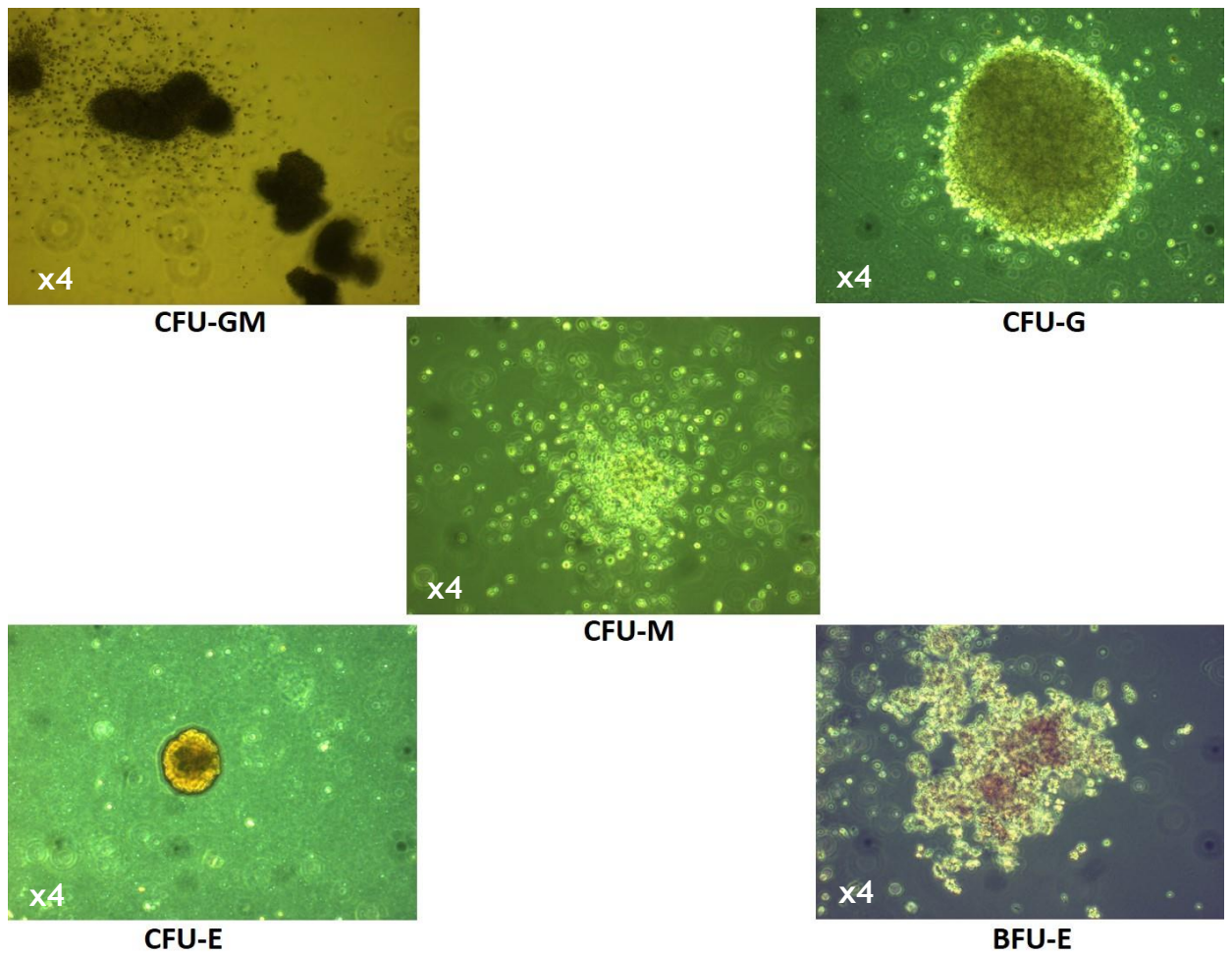
Figure 2.9 Different colonies formed by *Vav*-cre *Rictor*$^{fl/fl}$ BM (CD117 enriched cells) using the m3434 and m3334 MethoCult media.
CFU-GM (colony forming unit-granulocyte macrophage), CFU-G (colony forming unit-granulocyte), CFU-M (colony forming unit-macrophage), CFU-E (colony forming unit-erythroid), BFU-E (burst forming unit-erythroid). Pictures are taken using an inverted microscope (Olympus Life Sciences, Japan) at x4 magnification.

Chapter 3

The Role of mTOR in Erythropoiesis and Myelopoiesis

3 Role of mTOR in erythropoiesis and myelopoiesis

3.1 Aims and objectives

The mTOR pathway has previously been shown to play a role in RBC development(97). The aims of this chapter are to determine the role of mTORC1 and mTORC2 in RBC development and the role of mTORC1 in myelopoiesis using mouse models:

i) The *Vav*-cre *Raptor*/*Rictor*$^{fl/fl}$ mouse model, which excises either *Raptor* or *Rictor* (inactivating mTORC1 or mTORC2 respectively) at the HSC stage under the *Vav* promoter.

ii) The *Mx1*-cre *Raptor*$^{fl/fl}$ mouse model which excises *Raptor* (thus rendering mTORC1 inactive) in all tissues in a time controlled manner by the inoculation of poly(I:C) (Section 1.7.1.2).

3.2 Results

3.2.1 Mice lacking mTORC1 within the haemopoietic lineage do not survive after birth and *Raptor*-null adult mice display splenomegaly

To assess the role of mTORC1 at the HSC stage we used the *Vav*-cre model. To obtain the desired *Raptor* KO model, *Vav*-cre$^{+/-}$*Raptor*$^{wt/fl}$ were mated with *Vav*-cre$^{-/-}$*Raptor*$^{fl/fl}$ to obtain the possible mendelian phenotypic filial generations: *Vav*-cre$^{-/-}$*Raptor*$^{fl/fl}$ (*Vav-Raptor* control)*, Vav*-cre$^{+/-}$*Raptor*$^{wt/fl}$, *Vav*-cre$^{-/-}$*Raptor*$^{wt/fl}$, or the desired KO model *Vav*-cre$^{+/-}$*Raptor*$^{fl/fl}$ (*Vav-Raptor* KO). From previous literature, it is preferable to use heterozygous cre expression for the KO models, as homozygous expression of cre has shown to be 'leaky', leading to non-specific deletions due to the presence of pseudo-loxP sites present in the mouse genome(208). Therefore, cre$^{+/-}$*Raptor*$^{fl/fl}$ was the desired KO model.

Analysis of *Vav*-cre matings demonstrated a lack of *Vav-Raptor* KO mice specifically at weaning age (4 wk) (Table 3.1). We thus performed time-matings, obtaining foetus' at E13, E15 and E18, to determine whether the *Vav-Raptor* KO mice were present at these embryonic stages. Indeed, between E13-18, we obtained the desired model/phenotype of interest in the expected mendelian ratios (Table 3.1). This suggests that mice with *Raptor* KO at the HSC do not survive much longer after birth and undergo perinatal lethality. Post birth genotyping then revealed that *Vav-Raptor* KO mice do not survive more than 2 days (D2) after birth. Genotyping *Vav-Raptor* KO FL confirmed the KO as these FLs had a significant downregulation in *Raptor* expression (Figure 3.1A). Additionally, the *Raptor*-null foetus' had a much increased pallor (Figure 3.1B) alluding to a fundamental role of mTORC1 in RBC development.

To assess the role of mTORC1 at a later developmental stage, the *Mx1*-cre *Raptor*$^{fl/fl}$ model was used where *Mx1*-cre$^{-/-}$*Raptor*$^{fl/fl}$ mice were mated with *Mx1*-cre$^{+/-}$*Raptor*$^{fl/fl}$ to obtain the desired KO model *Mx1*-cre$^{+/-}$*Raptor*$^{fl/fl}$ (*Mx1-Raptor* cKO), along with the control *Mx1*-cre$^{-/-}$*Raptor*$^{fl/fl}$ (*Mx1-Raptor* control). Compared to *Vav-Raptor* KO mice, both possible genotypes *Mx1-Raptor* control and cKO models (without poly(I:C) inoculation) were obtained in the filial generations (Table 3.2) and induction of mTORC1 cKO, by poly(I:C) inoculations, in adult mice did not result in lethality (data not shown). The *Mx1* promoter is

only expressed under the activation of TLR3. Therefore, poly(I:C), an RNA mimetic which activates TLR3 was used to induce the cKO(202,244). Upon successful cKO, which was confirmed by a significant downregulation of *Raptor* gene expression in BM and spleen of *Mx1-Raptor* cKO compared to *Mx1-Raptor* control (Figure 3.1C), *Mx1-Raptor* cKO mice exhibited splenomegaly and a significant increase in spleen weight and spleen cellularity compared to *Mx1-Raptor* controls (Figure 3.1D-F).

3.2.2 *Raptor*-null mice have a disruption in RBC, myeloid, and B cell lineages *in vivo*

Analysis of haemopoietic lineages isolated from primary lymphoid organs in these mouse models, by flow cytometry, revealed a significant decrease in the percentage of Ter119^{+} erythroid populations in *Vav-Raptor* KO FL at E15 compared to *Vav-Raptor* controls (Figure 3.2A-D, Figure 3.3A). Additionally, there was a trend in decrease in the percentage of Ter119^{+} erythroid populations in the BM (Figure 3.2E-F), together with a significant increase in percentage of Ter119^{+} population in the spleen in *Mx1-Raptor* cKO mice compared to *Mx1-Raptor* controls (Figure 3.3B). A significant increase in percentage of Ter119^{+} expression in the spleen in *Mx1-Raptor* cKO mice suggests either a compensatory mechanism of the organism to overcome the loss in erythrocytes, or a functional role of the spleen in erythrocyte metabolism. Given the ability for mice to survive in the absence of white blood cell populations, and supported by previous literature(97) we concluded that the absence of *Vav-Raptor* KO mice was due to the critical role of mTORC1 in erythropoiesis.

Further assessing the mTORC1 KO models, both the mTORC1 KO models showed a significant increase in percentage of CD11b^{+} Gr1^{-} immature myeloid population along with a decrease in percentage of CD11b^{+}Gr1^{+} mature myeloid populations compared to controls (Figure 3.2, Figure 3.3C-E). This suggests that mTORC1 is not important for myeloid lineage commitment but is essential for myeloid maturation. Looking at the role of mTORC1 in B cell lineage generations, our results demonstrate that both the *Vav-Raptor* KO FL and *Mx1-Raptor* cKO mice exhibit a significant decrease in the percentage of CD19^{+} B cell populations in E15 and E17 FL of *Vav-Raptor* KO and in the BM, spleen and a trend in decrease in the blood of *Mx1-Raptor* cKO mice compared to their respective controls

(Figure 3.2, Figure 3.3F-H). These data suggest a vital role of mTORC1 in B cell lineage commitment at early and late stages of development.

3.2.3 Mice lacking *Raptor* at the HSC stage have a disruption in early B cell population and a block in RBC development at the MEP stage *in vivo*

To gain a deeper understanding of the stage at which *Raptor*-deficiency blocks lineage commitment/development we carried out flow cytometry analysis of the haemopoietic progenitor populations. Supporting the lack of CD19$^+$ B cells, a significant reduction in the percentage of proB cells was noted across E13-18 of *Vav-Raptor* KO FL (Figure 3.4, Figure 3.5A) and *Mx1-Raptor* cKO BM, along with a significant reduction in percentage of pre-proB cells in *Mx1-Raptor* cKO BM (Figure 3.5D), and trends in reduction in percentage of pre-proB cells across E13-18 of *Vav-Raptor* KO FL compared with their respective controls (Figure 3.5B). This was coupled with a trend in increase in percentage of LSK population at E13, along with a significant elevation at E15, while no significant difference was noted at E18 in *Vav-Raptor* KO FL. There was a significant elevation in the percentage of LSK in BM of *Mx1-Raptor* cKO adult mice compared to cre-controls (Figure 3.4, Figure 3.5C&D), suggesting a block in B cell development prior to lineage commitment with *Raptor* deficiency, at an early stage in gestation and in adult mice.

Analysis of the proportion of myeloid progenitors revealed a significant elevation in the percentage of Sca-1^{lo}CD117^{hi} population in *Vav-Raptor* KO FL at E13 and E15 (Figure 3.7A), a population consisting of CMP population, which gives rise to GMP and MEP populations (Figure 3.6). There were no changes in the percentages of CMP and GMP populations at E13, E15 or E18 of *Vav-Raptor* KO FL (Figure 3.7B, C). However, there was a trend towards an increase in percentage of GMP populations at E13, and E15 suggesting a skew towards myeloid lineages in *Raptor*-deficient mice at the HSC stage, which alludes to the observed accumulation of CD11b$^+$ immature myeloid population. Comparatively, the *Mx1-Raptor* cKO BM exhibit a decrease in the percentage (but not cellularity) of Sca-1^{lo}CD117^{hi} population, with no significant changes in the CMPs, but with a significant decrease in the percentage (but not cellularity) of GMPs compared to controls (Figure 3.6, Figure 3.8A&B), which confirms the decrease in percentage

of CD11b⁺Gr1⁺ mature myeloid population in BM of *Mx1-Raptor* cKO mice as GMPs give rise to myeloid lineages. The difference in progenitor populations between the FL and BM with *Raptor*-deficiency illustrates the varied functioning of the two organs and highlights that mTORC1 plays similar but not identical roles in lineage maintenance at different stages of development and ontogeny. Assessing the MEP population, there was an elevation in the percentage of MEPs at E13 and E15, with no observed change at E18 (Figure 3.7D) indicating a developmental block for erythropoiesis at the MEP stage in the absence of *Raptor* expression *in vivo* at the early HSC stage. The lack of change in early progenitors at E18 may be due to the shift of haemopoiesis towards the BM after E16.5 to prepare for birth (245). Adult mice with *Raptor*-deficiency exhibit a significant decrease in the percentage (not cellularity) of MEP population in the BM, which confirms the block in erythropoiesis at an earlier developmental stage in the BM. There is a significant decrease in the cellularity and trends in reduction in the percentage of MEP population in the spleen (Figure 3.8C&D), which suggests that there is a depletion of erythrocytes in the spleen. Therefore, the significant increase of erythrocytes in the spleen could allude to an acceleration in erythrophagocytosis, which occurs in the spleen(246). Interestingly, there is a significant increase in percentage and cellularity of MEP population with *Rictor*-deficiency at the HSC stage at 2 wk (*Vav-Rictor* KO mice) with similar trends at 8 wk compared to cre⁻ controls (*Vav-Rictor* control mice, Figure 3.8E&F). These are opposing trends to what is observed with *Raptor*-deficiency, suggesting a regulatory mechanism of erythropoiesis between mTORC1 and mTORC2 where mTORC1 is fundamental for the development of erythrocytes whereas mTORC2 suppresses erythrocyte generation.

In support of our phenotypic analysis showing a block in B cell and RBC development, expression analysis of key genes at the HSC stage responsible for enabling differential lineage commitment revealed a significant downregulation in the B cell specific transcription factors *Ebf1* and *Pax5*, while expression levels of the myeloid regulator *Cebpa* was unaltered. Assessing expression levels of vital TFs involved in erythroid lineage commitment, *Pu.1* and *Gata1* expression levels were significantly downregulated in the FL of *Vav-Raptor* KO mice with trends in an increase in *Gata2* levels alluding to aberrations in *Gata*-factor switching. Additionally, there was a significant downregulation in the expression

of *β-Globin*, *e-Klf/Klf1* and *Klf2*, TFs which play a role in embryonic and adult erythropoiesis and development (Figure 3.7E-G). Collectively, these results indicate an aberration B and RBC lineage commitment with *Raptor* deficiency in *Vav-Raptor* KO FLs.

3.2.4 Exploiting K562 CML cell line as an *in vitro* model for erythropoiesis

In order to further analyse the role of mTORC1 in RBC development *in vitro*, we made use of the BCR-Abl+ human CML cell line K562, an erythroleukaemia line that differentiates towards a RBC lineage when exposed to stressful environments(247–249). To induce differentiation, cells were treated with either 50 μM hemin(240) or 11 mM glucose was replaced with 11 mM galactose in complete media(241) and cultured till D5-7 *in vitro*. Hemin treatment showed the differentiation towards a RBC-like lineage as seen by the colour change in cells with hemin treatment (Figure 3.9A). As hemin is strongly auto-fluorescent, moving forward, we supplemented glucose for galactose in the media (Gal-media) to induce stress and thus RBC differentiation (as described in section 2.2.2). Indeed, we observed a significant increase in the percentage of $CD71^+GlyA^+$ cells (erythroid markers), an elevation in CD71 expression and a reduction in granularity (cell scatter – SSC-A) (Figure 3.9B-D, Figure 3.10A-C) in K562 cells cultured in Gal-media, coupled with a significant increase in gene expression of *B-GLOBIN*, and *GATA2*, which are involved in erythropoiesis (Figure 3.10D). Interestingly, we see a change in the activity of the mTOR pathway with erythroid differentiation *in vitro* as was indicated by an increase in expression of $pAKT^{S473}$, coupled with a decrease in RAPTOR and $p4EBP1^{T37/T46}$ expression in K562 cell cultured in Gal-media, suggesting an increase in mTORC2 and a decrease in mTORC1 activity (Figure 3.11A-D).

3.2.5 K562 cell line differentiation into RBCs is blocked with mTOR inhibition *in vitro*

To assess the role of mTORC1 in RBC differentiation, K562 cell line was treated with a partial mTORC1 inhibitor, rapamycin and the dual mTOR complex inhibitor AZD8055, and cultured in either complete media or Gal-media to induce RBC differentiation. Treatment of K562 cells with rapamycin or AZD8055 blocked erythroid differentiation *in vitro*, as indicated by a significant decrease

in the percentage of CD71$^+$GlyA$^+$ erythroid cells, and a reduction in gene expression of erythroid markers β-*GLOBIN, GATA1* and *GATA2*, (Figure 3.10A-D), indicating mTORC1 inhibition blocks RBC differentiation *in vitro*. Interestingly, there was a trend in increase in pAKT^{S473} and p4EBP1$^{T37/T46}$ levels with rapamycin treatment in K562 cells cultured in both complete or in Gal-media suggesting there was no change or an increase in activity of the downstream targets of mTORC1 including mTORC2 with rapamycin treatment (Figure 3.11A-D). Consistent with previous literature(250), as rapamycin is an allosteric inhibitor of mTORC1 and a partial inhibitor, these data suggest that even though rapamycin affects erythroid differentiation, the effects are not as potent. However, pAKT^{S473} is not a direct target of rapamycin and although rapamycin inhibits 4EBP1 function, this function is restored in prolonged treatments depending on the cell type(251).

Nevertheless, there was a significant decrease in pAKT^{S473} and p4EBP1$^{T37/T46}$ expression with AZD8055 in K562 cells cultured in complete media, alluding to the potent role of mTOR in leukaemia. There was also a significant decrease in pAKT^{S473} with an unexpected increase in p4EBP1$^{T37/T46}$ with AZD8055 in erythroid-like cells (Figure 3.11A-D).

3.2.6 mTORC1 and mTORC2 regulate RBC maintenance *ex vivo*.

To assess erythroid colony formation capacity of HPCs in the absence of mTORC1 activity, HPCs were isolated from BM of *Mx1-Raptor* control or *Mx1-Raptor* cKO mice and CFC assays were performed. We establish that *Mx1-Raptor* cKO mice lack CFC capacity, as indicated by the lack of colony formation of CFU-E, BFU-E or CFU-GEMM colonies in the absence of *Raptor* expression, compared to cre$^-$ controls (Figure 3.12A&B). Interestingly, myeloid progenitor CFC assays performed in *Vav*-cre$^-$*Rictor*$^{fl/fl}$ (*Vav-Rictor* control) and *Vav*-cre$^+$*Rictor*$^{fl/fl}$ (*Vav-Rictor* KO) HPCs to assess the role of mTORC2 in early myeloid/erythroid colony formation demonstrated a significant increase in CFU-E colonies, along with a trend in increase in GEMM colonies in *Vav-Rictor* KO HSPCs compared to controls (Figure 3.12C&D) suggesting a suppressive role of mTORC2 in erythropoiesis.

3.3 Discussion

The data presented in this chapter supports previously published data demonstrating a significant decrease in B cells with mTORC1 deficiency, together with an increase in CD11b$^+$ and decrease in CD11b$^+$Gr1$^+$ myeloid cells(91). Additionally, it has been reported that mTORC1 plays a role in erythropoiesis. Previous literature has identified mTORC1 a critical role in erythropoiesis whereby mTORC1 is regulated by dietary iron and *Raptor* ablation at the HSC stage leads to perinatal lethality(97). In turn, mTOR also regulates cellular iron homeostasis by its downstream target Tristetraprolin(252). Furthermore, *Raptor*$^{-/-}$ and overexpression leads to microcytic and macrocytic anaemia respectively(97). However, there remain discrepancies in the field as there are studies demonstrating the redundant role of mTORC1 in anaemia(253), while others indicate that mTORC1 inhibition improves anaemia in a sickle cell disease model(254). Thus, we proposed to elucidate the mechanism by which this is regulated. This was done by assessing two different KO models of mTORC1 using the cre-loxP system to identify the exact role of mTORC1 in haemopoiesis with a focus on erythropoiesis. The cre-loxP system was used to KO mTORC1 at the HSC stage, by excising *Raptor* under the *Vav* promoter, and across all tissues in adult mice using a conditional KO (cKO) system which excises *Raptor* under the *Mx1* promoter, which is expressed upon TLR3 activation. The *Mx1*-cre *Raptor* model was time controlled and cKO was induced upon the inoculation of poly(I:C) to activate TLR3. This enabled us to compare the role of mTORC1 at different stages of haemopoietic development.

While assessing the role of *Raptor* at the HSC stage, we demonstrated that *Raptor*-deficiency leads to perinatal lethality. *Raptor*-deficient embryos have an increased pallor, which is seen already at E13, suggesting that *Raptor*-deficient embryos are severely anaemic. In murine physiology, each foetus within the uterine horn has a dual supply of maternal blood – from the uterine branch of the ovarian artery and the uterine artery, which form a network of irrigation fields within each foetus. Additionally, the female bearing the litter undergoes vascular remodelling depending on the litter-size, as a larger litter size has shown to result in greater vascular remodelling to accommodate each foetus. Foetus' in the periphery of the horn have been shown to receive a greater blood supply as compared to those located in the middle of the horn. However, the

foetus' in the middle have shown to have a better survival capability, an example of evolutionary preservation of the litter in case of complications in the pregnancy(255). Genetic abnormalities within each foetus cause changes in the blood supply to accommodate for those changes to preserve the litter as best as possible. This could be one reason why *Vav-Raptor* KO (*Raptor*-deficient) mice are born but die soon after as they cannot survive after the circulation switch from maternal to new-born circulation, which takes place at birth. Additionally, circulation within the embryo is fully established after E10 in normal murine embryos, which is coupled together with vascular remodelling and vessel branching(256). However, our data shows that mTORC1 activity is involved in this circulation at an early stage due to the observed pallor in murine embryos as early as E13.

The pallor was likely due to a significant decrease in Ter119$^+$ erythrocytes with *Raptor*-deficiency at the early HSC stage. To assess whether erythropoiesis was blocked at an earlier developmental stage, we looked at surface markers for erythroid progenitors. There was a significant increase in the Sca^{lo}CD117^{hi} population with *Raptor*-deficiency, which gives rise to CMPs which further divide into GMP and MEPs. Indeed, we observed a significant increase in the MEP population suggesting a block at the MEP stage (the erythroid progenitor population) at E13 and E15 *Vav-Raptor* KO FL. It is seen that there is a reduction in the progenitor populations in all E18 *Vav-Raptor* FL, and there is no significant difference between the controls and the *Vav-Raptor* KO FL at E18. It is important to note here that haemopoiesis, broadly put, occurs in two waves, primitive and definitive. Primitive haemopoiesis mainly involves the formation of primitive erythrocytes from HSC residing in the yolk sac to induce oxygenation. The definitive wave comprises of the formation of other haemopoietic progenitors when haemopoiesis moves to the AGM region followed by the FL. In mice, the transition of haemopoiesis from the FL to the BM occurs before birth at E16.5(245). This confirms the steady decline in progenitor populations in all E18 FLs thereby diminishing any significant differences observed in FLs at E13 and E15, due to a shift in haemopoiesis from the FL to the BM.

The block in erythropoiesis was further confirmed by the significant downregulation in the gene expression of *Gata1, β-Globin, Klf1* and *Klf2* genes, which are vital for erythrocyte development, with *Raptor*-deficiency at the HSC

stage. *Gata2* is a transcription factor highly expressed in haematopoietic cells. Additionally, literature has shown that both transcription factors *Gata1* and *Gata2* in 'Gata-factor switching', which involves the decrease in *Gata2* and increase in *Gata1* expression with erythroid differentiation, occupy the same binding domains(10). *Gata1* plays a vital role in erythroid differentiation, sustaining its own expression and suppressing *Gata2* expression. *Gata1* expression is vital for erythropoiesis as it inhibits *Pu.1* expression(257) thereby repressing myeloid and lymphoid lineage generation and inhibiting *Cebpa* expression, a TF vital for myeloid differentiation. *Klf1* TF is vital for erythropoiesis as it regulates MEP lineage fate during erythrocyte development, is responsible for the globin switching from *γ-* to *β-Globin* for the maturation of erythrocytes(258) from the yolk sac to the FL(23). Whilst *KLF1* plays a major role in erythropoiesis, *Klf2* has shown to be involved in *γ-Globin* activation (involved in primitive erythropoiesis)(259) and also plays a role in endothelial growth, vascular remodeling(260) and inflammation responses(25), which are vital for embryonic development. Interestingly, there was no significant difference in *Gata2* expression alluding to *Gata*-factor switching, suggesting it is not *Gata2* but *Gata1,* which is affected by mTORC1.

To determine whether this block is apparent only at an early stage, we analysed the *Mx1*-cre *Raptor* model, where poly(I:C) was inoculated into adult mice to induce cKO. *Mx1-Raptor* cKO BM exhibit a decrease in percentages of Sca^{lo}CD117^{hi} and MEP populations with a significant decrease in the splenic MEP cellularity with *Raptor*-deficiency. There could be several reasons for the difference in Sca^{lo}CD117^{hi} and MEP population between the FL and BM. It is possible that haemopoiesis, and lineage potential of progenitors differs in foetal vs. adult mice. Indeed, HSCs residing in the FL differ from HSCs in the BM such that FL HSCs have a higher proliferative and metabolic capacity (increased oxidative phosphorylation) than BM-derived HSCs(261) which could affect Sca^{lo}CD117^{hi} and MEP primitive populations. Nevertheless, there is a trend in decrease in Ter119$^+$ erythroid population in the BM of adult mice with *Raptor*-deficiency. However, looking at the spleen, there is a significant increase in Ter119$^+$ population. Similar trends are seen literature where there is a decrease in the BM and an increase in the spleen in Ter119$^+$ expression in *Raptor*-deficient *Mx1*-cKO mice(262), which could suggest a possible compensatory mechanism

wherein the organism drives for erythropoiesis due to a lack in erythrocytes. Kalaitzidis *et al.*, also observe splenomegaly with *Raptor*-deficiency in adult mice and refer to the spleen as a site for extramedullary haemopoiesis due to an increase in splenic LSK cells(262). Therefore, the spleen could be a secondary site for haemopoiesis driving erythropoiesis. Additionally, as the spleen is known to be a main site for erythrophagocytosis, and it is possible that the function of erythrocytes is compromised and are accumulating in the spleen for phagocytosis(246). We observe splenomegaly and an increase in red pulp. As the red pulp is one of the major sites of erythrocyte destruction, it is a possibility that an accumulation of erythrocytes in the spleen indicates erythrocyte depletion.

To assess other haemopoietic lineages affected by *Raptor* deletion, surface markers for various lineages were assessed at the HSC stage and in adult mice lacking mTORC1. We observed a significant reduction of mature myeloid population CD11b$^+$Gr1$^+$ and an increase in immature myeloid (CD11b$^+$) population in the FL and BM suggesting a block in myelopoiesis with *Raptor* KO at both the HSC stage and in adult mice. Guo *et al.*, have shown a similar reduction in CD11b$^+$Gr1$^+$ myeloid population, together with a decrease in CMP population with conditional *mTOR* deletion in the BM(263), which suggests that mTORC1, and not mTORC2, is vital for myeloid maturation. Literature has also shown that *Mx1*-cKO of *Raptor* leads to a decline in CD11b$^+$Gr1$^+$ myeloid population with the accumulation of CD11b$^+$Gr1$^{mid/lo}$ immature myeloid population(262). However, whether this population is an immature myeloid population is debatable as a similar increase in CD11b$^+$Gr1$^-$ population with *Mx1-Raptor* cKO is classified as being a novel innate myelo-lymphoblastoid effector cell (IMLEC) population. This novel leukocyte population has similar phenotypic characteristic to myeloid cells and are produced by CMP progenitors which cause self-destructive innate immunity by producing excess IMLECs(104).

A significant decrease in mature B cell lineages was observed with *Raptor*-deficiency in the FL and BM at the HSC stage and in adult mice, together with a decrease in proB cell lineages. Furthermore, there was a significant reduction in pre-proB cells in *Raptor*-deficient BM along with trends in decrease in pre-proB cells in *Vav-Raptor* KO FL. The increase in LSK population, which give rise to pre-proB cells, in both BM and E15 FL (with trends increase in E13 FL) suggest a block

at the LSK stage in B cell development with *Raptor*-deficiency at the HSC stage and in adult mice. A similar trend has been observed, where *mTOR* cKO in the BM leads to an increase in LSK cells and a decrease in B cells. The increased LSK population was in S phase suggesting increased cell cycling thereby leading to HSC exhaustion with *mTOR* deficiency(263). Indeed, there was a decrease in mature B cells with an increase in LSK population in the spleen of *Mx1-Raptor* cKO mice which exhibit cell cycling and metabolic changes(262). Iwata *et al.,* demonstrate a block in B cell development at the preB cell stage with cKO of *Raptor* in B cells in adult mice (*Mb1-Raptor* cKO), which is not rescued by the introduction of an anti-apoptotic *Bcl$_{XL}$* transgene, suggesting that this block caused due to the lack of mTORC1 is independent of BCL$_{XL}$(109). Our data suggest a block in B cell development at an earlier LSK stage, as the *Mb1-Raptor* cKO model was specific to B cells and could have led to differing stages of B cell development block, with similar results.

Analysing the key master TFs that regulated lineage commitment, we show a significant downregulation in *Pu.1*. High levels *Pu.1* expression inhibit *Gata1* expression and is correlated with a myeloid population along with the expression of *Cebpa*. *Cebpa* KO causes an expansion in erythropoiesis(264) and its expression has shown to be a determining factor responsible for myeloid lineage generation by inhibiting erythropoiesis(15). As *Cebpa* levels were not altered in *Vav-Raptor* KO FL, it suggests that either *Raptor* does not regulate erythropoiesis via *Cebpa,* or that the significant downregulation of *Pu.1* prior to *Cebpa* expression is sufficient to abrogate myeloid lineage generation. Moreover, lower expression levels of *Pu.1* give rise to lymphoid populations and a decrease in *Pu.1* expression by *Gata1* is associated with a drive towards an erythroid lineage(14). The fact that *Pu.1* is a vital TF in regulating haemopoiesis, and our data show a reduction in *Pu.1* and *Gata1*, supports the aberrations in RBC and B cell lineage fates. Indeed, we observe a downregulation in *Ebf1* and *Pax5,* TFs responsible for the development of B cells. *PU.1* expression enhances the expression levels of *E2A*, which is a TF involved in the earliest stages of B cell development. Lack of *E2A* leads to a block in B cell development at the pre-proB and proB stages(32). *E2A* drives the expression of *EBF1*, which together with *E2A*, regulate the *RAG* and *PAX5* genes responsible for V(D)J recombination to form the pre-BCR complex on preB cells(265).

To assess the role of mTORC1 in erythropoiesis *in vitro*, we exploited the fact that the K562 cell line differentiates into an erythrocyte-like lineage when exposed to stress(247–249,266). Various methods exist to induce this differentiation, some of which include lactic acid treatment(267), nicotinic acid and by cisplatin analogues. We used two different methods to induce differentiation, hemin treatment(268) and galactose substitution for glucose in complete media(241). Hemin is an iron-porphyrin, protoporphyrin IX, and has a ferric ion with a chloride ligand. Upon treatment of K562 cells with hemin till D5 in culture, the cell pellet turned red indicative of RBC differentiation. However, as hemin is auto fluorescent, analysis of surface markers by flow cytometry was not possible. Therefore, erythrocyte differentiation was induced by replacing glucose in complete media with galactose (Gal-media) to initiate differentiation. Indeed, we observed an increase in CD71$^+$GlyA$^+$ erythroid-like population and a decrease in cell granularity with galactose substitution along with an increase in *GATA2*, and *B-GLOBIN* gene expression levels. We used established mTOR complex inhibitors to assess the role of mTORC1 in erythrocyte differentiation. We used rapamycin, which is an allosteric(269) and partial inhibitor of mTORC1(270), and AZD8055, which is a competitive and dual mTOR complex inhibitor(271). Treatment of K562 cells with either rapamycin, or AZD8055, led to a significant decrease in the gene expression levels and surface markers of erythroid-like cells suggesting a block in erythropoiesis with mTORC1 *in vitro*. The significant decrease in *GATA1*, *GATA2,* and *B-GLOBIN* expression levels with mTOR inhibitors is consistent with the results observed in *Raptor*-deficient FL thereby confirming the role of mTORC1 in erythrocyte development. As erythrocytes are less granular compared to K562 cells, it was reassuring that we observed a decrease in cell granularity between K562 cells cultured in complete media and Gal-media. As mTORC1 plays an important role in maintaining cell size(272), we also observed a decrease in cell granularity in K562 cells with both mTOR inhibitors regardless of erythroid differentiation confirming mTORC1 plays a role in cell size, regardless of the cell type.

K562 cells cultured in Gal-media to induce erythropoiesis have an increased mTORC2 functionality coupled with a decrease in mTORC1 activity, as there is an increase in pAKT^{S473} protein expression along with a decrease in RAPTOR and p4EBP1$^{T37/T46}$ protein expression. This suggests increased mTORC2 activity during

RBC differentiation. As not much is known about the role of mTORC2 in erythropoiesis, this is an interesting finding, which suggests that both mTORC1 and mTORC2 modulate erythrocyte development. FOXO3 has shown to be vital for erythrocyte maturation, and metabolic regulation as a lack of *Foxo3* leads to increased ROS mediated by an increase in expression of *Cdkn1a* and a shortened life span of animals[273]. As AKT lies upstream of FOXO3, mTOR/AKT/FOXO3 cross-talk has shown to be vital for erythrocyte maturation[274]. This directly implicates a role of mTORC2 in erythrocyte maturation.

We would have expected to see a decrease in expression in downstream targets of mTORC1 targets with rapamycin treatment in K562 cells. However, rapamycin treatment did not have any significant change on RAPTOR, $p4EBP1^{T37/T46}$ levels with a trend in increase in $pAKT^{S473}$ expression, suggesting that rapamycin treatment leads to a strong induction of the mTORC2 complex. Carayol *et al.*, see similar results of rapamycin treatment on K562 cells with no changes and trends in increase in $pAKT^{S473}$ and $p4EBP1^{T37/T46}$ expression[250]. This could be because rapamycin is a partial inhibitor of mTORC1, and the data suggest a continuous activation of the mTOR pathway regardless of the inhibitor. Indeed, rapamycin inhibits mTORC1 via 4EBP1 and S6K inhibition. However, prolonged treatment with rapamycin increased 4EBP1 phosphorylation which is insensitive to rapamycin, whereas S6K inhibition remains constant[251] making $p4EBP1^{T37/T46}$ an unfavourable target to assess rapamycin function. Therefore, as we observe phenotypic (CD71$^+$GlyA$^+$ expression) and genotypic (*GATA1, GATA2, βGLOBIN*) changes suggesting a block in erythropoiesis with rapamycin treatment, S6K or $pS6^{S235/S236}$ expression levels could be assessed to determine the effects of rapamycin on downstream mTORC1 targets. However, there was an expected decrease in $pAKT^{S473}$ levels with the dual mTOR complex inhibitor, AZD8055 in both K562 cells and erythrocyte-like cells alluding to the antileukemic potential of the drug in K562 cells and the role of mTOR in erythropoiesis. Interestingly, there was a significant increase in $p4EBP1^{T37/T46}$ expression with rapamycin and AZD8055 treatment in cells differentiated into an erythrocyte-like lineage. 4EBP1, when dephosphorylated binds to eIF-4E cap-protein which is a part of the eIF-4F complex. This binding inhibits the interaction of eIF-4E with eIF-4G (part of the complex), thereby inhibiting protein translation [275]. The activation of the mTOR pathway has shown to directly influence and increase 4EBP1

phosphorylation(276). However, protein phosphatases (PP) including PP1, PP2A(277), and PPM1G(278) have been shown to be responsible for the dephosphorylation of 4EBP1 thereby inhibiting translation thereby regulation translation. As we see an unexpected increase in 4EBP1 phosphorylation at T37/T46 with rapamycin and AZD8055 mTOR inhibitors in erythrocyte-like cells, an evaluation of the functional levels of these PPs (PP1, PP2a and PPM1G) would give us more information about the reasons for increase in 4EBP1 phosphorylation. Previous literature has demonstrated that PP1 and PP2a are important for erythroid colony formation(279). Additionally, PP2A is known to be important for the maintained survival of mature erythrocytes(280). There is a possibility of abrogated PP levels with a block in erythrocyte-like cells with mTOR inhibitors which lead to an increase in 4EBP1$^{T37/T46}$ phosphorylation.

Lastly, we wanted to assess the colony formation capacity of *Raptor*-deficient cells. Thus, we harvested *Mx1*-cre *Raptor$^{fl/fl}$* BM to assess erythroid colony formation capacity. As expected, *Raptor*-deficient BM lacked colony formation capacity altogether demonstrating a lack in formation of CFU-E, CFU-GEMM or BFU-E colonies. This also confirms the perinatal lethality in *Vav-Raptor* KO mice due to their inability to generate haemopoietic lineages to survive. Interestingly, when we assessed *Rictor*-deficient BM and their capacity of myeloid colony formation, we observed that HPCs from the BM of *Vav-Rictor* KO mice formed significantly higher CFU-E erythroid colonies than their controls together with a trend in increase in CFU-GEMM colonies. Furthermore, there was a significant increase in the percentage and cellularity of the MEP population in *Vav-Rictor* KO BM compared to controls, suggesting a skew in erythrocyte generation in the absence of *Rictor*. This suggests a possible regulatory system for erythroid regulation wherein mTORC1 drives erythroid formation, whereas mTORC2 limits erythropoiesis suggesting mTORC1 and mTORC2 play opposing roles in regulating erythropoiesis. Interestingly, a conditional *mTor* KO results in diminished CFU-E and BFU-E colonies, with a block in erythropoiesis at the proerythroblast stage compared to controls(263) suggesting that mTORC1 is vital for the generation of erythrocytes whereas mTORC2 might be involved in the regulation of erythrocytes. As a future direction, it would be interesting to culture erythroid cells or an erythroid cell line: Bristol Erythroid Line Adult (BEL-A)(281) to directly test the role of mTORC1 and mTORC2 in erythropoiesis by performing

*sh*RNA or CRISPR knock down (KD) of mTORC1 and mTORC1 *in vitro*. From our data, we would expect to see an enhanced erythrocyte generation with mTORC2 KD with a concomitant decline in RBC generation with mTORC1 KD.

3.4 Tables and Diagrams

Breeding	Ratios	*Vav* cre⁻ *Raptor*$^{wt/fl}$	*Vav*-cre⁻ *Raptor*$^{fl/fl}$	*Vav*-cre⁺ *Raptor*$^{wt/fl}$	*Vav*-cre⁺ *Raptor*$^{fl/fl}$	Chi Test Value (x^2)	*p* value
At weaning (n=26)	Expected mendelian ratios	6.5	6.5	6.5	6.5	14.92	**
	Actual Genotypes	13	9	4	0		
Embryonic Day 13 (n=49)	Expected mendelian ratios	12.25	12.25	12.25	12.25	2.92	0.50 (ns)
	Actual Genotypes	12	8	15	14		

Table 3.1: *Vav*-cre⁺*Raptor*$^{fl/fl}$ mice do not survive to weaning (4 wk old), exhibiting perinatal lethality.
Timed-mated mice were generated where *Vav*-cre$^{+/-}$*Raptor*$^{wt/fl}$ mice mated with *Vav*-cre$^{+/-}$*Raptor*$^{fl/fl}$ to obtain filial generations with *Vav*-cre$^{-/-}$*Raptor*$^{wt/fl}$, *Vav*-cre$^{-/-}$*Raptor*$^{fl/fl}$, *Vav*-cre$^{+/-}$*Raptor*$^{wt/fl}$, or *Vav*-cre$^{+/-}$*Raptor*$^{fl/fl}$ genotypes according to Mendel's law. Table shows expected mendelian ratios and the actual genotyped ratios of the mice at weaning and E13, together with chi test values and whether they are statistically different. (p, **≤0.001).

Breeding	Ratios	$Mx1$-cre$^-$ $Raptor^{+/+}$	$Mx1$-cre$^+$ $Raptor^{+/+}$	Chi Test Value (x^2)	p value
At weaning (n=76)	Expected mendelian ratios	38	38	0.053	3.84 (ns)
	Actual Genotypes	37	39		

Table 3.2: *Mx1*-cre *Raptor^fl/fl* mice genotypes at weaning (4 wk).
Mx1-cre*^+/-^Raptor^fl/fl* mice were mated with *Mx1*-cre*^-/-^Raptor^fl/fl* mice and the obtained genotypes of the filial generations were recorded. Table shows the expected medelian ratios and the actual genotyping of the filial generations upon matings, together with chi test values and whether they are statistically different. (p, *≤0.05).
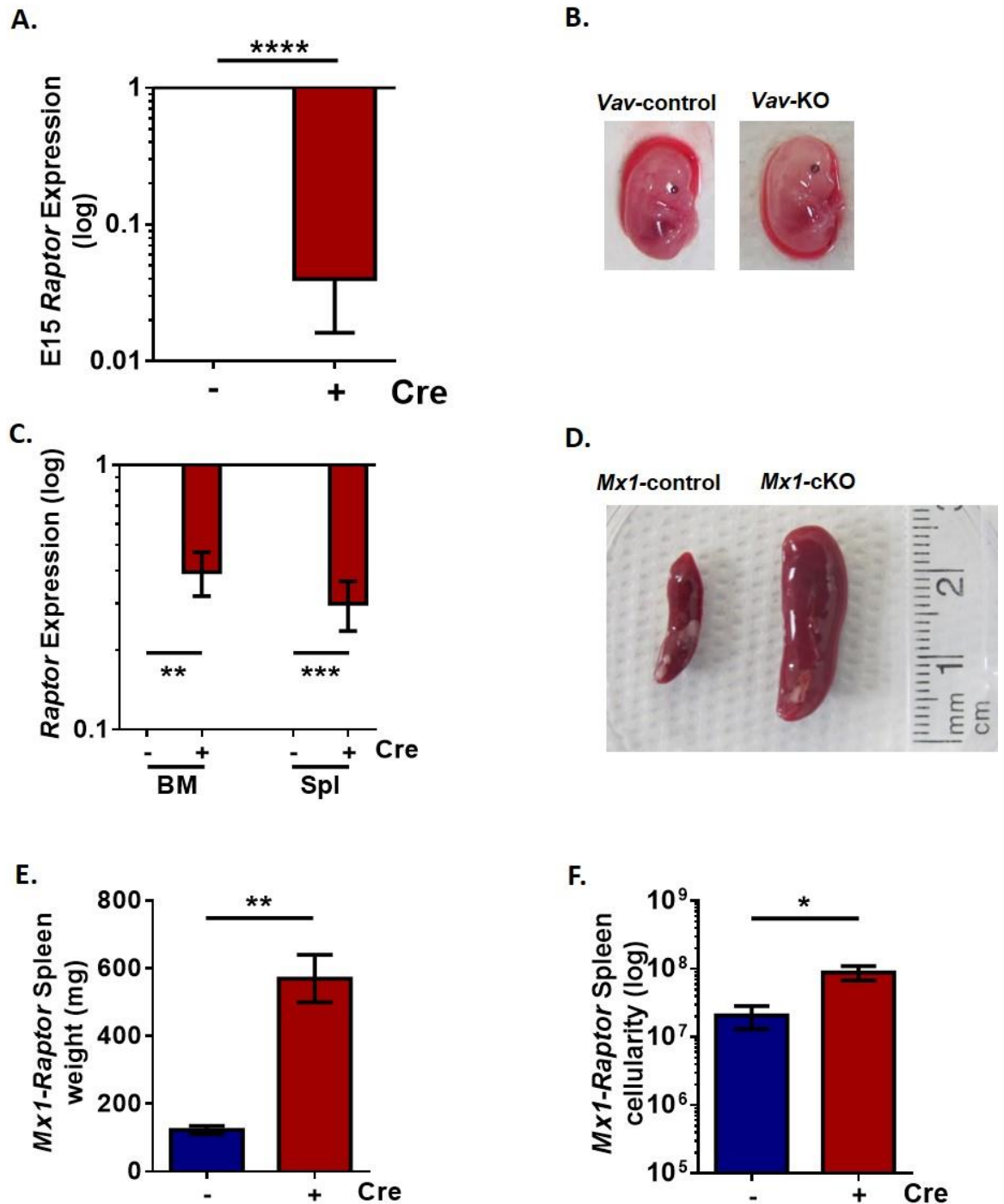
Figure 3.1: *Vav-Raptor* KO mice are perinatally lethal and *Raptor*-null adult mice exhibit splenomegaly *in vivo.*

A. Gene expression data showing expression of *Raptor* with cre expression in *Vav-cre⁺Raptor^fl/fl* (*Vav-Raptor* KO) compared to *Vav*-cre⁻*Raptor^fl/fl* (*Vav-Raptor* control) E15 FL. **B.** Picture showing the difference in pallor in E13 FL between *Vav*-cre⁻*Raptor^wt/fl* and *Vav-Raptor* KO foetal mice. **C.** Gene expression of *Raptor* in the BM and spleen in *Mx1*-cre⁻*Raptor^fl/fl* (*Mx1-Raptor* control, blue bar) and *Mx1*-cre⁺*Raptor^fl/fl* mice (red, Mx1-*Raptor* cKO). **D.** Picture showing splenomegaly in *Mx1-Raptor* cKO mice compared to *Mx1-Raptor* control. Graphs showing spleen weight (mg) **(E)** and cellularity **(F)** of *Mx1- Raptor* control and *Mx1-Raptor* cKO mice. Data are expressed as mean±SEM (p *≤0.05, p **≤0.001, p ***≤0.0001, p ****≤0.00001).
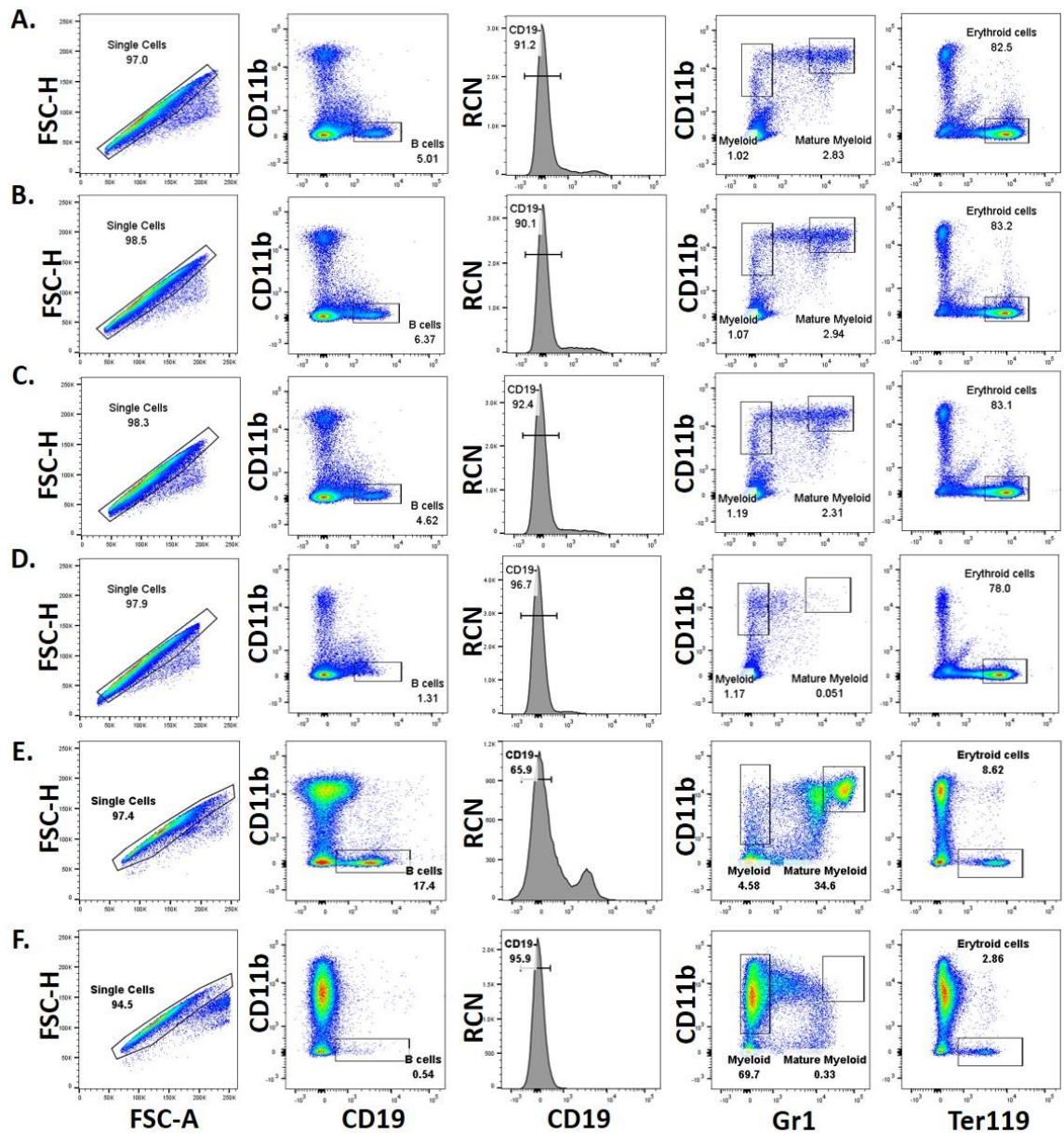
Figure 3.2: Gating strategy of haemopoietic lineages in *Vav*-cre *Raptor* and *Mx1*-cre *Raptor^fl/fl* primary lymphoid organs.
Representative flow cytometry plots demonstrating the proportion of B cells (CD19$^+$CD11b$^-$), mature myeloid cells (CD19$^-$CD11b$^+$Gr1$^+$), myeloid cells (CD19$^-$CD11b$^+$), and erythroid (CD19$^-$CD11b$^-$Ter119$^+$) lineages in *Vav*-cre$^-$ *Raptor^wt/fl* **(A)**, *Vav-Raptor* control **(B)**, *Vav*-cre$^+$*Raptor^wt/fl* **(C)** and *Vav-Raptor* KO **(D)** E15 FL, and the same of *Mx1-Raptor* control **(E)** and *Mx1-Raptor* cKO **(F)** BM. Plots are live and size (FSC-A/SSC-A) gated prior to the gating shown. RCN – relative cell number.
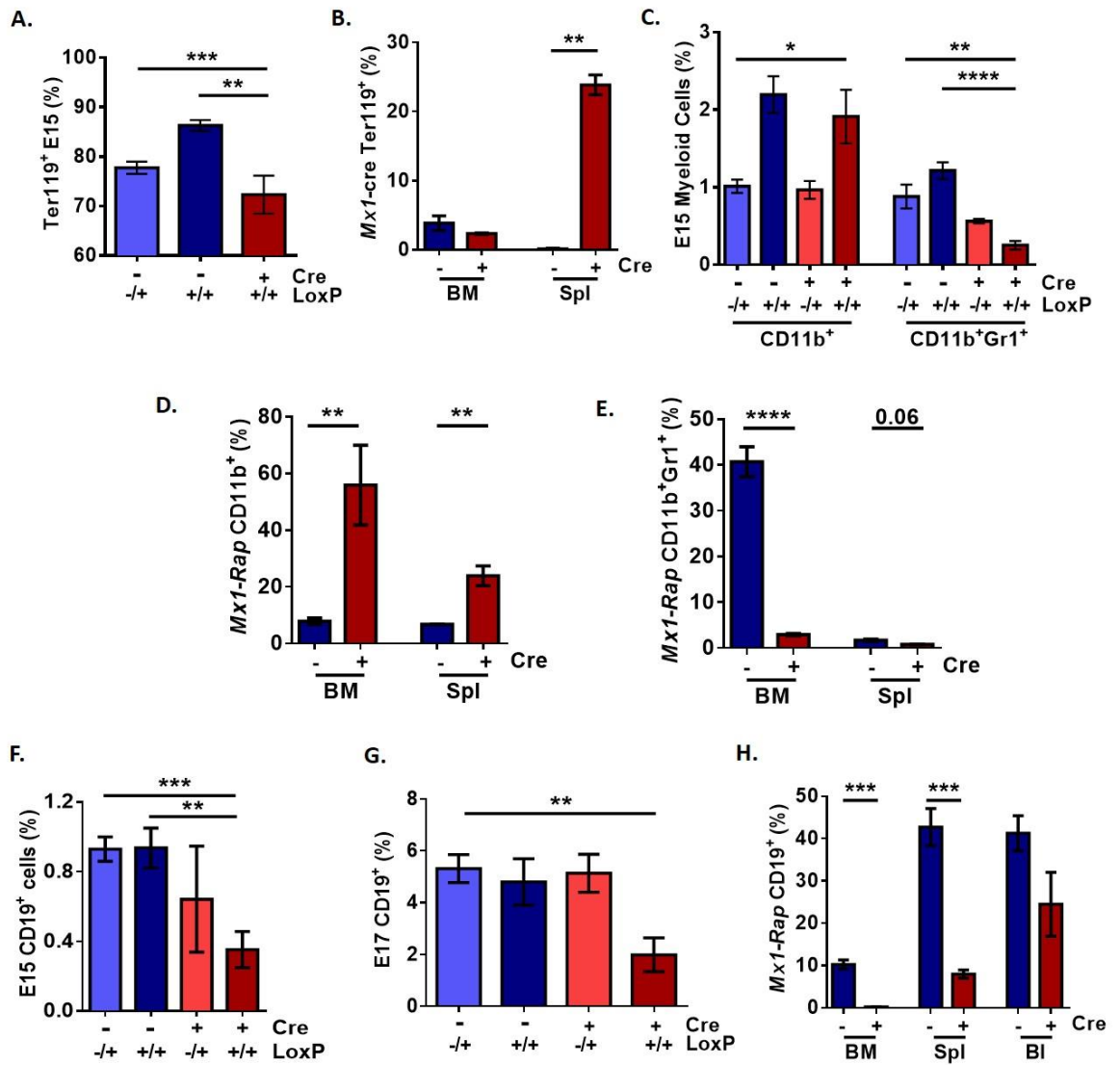
Figure 3.3: *Vav/Mx1*-cre⁺*Raptor^{fl/fl}* mice exhibit a disruption in haemopoiesis *in vivo.*
Graph demonstrating the percentage of surface expression of Ter119 in *Vav-Raptor* KO FL (n=7, cre+ ; loxP +/+) compared to *Vav*-cre⁻*Raptor^{wt/fl}* (n=10, cre- ; loxP -/+) and *Vav-Raptor* control (n=8, cre- ; loxP +/+) of E15 FL **(A)**, and in the BM and spleen of *Mx1-Raptor* cKO (cre+, red bars) compared to *Mx1-Raptor* control mice (cre-, blue bars) **(B)**. Flow cytometry graphs showing surface expression of percentage of CD11b⁺ myeloid population, and CD11b⁺Gr1⁺ myeloid lineage **(C)** in *Vav-Raptor* KO (n=8) compared to *Vav*-cre⁻*Raptor^{wt/fl}* (n=11), *Vav-Raptor* control (n=8) and *Vav*-cre⁺*Raptor^{wt/fl}* (n=6, cre+ ; loxP -/+) E15 FL. Flow cytometry data of BM and spleen of *Mx1-Raptor* cKO and *Mx1-Raptor* control mice showing surface expression of percentage of CD11b⁺ myeloid population **(D)** and CD11b⁺Gr1⁺ myeloid lineage **(E)**. Bar graphs showing expression of percentage of CD19⁺ B cells in *Vav*-cre⁻*Raptor^{wt/fl}*, *Vav-Raptor* control, *Vav*-cre⁺*Raptor^{wt/fl},* and *Vav-Raptor* KO FL at E15 **(F)** and E17 **(G)**, together with expression of percentage of CD19⁺ B cell population in the BM, spleen and blood in *Mx1-Raptor* cKO compared to *Mx1-Raptor* controls **(H)**. Data are expressed as mean±SEM (p *≤0.05, p **≤0.001, p ***≤0.0001, p ****≤0.00001).
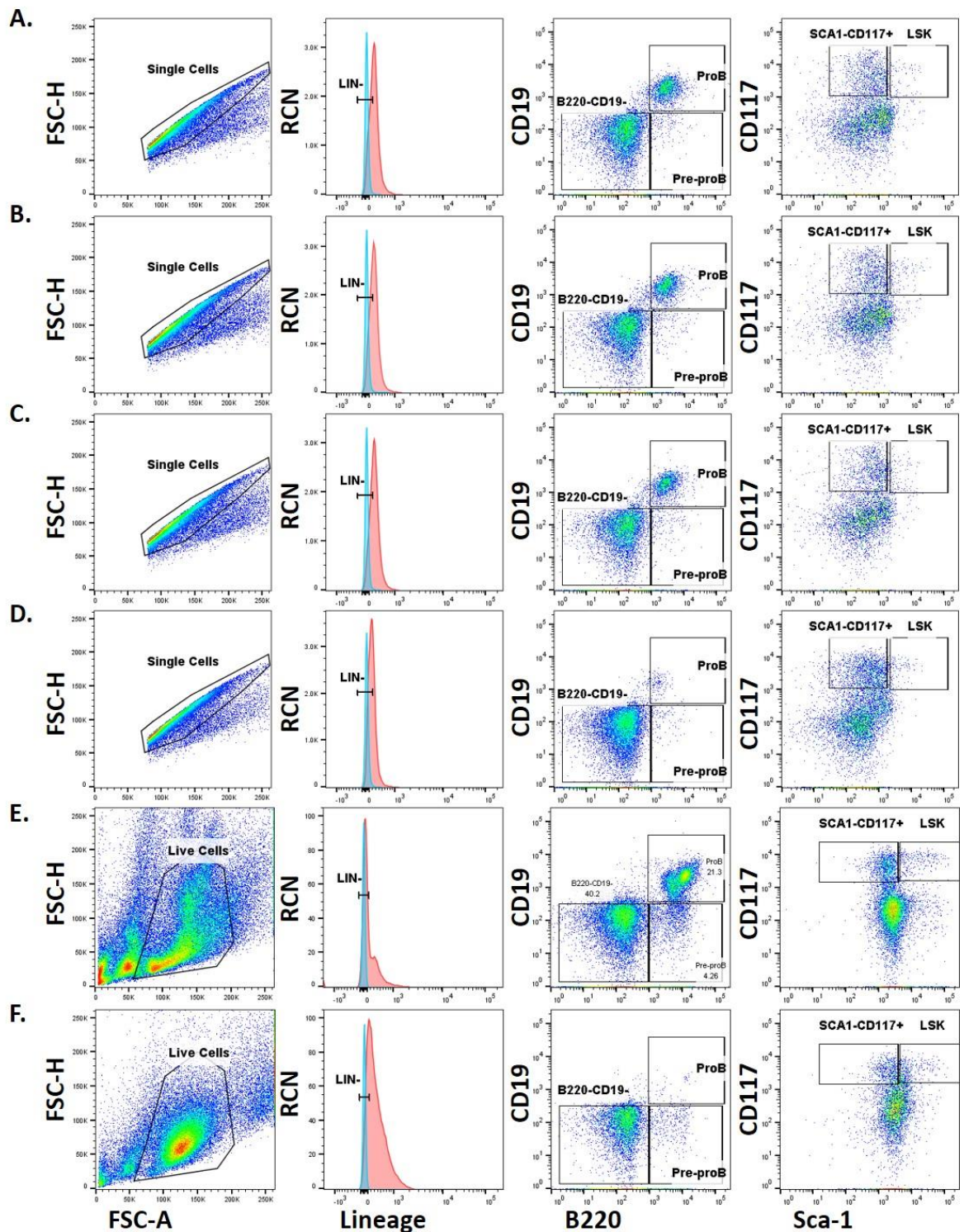
Figure 3.4: Gating strategy of progenitor cells and early B haemopoietic lineages in *Vav*-and *Mx1*-cre *Raptor* models.
Representative flow cytometry plots demonstrating the proportion of proB (Lin⁻B220⁺CD19⁺), pre-proB (Lin⁻B220⁺CD19⁻), Sca-1^{lo}CD117^{hi} (Lin⁻B220⁻CD19⁻ Sca-1^{lo}CD117^{hi}) and LSK (Lin⁻B220⁻CD19⁻ Sca-1⁺CD117⁺) cell populations in *Vav*-cre⁻*Raptor*$^{wt/fl}$ **(A)**, *Vav-Raptor* control **(B)**, *Vav*-cre⁺*Raptor*$^{wt/fl}$ **(C)** and *Vav-Raptor* KO **(D)** E15 FL, and the same in BM of *Mx1-Raptor* control **(E)** and *Mx1-Raptor* cKO **(F)** mice. Lin⁻ gating is done by taking into account the unstained control (blue peak), where the red peak represents Lin⁺ cells. Plots are live and size (FSC-A/SSC-A) gated prior to the gating shown. RCN – relative cell number.
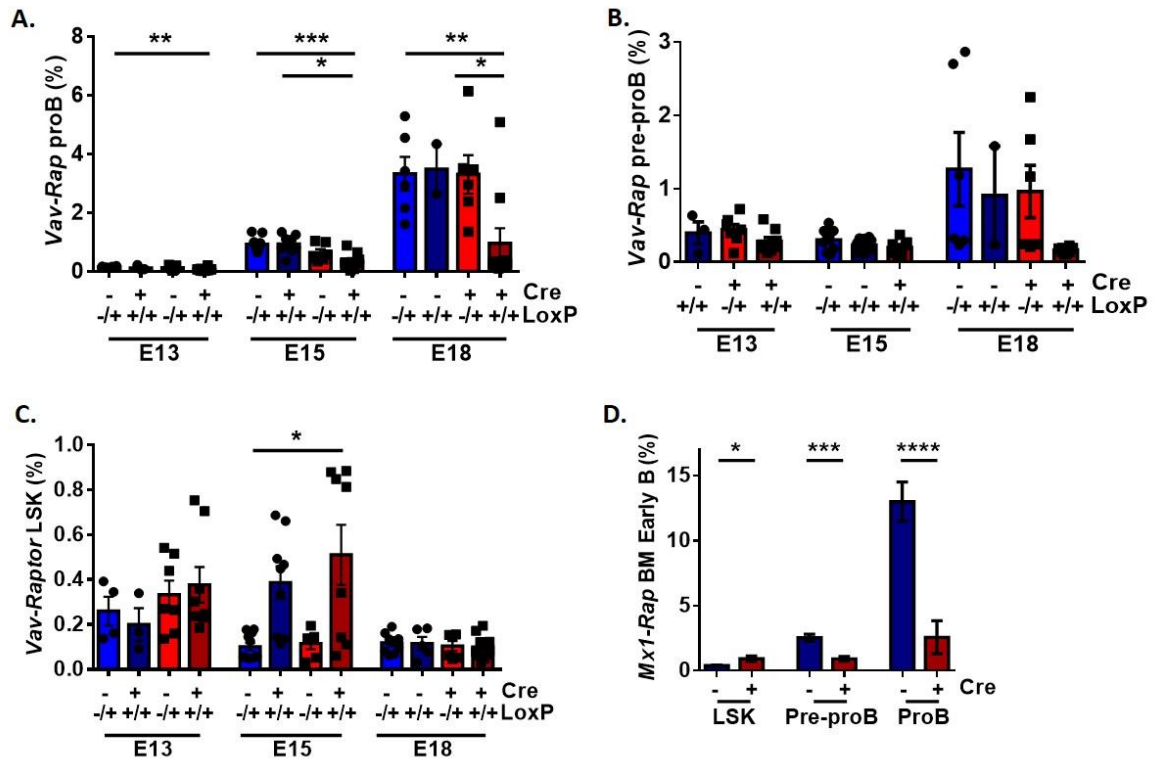
Figure 3.5: *Mx1-* and *Vav-cre⁺Raptor^{fl/fl}* mice exhibit a block in B cell development at the LSK stage.

Surface expression of percentage of proB (CD19⁺B220⁺) **(A)**, pre-proB (B220⁺CD19⁻) **(B)** and LSK **(C)**, populations in E13, E15, E18 in *Vav-*cre⁻*Raptor^{wt/fl}* (cre-, loxP -/+), *Vav-Raptor* control (cre-, loxP +/+), *Vav-*cre⁺*Raptor^{wt/fl}* (cre+, loxP -/+) and *Vav-Raptor* KO (cre+, loxP +/+) FL, and in BM of *Mx1-Raptor* control (blue, cre-) compared to *Mx1-Raptor* cKO (red, cre+) mice **(D)**. Data are expressed as mean±SEM (p *≤0.05, p **≤0.001, p ***≤0.0001, p ****≤0.00001).
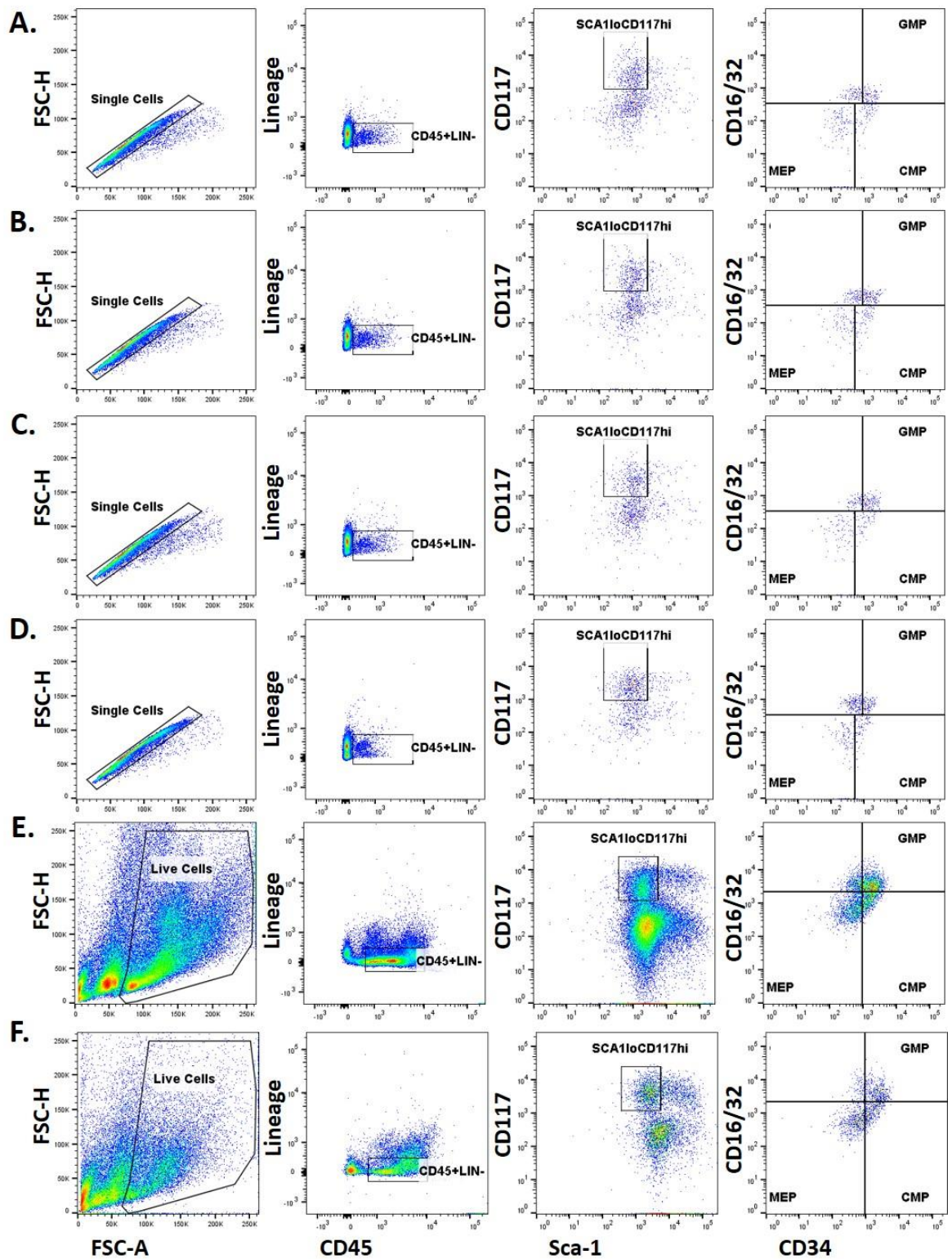
Figure 3.6: Gating strategy of early myeloid progenitors in *Vav-* and *Mx1-*cre *Raptor* models.
Representative flow cytometry plots demonstrating the proportion of Sca-1^{lo} CD117^{hi} cells, common myeloid progenitors (CMP) (CD45$^+$Lin$^-$Sca^{lo}CD117^{hi}CD34$^+$CD16/32$^-$), megakaryocyte-erythrocyte progenitors (MEP) (CD45$^+$Lin$^-$Sca^{lo}CD117^{hi}CD34$^-$CD16/32$^-$) and granulocyte-macrophage progenitors (GMP) (CD45$^+$Lin$^-$Sca^{lo}CD117^{hi}CD34$^+$CD16/32$^+$) cell populations in *Vav-*cre$^-$*Raptor$^{wt/fl}$* **(A)**, *Vav-Raptor* control **(B)**, *Vav-*cre$^+$*Raptor$^{wt/fl}$* **(C)** and *Vav-Raptor* KO **(D)** in E15 FL, and in BM of *Mx1-Raptor* control **(E)** and *Mx1-Raptor* cKO **(F)** mice. Plots are live and size (FSC/SSC) gated prior to the gating shown.
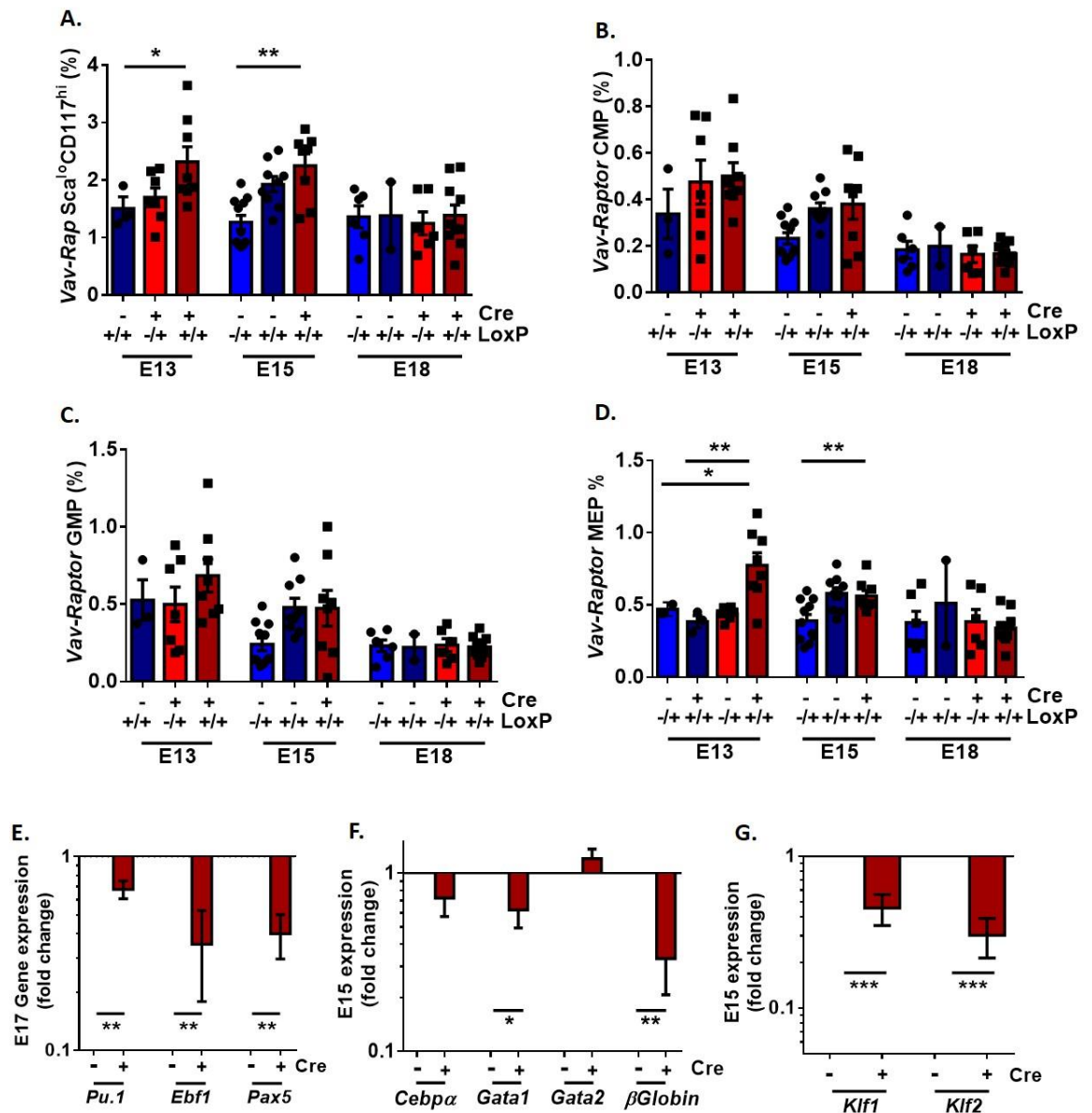
Figure 3.7: *Vav-Raptor* **KO mice exhibit a block in RBC development at MEP stage** *in vivo.*
Graph showing surface expression of percentage of S1^{lo}CD117^{hi} (Sca-1^{lo}CD117^{hi}) **(A)**, CMP **(B)**,
GMP **(C)**, MEP **(D)** populations in E13, 15, 18 FL in *Vav*-cre$^-$*Raptor*$^{wt/fl}$ (light blue, cre-, loxP -/+) and
Vav-Raptor control (blue, cre-, loxP +/+), *Vav*-cre$^+$*Raptor*$^{wt/fl}$ (pink, cre+, loxP -/+) and *Vav-Raptor*
KO (red, cre+, loxP +/+). Gene expression of E17 FL demonstrating the fold change (log$_{10}$) in *Pu.1,*
early B cell factor 1 (*Ebf1*), and *Pax5* **(E)**, along with fold changes (log$_{10}$) in gene expression of
Cebpα, *Gata1*, *Gata2*, *βGlobin* **(F)**, and Krüppel-like factor (*Klf1*) and *Klf2* **(G)** at E15 FL in *Vav-
Raptor* KO (cre+) compared to *Vav-Raptor* control (cre-) FL. Data are expressed as mean±SEM (p
*≤0.05, p **≤0.001, p ***≤0.0001).
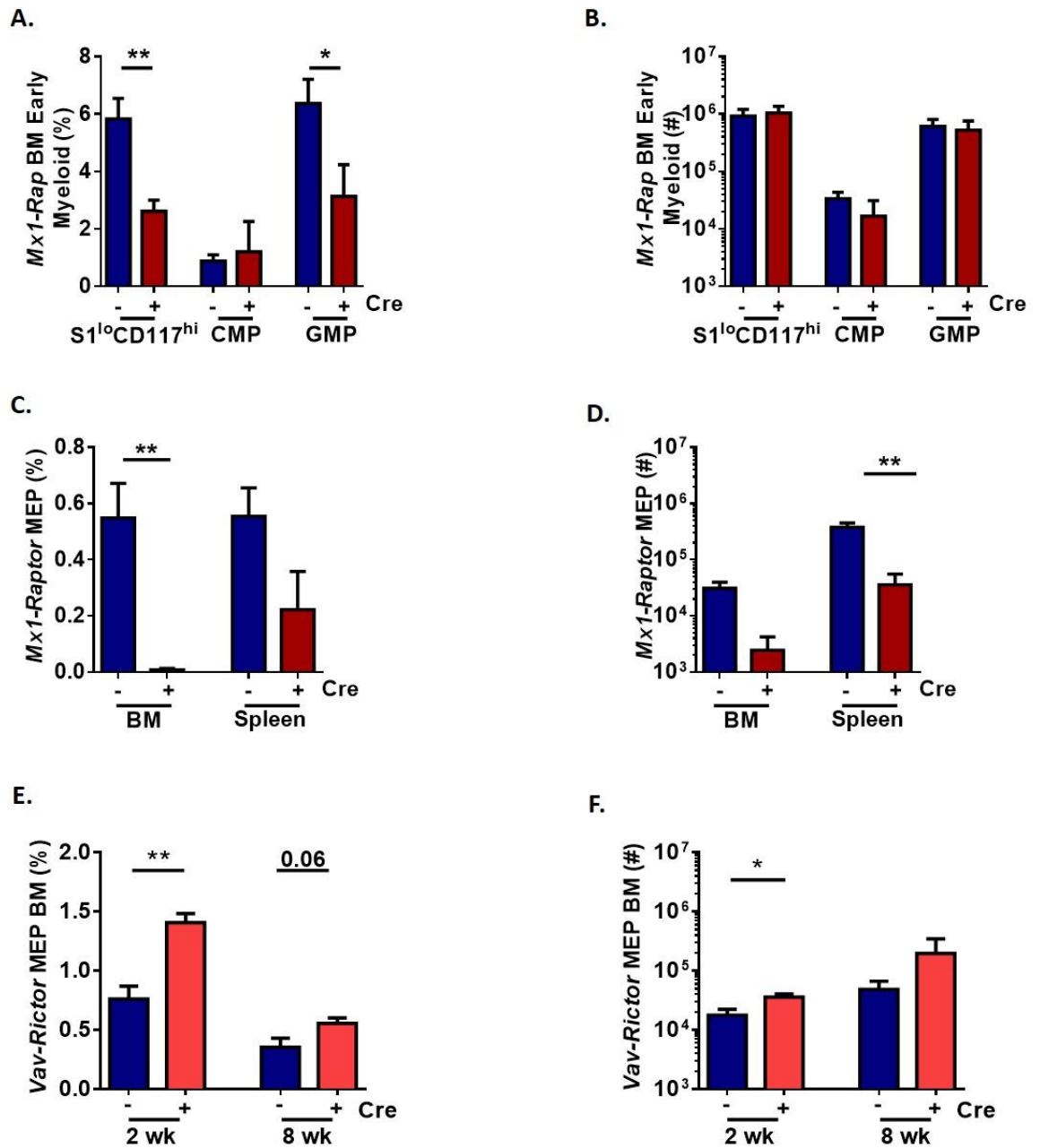
Figure 3.8: *Mx1-Raptor* **cKO mice have aberrations at the MEP stage with opposite trends in** *Vav-Rictor* **KO mice** *in vivo.*
Graph showing surface expression of the percentage **(A)** and cellularity **(B)** of S1^{lo}CD117^{hi} (Sca-1^{lo}CD117^{hi}), CMP, GMP populations in BM of *Mx1-Raptor* control (cre-) or *Mx1-Raptor* cKO (cre+) mice. Graph showing surface expression of the percentage **(C)** and cellularity **(D)** of MEP in BM of *Mx1-Raptor* control or *Mx1-Raptor* cKO mice. Graph showing surface expression of the percentage **(E)** and cellularity **(F)** of MEP in BM of *Vav*-cre^{-}*Rictor*$^{fl/fl}$ (*Vav-Rictor* control, cre-) or *Vav*-cre^{+}*Rictor*$^{fl/fl}$ (*Vav-Rictor* KO, cre+) mice. Data are expressed as mean±SEM (p *≤0.05, p **≤0.001, p ***≤0.0001, p ****≤0.00001).
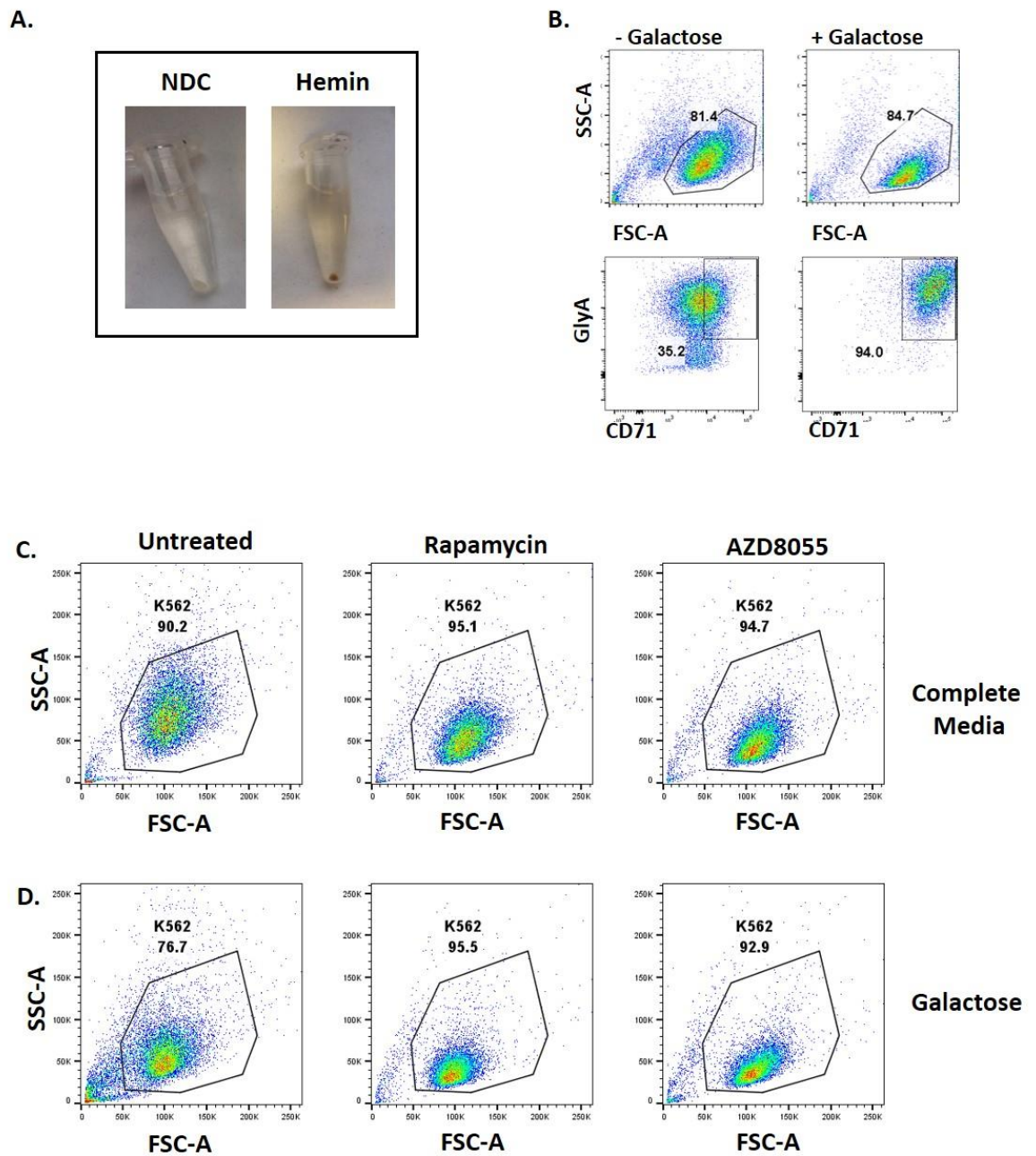
Figure 3.9: K562 cells differentiate into an erythrocyte-like lineage with changes in surface markers and size, which are changed with mTOR inhibitors.
A. Picture showing the colour change in the cell pellet confirming RBC-like differentiation upon treatment of 5×10^5 K562 cells with 50 μM hemin treatment till D5 (right) compared with the white pellet observed in untreated K562 cells (NDC – no drug control, left). **B.** Flow cytometry plots showing expression of CD71$^+$GlyA$^+$ population in K562 cells cultured in either complete media (-Galactose) or in Gal-media (+Galactose). Representative flow cytometry plots demonstrating changes in FSC-A and SSC-A in K562 cells cultured in complete media **(C)** or in Gal-media **(D)** with no drug (untreated; left) or treated with rapamycin (middle) or AZD8055 (right).
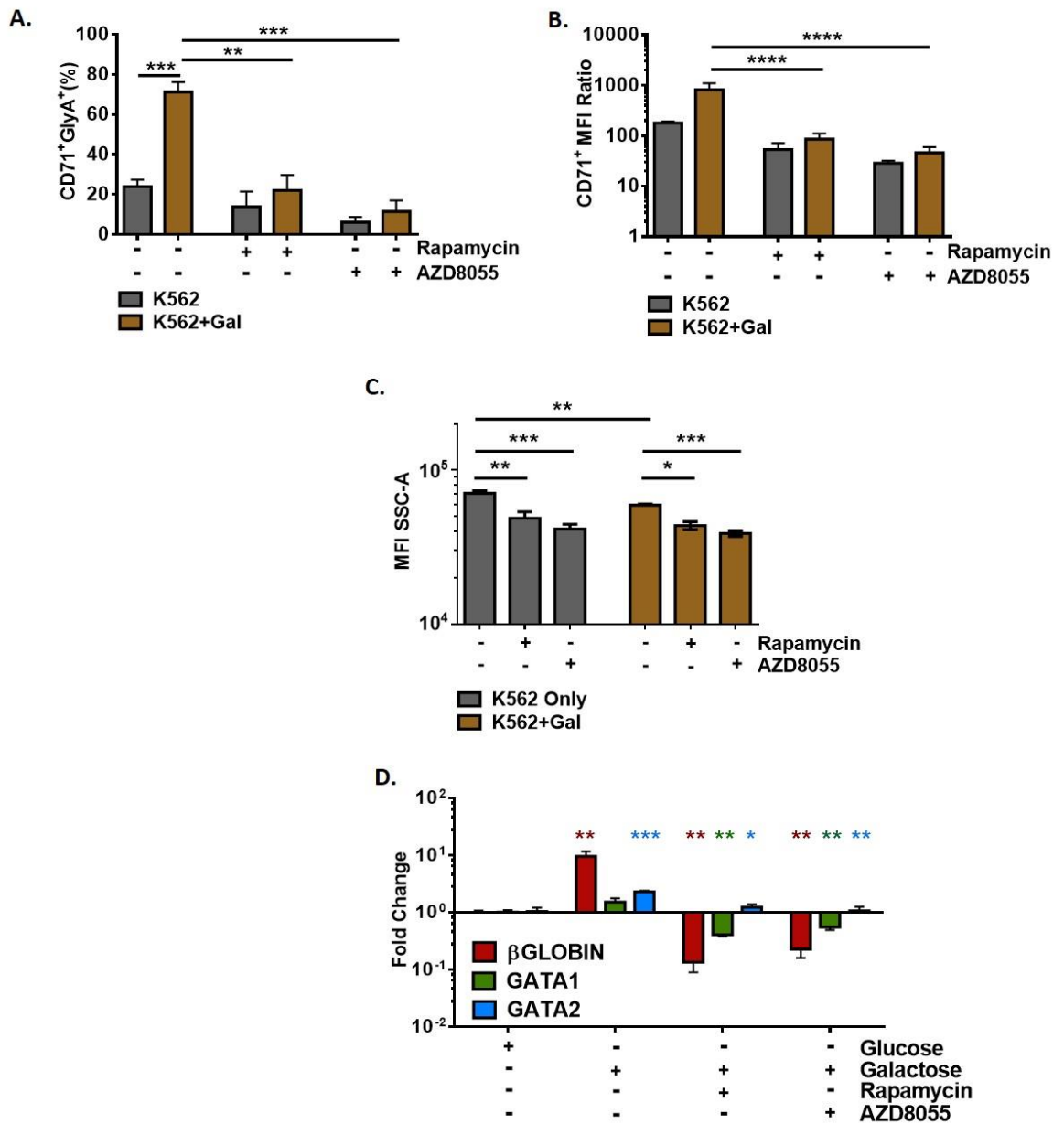
Figure 3.10: mTOR inhibitors abrogate RBC differentiation in a human cell model.
Percentage of CD71+GlyA+ surface expression **(A)**, mean fluorescent intensity (MFI) ratio of CD71+ erythroid cells **(B)** and MFI of side scatter area (SSC-A) **(C)** of K562 cells and K562 cells treated with mTOR inhibitors cultured in either complete media or in Gal-media. **D.** Gene expression data showing fold changes (log$_{10}$) of *β-GLOBIN, GATA1* and *GATA2* in K562 cells cultured in complete media and in Gal-media with or without mTOR inhibitors – rapamycin (mTORC1 inhibitor), AZD8055 (dual mTOR complex inhibitor). Data are expressed as mean±SEM (p *≤0.05, p **≤0.001, p ***≤0.0001, p ****≤0.00001).
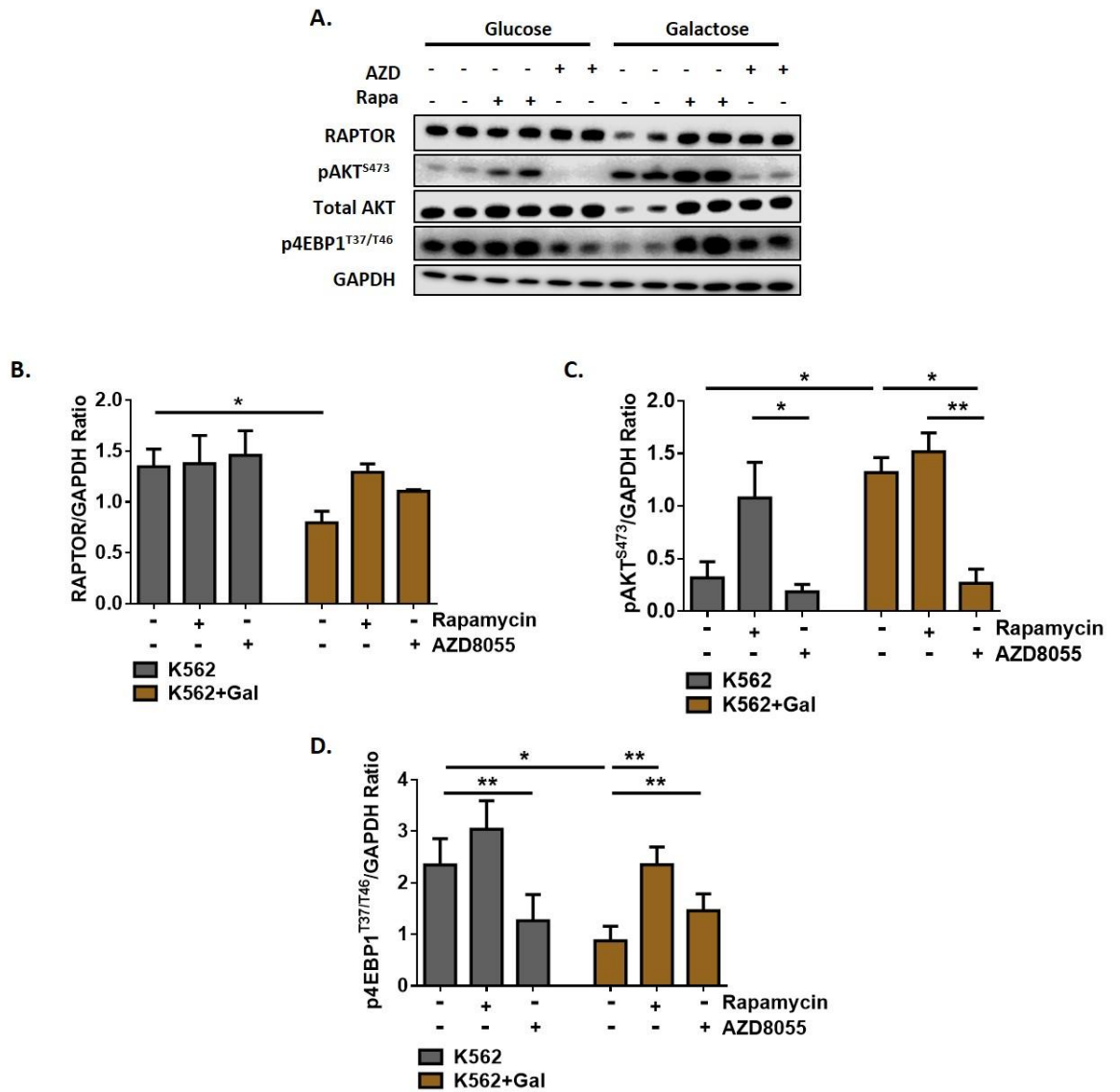
Figure 3.11: Proving the role of mTORC1 in the differentiation of RBCs in K562 cells at the phenotype and molecular level.
Representative western blot **(A)** and ratios of protein expression levels of RAPTOR/GAPDH **(B)**, pAKT^{S473}/GAPDH **(C)**, and p4EBP1$^{T37/T46}$/GAPDH **(D)** in K562 cells either cultured in complete media (with glucose) or in Gal-media and treated with AZD8055 (AZD) or rapamycin (rapa). Data are expressed as mean±SEM (p *≤0.05, p **≤0.001).
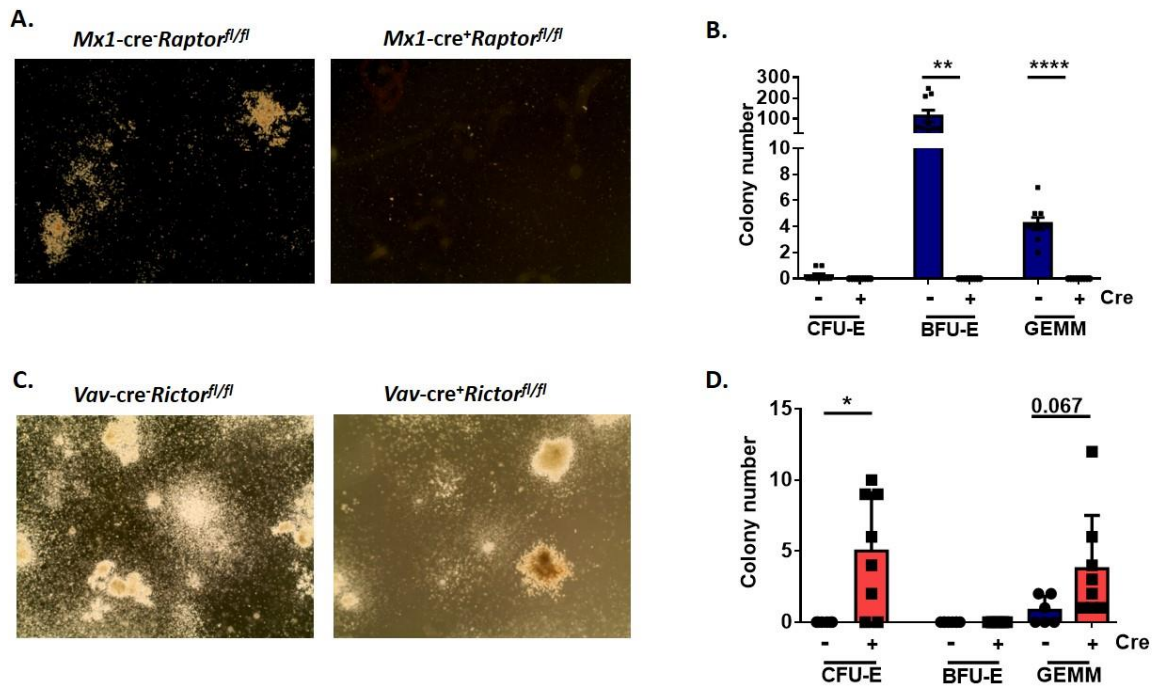
Figure 3.12: Demonstrating a functional block in RBC development in *Mx1-Raptor* cKO mice, together with an increase in RBC generation in *Vav-Rictor* KO mice.
A. CFCs which optimise for the growth of erythroid cells were carried out on *Mx1-Raptor* control (left) and *Mx1-Raptor* cKO (right) BM enriched for HPCs. **B.** Colony counts of different erythroid colonies: CFU-E, BFU-E and CFU-GEMM in *Mx1-Raptor* cKO models and in *Mx1-Raptor* controls. **C.** CFCs which optimise for the growth of HPCs were carried out on *Vav-Rictor* control (left) and *Vav-Rictor* KO (right) BM enriched for HPCs. **D.** Colony counts of different haemopoietic colonies: CFU-E, BFU-E and CFU-GEMM in *Vav-Rictor* KO models and in *Vav-Rictor* controls. Data are expressed as mean±SEM (p *≤0.05, p **≤0.001, p ***≤0.0001, p ****≤0.00001).

Chapter 4

Role of mTORC1 and mTORC2 in Lymphopoiesis

4 Role of mTORC1 and mTORC2 in lymphopoiesis

4.1 Aims and Objectives

The mTOR pathway has previously known to play an important role in haemopoiesis(282). Here, we use the cre-loxP system to individually KO *Raptor* (mTORC1) and *Rictor* (mTORC2) at different stages of development to assess the individual roles of the mTOR complexes during haemopoiesis. The complexes were removed at the HSC stage (*Vav*-cre model) resulting in a KO specifically in haemopoietic lineage cells, in the whole organ system in adult mice by using the cKO system (*Mx1*-cre model) and specifically in B cells by using the *CD19*-cre model. This enabled us to determine the exact role of mTORC1 and mTORC2 in haemopoiesis and allowed us to elucidate the stages at which these complexes play a role (if any) in lineage development/commitment.

4.2 Results

4.2.1 Mice with induced *Raptor* deficiency at an adult stage exhibit optimal characteristics of KO when assessed 5 wk post 4 poly(I:C) inoculations.

As the *Vav-Raptor* KO mouse model is lethal at the perinatal stage (Chapter 3, Figure 3.1), two mTORC1 KO models, the *Mx1*-cre and *CD19*-cre models were used to assess the role of mTORC1 in adult mice and specifically in B cells respectively, during normal haemopoiesis. As the cKO system in the *Mx1*-cre model is dependent upon the inoculation of poly(I:C), it was essential to optimize the cKO system, assessing the dose of poly(I:C) to be given to the mice, and the time taken to induce the cKO. Due to the discrepancies in the dosage of poly(I:C), in terms of number and concentration, along with the timeline at which these mice were assessed in previous literature(91,263), optimization of this model was carried out with variables being the number of doses (3, 4, 5 inoculations on alternate days) and time of analysis after inoculations (3, 5, 8, 10 wk) at 10 mg/kg poly(I:C).

Mx1-cre⁻*Raptorᶠˡ/ᶠˡ* (*Mx1-Raptor* control) and *Mx1*-cre⁺*Raptorᶠˡ/ᶠˡ* (*Mx1-Raptor* cKO) mice, inoculated with 3 doses of 10 mg/kg poly(I:C) every alternate day, were assessed at 3, 5, 8 or 10 wk post the last inoculation. There was significant splenomegaly in *Mx1-Raptor* cKO spleens 5 and 8 wk post poly(I:C) inoculation with similar trends 3 and 10 wk post inoculation compared to *Mx1-Raptor* controls (Figure 4.1A). Although there was no trend in increase in spleen organ cellularity, there was a greater difference between *Mx1-Raptor* cKO splenic organ cellularity 5 wk post poly(I:C) compared to analysis at other weeks (Figure 4.1B). Moreover, there was no significant difference in BM or LN organ cellularity over time, however there was a strong trend in decrease in *Mx1-Raptor* cKO LN organ cellularity 5 wk post poly(I:C), and a significant decrease in thymic cellularity in *Mx1-Raptor* cKO mice 5 wk after 3 poly(I:C) inoculations compared to control mice (Figure 4.1C-E). These data suggested that the cKO was more pronounced 5 wk post 3 poly(I:C) inoculations compared to earlier or later weeks. To test whether increasing the dose frequency would improve the cKO model, the frequency of the dose was increased from 3 to 5 doses at 10 mg/kg poly(I:C) and the mice were assessed 5 wk post inoculation. Greater

splenomegaly was noted in *Mx1-Raptor* cKO mice with 5 poly(I:C) doses compared to those with 3 doses. These cKO mice exhibited a significant increase in splenic cellularity and a decrease in thymic cellularity, with no changes in BM and LN cellularity compared to 5 wk 5 poly(I:C) control mice (Figure 4.1F&G).

To assess the *Mx1-Raptor* cKO model treated with 3 and 5 doses of poly(I:C), B cell lineage was assessed at different developmental stages, compared to *Mx1-Raptor* controls. There was a trend in increase in percentage of lineage⁻sca-1⁺CD117⁺ (LSK) population, and a significant increase in LSK cellularity in the BM of *Mx1-Raptor* cKO mice compared to *Mx1-Raptor* controls with 5 doses compared with 3 doses of poly(I:C) (Figure 4.2A,B,E,F). Additionally, with 3 doses of poly(I:C), there was a significant decrease in the percentage of pre-proB cells (lin⁻B220⁺CD19⁻) after 3 and 10 wk, with a greater significant reduction at 5 wk post inoculation, and a significant decrease in the pre-proB cell cellularity in the BM 5 wk post inoculation in *Mx1-Raptor* cKO mice compared to controls (Figure 4.2C,D). A similar trend in percentage and cellularity decrease of pre-proB cells was noted in the BM with a trend in increase of the same in the spleen 5 wk post 5 poly(I:C) inoculation in *Mx1-Raptor* cKO mice compared to controls (Figure 4.2G,H). These results suggested that there may be a block in B cell lineage commitment in the *Mx1-Raptor* cKO mouse model, which was supported by a significant decrease in the percentage of mature B cell (CD11b⁻CD19⁺) lineage in the BM and spleen 3, 5 and 10 wk post 3 poly(I:C) inoculation, coupled with a decrease in B cell lineage percentage in the blood at 5 and 8 wk post 3 poly(I:C) inoculation. Similar trends were seen in the LN across the weeks in *Mx1-Raptor* cKO mice compared to *Mx1-Raptor* controls (Figure 4.3A). *Mx1-Raptor* cKO mice assessed 5 wk post 5 poly(I:C) doses showed a significant decrease in B cell lineage percentage in the BM, spleen and thymus and a decreasing trend in the blood compared to *Mx1-Raptor* controls (Figure 4.3B). Lastly, to determine whether late stages of B cell development were also affected in *Mx1-Raptor* cKO mice, and to compare 5 doses of poly(I:C) treatment with 3 doses, the presence of the following B cell populations were assessed. *Mx1-Raptor* cKO mice treated with 3 poly(I:C) doses showed a significant decrease in percentage of transitional 1 (T1, CD19⁺CD23⁻IgM^hiCD21^int) B cell population after 3 wk, together with a decrease in percentage of fol1 (CD19⁺CD23⁺CD21^loCD1d^intIgD^hiIgM^loAA4.1⁻) B cells after 5 wk, and a decrease in

percentage of fol2 (CD19$^+$CD23$^+$CD21^{lo}CD1d^{int}IgD^{hi}IgM^{hi}AA4.1$^-$) B cells after 3, 5 and 10 wk in the spleen compared to controls (Figure 4.4A&B). Similarly, treatment of mice with 5 poly(I:C) doses showed *Mx1-Raptor* cKO mice exhibit a significant decrease in the percentage of T1, T3 (CD19$^+$CD23$^+$CD21^{int}CD1d^{int}IgD^{hi}IgM^{lo}AA4.1$^+$), MZ (CD19$^+$CD23$^-$IgM^{hi}CD21^{hi}) and fol2 B cells with a trend of a decrease in T2 (CD19$^+$CD23$^+$CD21^{int}CD1d^{int}IgD^{hi}IgM^{hi}AA4.1$^+$), fol1 and MZP (CD19$^+$CD23$^+$CD21^{hi}CD1d^{hi}) percentages in the spleens compared to controls (Figure 4.4C&D).

These data suggest that analysis of the mice 5 wk post 5 poly(I:C) inoculations results in a more potent cKO compared to 3 poly(I:C) doses. However, treatment of mice aged >18 wk with 5 poly(I:C) doses resulted in death soon after the last poly(I:C) dose (data not shown), therefore 5 poly(I:C) inoculations was considered too severe. Thus, for the remainder of the experiments, we treated mice with 4 poly(I:C) inoculations and assessed them at 5 wk post the last injection. The cKO in mice with 4 poly(I:C) inoculations was as robust as seen in cKO mice with 5 poly(I:C) inoculations as indicated by the spleen weight (mg) in *Mx1-Raptor* cKO mice with 3, 4 and 5 poly(I:C) injections assessed after 5 wk (Figure 4.6A), and *Raptor* expression data (see below – Figure 4.7). Before proceeding with additional experiments, it was vital to assess whether the transgenic cre-loxP system initiates phenotypic changes in mice compared to WT mice without the cre-loxP background. Therefore, phenotypic analyses of different haemopoietic lineages were compared between *Mx1-Raptor* control and WT mice assessed 5 wk post 10 mg/kg 4 poly(I:C) inoculations. As expected, no significant difference was seen between the spleen weight or whole organ counts of the BM, spleen and thymus between the two sets of mice. Furthermore, there was no significant difference in the percentage and cellularity of CD19$^+$ B cells and CD11b$^+$Gr1$^+$ mature myeloid cells in the BM, spleen and thymus along with no difference in CD4$^+$CD8$^+$ DP and CD4$^-$CD8$^-$ DN T cell populations in the thymus (Figure 4.5) suggesting that both the *Mx1-Raptor* control and WT mice are phenotypically similar after treatment with poly(I:C), thereby defining *Mx1-Raptor* control mice as a 'wildtype' reference for comparison to *Mx1-Raptor* cKO mice.

4.2.2 mTORC1 plays a role in developmental haemopoiesis *in vivo.*

To assess the role of mTORC1 in normal B lymphopoiesis, *Mx1*-cre and *CD19*-cre models were used which KO *Raptor* in adult mice upon poly(I:C) inoculation (*Mx1-Raptor* cKO) and specifically in B cells at the proB cell stage (*CD19-Raptor* KO). As seen in Section 4.2.1, *Raptor* deficiency in adult mice led to a significant increase in splenic weight and cellularity along with similar trend towards an increase in the BM, and a significant decrease in thymic cellularity (Figure 4.6A&B). To further analyse the spleen in *Mx1-Raptor* cKO mice with splenomegaly, H&E staining was carried out, which demonstrated a disruption of splenic architecture with a lack of GC and MZ and an increase in red pulp. Ki67 staining was increased suggesting increased cell cycling/proliferation (Figure 4.6C) in *Mx1-Raptor* cKO mice compared to *Mx1-Raptor* controls. As the *CD19*-cre model excises *Raptor* solely in B cells, there was no difference in the spleen weight between *CD19*-cre⁻*Raptor*$^{fl/fl}$ (*CD19-Raptor* control) and *CD19*-cre$^{+/-}$*Raptor*$^{fl/fl}$ (*CD19*-cre$^{+/-}$*Raptor* KO) mice. However, there was a significant decrease in the spleen weight along with BM and spleen cellularity in *CD19*-cre$^{+/+}$*Raptor*$^{fl/fl}$ mice (*CD19*-cre$^{+/+}$*Raptor* KO) compared to both the *CD19-Raptor* control and *CD19*-cre$^{+/-}$*Raptor* KO mice (Figure 4.6D&E).

To confirm the cKO in *Mx1-Raptor* cKO mice, levels of Raptor were assessed at the protein and genomic levels. Although there was no signal in the BM at the protein level, there was a significant decrease in RAPTOR expression in the spleen and thymus. Furthermore, there was a trend towards a decrease in RICTOR expression in the spleen, and a significant decrease in the thymus of *Mx1-Raptor* cKO mice compared to controls (Figure 4.7A-C). These data were supported by a significant decrease in *Raptor* expression in the BM, spleen and liver, coupled with a decreasing trend in *Rictor* expression in the spleen (Figure 4.7F&G) of *Mx1-Raptor* cKO mice compared to control mice. These data confirm that *Raptor* is excised upon treatment with poly(I:C) in adult *Mx1-Raptor* cKO mice.

The representative Western blot also showed a decrease in t4EBP1 expression in the BM, spleen and thymus and a similar trend in reduction of p4EBP1$^{T37/T46}$/isotype MFI ratio in the BM, spleen and thymus of mice with

Raptor-deficiency (Figure 4.7A,D). However, no reduction in pAKT^{S473} or pS6$^{S235/S236}$ was seen in the absence of *Raptor* expression (Figure 4.7A&E).

To assess the effect of *Raptor*-deficiency in adult mice on all major haemopoietic lineages, surface markers for B, T, myeloid and NK cells were assessed in the BM, spleen, thymus, LN and blood. A significant reduction in CD19$^+$CD11b$^-$ B cell lineage percentage was observed in the BM (Figure 4.8A&B) and spleen, together with a significant decrease in B cell cellularity in the BM and thymus. No difference in the B cell splenic cellularity was seen due to the significant increase in splenic cells altogether in *Mx1-Raptor* cKO mice compared to controls (Figure 4.6B, Figure 4.9A&B). Furthermore, there was a significant decrease in percentage of CD11b$^+$Gr1$^+$ mature myeloid population in the BM (Figure 4.8A&B) and blood, while significantly increased in the spleen and LN, with similar trends noted in cellularity of CD11b$^+$Gr1$^+$ myeloid population in *Mx1-Raptor* cKO mice (Figure 4.8A&B, Figure 4.9C&D). Analysing the CD11b$^+$Gr1$^-$ immature myeloid population, there was a significant increase in percentage of this population in the BM and spleen (data not shown). A significant decrease in NK cells percentage was observed in the BM and spleen, with a significant decrease in cellularity of NK cells in the thymus (Figure 4.8A&B, Figure 4.9E&F). Analysing T lineage cells in the thymus, a significant decrease in the percentage and cellularity of CD4$^+$CD8$^+$ DP thymocytes was seen, together with a significant increase in percentage of CD4$^-$CD8$^-$ DN thymocytes, however the CD4$^-$CD8$^-$ population cell number remained largely unchanged (Figure 4.8A&B, Figure 4.9G&H) in *Mx1-Raptor* cKO mice compared to controls. There was also an increase in percentage of CD8$^+$ T cells with no change in CD4$^+$ T cell lineage with *Mx1-Raptor* cKO compared to controls (data not shown). These data suggest a significant role of mTORC1 in B cell development and a role in myeloid and T cell lineages *in vivo*.

The *Mx1*-cre model excises *Raptor* in all haemopoietic tissues, enabling analysis of *Raptor*-deficiency in various haemopoietic organs and cell lineages, generating results that were consistent with previously published data (282). However, by generating *Raptor*-deficiency specifically in B cells in the *CD19-cre* model, we wanted to assess the extent of this deficiency in B cells and whether the KO affected the ratio and composition of other haemopoietic lineages. Analysing the *CD19*-cre$^{+/-}$*Raptor* KO mice initially, there was a significant

decrease in percentage and cellularity of CD19$^+$ B cell lineages in the BM and LN, with a further significant decrease in the percentage of CD19$^+$ B cells in the spleen and blood compared to *CD19-Raptor* controls (Figure 4.8C&D, Figure 4.10A&B). However, as we solely assessed CD19$^+$ B cells, it is important to note that there still exist early B cells, just not B cells with CD19 as a marker. The percentage of NK cells in the spleen of *CD19*-cre$^{+/-}$*Raptor* KO mice increased significantly with no other changes in other haemopoietic lineages compared to controls (Figure 4.8C&D, Figure 4.10C-H). Assessment of *CD19*-cre$^{+/+}$*Raptor* KO mice revealed a significant reduction in B cell lineage percentage and cellularity in BM, spleen and LN together with reduction in percentage in the blood compared to both *CD19*-cre$^{+/-}$*Raptor* KO and control mice as expected (Figure 4.8C-E, Figure 4.10A&B). There was also a significant increase in the percentage of mature myeloid cells in the spleen coupled with an increase in NK cell lineage population in the BM and spleen in *CD19*-cre$^{+/+}$*Raptor* KO mice (Figure 4.8C-E, Figure 4.10C&E). Moreover, a significant decrease in the cellularity of CD11b$^+$Gr1$^+$ myeloid cells and NK cells was observed with no changes in T cell lineage in *CD19*-cre$^{+/+}$*Raptor* KO mice compared to *CD19*-cre$^{+/-}$*Raptor* KO mice (Figure 4.10D,F-H). These data suggest that *CD19*-cre$^{+/-}$*Raptor* KO mice do indeed have a decline in B cell lineage across haemopoietic organs compared to controls with a compensatory increase in the percentage of NK cells. However, changes in B cell percentage/cellularity is expected in *CD19*-cre$^{+/+}$*Raptor* KO mice due to the placement of the cre recombinase gene within the first coding exon of *CD19* antigen gene thereby blocking the expression of CD19 altogether (283). Thus, *CD19*-cre$^{+/-}$*Raptor$^{fl/fl}$* mice were considered the KO mice, while *CD19*-cre$^{+/+}$*Raptor* KO mice were disregarded for further analyses of early and late B cell phenotyping due to the lack of CD19 antigen expression.

In order to further assess the nature of B cell subsets affected by *Raptor*-deficiency, late B cell subsets were analysed in the spleen and LN of control, *Mx1-Raptor* cKO and *CD19*-cre$^{+/-}$*Raptor* KO mice. There was a significant decrease in the percentage of T2, MZP, MZ and fol2 cells in the spleen along with decreasing trends in the percentage of T2, MZ and fol2 cells in the LN of *Mx1-Raptor* cKO mice compared to controls (Figure 4.11A&B, Figure 4.12). However, these changes were not mirrored by changes in cellularity of late B

cell subsets in the spleen or LN likely due to the increase in splenic organ cellularity with *Mx1-Raptor* cKO.

Analysis of the splenic late B cell populations in *CD19*-cre^{+/-}*Raptor* KO mice revealed a similar phenotype to *Mx1-Raptor* cKO mice, with a significant decrease in percentage of T2, MZP, MZ and fol2 late B cell populations in the spleen compared to controls (Figure 4.11C&D, Figure 4.13A&C). Additionally, there was a significant decrease in percentage of fol1 and fol2 cells in the LN together with a decrease in cellularity of T2 population in the spleen and fol2 population in the LN in *CD19*-cre^{+/-}*Raptor* KO mice compared to controls (Figure 4.13B,G&H).

The role of mTORC1 on B cell viability was assessed by analysing apoptotic markers (Annexin V/7AAD) in BM cells. Induced *Raptor*-deficiency in adult *Mx1-Raptor* cKO mice led to a significant decrease in percentage and cellularity of viable B cells (CD19$^+$AnnV$^-$7AAD$^-$) and increased apoptotic cells (CD19$^+$AnnV$^+$7AAD$^+$), with a significant decrease in the percentage of early apoptotic B cells (CD19$^+$AnnV$^+$7AAD$^-$) in the BM compared to controls (Figure 4.14A&B, Figure 4.15A&B). While there was an increase in apoptosis in B cells with *Raptor*-deficiency, there were only trends towards an increase in apoptotic cells in all haemopoietic cells, with a significant decrease in percentage of early apoptotic cells and an increase in 7AAD$^+$ cells in the BM in *Mx1-Raptor* cKO mice (Figure 4.15C&D). As there was an increase in apoptosis in B cells with *Raptor*-deficiency in adult mice, the *CD19*-cre model was assessed to determine whether a similar trend was observed. Indeed, there were trends of an increase in the percentage of apoptosis, with a decrease in viability in B cells in *CD19*-cre^{+/-}*Raptor* KO BM compared to controls, with no difference in all cells (Figure 4.14C&D, Figure 4.15E-H). These data suggest that *Raptor*-deficiency in B cells causes death by apoptosis without affecting other haemopoietic lineages.

4.2.3 mTORC2 plays a role in later stages of development.

To assess the role of mTORC2 in haemopoiesis, *Vav*-cre *Rictor$^{fl/fl}$*, *Mx1*-cre *Rictor$^{fl/fl}$* and *CD19*-cre *Rictor$^{fl/fl}$* KO models were generated and analysed to determine whether the role of mTORC2 differed when removed at the HSC stage vs. in all haemopoietic lineages of adult mice. Moreover, to specifically assess

the role of mTORC2 in B cells, the *CD19*-cre *Rictor$^{fl/fl}$* model was used. As with *Raptor*-KO models, it was vital to first determine the optimal timepoints (for the *Vav*-cre *Rictor$^{fl/fl}$*) and frequency of inoculations of poly(I:C) (*Mx1*-cre *Rictor$^{fl/fl}$*) for the mouse models.

To determine the optimal timepoint for phenotypic changes in haemopoietic lineages upon *Rictor*-deficiency at the HSC stage, *Vav*-cre⁻*Rictor$^{fl/fl}$* (*Vav-Rictor* control) mice and *Vav*-cre⁺*Rictor$^{fl/fl}$* (*Vav-Rictor* KO) mice were analysed at E18 (data not shown), 2, 8, and 24 wk of age. A significant decrease in splenic weight was seen at all ages (Figure 4.16B). Additionally, splenic cellularity was reduced at 2 and 8 wk of age, along with a decreasing trend in LN cellularity at all ages (Figure 4.16C).

B cell cellularity was significantly reduced in the spleen at 8 wk with similar trends in the percentage and cellularity over different ages in the spleen of *Vav-Rictor* KO mice (Figure 4.16D&E). Due to the known role of mTORC2 in T cell development (284), surface markers of haemopoietic lineages were analysed to assess the effect of *Rictor*-deficiency at the HSC stage over different age groups. A significant decrease in the percentage of CD4⁺CD8⁺ DP thymocytes cells was seen with a concomitant increase in CD4⁻CD8⁻ DN T cells in the thymus at 8 and 24 wk of age in *Vav-Rictor* KO mice compared to controls. Furthermore, there was a significant decrease in cellularity of CD4⁺CD8⁺ DP T cells at 8 wk in *Vav-Rictor* KO mice compared to controls (Figure 4.17A&B). NK cell lineage cellularity significantly decreased in the spleen at 8 wk in *Vav-Rictor* KO mice compared to control due to the significant decrease in splenic cellularity in *Vav-Rictor* KO mice (Figure 4.16B, Figure 4.17E&F). No other changes in other haemopoietic lineages (including myeloid lineage) were observed in mice over weeks (Figure 4.17C&D), which led us to conclude that *Vav-Rictor* KO mice at 8 wk time was the optimal timepoint to view phenotypic changes in the *Vav-Rictor* KO model.

Mx1-cre⁺*Rictor$^{fl/fl}$* (*Mx1-Rictor* cKO) mice assessed 5 wk post 4 inoculations of poly(I:C) had a more pronounced phenotype by the cKO compared to mice assessed 3 wk post 4 poly(I:C) inoculations (data not shown). *Rictor*-deficiency at the HSC stage, in adult mice and in B cells specifically led to a significant decrease in spleen weight together with a significant or decreasing trend in

spleen organ cellularity compared to controls (Figure 4.16A, Figure 4.18A-B). Furthermore, there was a significant decrease in thymic and LN cellularity in *Mx1-Rictor* cKO mice with similar trends of the same in *Vav-Rictor* KO mice compared to controls (Figure 4.18B). A significant loss in splenic architecture was observed in *Vav-Rictor* KO mice compared to controls, with an increase in Ki67 staining. No visible changes in pS6$^{S235/S236}$ staining was seen with loss in splenic architecture in mice with *Rictor*-deficiency at the HSC stage. On the contrary, *Mx1-Rictor* cKO mice did not lead to a complete loss in splenic architecture and showed an increase in Ki67 and pS6$^{S235/S236}$ staining within the GCs suggesting increased proliferation/cell cycling in these regions of the spleen compared to controls. Additionally, unlike in *Vav-Rictor* KO mice, *Mx1-Rictor* cKO spleens also had an increased MZ area as compared to controls (Figure 4.18C&D) alluding to accumulation of MZ B cell population. Successful KO of *Rictor* at the HSC stage and in adult mice was confirmed by a significant decrease in RICTOR expression in the spleen with a decreasing trend in the thymus of *Vav-Rictor* and *Mx1-Rictor* KO models coupled with a significant decrease in RICTOR expression in the liver in *Mx1-Rictor* cKO mice compared to controls (Figure 4.19A-C,F). Furthermore, *Rictor*-deficiency was confirmed by a reduction in *Rictor* expression in the BM, spleen and thymus in *Vav-Rictor* KO mice and in the BM, spleen and liver in *Mx1-Rictor* cKO mice compared to controls (Figure 4.19I&K). This was coupled with a significant decrease in downstream target pAKT^{S473} in the BM and spleen with a decreasing trend in the thymus of *Vav-Rictor* KO mice with similar decreasing trends in the BM of *Mx1-Rictor* cKO mice compared to controls. As expected, RAPTOR expression was unaffected by *Rictor*-deficiency (Figure 4.19D,E,G,H,J,L). These studies suggest a cleaner KO in the *Vav*-cre *Rictor$^{fl/fl}$* model as compared to the *Mx1*-cre *Rictor$^{fl/fl}$* model.

To assess the extent by which *Mx1*- and *CD19-Rictor* KO models differ from the *Vav-Rictor* KO model, different haemopoietic lineages were assessed in all three models. *Mx1-Rictor* cKO and *Vav-Rictor* KO mice exhibited a significant decrease in the CD4$^+$CD8$^+$ DP T cell percentage, together with an increase in percentage of CD4$^-$CD8$^-$ DN T cells in the thymus (Figure 4.20, Figure 4.21D-F). There was no change in CD4$^+$ T cells with an increasing trend in CD8$^+$ T cells with *Rictor*-deficiency in all three models (data not shown). Moreover, there were no

changes in the CD11b⁺Gr1⁺, B or NK populations with *Rictor*-deficiency at the HSC stage suggesting a vital role of mTORC2 in T cell development (Figure 4.20A&B, Figure 4.21A,G,J). In addition to aberrations in T cell lineage, a significant decrease in percentage of B cell and an increase in NK cell lineage was observed in the LN and spleen respectively with *Rictor*-deficiency in adult mice (*Mx1-Rictor* cKO) (Figure 4.20C&D, Figure 4.21B,H,K). *CD19*-cre⁺/⁻*Rictor*ᶠˡ/ᶠˡ (*CD19-Rictor* KO) led to a significant decrease in percentage of B cells in the BM, spleen and blood with an increase in percentage of CD11b⁺Gr1⁺ cells (with no changes in cell number – data not shown) in the spleen and blood compared to *CD19*-cre⁻/⁻*Rictor*ᶠˡ/ᶠˡ (*CD19-Rictor* control) (Figure 4.21C,I). Furthermore, there was a significant increase in percentage of NK cells in the blood, with no changes in T cell lineage in *CD19-Rictor* KO mice compared to *CD19-Rictor* controls (Figure 4.21F,L). These data suggest that *Rictor*-deficiency at the HSC and in adult mice leads to aberrations in mature B, T cell populations. As expected, *Rictor*-deficiency specifically in B cells leads to significant changes in mature B cells, with increased percentages of myeloid and NK cells lineages likely due to the decrease in B cells. Interestingly, there was no change in the percentage of apoptotic cells in all haemopoietic or in B cells in the BM (Figure 4.22). However, there was a decreasing trend in live cells with an increasing trend in early and late apoptotic haemopoietic cells and B cells in the spleen of *Vav-* and *Mx1-Rictor* KO mice (Figure 4.23A-H). Moreover, there was a significant increase in the percentage of apoptotic B cells, together with trends in decrease in percentage of live cells with *CD19-Rictor* KO (Figure 4.23I,J), suggesting only a subtle role of mTORC2 in apoptosis in B cells and other haemopoietic lineages.

To assess the role of *Rictor* in B cells, early and late B cells markers were assessed in the BM, spleen, and LN. Unlike with *Raptor*-deficiency, *Rictor*-deficiency did not lead to any changes in the percentage or cellularity (data not shown) of early B progenitors including LSK, pre-proB and proB cells in the BM of *Vav-* and *Mx1-Rictor* KO mice compared to their respective controls (Figure 4.24, Figure 4.26A&B). However, there was a significant increase in the percentage of pre-proB cells in the BM of *CD19-Rictor* KO mice, together with a significant decrease in the percentage of proB cells compared to controls, suggesting a block in B cell development at the pre-proB cell stage within the *CD19-Rictor* KO model specifically (Figure 4.26C). To assess late B cell lineage development, we

focussed on the percentages, not cellularity, of late B cell populations due to the significant decrease in total splenic cellularity thereby decreasing the cellularity of most late B cell populations with *Rictor*-deficiency at the HSC stage and in adult mice (Figure 4.18B). There was a significant decrease in the percentage of T1 cells in the LN, and a decreasing trend in T3 B cell populations in the spleen of *Vav-Rictor* and *Mx1-Rictor* KO mice respectively compared to controls (Figure 4.25, Figure 4.26D&E), along with a significant decrease in T1 and T3 percentages in the spleen and T1 B cells in the LN of *CD19-Rictor* KO mice compared to controls (Figure 4.26F). As T1 B cells transition to T2 and subsequently fol2 which give rise to MZ cells, looking at mature B cell lineages, it was not surprising to observe a significant decrease in MZP and MZ percentages in spleens of *Vav-Rictor* KO mice, which is consistent with H&E staining showing a decrease in MZ (Figure 4.26G, Figure 4.16C). Additionally, a decrease in the percentage of fol1 B cell population in the LN with a decreasing trend in the spleen in *Mx1-Rictor* cKO mice was observed compared to controls. There was also a trend in increase in the MZP and MZ population which was consistent with the H&E staining in the spleens of *Mx1-Raptor* cKO mice (Figure 4.26H, Figure 4.16D) suggesting an accumulation of MZ B cell population. Lastly, a significant decrease in the MZ percentage was observed in the spleen and LN of *CD19-Rictor* KO mice suggesting aberrations in late B cell populations, specifically in MZ and fol1 B cells with *Rictor*-deficiency *in vivo* (Figure 4.26I). These data suggest an important role of mTORC2 in later stages B cell subtypes.

4.3 Discussion

In order to determine the individual roles of mTORC1 and mTORC2 in normal haemopoiesis, the *Vav*-cre, *Mx1*-cre and *CD19*-cre *Raptor* and *Rictor* KO mouse models were used to assess haemopoiesis at various stages – the HSC stage, adult mice and specifically in B cells. However, in order to do so, each model needed to be optimised to obtain the robust phenotypic evidence of changes in haemopoietic cell development upon KO/cKO of mTORC1/mTORC2.

4.3.1 Optimisation

Previous literature comprising the *Mx1*-cre *Raptor*$^{fl/fl}$ and *Mx1*-cre *Rictor*$^{fl/fl}$ models used differing doses and volume of poly(I:C) to induce a cKO in mice. Kalaitzidis *et al.*, induced *Mx1-Raptor* cKO with 3 poly(I:C) inoculations every other day at 15 mg/kg(91), whereas Guo *et al.*, carried out 6-8 poly(I:C) inoculations at 10 mg/kg(263), with no reference to the timepoint these mice were assessed post poly(I:C) inoculation. The *Mx1-Rictor* cKO has previously been induced by 4 poly(I:C) inoculations at 5 mg/kg and assessed at either 1 or 6 months(92). However, data for 1 month was not shown in the paper suggesting a poorer cKO. In other laboratories *Rictor* cKO has been induced by 7 poly(I:C) inoculations every other day at 400 μg with no mention of the age of the mice when assessed(115). Due to additional papers suggesting 4 poly(I:C) or fewer inoculations(93) reproduced the desired phenotype, a dose of 4 poly(I:C) at 10 mg/kg was delivered to our mice where the timepoint at which the mice were assessed differed between 3 and 5 wk post 4 poly(I:C) inoculation in the *Mx1-Rictor* model. Kuhn *et al.*, showed that one dose of poly(I:C) is sufficient to induce a 100% KO in the liver suggesting that fewer doses can lead to potent KO(234). We determined that the *Mx1*-cre induced cKO via poly(I:C) inoculation was optimal 5 wk post 4 rounds of poly(I:C) at 10 mg/kg in both *Mx1*-cre *Raptor*$^{fl/fl}$ and *Mx1*-cre *Rictor*$^{fl/fl}$ models. Successful excision of *Raptor* and *Rictor* in these mouse models was confirmed. Additionally, *Mx1-Raptor* control mice were compared with WT mice inoculated with 4 poly(I:C) inoculation and assessed 5 wk post to assess any changes between the two models with poly(I:C) inoculation. As both the models did not show any significant difference, *Mx1-Raptor* control mice were used as reference whilst assessing *Mx1-Raptor* cKO

mice as it suggested that polyI:C inoculation did not produce any drastic effects in either WT or *Mx1-Raptor* control model.

Discrepancies in the field existed for the timepoint at which the *Vav*-cre *Rictor^{fl/fl}* mouse model should be assessed to obtain the best phenotype for the KO. Indeed, *Vav*-cre *Rictor^{fl/fl}* mice have been assessed at 3-4 wk(285) or at 6-8 wk(116) in previous studies. Therefore, the mice were assessed at 2, 8, and 24 wk of age to determine the optimal timepoint for the best phenotype from the KO. Analysis of the development of B, T, NK and myeloid lineages concluded that mice with *Rictor* deficiency at the HSC stage have an optimal phenotype from the KO at 8 wk of age.

The *CD19*-cre models for *Raptor* and *Rictor* were analysed between 8-10 wk and 18-24 wk respectively due to the known role of *Raptor* and *Rictor* at early and later stages of B cell lineage haemopoiesis respectively(282). *CD19*-cre^{+/+}*Raptor^{fl/fl}* mice, having homozygous cre expression, exhibited a severe phenotype with a drastic decrease in mature B cells due to the insertion of cre recombinase gene into the first exon of *CD19* antigen gene thereby causing a block in *CD19* expression and essentially creating a *CD19* KO (283). Moreover, *Vav*-cre model has been shown to be better at the excision of a gene of interest than *CD19*-cre models, where cre excision is 75-80% and 95% accurate in the BM and spleen respectively (206). The *Mb1*-cre model (*Mb1* is expressed at the pro-proB cell stage) is a better B cell specific model with a better deletion efficiency than *CD19*-cre model (208). Additionally, the homozygous expression of cre has been well known to be associated with non-specific excisions within the genome due to the presence of pseudo-loxP sites within the murine genome leading to toxicity(208). Therefore, a heterozygous expression of cre was used for all the models to limit non-specific excisions and the *CD19*-cre^{+/+}*Raptor^{fl/fl}* model was not considered for further B cell lineage analysis.

4.3.2 Validation of KO Targets

Testing the gene and protein expression levels of Rictor and Raptor together with their downstream targets in deficient mouse models revealed a significant downregulation of *Raptor* in haemopoietic organs in *Mx1-Raptor* cKO as expected. Less expected was the decrease in *Rictor* expression in the spleen

with *Raptor*-deficiency in *Mx1-Raptor* cKO mice. Similarly, there was a significant decrease in RAPTOR and RICTOR expression in haemopoietic organs in *Mx1-Raptor* cKO mice. It is possible that mTORC1 controls the protein synthesis of RICTOR thereby decreasing RICTOR expression altogether. This is supported by the finding that *Rictor* gene expression was not significantly modulated in *Mx1-cre Raptor^{fl/fl}* mice. mTORC1 is known to phosphorylate S6K1 which negatively regulates mTORC2 activity (65). However, as our data presented did not show a reduction in S6 phosphorylation, there could be other possible substrates phosphorylating S6. Five phosphorylation sites have been identified for S6, at S235, S236, S240, S244 and S247, where there is an orderly progression of phosphorylation with S236 as the primary phosphorylation site(286). Interestingly, Pende *et al.*, have shown that although S6K2 is primarily responsible for S6 phosphorylation, there are still lower levels of detection of S235 and S236 phosphorylation, after the KO of S6K1 and S6K2, by MAPKs (287) which could be responsible for the phosphorylation of S6. Nevertheless, it is possible that the upstream S6K, a primary effector of S6, is being modulated by other pathways despite *Raptor* cKO thereby phosphorylating S6. Previous literature suggests that S6K1 is phosphorylated directly by PDK1 at T308 residue(288), and by insulin stimulated MAPKs (289,290) which could be other possible upstream substrates phosphorylating S6K1.

Analysis of p4EBP1^{T37/T46} in *Raptor*-deficiency in adult mice, showed a slight decrease in phosphorylation. A reason behind the lack of significant decrease of p4EBP1 could be due to the antibody used for western blotting. The signal seen on the Western blot was weak, with no signal on various occasions in tissues of *Raptor*-control mice thereby explaining the lack of significance.

Similarly, *Rictor*-deficiency at the HSC stage (*Vav-Rictor* KO) and in adult mice (*Mx1-Rictor* cKO) showed a significant decrease in Rictor expression at the mRNA and protein levels. It was interesting to observe a significant decrease in *Raptor* expression at the mRNA level in the BM and thymus of *Vav-Rictor* KO mice. However, there was no difference in RAPTOR expression at the protein level in these mice suggesting mTORC2 does not regulate mTORC1 at the early HSC stage (*Vav-Rictor* KO model). Moreover, *Mx1-Rictor* cKO mice did not show any changes in RAPTOR expression at the protein/mRNA levels. These studies indicate that mTORC1 regulation of mTORC2/RICTOR expression is more potent

compared to mTORC2 vs. mTORC1 dysregulation. Assessing a downstream substrate of mTORC2, *Vav-Rictor* KO mice displayed a significant decrease in the downstream AKT^{S473} phosphorylation as compared to *Mx1-Rictor* cKO mice, which displayed similar, yet non-significant trends in the BM, spleen, and thymus. As mentioned, *Vav*-cre model is regarded as system with a very high efficiency in deletion of the target(208). The *Mx1*-cre model on the other hand has shown to have other immunogenic side effects(204) and may not represent a complete KO(234). Previous literature has shown that an inducible model of *Rictor*-deficiency in adult mice (*Rosa*-cre ER) results in a significant reduction of AKT^{S473} phosphorylation with increased AKT^{T308} phosphorylation and increased *FoxO1* activity(111). This suggests there is an increase in PDK1 activity(291) potentially activating the mTORC1 complex, evident by no change in RAPTOR expression with *Rictor* deficiency in both *Rosa*-cre and *Mx1*-cre models. Nevertheless, the difference observed between the phosphorylation of AKT^{S473} in *Mx1*-cre vs. *Rosa*-cre could be model specific. *Rosa26* is a promoter which is ubiquitously expressed in all tissues and is expressed at an early stage in ES cells, but its function is not yet known(292). On the other hand, *Mx1* promoter is expressed in the nucleus of most tissues including spleen, liver, uterus, kidneys, BM, peripheral blood mononuclear cells (PBMCs)(293) in mice, and in most tissues with lower expression in smooth muscle in humans(199). However, its ubiquitous expression in mice has not been confirmed. This difference in the nature of the promoter expression and function together with the mechanism of cre induction (via tamoxifen vs. poly(I:C)) could account for the potent KO in *Rosa*-cre vs. *Mx1*-cre transgenic mice.

4.3.3 Splenic Architecture in KO models

Mx1-Raptor cKO in mice resulted in an increase in splenic weight and cellularity and a decrease in BM cellularity, which has been demonstrated previously, together with a disruption in splenic structure with *Raptor* cKO 5-7 months post poly(I:C) inoculation(91). The reasons for the aberrations in the spleen are unclear. mTORC1 has shown to play a role in cytoskeletal reorganisation, as rapamycin has shown to inhibit IGF1 activated cytoskeletal structure and cell motility in a RhoA dependent manner in tumour cell lines(294). Therefore, it is a possibility that there is an aberration in the F-actin filaments with mTORC1 deficiency thereby demolishing the structure of the spleen as our data

demonstrate a loss of GC and MZ in the spleen altogether with *Raptor* cKO. However, literature has also shown that mTORC2 controls actin cytoskeleton in a rapamycin independent manner(295) and is mediated by PKCα(296), thereby suggesting contradictory roles of mTOR complexes in actin organisation. Recently, *Rictor* has shown to positively regulate BCR signalling as *Rictor*-deficiency in B cells results in overactivation of ezrin, a protein responsible for connecting actin filaments, leading to the formation of a rigid fence of actin thereby restricting lateral BCR movement on the membrane(297). Indeed, we do see a disruption of splenic morphology and architecture in *Vav-Rictor* KO mice suggesting that both mTOR complexes play a role in splenic architecture. However, whether this is dependent on actin organisation is unclear. Additionally, the increase in spleen weight with a loss of *Raptor* has been associated with a compensatory mechanism of the body to increase the population of other cells such as erythrocytic, dendritic (not tested) or macrophages leading to extramedullary haemopoiesis due to the decrease in other lymphoid haemopoietic lineages(91).

Interestingly, we show an increase in Ki67 staining in the red pulp of the spleen in *Mx1-Raptor* cKO mice. Ki67 is a marker for proliferating cells with expression present in all stages of cell cycling - G_1, G_2, S phases(298). Therefore, observing an increase in Ki67 expression with *Raptor* cKO suggests a disruption in cell cycling. Dowling *et al.*, have published an essential role of 4EBPs in regulating cell proliferation and cycling in an mTORC1 dependent manner confirming the observed increase in Ki67 expression in mice with *Raptor*-deficiency(299). In *Vav-Rictor* KO mice there was no change in proliferation and cycling. Nevertheless, *Mx1-Rictor* cKO mice (and not *Vav-Rictor* KO) showed increased accumulation of Ki67 expression in the GCs of the spleen. This suggests a block in proliferation and cell cycling in adult mice alluding to a specific role of *Rictor* in later stages of development as opposed to at the HSC stage. Wang *et al.*, demonstrated a decrease in proliferation in adult murine endothelial cells with a decrease in vascular endothelial growth factor (VEGF) with *Rictor* deficiency(300). Similarly, *Rictor*-deficiency in B cells affected proliferation with the significant decrease in MZ B cells(111).

4.3.4 mTORC1/2 signalling in apoptosis

As discussed in section 3.3, the increase in spleen weight due to *Raptor*-deficiency correlates with an increase in the red pulp as seen from the H&E staining, which could suggest an increase in erythrophagocytosis in the spleen (301). *Mx1-Raptor* cKO in adult mice led to increased apoptotic death of B cells with similar trends in mice with deletion of *Raptor* in B cells. As *Raptor*-deficiency did not demonstrate other significant changes (but trends in increase in apoptotic cellularity due to the likely effect of mTORC1 on apoptosis in B cells) in other haemopoietic lineages, it is a possibility that B cells are particularly sensitive to apoptosis in the absence of *Raptor*. Guo *et al*., observe an increase in apoptosis in myeloid, erythroid and B cell lineages in the BM coupled with a decrease in the anti-apoptotic protein, MCL-1, with *mTOR*-deficiency(263). These data could allude to the role of both mTORC1 and mTORC2 in apoptosis as they did not assess the individual roles of mTOR complexes. Additionally, induced deletion of *Raptor* in adult mice led to an increase in apoptosis of differentiated, but not leukaemic stem cells (LSCs), in a mouse model of AML(100). However, these data focusses on a murine model of AML and not healthy haemopoietic lineages. Our data show that B cells are particularly sensitised to apoptosis with *Raptor*-deficiency in the BM. The BM does not have many T cell subsets but has an increased population of myeloid cells. It would be interesting to assess other haemopoietic organs such as the spleen or thymus and assess myeloid, and other lymphoid lineages to determine the exact role of mTORC1 in apoptosis within different haemopoietic lineages.

Our data suggest a subtle role of mTORC2 in apoptosis as there exist slight trends illustrating an increase in early and late apoptotic cells in the spleens of *Vav-Rictor* KO and *Mx1-Rictor* cKO mice and a significant increase in apoptotic B cells in *CD19-Rictor* KO mice. In agreement with this, published data demonstrates an important role of *Rictor* in apoptosis. It has previously been shown that *Vav-Rictor* KO mice exhibit an increase in the pro-apoptotic target *Bim* with a decrease in the anti-apoptotic Bcl_{XL} in mature B cells by impairing the canonical and non-canonical NFκB pathway, thereby demonstrating a balance of apoptosis in mature B cells by mTORC2(111). Furthermore, Brunet *et al*., demonstrated an important role of AKT in phosphorylating and inhibiting the forkhead TF FKHRL1 (FOXO3), thereby inhibiting apoptosis suggesting a role of

mTORC2 in balancing apoptosis(70). *RICTOR* (and not *RAPTOR*) knock down (KD) in MCF-7 cells (human breast cancer cell line) revealed that mTORC2 regulates apoptosis in B cells and epithelial cells in a *C-MYC* dependent manner whereby *RICTOR* KD upregulates *C-MYC* expression and subsequent downregulation of E2F1(113). In contrast, conditional *Rictor* deletion in CD8$^+$ effector T cells did not affect the rate of apoptosis suggesting a redundant role of mTORC2 in regulating T cell mediated apoptosis(125). This suggests a role of mTORC2 in apoptosis in B cells and in other haemopoietic lineages excluding T cells. Clearly there exist discrepancies between our data and in previous literature as our data does not allude to significant apoptosis in B cells with *Rictor*-deficiency. Perhaps the trends observed in our data could allude to other lineages not affected by mTORC2 which skew the percentages.

4.3.5 Impact of mTORC1/2 deletion on haemopoietic lineage development

4.3.5.1 B cells

To assess the individual roles of mTORC1 and mTORC2 in normal haemopoiesis, haemopoietic lineages were assessed in mice with *Raptor* and *Rictor*-deficiency. In agreement with previously published literature (91), *Mx1-Raptor* cKO mice lacked mature B cells in haemopoietic organs, while *Rictor*-deficient mice only revealed major phenotypic changes later in development. To determine the exact role of mTORC1 and mTORC2 in B cells, populations of early B cells in the BM and late B cells in the spleen and LN were assessed. There was a significant elevation of LSK cells in the BM of *Vav-Raptor* KO and *Mx1-Raptor* cKO mice (chapter 3) suggesting a block in B cell development and B cell lineage commitment with *Raptor*-deficiency. Iwata *et al.*, have shown a block in B cell development at the preB cell stage along with a lack in peripheral B cells independent of BCL$_{XL}$ in mice with *Raptor*-deficiency in B cells specifically (*Mb1*-cre cKO). B cell populations with *Raptor*-deficiency had decreased glycolysis and oxidative phosphorylation indicating an aberration in metabolism(109). This group used a different KO model, which rendered only B cells deficient of mTORC1 via the *Mb1*-cre cKO model (*Mb1* is expressed at the pre-proB cell stage), which will be the reason for the difference observed in the stage at which B cell development is blocked. Additionally, mTORC1 deficiency, and not

mTORC2, is responsible for a decrease in 18 genes encoding for electron transport chain (ETC) proteins together with a decrease in oxidative phosphorylation(302). While assessing the model with *Raptor*-deficiency in B cells (*CD19*-cre$^{+/-}$*Raptor* KO) for early B cell progenitors, we observed an increase in LSK and pre-proB cells with a decrease in proB cells with *Raptor*-deficiency (data not shown), thereby blocking B cell development at the pre-proB cell stage as opposed to at the LSK stage in mice lacking *Raptor* at the HSC stage (*Vav*-cre) or in adult mice (*Mx1*-cre). This suggests that sufficient *Raptor* expression is required throughout the early stages of B cell development to support maturation of the B cell lineage. Interestingly, Tze *et al.*, demonstrated that a conditional BCR deletion or inhibition of PI3K resulted in a de-differentiation of mature B cells to having early B cell characteristics(303). Whether mTORC1 inactivation leads to the reversal or depletion of B cells is currently unknown.

Rictor-deficiency in *Vav*-cre (HSC stage) or *Mx1*-cre (adult mice) mice did not affect B cell lineage commitment suggesting mTORC2 does not play a role in early B cell lineage commitment. However, previous literature has shown that *Mx1-Rictor* cKO mice exhibit an increase in proB cells with a decrease in mature B cells 6 months post poly(I:C) with an increase *Rag1* expression and an increase in cell cycling as there was a significant increase in B cells in G_2/S phase with a decrease in cells in G_0 phase which was *Foxo1* dependent(92). As our conditional mouse model is assessed 5 wk post poly(I:C) inoculation, it is possible that this phenotype has not become evident after about 1 month and needed to be assessed 6 months post inoculation. Additionally, B cells lacking *mSIN1* (a component of mTORC2 which is known modulate activity of mTORC2) led to an increase in *Rag* and *Il7r* expression (also causing augmentation in V(D)J activity) via the regulation of *Foxo1,* which is mediated by *Akt*(112). Our data show that *Rictor*-deficiency solely in B cells leads to a significant decrease in B cells with an increase in pre-proB cells alluding to a potent role of mTORC2 in B cell maturation. However, as cre excision is not as efficient in CD19 models (206), a more potent *Rictor* KO in B cells in the BM, such as the *Mb1*-cre models, may have shown deregulated mTORC1 and *Foxo1* activity (via upstream mTORC2 activity).

Given that B cell development is blocked with mTORC1 deficiency, it was not surprising to see aberrations in late B cell populations. Significant reductions in T2 B cells with reductions in MZP, MZ and fol2 populations in the spleen of *Mx1-Raptor* cKO mice with similar reductions in T2, fol1 and fol2 B cell subsets in *CD19*-cre^{+/-}*Raptor* KO mice. Interestingly, *Rictor*-deficiency was also associated with a decrease in T1 and T3 B cells and reductions in MZP, MZ and fol1 B cells. These results were in agreement with previous literature determining the function of late B cell populations. T1 cells transition into T2 cells leading to subsequent fol2 B cells. Fol2 B cells are more primitive, quiescent and less abundant compared to fol1 cells, which form the majority of the recirculating pool. MZP B cells arise from fol2 cells leading to MZ B cells. Fol2 cells also generate fol1 cells(44). Therefore, it is appropriate to observe a significant decrease in T2 and the primitive fol2 cells and a concomitant decrease in MZP and MZ cells in *Mx1-Raptor* mice due to the fundamental role of mTORC1 in B cell development as discussed previously. *Rictor*-deficiency is associated with disruption in migration and cell cycling, which explains the observed reduction in T1, T3 cells which give rise to the recirculating fol1 B cell population. There were no significant changes observed in fol2 B cells suggesting that mTORC2 plays a role in the ability of fol2 B cells to further develop into fol1, MZP and MZ cells. Lee *et al.,* demonstrate a block in late B cell populations in mice with *Rictor*-deficiency at the HSC stage with similar results in adult mice via a decrease in T3 B cells and an increase in T1/T2 ratio together with a decrease in MZ cells. They also observe a modest decrease in follicular cells(111), however they did not distinguish between fol1 and fol2 cells. All these data support our results thereby confirming a role for mTORC2 in late B cell development. Although, there is a decrease in MZ population in *Vav-Rictor* KO mice, there is a trend in increase in MZ and MZP populations when *Rictor*-deficiency is induced in adult mice (*Mx1-Rictor* cKO) seen from H&E staining and from phenotypic analysis by flow cytometry. This suggests an accumulation of MZ cells with induced *Rictor*-deficiency in adult mice, as there is a decline in fol2 cells.

4.3.5.2 Other haemopoietic lineages

A significant reduction in the mature myeloid (CD11b^{+}Gr1^{+}) population was observed in the BM and blood but an increase in percentage of mature myeloid cells in the secondary lymphoid organs: spleen and LN, in *Mx1-Raptor* cKO mice.

As lymphopoiesis takes place in the BM, it is possible that there was an accumulation of CD11b$^+$ myeloid cells (as seen in the BM) blocking the maturation into CD11b$^+$Gr1$^+$ myeloid cells with *Raptor*-deficiency in adult mice. Therefore, there was an increase in the remaining CD11b$^+$Gr1$^+$ myeloid cells in the secondary lymphoid organs. Additionally, secondary lymphoid organs would have a reduced population of B and T cells thereby increasing the percentage of myeloid cells. It would be interesting to analyse this population at later timepoint (6 months) post poly(I:C) inoculation and to determine whether there is a decrease in mature myeloid population with induced *Raptor*-deficiency in adult mice. Indeed, *mTOR*-deficiency leads to a block in myeloid development *in vivo* and *in vitro* via the reduction of M-CSF(102) receptor CD115 and the overactivation of STAT5 leading to the downregulation of IRF8(101). *Rictor* KO in myeloid cells has been shown to result in a bias towards an M1, and not M2, population and increased their sensitivity to apoptotic stimuli(304) and promoted pro-inflammatory M1 genes in response to TLR ligands in a FOXO1/3 dependent manner(106), suggesting a role of mTORC2 in myeloid viability and inflammatory responses. Our data was not focussed on the role of mTORC2 in myeloid lineages. However, assessing the viability of this lineage in the three different models would give us a better insight on the cycling and underlying mechanisms behind this characteristic caused due to mTORC2 abrogation.

Raptor-deficiency also affected NK cell populations and T cell lineages. The earliest thymocytes within the thymus lacking CD4 and CD8 expression and are termed as double negative (DN) thymocytes. About 95% of DN cells give rise to αβ-T cells via successful rearrangement of αβ-TCR via a process known as beta-selection. It is during this proliferative period of selection that T cells either die of apoptosis or express both CD4 and CD8 to become DP. These cells subsequently down-regulate a co-receptor to fully differentiate into either CD4$^+$ or CD8$^+$ T cells(305). We demonstrate a decrease in CD4$^+$CD8$^+$ DP thymocytes with a concomitant increase in CD8$^+$ and CD4$^-$CD8$^-$ DN thymocytes with *Raptor*-deficiency. Although reduced, there is a generation of DP T cells suggesting a role of mTORC1 in the proliferation of naïve cells, which is consistent with previously published data(306). In agreement with our data, rapamycin (mTORC1 inhibitor) treatment of mice with lymphocytic choriomeningitis virus (LCMV) has shown to increase the quantity and quality of CD8+ T cells(306) demonstrating a

role of mTORC1 in the proliferation with redundant roles in T cell development. Nevertheless, there remain discrepancies in the field as Pollizzi *et al.*, have shown a potent role of mTORC1 in effector cells as RHEB mediated deletion of mTORC1 in CD8^{+} T cells did not differentiate into effector cells, but retained ability to differentiate into memory T cells, but were dysfunctional due to metabolic defects(120). *Rictor*-deficiency in the *Vav-* and *Mx1*-cre mouse models strongly affected T cell development with a decrease in CD4^{+}CD8^{+} DP T cells together with an increase in the CD4^{-}CD8^{-} DN T cell populations with a modest increase in NK cell population in the spleen of adult mice with *Rictor*-deficiency. mTORC2 has been shown to regulate T cell development as *Mx1-Rictor* cKO partially blocks T cell development at the DN3 (CD3^{+}CD44^{-}CD25^{+}) stage(115) and involves NFκB and FOXO1 pathways(116). Mice with *mTOR*-deficiency exhibit a block in Th1, Th2, and Th17 cells due to abrogation in the STAT signalling and differentiate towards T-regulatory (T-reg) cells which is independent of mTORC1 suggesting an important role of mTORC2 in T-reg development(307). Additionally, *Rictor* deficiency in T cells causes a block in Th1 and Th2 CD4^{+} T cell development which is rescued by AKT (via increased expression of *Tbet* TF) and PKC-θ (via reverting *Gata3* expression)(123). Conditional deletion of *Rictor* in CD8^{+} T cells demonstrates an increased ability of CD8^{+} T cells to commit to memory precursor effector cells (MPECs) together with more potent recall responses and CD8^{+} T cells also exhibited a reduction in short-lived effector cell (SLECs) commitment in a *Foxo1* dependent manner(125) suggesting mTORC2 regulates effector cell commitment. These published papers suggest a vital role of mTORC2 in T cell development. As the *CD19*-cre model should only effect CD19^{+} B cells, is was reassuring to see the majority of effects on B cells with *Raptor* and *Rictor*-deficiency. Nevertheless, there were slight increases in NK and myeloid lineages in the spleen and blood of transgenic mice lacking *Raptor* and *Rictor*, which could be attributed to the significant decrease in B cell lineage in these mice.

Taken together, upon successful deletion of *Raptor* and *Rictor*, our data show an important role of mTORC1 predominantly in B and T cell development. mTORC1 inactivation blocks B cell development at the LSK or the pre-proB cell stage (depending on the individual models used). Additionally, we demonstrate that mTORC2 is not vital for early B cell development but plays a role in late B cells

by blocking fol2 development into MZ and fol1 cells. mTORC2 also plays an important role in T cell development. Therefore, we demonstrate that although there is a cross-talk between both the complexes, mTORC1 and mTORC2 have unique roles during haemopoiesis.

4.4 Figures
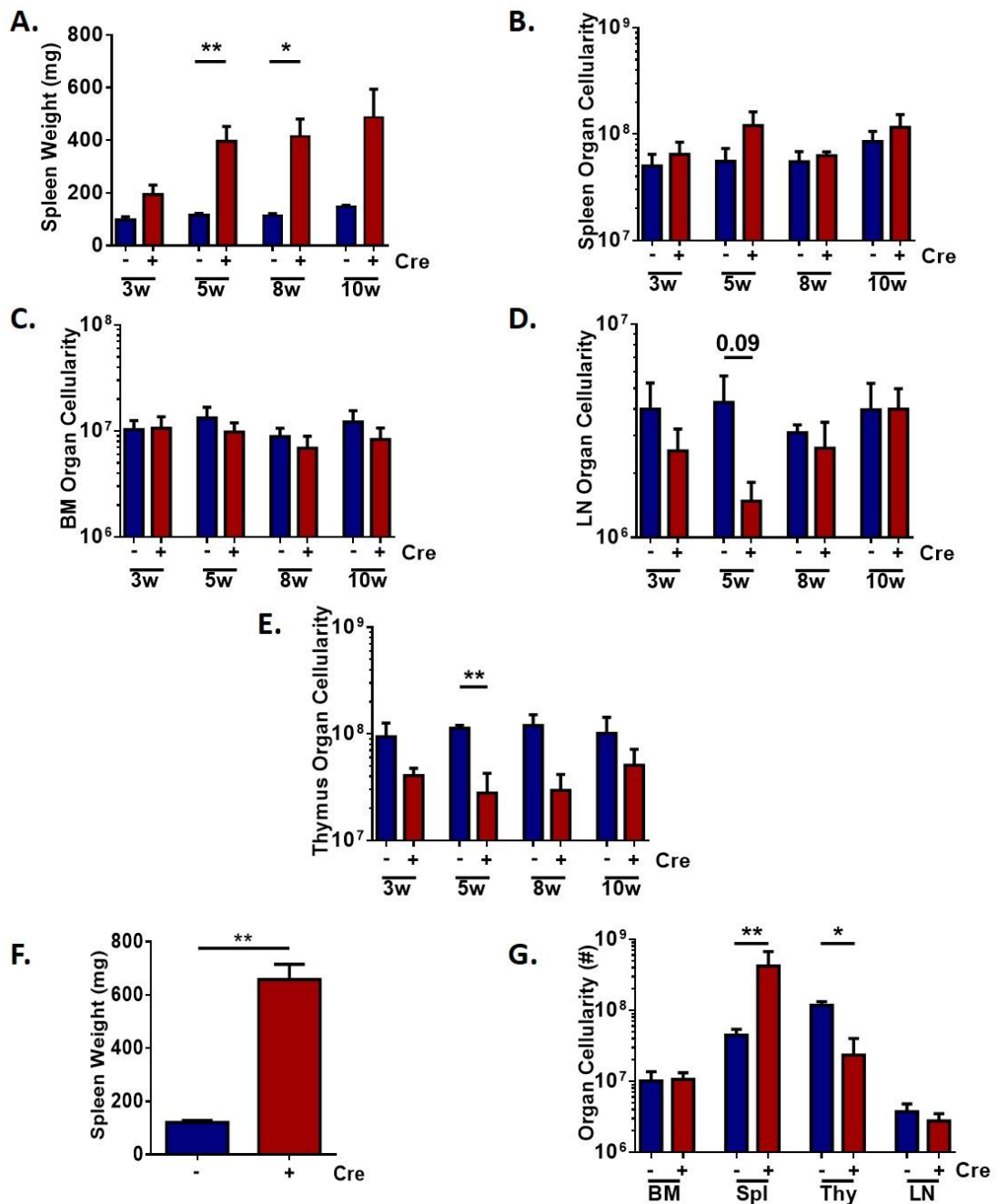
Figure 4.1:Optimization of the *Mx1*-cre *Raptor* cKO model.
Mx1-cre⁻ (cre-, *Mx1-Raptor* control) and *Mx1*-cre⁺*Raptor^(fl/fl)* (cre+, *Mx1-Raptor* cKO) mice were inoculated with either 3 or 5 doses of 10 mg/kg poly(I:C) and analyzed at either 3 (n=5), 5 (n=5), 8 (n=4) or 10 (n=3) wk or 5 wk post inoculations respectively. Spleen weight (mg) **(A)** and cellularity (log₁₀) **(B)** of *Mx1-Raptor* control and *Mx1-Raptor* cKO mice inoculated with 3 poly(I:C) doses and assessed at either 3, 5, 8 or 10 wk post inoculation. BM **(C)**, LN **(D)**, and thymus **(E)** cellularity (log₁₀) of *Mx1-Raptor* control and *Mx1-Raptor* cKO mice inoculated with 3 poly(I:C) doses and assessed at either 3, 5, 8 or 10 wk post inoculation. Spleen weight (mg) **(F)** and cellularity (log₁₀) of BM, spleen, thymus and LN **(G)** of *Mx1-Raptor* control (n=3) and *Mx1-Raptor* cKO (n=3) mice inoculated with 5 poly(I:C) doses and assessed 5 wk post inoculation. Data are expressed as mean±SEM (p *≤0.05, p **≤0.001).
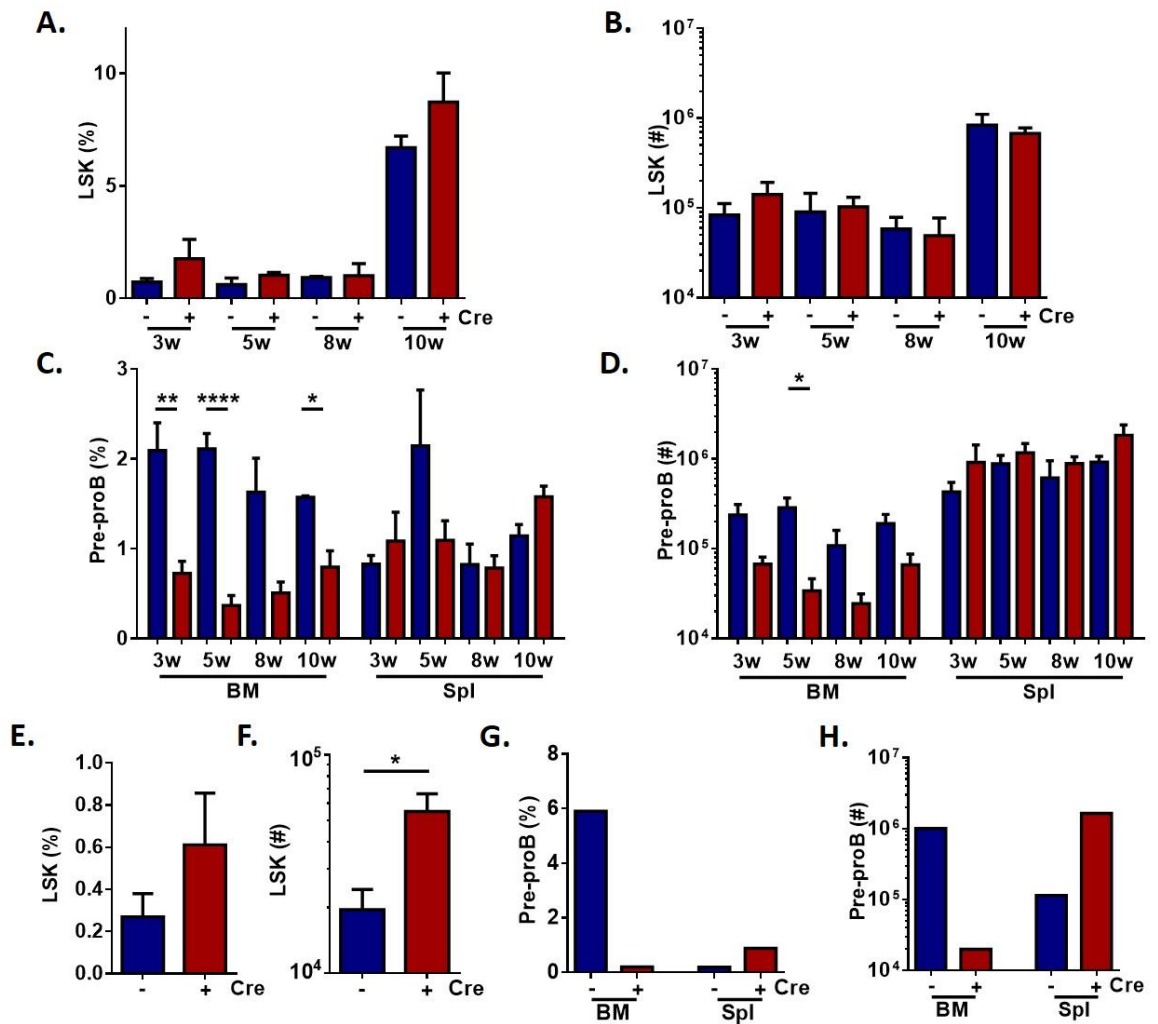
Figure 4.2: Optimization of the *Mx1*-cre *Raptor* cKO model assessing stem and early B cell progenitors *in vivo*.
Mx1-Raptor control (cre-) and *Mx1-Raptor* cKO (cre+) mice were inoculated with either 3 or 5 doses of 10 mg/kg poly(I:C) and analyzed at either 3 (n=5), 5 (n=5), 8 (n=2) or 10 (n=3) wk or 5 wk post inoculation respectively. Bar graphs demonstrating the percentage **(A)** and cellularity (log$_{10}$) **(B)** of LSK (lin-sca-1+CD117+) cells in the BM along with percentage **(C)** and cellularity (log$_{10}$) **(D)** of pre-proB cells (lin-B220+CD19-) in the BM and spleen of *Mx1-Raptor* control and *Mx1-Raptor* cKO mice inoculated with 3 poly(I:C) doses and assessed at either 3, 5, 8 or 10 wk post inoculation. Percentage **(E)** and cellularity (log$_{10}$) **(F)** of LSK cells in the BM (n=3) along with percentage **(G)** and cellularity (log$_{10}$) **(H)** of pre-proB cells in the BM (n=1) and spleen of *Mx1-Raptor* control and *Mx1-Raptor* cKO mice inoculated with 5 poly(I:C) doses and assessed 5 wk post inoculation. Data are expressed as mean±SEM (p *≤0.05, p **≤0.001, p ***≤0.0001, p ****≤0.00001).
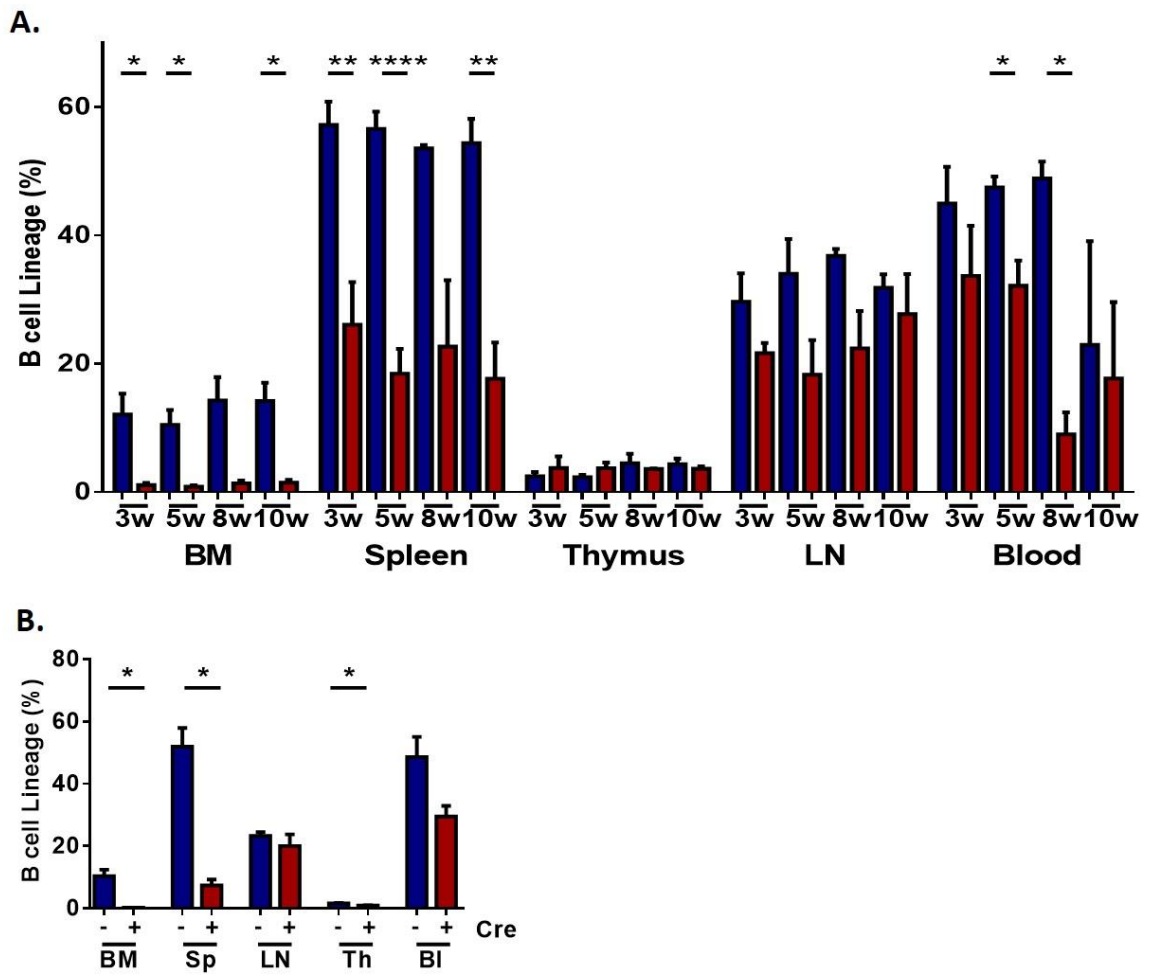
Figure 4.3: Optimization of the *Mx1*-cre *Raptor* cKO model assessing B cell lineages *in vivo*. *Mx1-Raptor* control (cre-) and *Mx1-Raptor* cKO (cre+) mice were inoculated with either 3 or 5 doses of 10 mg/kg poly(I:C) and analyzed at either 3 (n=5), 5 (n=5), 8 (n=2) or 10 (n=3) wk or 5 wk (n=3) post inoculation respectively. Percentage of B cell lineage (CD19⁺CD11b⁻) in the BM, spleen, thymus, LN and blood of *Mx1-Raptor* control and *Mx1-Raptor* cKO mice inoculated with 3 doses of poly(I:C) and analyzed at either 3, 5, 8 or 10 wk post inoculation **(A)** or with 5 doses of poly(I:C) and assessed 5 wk post inoculation **(B)**. Data are expressed as mean±SEM (p *≤0.05, p **≤0.001, p ***≤0.0001, p ****≤0.00001).
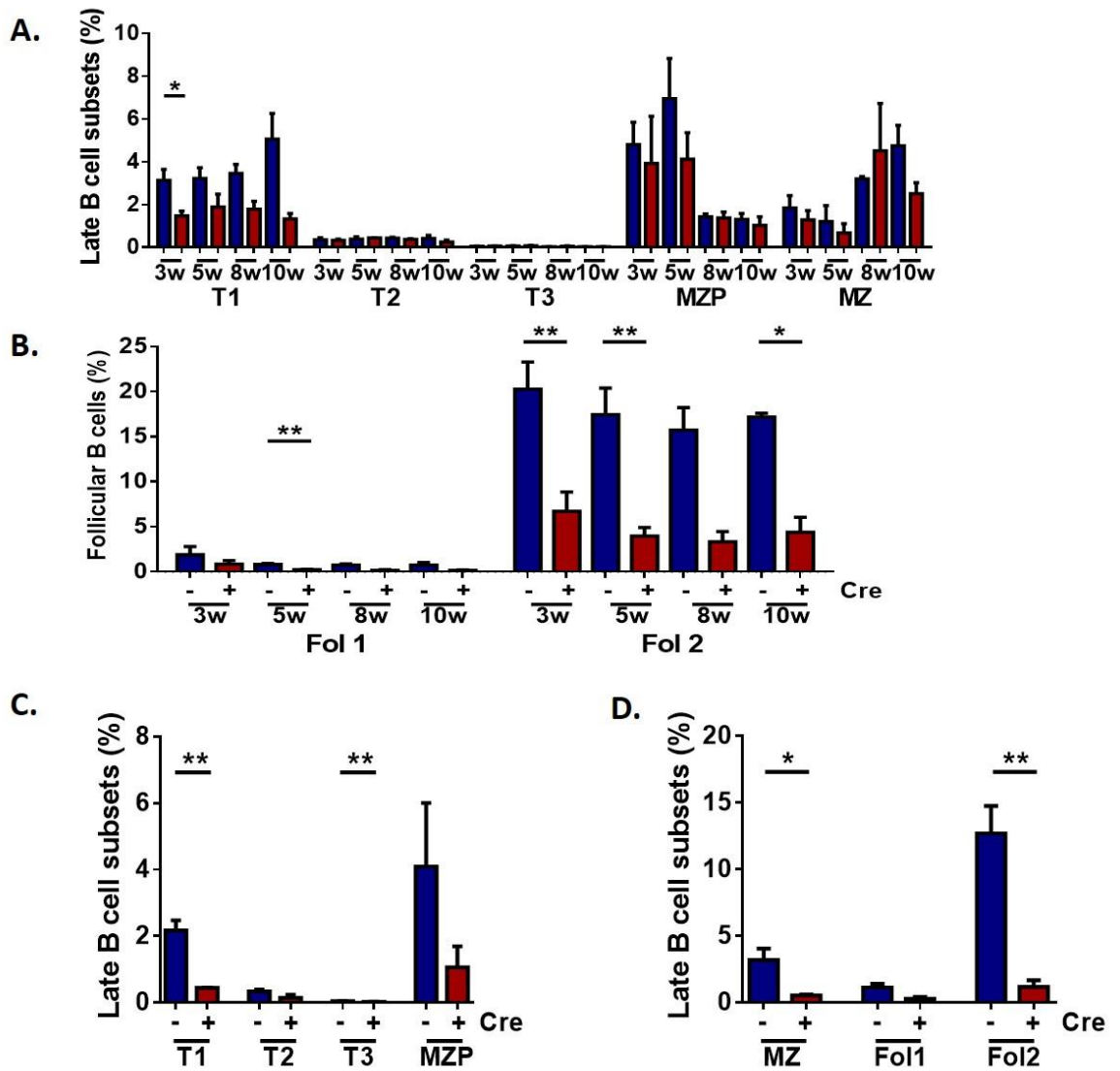
Figure 4.4: Optimization of the *Mx1*-cre *Raptor* cKO model assessing late B cell lineages *in vivo*.

Mx1-Raptor control (cre-) and *Mx1-Raptor* cKO (cre+) mice were inoculated with either 3 doses of 10 mg/kg poly(I:C) and analyzed at either 3 (n=5), 5 (n=5), 8 (n=2) or 10 (n=3) wk post inoculation or with 5 doses (n=3) of poly(I:C) and assessed 5 wk post inoculation. Bar graphs demonstrating the percentage of T1 (CD19+CD23-IgM+CD21-), T2 (CD19+CD23+CD21-CD1d^{lo}IgD+IgM+AA4.1+), T3 (CD19+CD23+CD21-CD1d^{lo}IgD+IgM-AA4.1+), MZP (CD19+CD23+CD21+CD1d+) and MZ (CD19+CD23-IgM+CD21+) B cells **(A)**, and percentage of fol1 (CD19+CD23+CD21-CD1d^{lo}IgD+IgM-AA4.1-) and fol2 (CD19+CD23+CD21-CD1d^{lo}IgD+IgM+AA4.1-) B cells **(B)** in the spleen of *Mx1-Raptor* control and *Mx1-Raptor* cKO mice inoculated with 3 poly(I:C) doses and assessed at either 3, 5, 8 or 10 wk post inoculation. Percentage of T1, T2, T3, and MZP B cells **(C)**, and percentage of MZ, fol1 and fol2 B cells **(D)** in the spleen of *Mx1-Raptor* control and *Mx1-Raptor* cKO mice inoculated with 5 doses of poly(I:C) and assessed 5 wk post inoculation. Data are expressed as mean±SEM (p *≤0.05, p **≤0.001). T – transitional 1 B cells, MZP – marginal zone B cells, fol – follicular B cells.
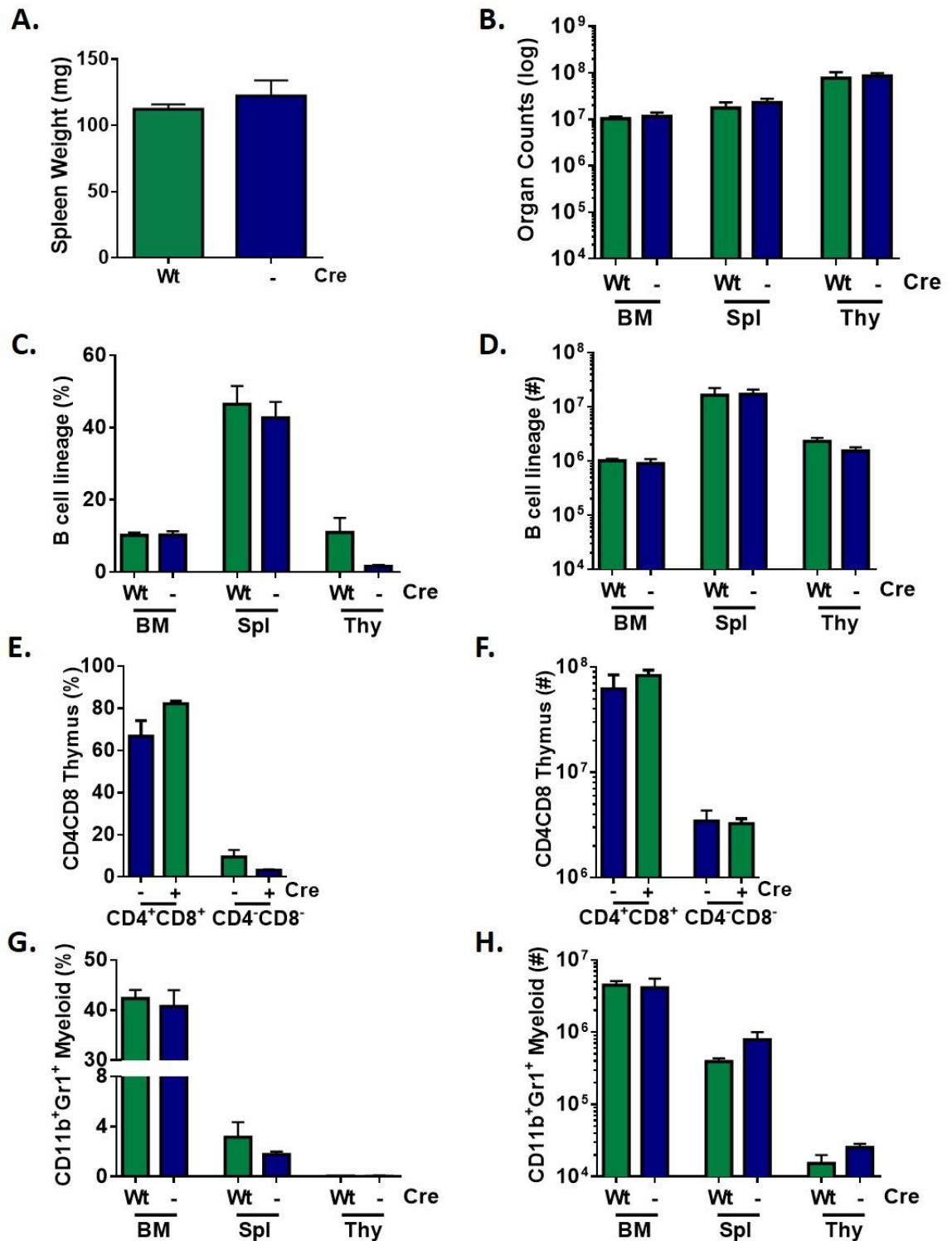
Figure 4.5: Control experiment showing no difference between WT mice and mice expressing cre⁻ on alleles.
Comparison of spleen weight (mg) **(A)** and total organ counts (BM, spleen, and thymus) in logarithmic axis **(B)** between wild type (Wt) (n=8) mice and cre⁻ (n=9, *Mx1-Raptor* control) mice assessed 5 wk post 10 mg/kg 4 poly(I:C) inoculation. Bar graphs demonstrating the percentage **(C)** and cellularity (log₁₀) **(D)** of B cells in the BM, spleen, and thymus of Wt (n=8) and cre⁻ (n=6) mice assessed 5 wk post 10 mg/kg 4 poly(I:C) inoculation. Percentage **(E)** and cellularity (log₁₀) **(F)** of CD4⁺CD8⁺ DP and CD4⁻CD8⁻ DN T cells in the thymus of wild type (Wt) and cre⁻ mice assessed 5 wk post 4 poly(I:C) inoculation. Percentage **(G)** and cellularity (log₁₀) **(H)** of CD11b⁺Gr1⁺ mature myeloid cells in the BM, spleen and thymus of wild type (Wt) (n=8) and cre⁻ (n=6) mice assessed 5 wk post 10 mg/kg 4 poly(I:C) inoculation. Data are expressed as mean±SEM.
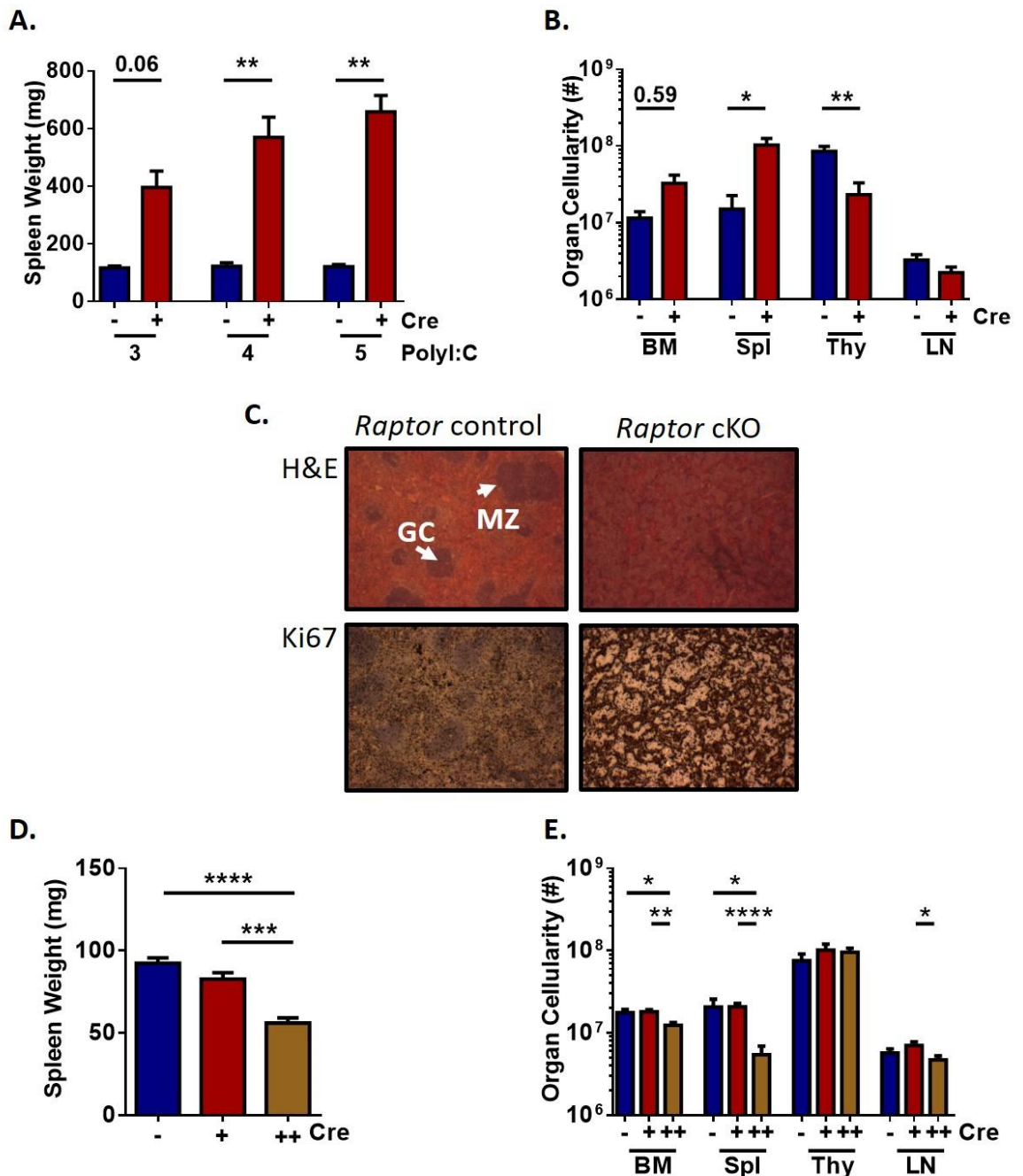
Figure 4.6: Characterization of lymphoid organs in *Raptor* KO models.
A. Spleen weights (mg) of *Mx1-Raptor* control (cre-) or *Mx1-Raptor* cKO (cre+) mice inoculated with 3 (n=5), 4 (n=6) or 5 (n=3) doses of 10 mg/kg poly(I:C) were assessed 5 wk post-inoculation to induce the cKO. **B.** Total organ counts ($\log_{10}$; BM, spleen, thymus and LN) of *Mx1-Raptor* control or *Mx1-Raptor* cKO mice assessed 5 wk post 4 poly(I:C) inoculation. **C.** Histology slides showing haematoxylin and eosin (H&E) staining (top row) and Ki67 staining (bottom row) of spleen section of *Mx1-Raptor* control or *Mx1-Raptor* cKO mice assessed 5 wk post 4 poly(I:C) inoculation. Spleen weights **(D)** and organ cellularity ($\log_{10}$) **(E)** of *CD19*-cre$^{-/-}$*Raptor*$^{fl/fl}$ (cre-, *CD19-Raptor* control, n=5), *CD19*-cre$^{+/-}$*Raptor*$^{fl/fl}$ (cre+, *CD19-Raptor* KO, n=7) or *CD19*-cre$^{+/+}$*Raptor*$^{fl/fl}$ (cre++, *CD19*-cre$^{+/+}$*Raptor* KO, n=6) mice. Data are expressed as mean±SEM (p *≤0.05, p **≤0.001, p ***≤0.0001, p ****≤0.00001). GC – germinal centre, MZ – marginal zone.
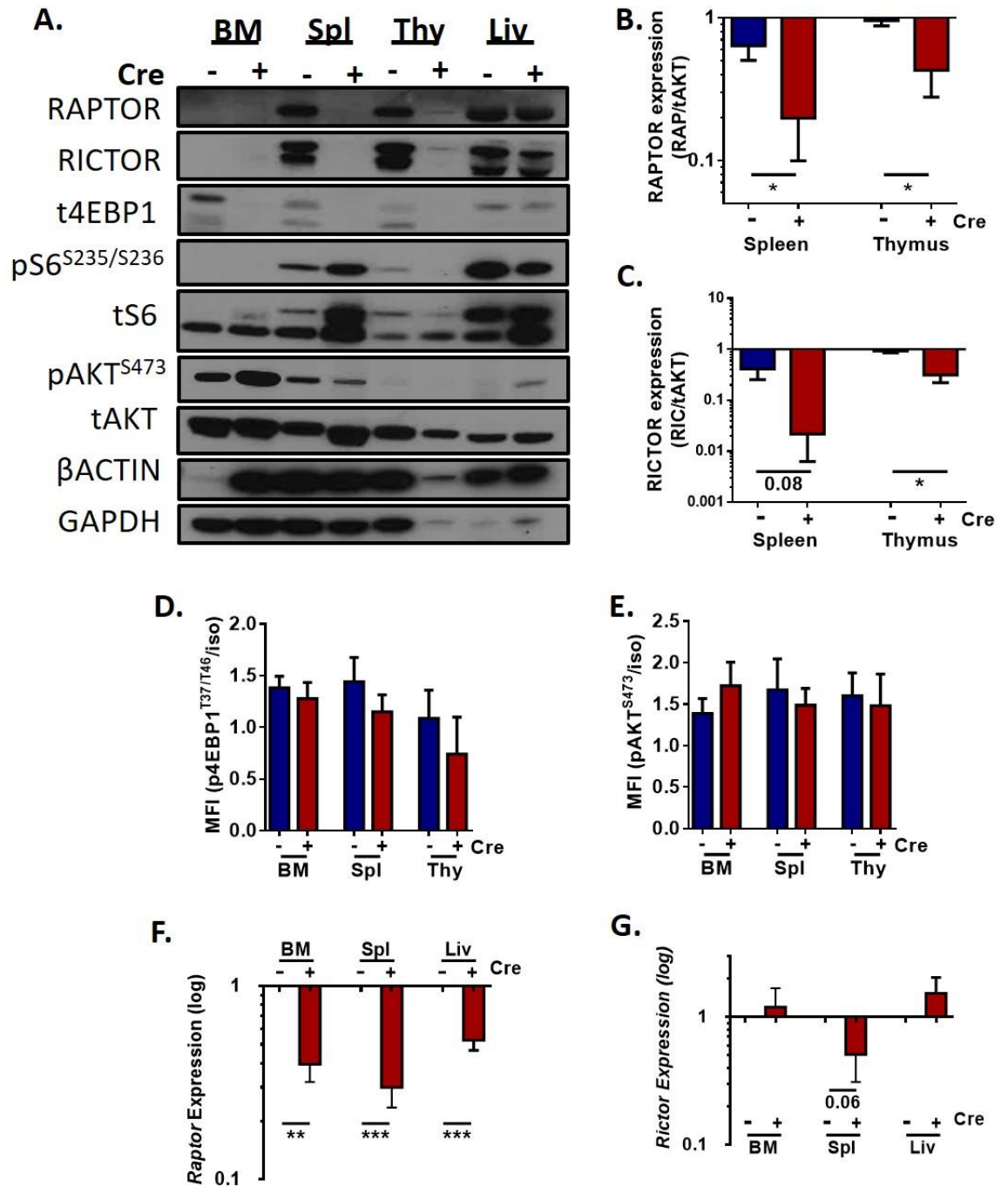
Figure 4.7: Confirmation of *Raptor* cKO at the protein, gene and at the substrate level for mTOR pathway members in *Mx1-Raptor* cKO mice.
Representative western blot showing protein expression of RAPTOR and RICTOR, and downstream mTOR proteins: t4EBP1, pS6$^{S235/S236}$, tS6, pAKT^{S473}, tAKT and loading controls βACTIN and GAPDH in the BM, spleen, thymus and liver from *Mx1-Raptor* control and *Mx1-Raptor* cKO mice 5 wk post 4 poly(I:C) inoculation **(A)**. Densitometry of protein expression of RAPTOR/tAKT (n=5 *Mx1-Raptor* control, n=7 *Mx1-Raptor* cKO) **(B)** and RICTOR/tAKT (n=4) in the spleen and thymus *Mx1-Raptor* control and *Mx1-Raptor* cKO mice 5 wk post 4 poly(I:C) inoculation **(C)**. MFI ratios of p4EBP1$^{T37/T46}$/isotype control (n=3) **(D)** and pAKT^{S473}/isotype control (n=5) **(E)** in the BM, spleen and thymus of *Mx1-Raptor* control and *Mx1-Raptor* cKO mice 5 wk post 4 poly(I:C) inoculation. Gene expression of *Raptor* **(F)** and *Rictor* **(G)** in the BM (n=4), spleen (n=5) and liver (n=4) of *Mx1-Raptor* control and *Mx1-Raptor* cKO mice 5 wk post 4 poly(I:C) inoculation. Data is shown relative to *Mx1-Raptor* controls with *Tbp* as the reference gene. Data are expressed as mean±SEM (p *≤0.05, p **≤0.001, p ***≤0.0001).
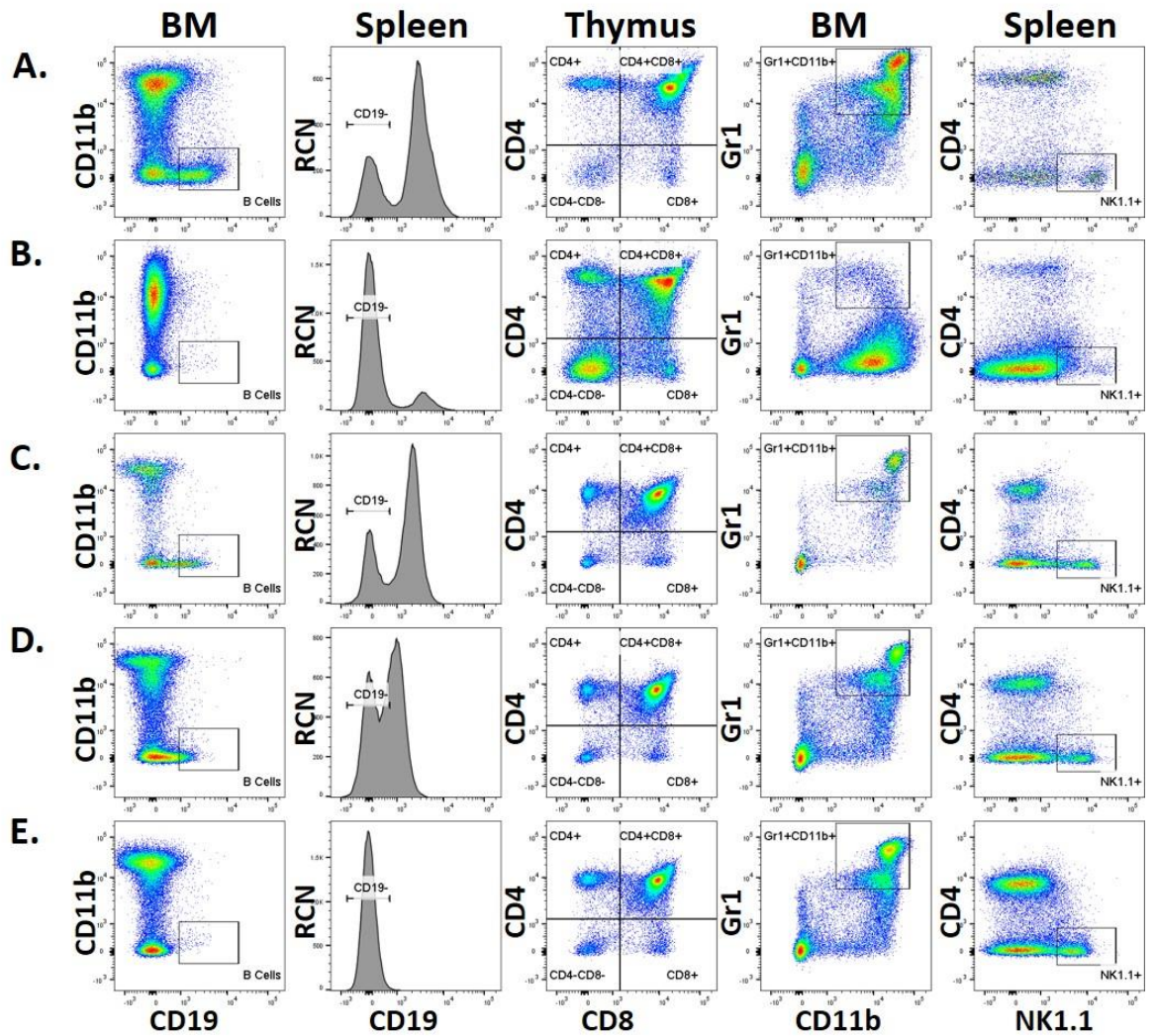
Figure 4.8: Gating strategy of haemopoietic lineages in *Mx1*-cre and *CD19*-cre *Raptor* mouse models.

Representative flow cytometry plots demonstrating the proportion of B cells (CD19$^+$CD11b$^-$) in the BM, CD4$^+$ (CD19$^-$CD4$^+$CD8$^-$), CD8$^+$ (CD19$^-$CD8$^+$CD4$^-$), CD4$^+$CD8$^+$ (CD19$^-$CD4$^+$CD8$^+$) T cells in the thymus, mature myeloid cells (CD19$^-$CD11b$^+$Gr1$^+$) in the BM, and NK cells (CD19$^-$CD4$^-$NK1.1$^+$) in the spleen in *Mx1-Raptor* control **(A)** *Mx1-Raptor* cKO 5 wk post 4 poly(I:C) inoculation **(B)**, *CD19-Raptor* control **(C)** *CD19*-cre$^{+/-}$*Raptor* KO **(D)**, and *CD19*-cre$^{+/+}$*Raptor* KO **(E)** mice. Plots are live and size (FSC-A/SSC-A) gated prior to the gating shown. RCN – relative cell number.
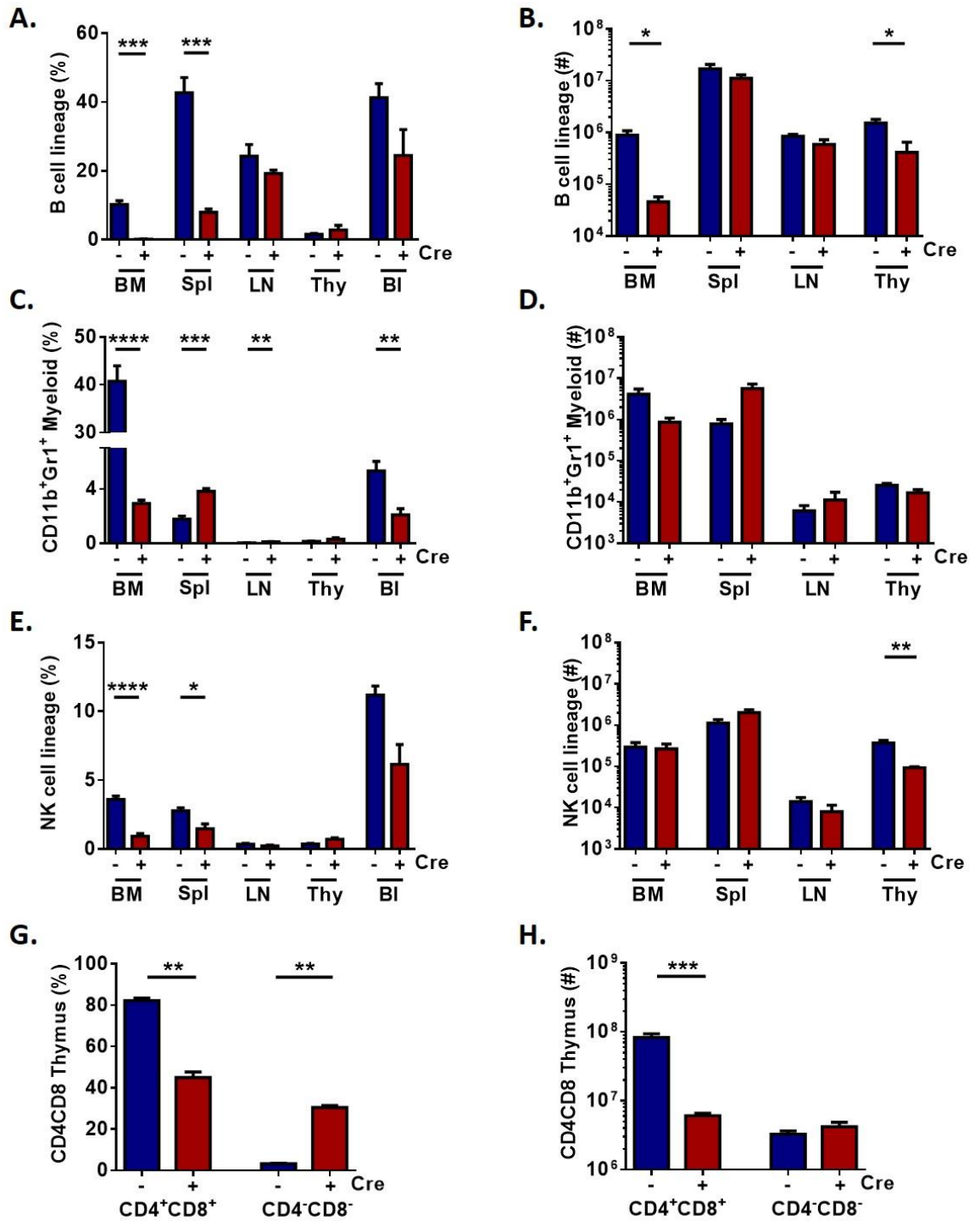
Figure 4.9: *Raptor* cKO in adult mice leads to significant aberrations in haemopoietic lineages *in vivo.*
Bar graphs showing the percentage of B cells **(A)**, CD11b⁺Gr1⁺ mature myeloid cells **(C)**, NK cells **(E)** in the BM, spleen, LN, thymus and blood and cellularity of B cells **(B)**, CD11b⁺Gr1⁺ mature myeloid cells **(D)**, NK cells **(F)** in the BM, spleen, LN and thymus of *Mx1-Raptor* control (n=6) and *Mx1-Raptor* cKO (n=3) mice 5 wk post 4 poly(I:C) inoculation. Percentage **(G)** and cellularity **(H)** of CD4⁺CD8⁺ DP and CD4⁻CD8⁻ DN thymocytes in the thymus of *Mx1-Raptor* control (n=6) and *Mx1-Raptor* cKO (n=3) mice 5 wk post 4 poly(I:C) inoculation. Data are expressed as mean±SEM (p *≤0.05, p **≤0.001, p ***≤0.0001, p ****≤0.00001).
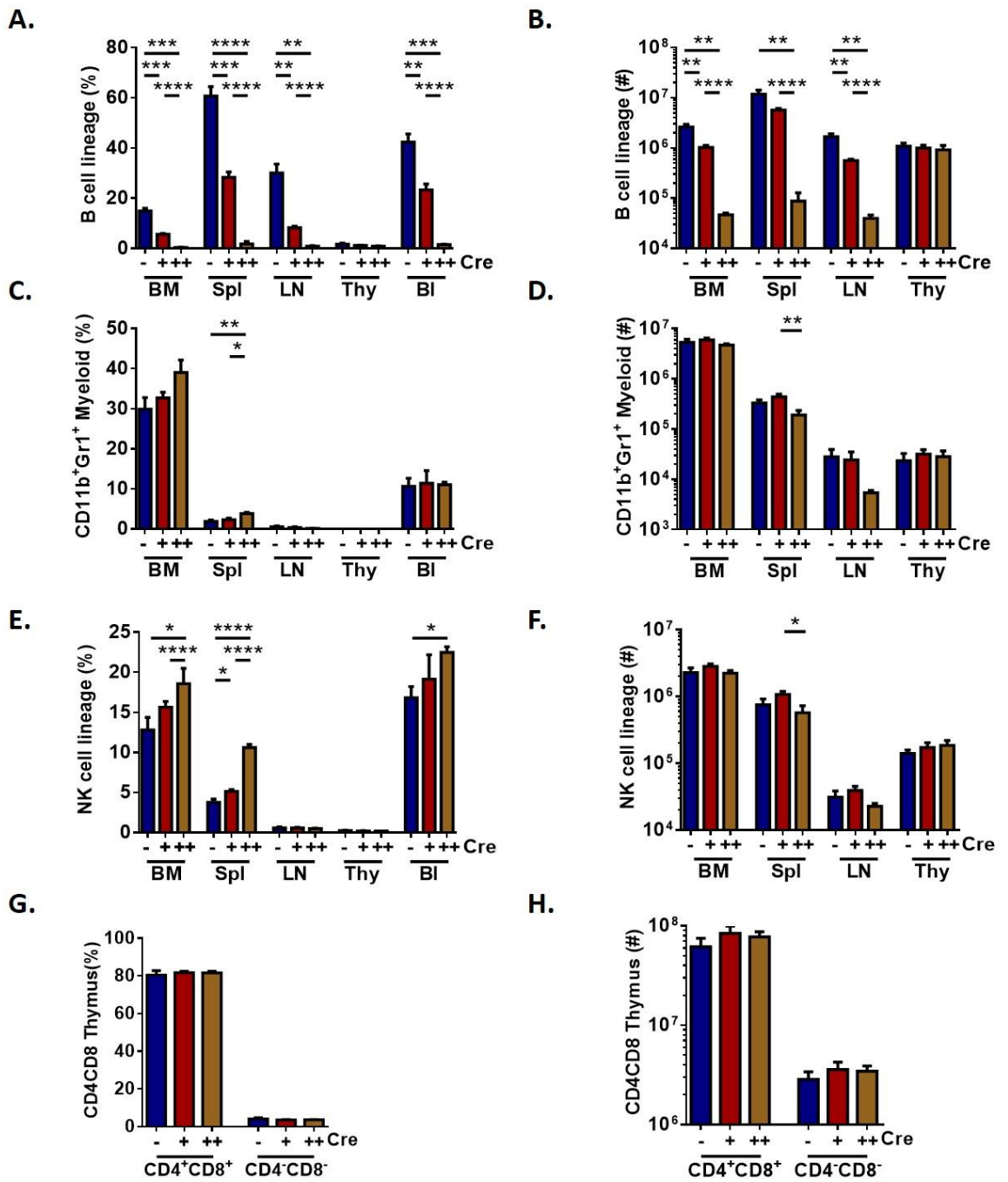
Figure 4.10: *Raptor*-deficiency in B cells leads to a decline in B cell lineage *in vivo.*
Bar graphs showing the percentage of CD19+ B cells **(A)**, CD11b+Gr1+ mature myeloid cells **(C)**, NK cells **(E)** in the BM, spleen, LN, thymus and blood and cellularity of CD19+ B cells **(B)**, CD11b+Gr1+ mature myeloid cells **(D)**, NK cells **(F)** in the BM, spleen, LN and thymus of *CD19-Raptor* control, *CD19*-cre+/- *Raptor* KO, and *CD19*-cre+/+ *Raptor* KO mice. Percentage **(G)** and cellularity **(H)** of CD4+CD8+ and CD4-CD8- T cells in the thymus in *CD19-Raptor* control (n=5), *CD19*-cre+/- *Raptor* KO (n=7), and *CD19*-cre+/+ *Raptor* KO (n=6) mice. Data are expressed as mean±SEM (p *≤0.05, p **≤0.001, p ***≤0.0001, p ****≤0.00001).
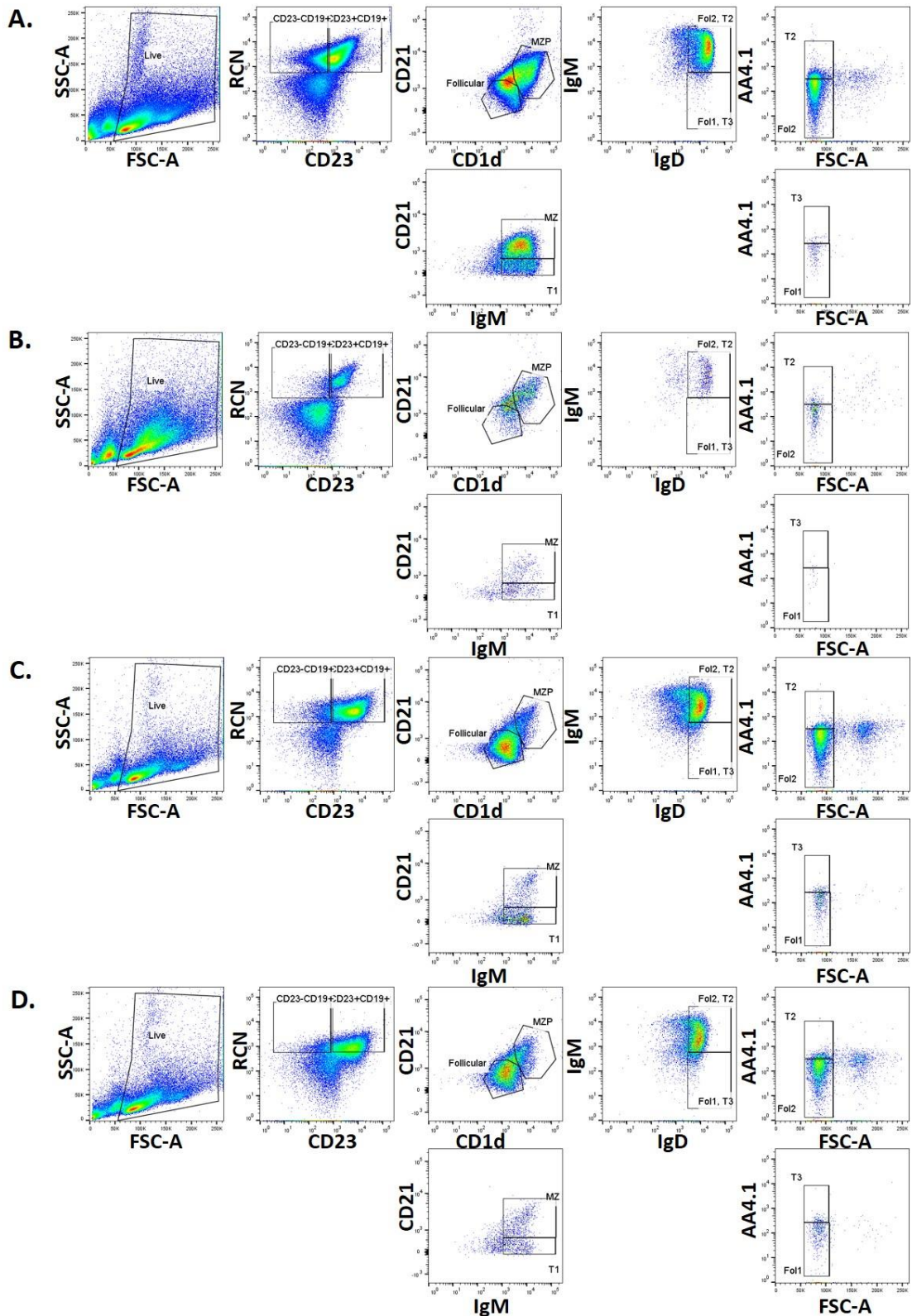
Figure 4.11: Gating strategy of late B cell lineages in *Mx1*-cre and *CD19*-cre *Raptor* models.
Representative flow cytometry plots showing the proportion of late B cells comprising transitional 1 (T1) cells (CD19$^+$CD21^{int}CD23$^-$IgM^{hi}); T2 (CD19$^+$AA4.1$^+$CD21^{int}CD23$^+$CD1d^{int}IgD^{hi}IgM^{hi}); T3 (CD19$^+$AA4.1$^+$CD21^{int}CD23$^+$CD1d^{int}IgD^{hi}IgM^{lo}); marginal zone precursor (MZP): (CD19$^+$CD21^{hi}CD23$^+$CD1d^{hi}); marginal zone (MZ) (CD19$^+$CD21^{hi}CD23$^-$IgM^{hi}); Fol1 (CD19$^+$AA4.1$^-$CD21^{lo}CD23$^+$CD1d^{int}IgD^{hi}IgM^{lo}) Fol2 (CD19$^+$AA4.1$^-$CD21^{lo}CD23$^+$CD1d^{int}IgD^{hi}IgM^{hi}) in the spleen in *Mx1-Raptor* control **(A)**, *Mx1-Raptor* cKO mice assessed 5 wk post 4 poly(I:C) inoculation **(B)**, *CD19-Raptor* control **(C)** and *CD19*-cre$^{+/-}$*Raptor* KO **(D)** mice. Plots are live and size (FSC-A/SSC-A) gated. RCN – relative cell number.
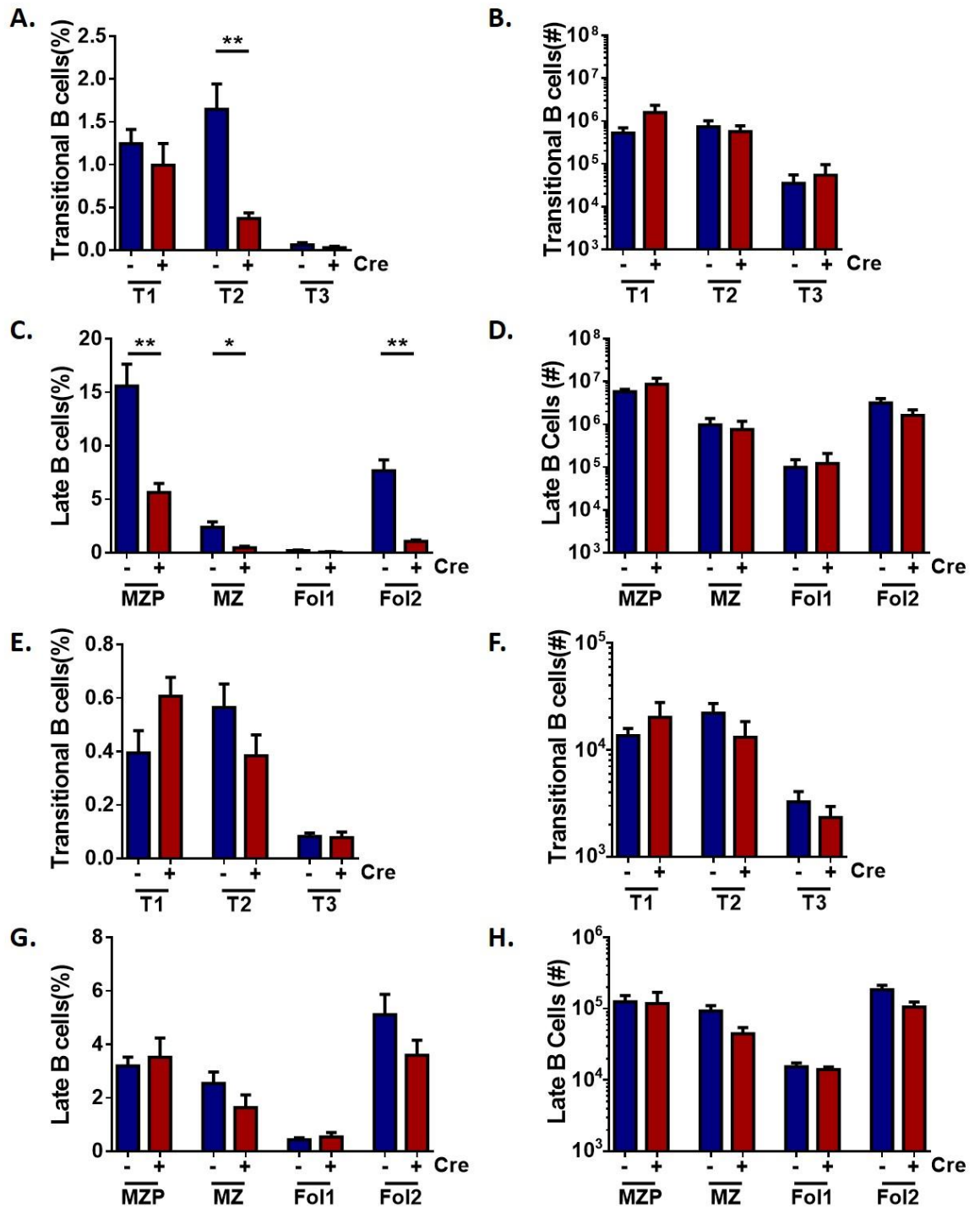
Figure 4.12: *Raptor*-deficiency in adult mice leads to aberrations in late B cells *in vivo.*
Bar graphs showing the percentage **(A)** and cellularity ($\log_{10}$) **(B)** of T1, T2 and T3 B cells, and percentage **(C)** and cellularity ($\log_{10}$) **(D)** of MZP, MZ, Fol1, and Fol2 cells in the spleen in *Mx1-Raptor* control and *Mx1-Raptor* cKO mice 5 wk post 4 poly(I:C) inoculation. Percentage **(E)** and cellularity ($\log_{10}$) **(F)** of T1, T2 and T3 B cells, along with percentage **(G)** and cellularity ($\log_{10}$) **(H)** of MZP, MZ, Fol1, and Fol2 cells in the LN of *Mx1-Raptor* control (n=6) and *Mx1-Raptor* cKO (n=3) mice 5 wk post 4 poly(I:C) inoculation. Data are expressed as mean±SEM (p *≤0.05, p **≤0.001).
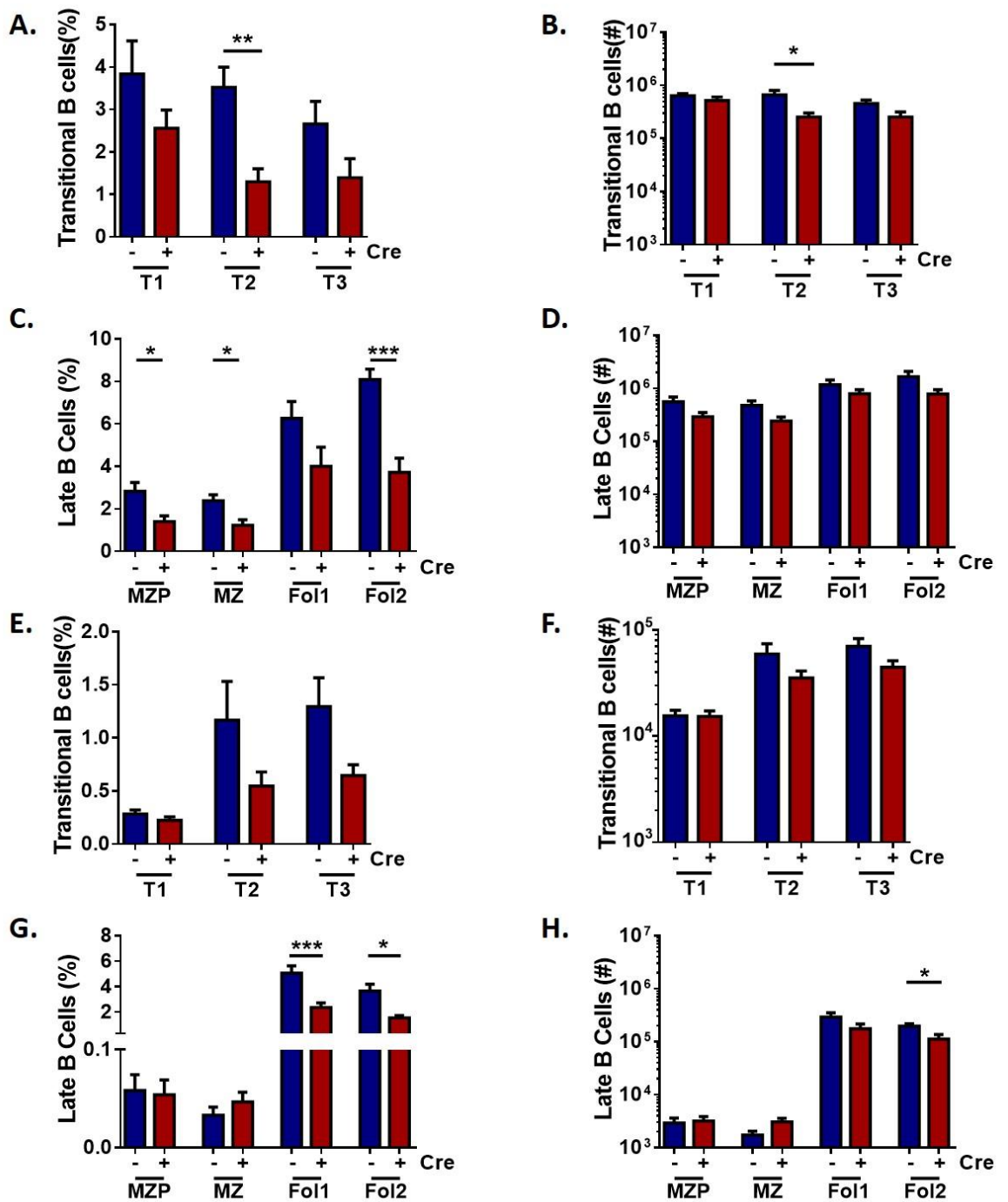
**Figure 4.13: *Raptor*-deficiency in B cells leads to aberrations in late B cells *in vivo.***
Bar graphs showing the percentage **(A)** and cellularity (log_{10}) **(B)** of T1, T2 and T3 B cells, and percentage **(C)** and cellularity (log_{10}) **(D)** of MZP, MZ, Fol1, and Fol2 cells in the spleen of *CD19-Raptor* control and *CD19*-cre$^{+/-}$*Raptor* KO mice. Percentage **(E)** and cellularity (log_{10}) **(F)** of T1, T2 and T3 B cells, and percentage **(G)** and cellularity (log_{10}) **(H)** of MZP, MZ, Fol1, and Fol2 cells in the LN in *CD19-Raptor* control (n=5) and *CD19*-cre$^{+/-}$*Raptor* KO (n=7) mice. Data are expressed as mean±SEM (p *≤0.05, p **≤0.001, p ***≤0.0001, p ****≤0.00001).
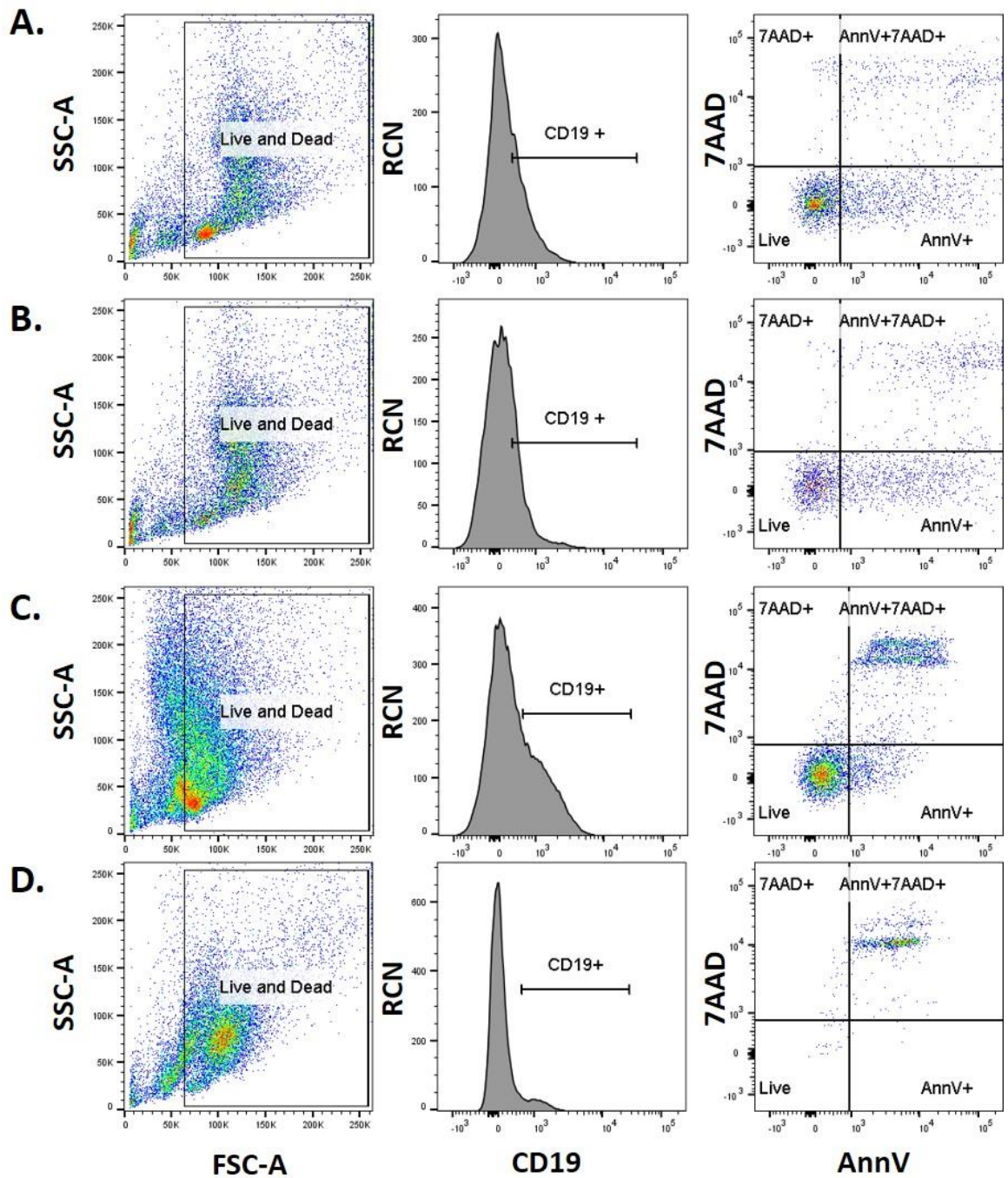
Figure 4.14: Gating strategy for determining live, early apoptosing and apoptotic cells in *Mx1*-cre and *CD19*-cre *Raptor* models.
Representative flow cytometry plots showing B cells (CD19+) and the proportion of live B cells (CD19+AnnV-7AAD-), early apoptosing B cells (CD19+AnnV+7AAD-) and apoptotic B cells (CD19+AnnV+7AAD+) in BM of *Mx1-Raptor* control **(A)** *Mx1-Raptor* cKO mice assessed 5 wk post 4 poly(I:C) inoculation **(B)**, *CD19-Raptor* control **(C)** *CD19*-cre+/-*Raptor* KO **(D)** mice. Plots are live and size (FSC-A/SSC-A) gated as shown. RCN – Relative cell number.
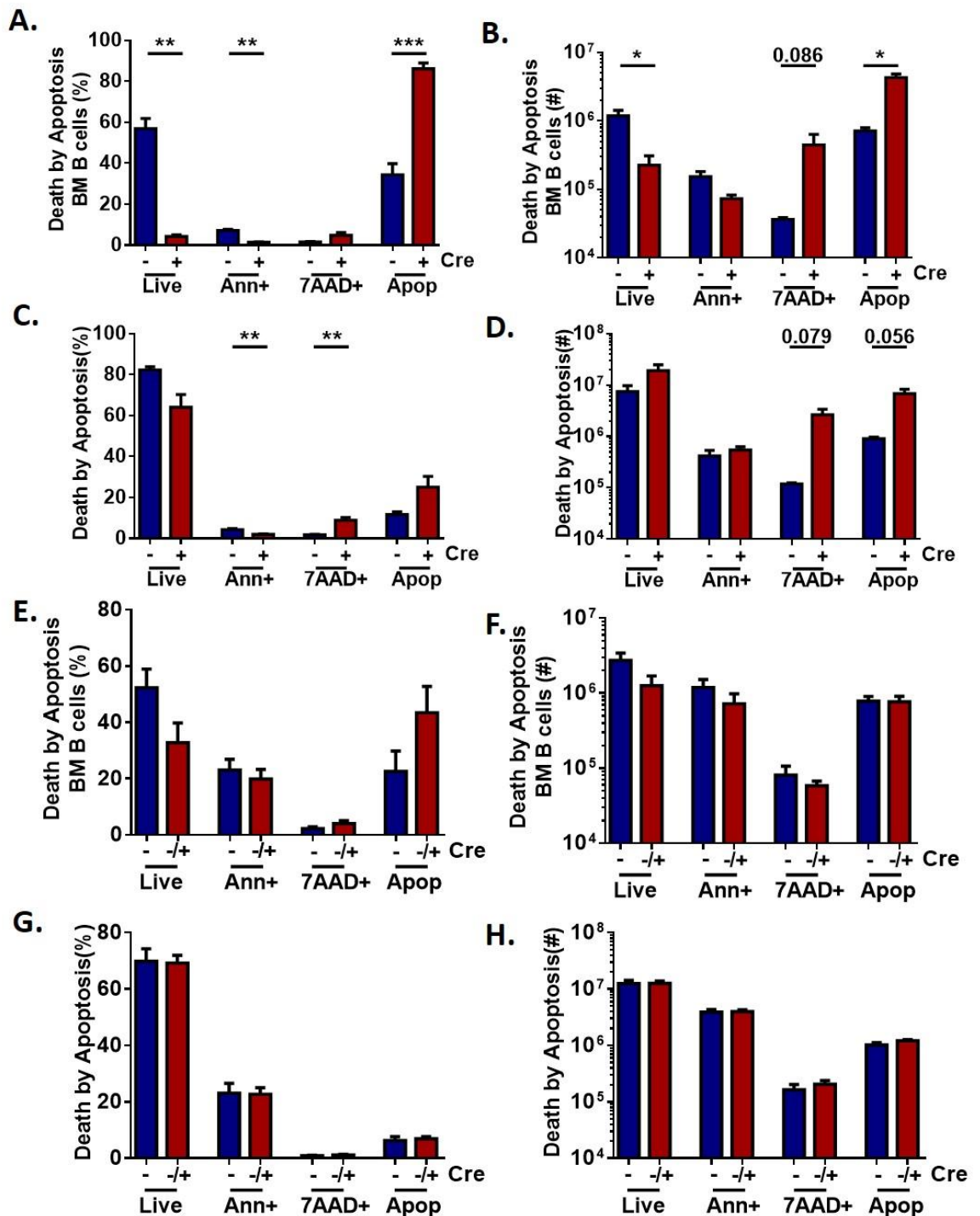
Figure 4.15: *Raptor*-deficiency in adult mice leads to increased apoptosis in B cells *in vivo.* Bar graphs demonstrate the percentage **(A)** and cellularity ($\log_{10}$) **(B)** of $CD19^+$ B cells (n=4) along with the percentage **(C)** and cellularity ($\log_{10}$) **(D)** of all haemopoietic lineages which are live ($AnnV^-$ $7AAD^-$), early apoptotic ($AnnV^+7AAD^-$), necrotic ($AnnV^-7AAD^+$) or apoptotic cells (Apop; $AnnV^+7AAD^+$) in BM of *Mx1-Raptor* control (n=6) and *Mx1-Raptor* cKO (n=3) mice assessed 5 wk post 4 poly(I:C) inoculation. Percentage **(E)** and cellularity ($\log_{10}$) **(F)** of $CD19^+$ B cells along with the percentage **(G)** and cellularity ($\log_{10}$) **(H)** of all haemopoietic cells which are live ($AnnV^-7AAD^-$), early apoptotic ($AnnV^+7AAD^-$), necrotic ($AnnV^-7AAD^+$) or dead by apoptosis ($AnnV^+7AAD^+$) in BM of *CD19-Raptor* control (n=5) and *CD19*-cre$^{+/-}$-*Raptor* KO (n=7) mice. Data are expressed as mean±SEM (p *≤0.05, p **≤0.001, p ***≤0.0001).
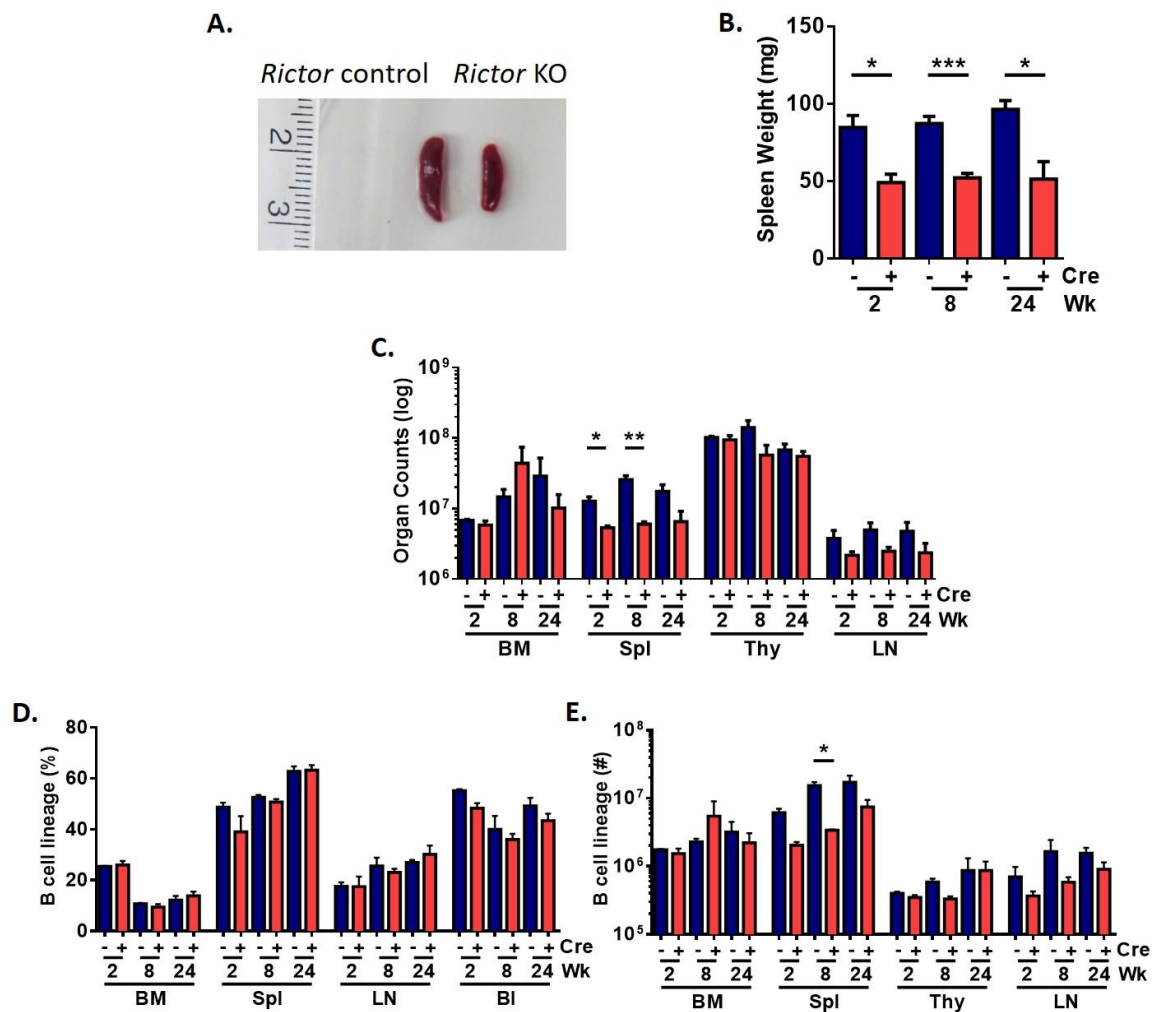
Figure 4.16: Optimization of the *Vav*-cre *Rictor* KO model.
Vav-cre⁻ (cre-, *Vav-Rictor* control) and *Vav*-cre⁺*Rictor^{fl/fl}* (cre+, *Vav-Rictor* KO) mice were analyzed after 2 (n=3), 8 (n=3), or 24 (n=5) wk to assess the KO at different time points. **A.** Picture showing differences in spleen size of *Vav-Rictor* control (left) and *Vav-Rictor* KO (right) mice 8 wk of age. Spleen weight (mg) **(B)** and organ cellularity (log_{10}) of BM, spleen, thymus and LN **(C)** of *Vav-Rictor* control and *Vav-Rictor* KO mice assessed after 2, 8, or 24 wk. B cell percentage in the BM, spleen LN and blood **(D)** and B cell lineage cellularity (log_{10}) in the BM, spleen, thymus and LN **(E)** of *Vav-Rictor* control and *Vav-Rictor* KO mice assessed after 2, 8, or 24 wk. Data are expressed as mean±SEM (p *≤0.05, p **≤0.001, p***≤0.0001).
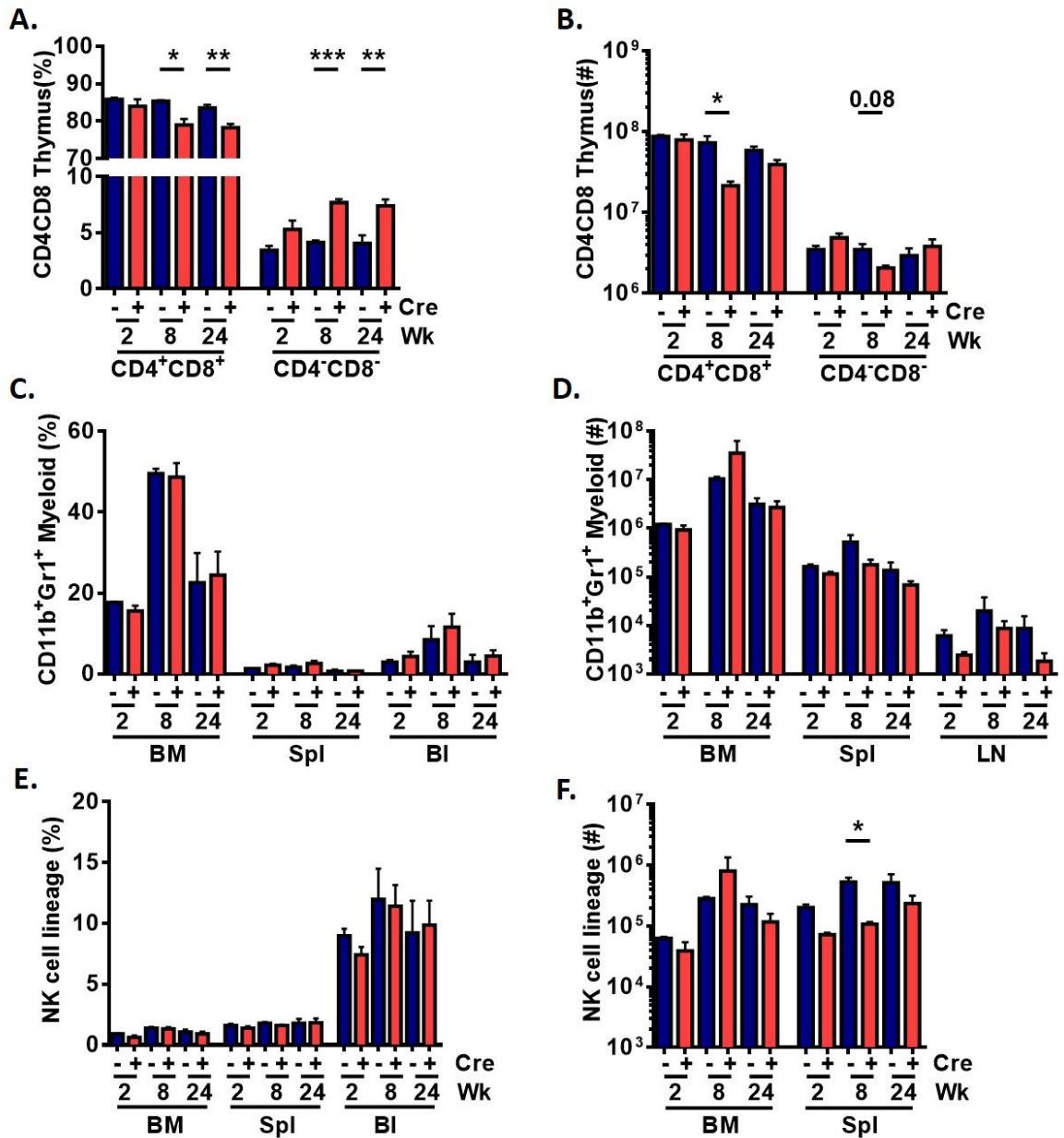
Figure 4.17: Optimization of the *Vav*-cre *Rictor* KO model age for phenotypic analysis of haemopoietic lineages.

Vav-Rictor control (cre-) and *Vav-Rictor* KO (cre+) mice were analyzed after 2 (n=3), 8 (n=3), or 24 (n=5) wk to assess the KO at different time-points. Percentage **(A)** and cellularity (log$_{10}$) **(B)** of CD4$^+$CD8$^+$ DP and CD4$^-$CD8$^-$ DN thymocytes in the thymus of *Vav-Rictor* control and *Vav-Rictor* KO mice analysed at 2, 8, or 24 wk of age. Percentage **(C)** and cellularity (log$_{10}$) **(D)** of CD11b$^+$Gr1$^+$ mature myeloid cells in the BM, spleen, blood and LN as indicated of *Vav-Rictor* control and *Vav-Rictor* KO mice analysed aged 2, 8, or 24 wk. Percentage **(E)** and cellularity (log$_{10}$) **(F)** of NK cells in the BM, spleen and blood as indicated of *Vav-Rictor* control and *Vav-Rictor* KO mice analysed aged 2, 8, or 24 wk. Data are expressed as mean±SEM (p *≤0.05, p **≤0.001, p ***≤0.0001).
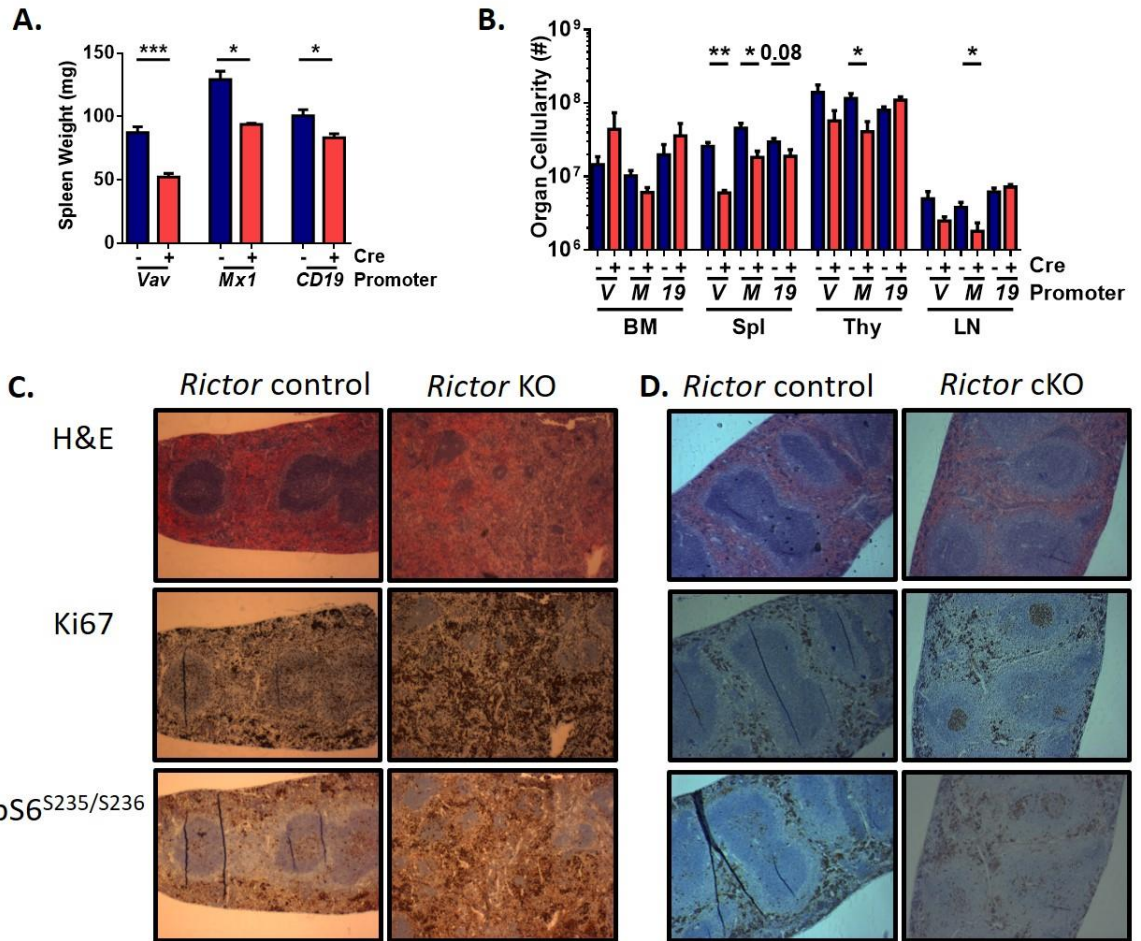
Figure 4.18: Characterization of *Rictor* KO models.
Spleen weight (mg) **(A)** and total organ counts ($\log_{10}$) (BM, spleen, thymus and LN) **(B)** of *Vav-Rictor* control and *Vav-Rictor* KO mice at 8 wk (n=3); *Mx1-Rictor* control and *Mx1-Rictor* cKO mice assessed 5 wk post 4 poly(I:C) inoculation (n=5); and *CD19-Rictor* control and *CD19-Rictor* KO mice (n=6) ≥18 wk of age. Histology slides showing H&E staining (top row), Ki67 staining (middle row), and pS6$^{S235/S236}$ (bottom row) in spleens of *Vav-Rictor* control and *Vav-Rictor* KO mice at 8 wk of age **(C)** and of *Mx1-Rictor* control and *Mx1-Rictor* cKO mice assessed 5 wk post 4 poly(I:C) inoculation **(D)**. Data are expressed as mean±SEM (p *≤0.05, p **≤0.001, p ***≤0.0001).
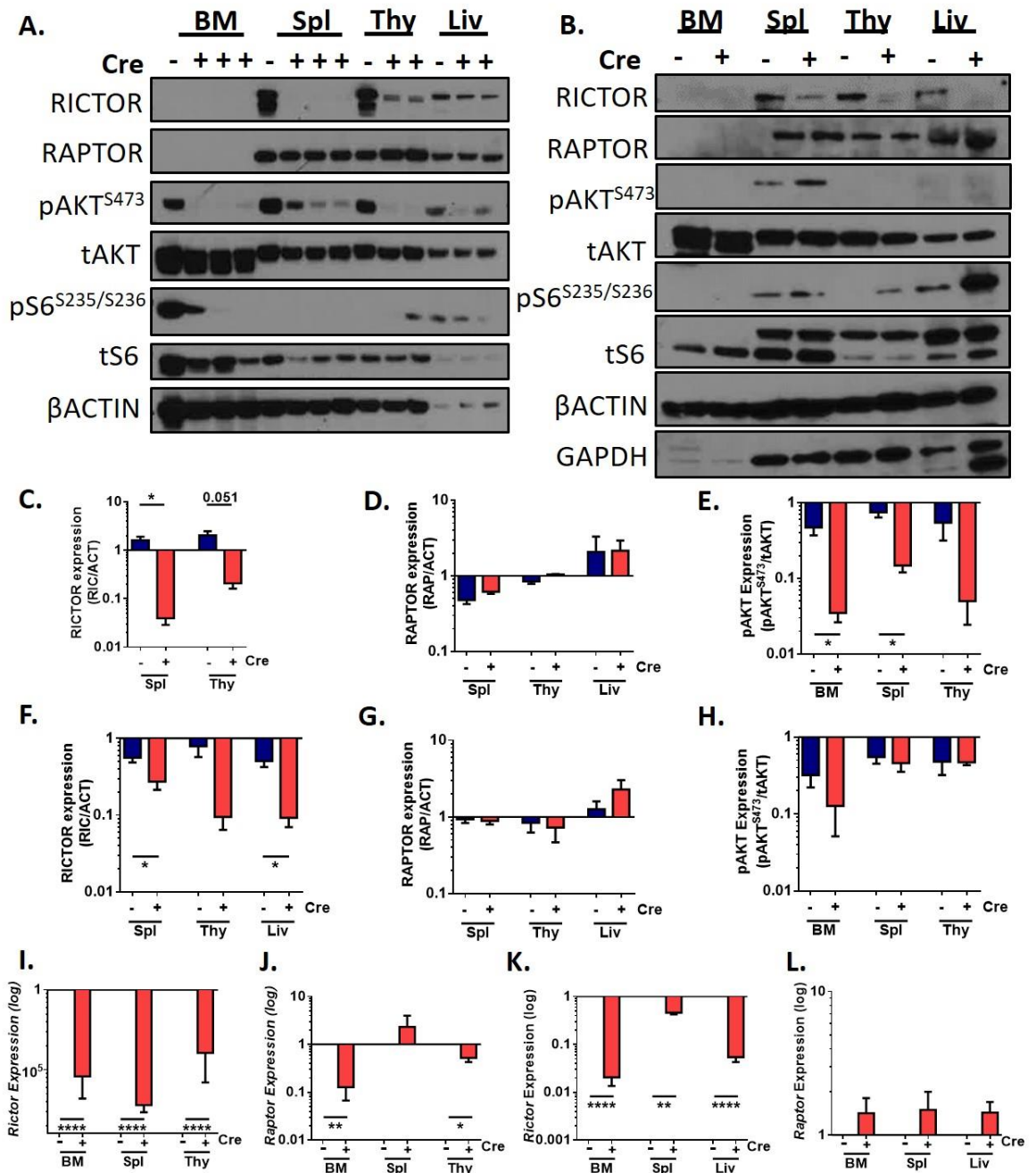
Figure 4.19: Confirming *Rictor* cKO by assessing protein and gene expression of mTOR pathway members.
Representative western blot showing protein expression of mTOR pathway proteins: RICTOR, RAPTOR, pAKT^{S473}, tAKT, pS6$^{S235/S236}$, tS6, βACTIN and GAPDH in the BM, spleen, thymus and liver of *Vav-Rictor* control and *Vav-Rictor* KO mice 8 wk of age **(A)** and of *Mx1-Rictor* control and *Mx1-Rictor* cKO mice assessed 5 wk post 4 poly(I:C) inoculation **(B)**. Densitometry showing protein expression (log fold change) of RICTOR/βACTIN in the spleen and thymus **(C)**, RAPTOR/βACTIN in the spleen, thymus and liver **(D)**, and of pAKT^{S473}/tAKT in the BM, spleen, thymus **(E)** of *Vav-Rictor* control and *Vav-Rictor* KO mice 8 wk of age (n=3), and densitometry showing protein expression (log fold change) of RICTOR/βACTIN in the spleen (n=5), thymus (n=3) and liver (n=4) **(F)**, of RAPTOR/βACTIN in the spleen (n=5), thymus (n=3) and liver (n=4) **(G)**, and of pAKT^{S473}/tAKT in the BM (n=4), spleen (n=5), thymus (n=2) **(H)** of *Mx1-Rictor* control and *Mx1-Rictor* cKO mice assessed 5 wk post 4 poly(I:C) inoculation. Gene expression (log fold change) of *Rictor* **(I)** and *Raptor* **(J)** in the BM, spleen and thymus of *Vav-Rictor* control and *Vav-Rictor* KO mice 8 wk (n=3) of age, along with gene expression (log fold change) of *Rictor* **(K)** and *Raptor* **(L)** in the BM (n=8), spleen (n=6) and liver (n=5) of *Mx1-Rictor* control and *Mx1-Rictor* cKO mice assessed 5 wk post 4 poly(I:C) inoculation. Data are expressed as mean±SEM (p *≤0.05, p **≤0.001, p ***≤0.0001).
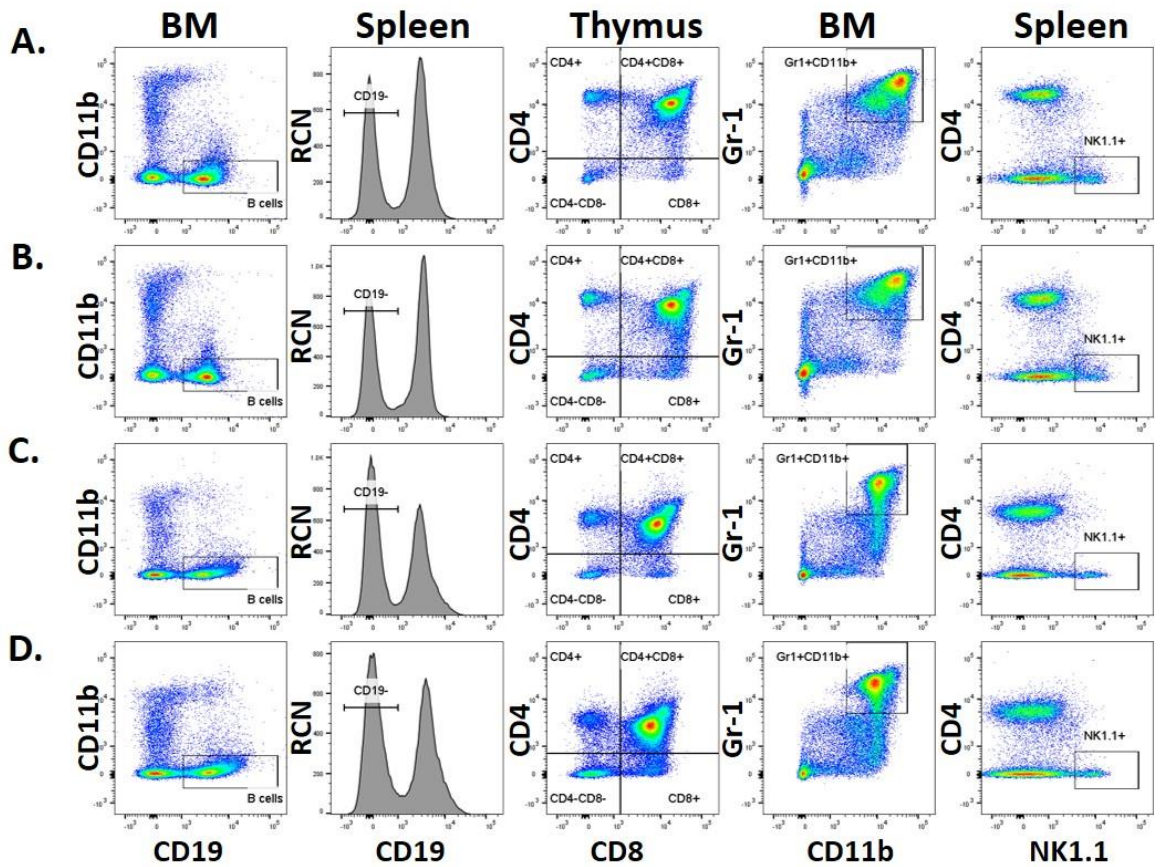
Figure 4.20: Gating strategy of haemopoietic lineages in *Vav*-cre and *Mx1*-cre *Rictor* models. Representative flow cytometry plots demonstrating the proportion of B cells (CD19$^+$CD11b$^-$) in the spleen, CD4$^+$ (CD19$^-$CD8$^-$CD4$^+$), CD8$^+$ (CD19$^-$CD4$^-$CD8$^+$), CD4$^+$CD8$^+$ (CD19$^-$CD4$^+$CD8$^+$) T cells in the thymus, mature myeloid cells (CD19$^-$CD11b$^+$Gr1$^+$) in the BM, and NK cells (CD19$^-$CD4$^-$NK1.1$^+$) in the spleen in *Vav-Rictor* control **(A)** *Vav-Rictor* KO aged 8 wk **(B)**, *Mx1-Rictor* control **(C)**, and *Mx1-Rictor* cKO mice assessed 5 wk post 4 poly(I:C) inoculation **(D)**. Plots are live and size (FSC-A/SSC-A) gated prior to the gating shown. RCN – relative cell number.
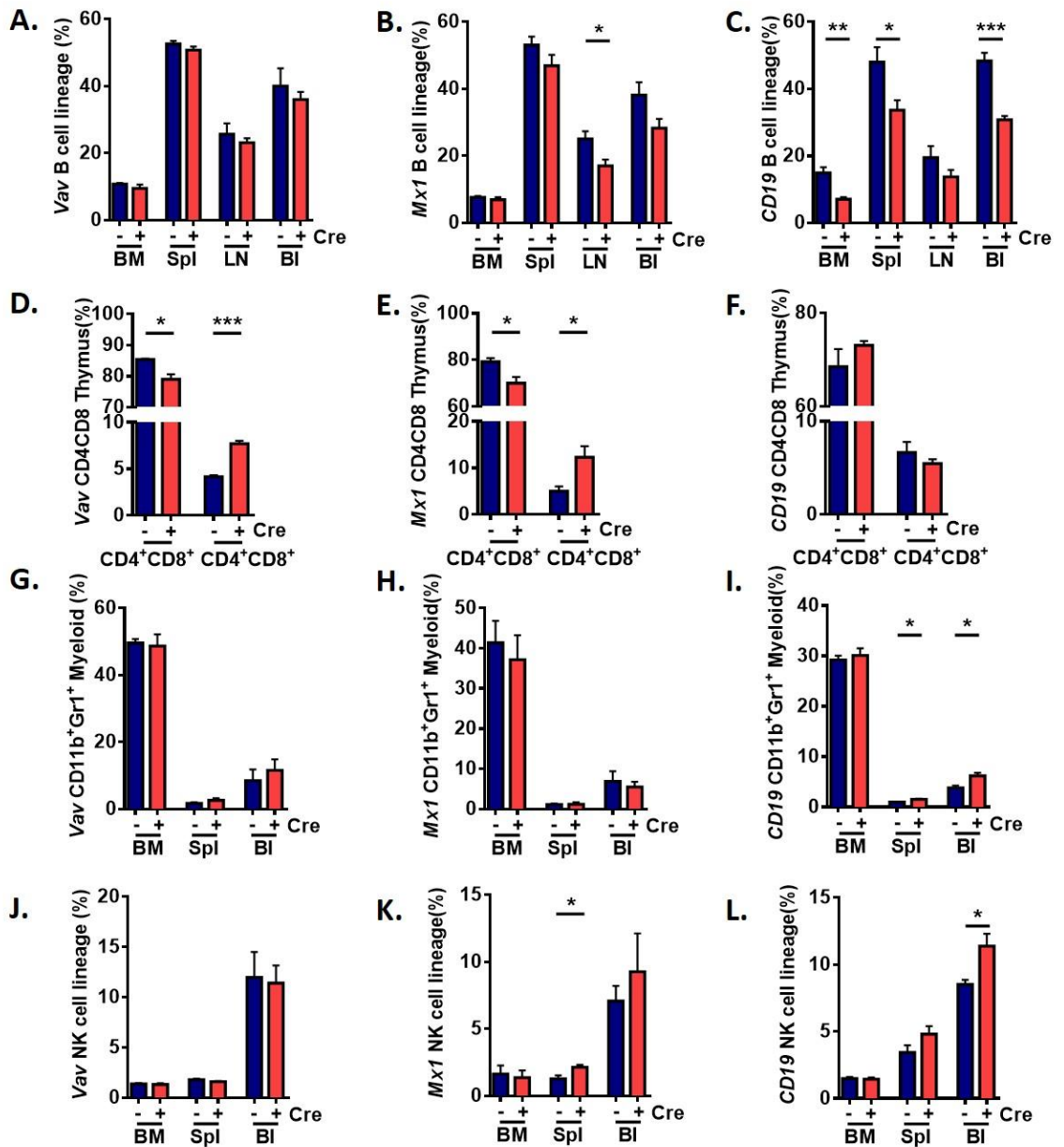
Figure 4.21: *Rictor*-deficiency leads to B and T cell aberrations *in vivo.*
Bar graphs showing the percentage of B cells in the BM, spleen, LN, and blood of *Vav-Rictor*
control and *Vav-Rictor* KO mice aged 8 wk (n=3) **(A)**, *Mx1-Rictor* control and *Mx1-Rictor* cKO mice
assessed 5 wk post 4 poly(I:C) inoculation (n=6) **(B)**, and *CD19-Rictor* control and *CD19-Rictor* KO
mice (n=6) **(C)**. Percentage of CD4+CD8+ DP and CD4-CD8- DN T cells in the thymus of *Vav-Rictor*
control and *Vav-Rictor* KO mice aged 8 wk (n=3) **(D)**, *Mx1-Rictor* control and *Mx1-Rictor* cKO mice
assessed 5 wk post 4 poly(I:C) inoculation (n=6) **(E)**, and *CD19-Rictor* control and *CD19-Rictor* KO
mice (n=6) **(F)**. Percentage of CD11b+Gr1+ mature myeloid cells in the BM, spleen and blood of
Vav-Rictor control and *Vav-Rictor* KO mice aged 8 wk (n=3) **(G)**, *Mx1-Rictor* control and *Mx1-Rictor*
cKO mice assessed 5 wk post 4 poly(I:C) inoculation (n=6) **(H)**, and *CD19-Rictor* control and
CD19-Rictor KO mice (n=6) **(I)**. Percentage of NK cells in the BM, spleen and blood of *Vav-Rictor*
control and *Vav-Rictor* KO mice aged 8 wk (n=3) **(J)**, *Mx1-Rictor* control and *Mx1-Rictor* cKO mice
assessed 5 wk post 4 poly(I:C) inoculation (n=6) **(K)**, and *CD19-Rictor* control and *CD19-Rictor* KO
mice (n=6) **(L)**. Data are expressed as mean±SEM (p *≤0.05, p **≤0.001, p ***≤0.0001).
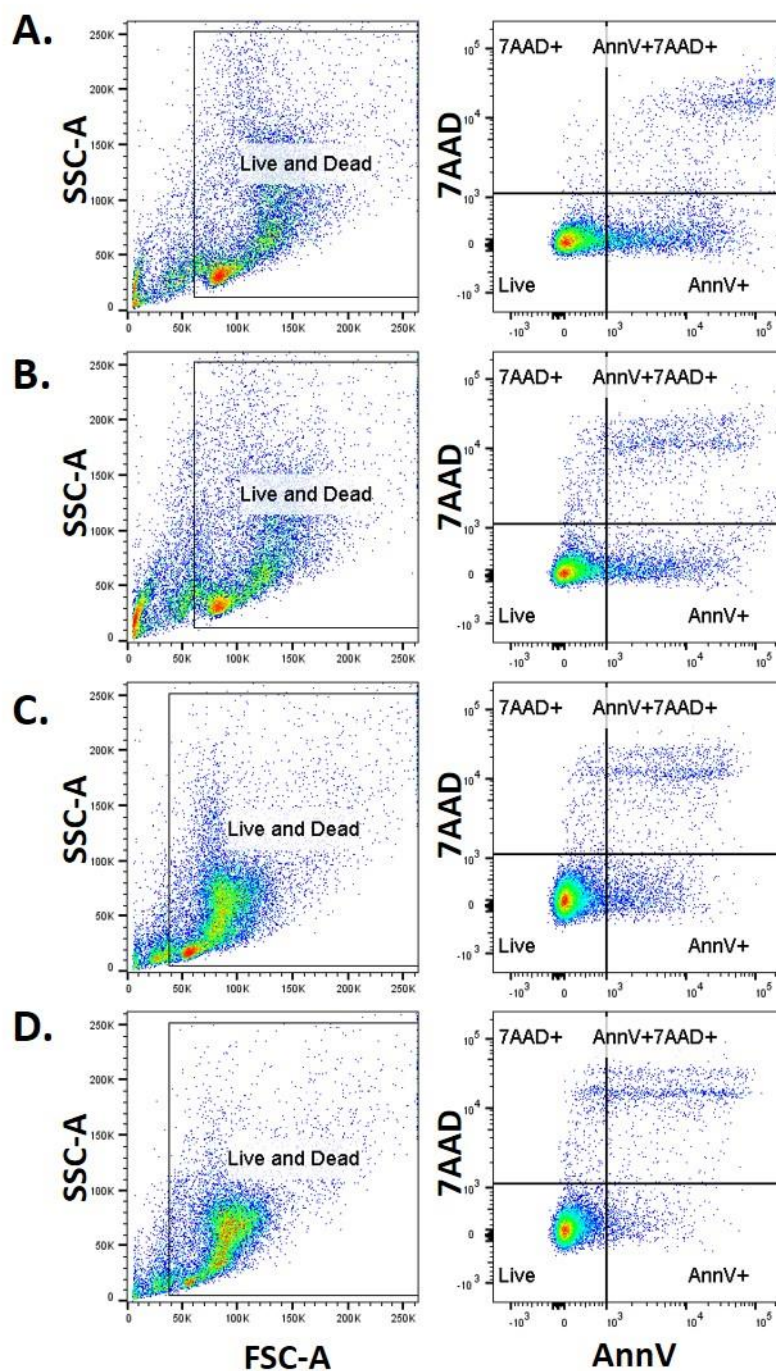
Figure 4.22: Gating strategy for determination of cell viability in *Vav*-cre and *Mx1*-cre *Rictor* models.
Representative flow cytometry plots showing the proportion of live (AnnV⁻7AAD⁻), early apoptosing (AnnV⁺7AAD⁻) and apoptotic (AnnV⁺7AAD⁺) cells in BM of *Vav-Rictor* control **(A)** *Vav-Rictor* KO mice aged 8 wk **(B)**, *Mx1-Rictor* control **(C)** and *Mx1-Rictor* cKO mice assessed 5 wk post 4 poly(I:C) inoculation **(D)**. Plots are live and size (FSC-A/SSC-A) gated as shown.
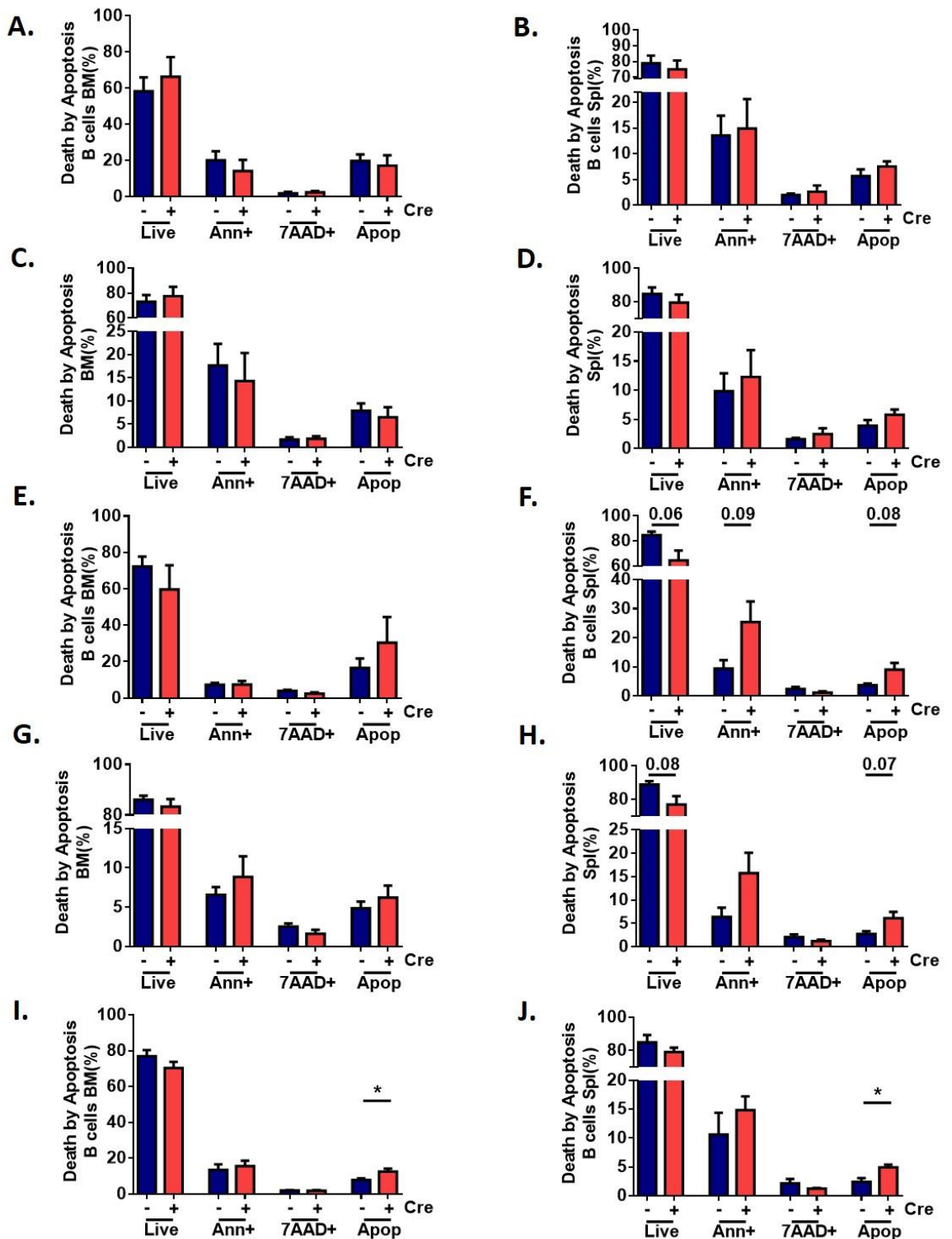
Figure 4.23: *Rictor*-deficiency does not cause apoptosis *in vivo.*
Bar graphs showing the percentage of CD19$^+$ B cells in the BM **(A)** and spleen **(B)**, and percentage of all cells in the BM **(C)** and spleen **(D)** which are live, early apoptotic (AnnV$^+$), necrotic (7AAD$^+$) or dead by apoptosis (Apop) in BM of *Vav-Rictor* control and *Vav-Rictor* KO mice aged 8 wk (n=5). Percentage of CD19$^+$ B cells in the BM **(E)** and spleen **(F)**, and percentage of all cells in the BM **(G)** and spleen **(H)** which are live, early apoptotic (AnnV$^+$), necrotic (7AAD$^+$) or dead by apoptosis in BM of *Mx1-Rictor* control and *Mx1-Rictor* cKO mice assessed 5 wk post 4 poly(I:C) inoculation (n=5). Bar graphs demonstrating the percentage of CD19$^+$ B cells in the BM **(I)** and spleen **(J)** which are live, early apoptotic (AnnV$^+$), necrotic (7AAD$^+$) or dead by apoptosis in BM of *CD19-Rictor* control and *CD19-Rictor* KO mice (n=6). Data are expressed as mean±SEM (p *≤0.05).
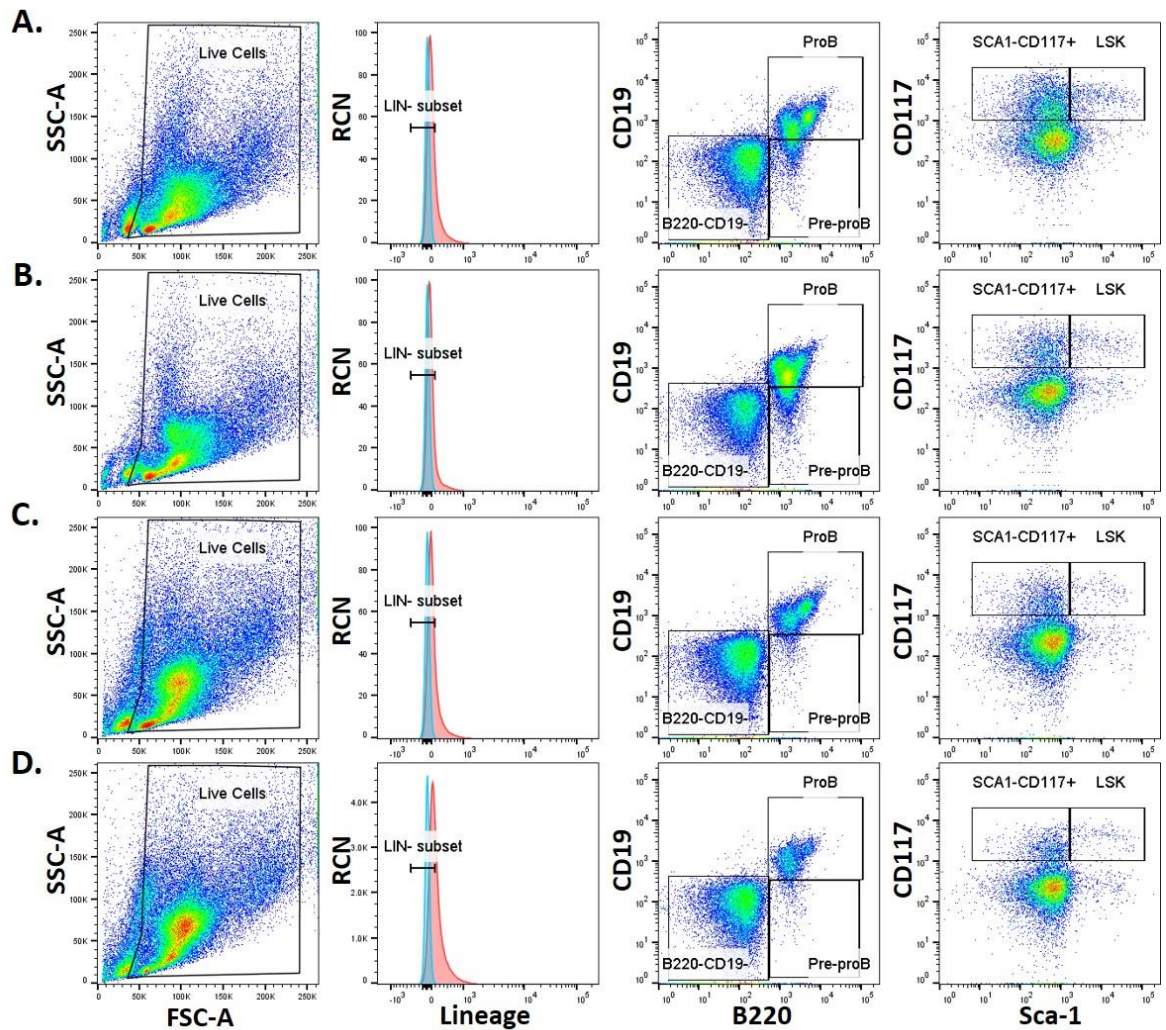
**Figure 4.24: Gating strategy of early B cell lineages in *Vav*-cre and *Mx1*-cre *Rictor* models.**
Representative flow cytometry plots showing the proportion of proB cells (Lineage⁻B220⁺CD19⁺), pre-proB cells (Lineage⁻B220⁺CD19⁻), LSK cells (Lineage⁻B220⁻CD19⁻Sca-1^{hi}CD117^{hi}), and sca-1^{lo}CD117^{hi} (Lineage⁻B220⁻CD19⁻Sca-1^{lo}CD117^{hi}) cells in the BM of *Vav-Rictor* control **(A)** and *Vav-Rictor* KO mice of 8 wk **(B)**, *Mx1-Rictor* control **(C)** and *Mx1-Rictor* cKO 5 wk post 4 poly(I:C) inoculation **(D)**. Lineage peak is shown in red and lineage negative subset was gated based on the unstained population (blue peak). Plots are live and size (FSC-A/SSC-A) gated as shown. RCN – relative cell number.
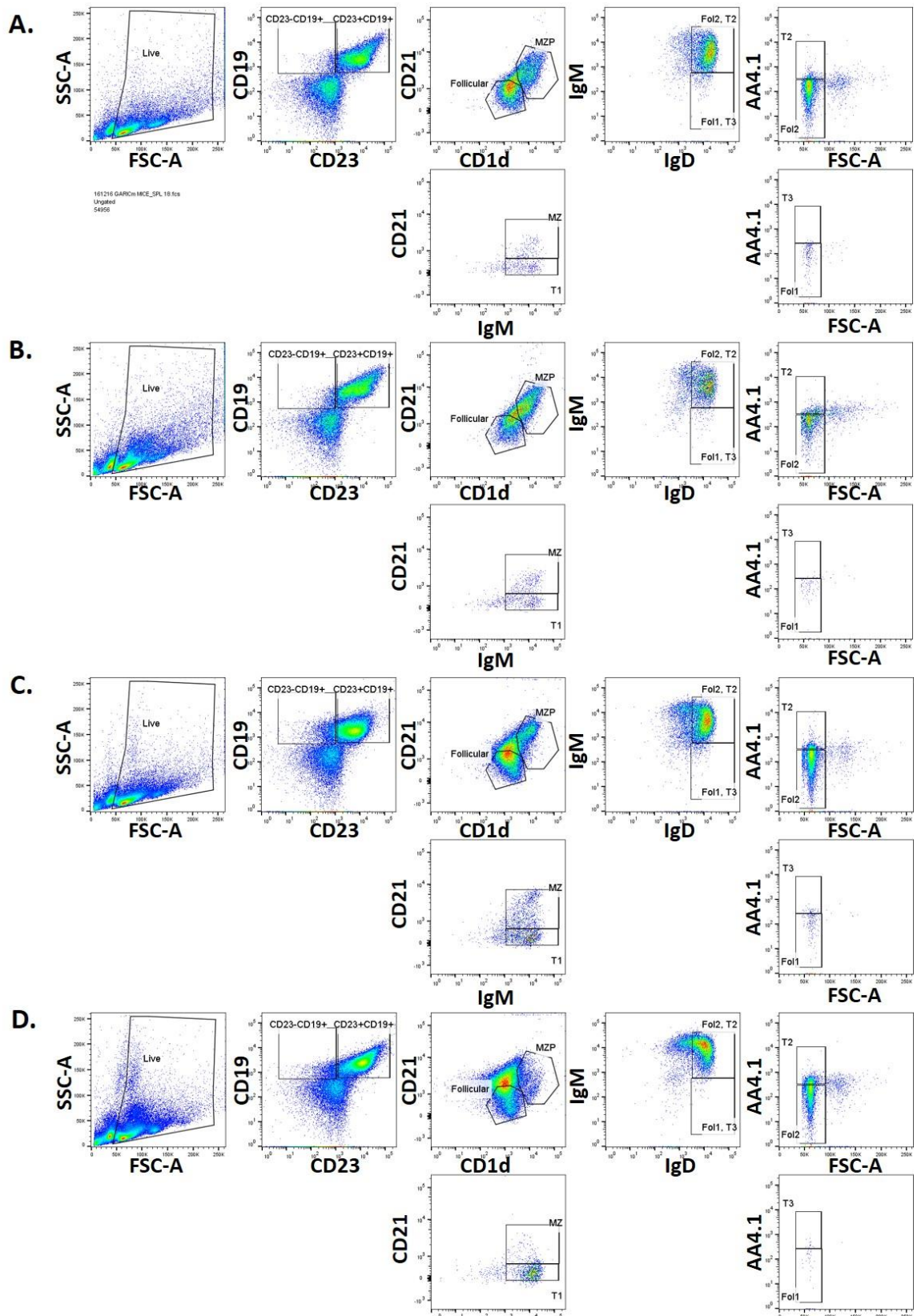
Figure 4.25: Gating strategy of late B cell lineages in *Vav*-cre and *Mx1*-cre *Rictor* models.
Representative flow cytometry plots demonstrating the proportion of late B cells which comprise
transitional 1 (T1) cells (CD19$^+$CD21^{int}CD23$^-$IgM^{hi}); T2
(CD19$^+$AA4.1$^+$CD21^{int}CD23$^+$CD1d^{int}IgD^{hi}IgM^{hi}); T3 (CD19$^+$AA4.1$^+$CD21^{int}CD23$^+$CD1d^{int}IgD^{hi}IgM^{lo});
marginal zone precursor (MZP): (CD19$^+$CD21^{hi}CD23$^+$CD1d^{hi}); marginal zone (MZ)
(CD19$^+$CD21^{hi}CD23$^-$IgM^{hi}); Fol1 (CD19$^+$AA4.1$^-$CD21^{lo}CD23$^+$CD1d^{int}IgD^{hi}IgM^{lo}) Fol2 (CD19$^+$AA4.1$^-$
CD21^{lo}CD23$^+$CD1d^{int}IgD^{hi}IgM^{hi}) in the spleen of *Vav-Rictor* control **(A)** and *Vav-Rictor* KO mice of
8 wks **(B)**, *Mx1-Rictor* control **(C)** and *Mx1-Rictor* cKO 5 wks post 4 poly(I:C) inoculation **(D).** Plots
are live and size (FSC-A/SSC-A) gated as shown.
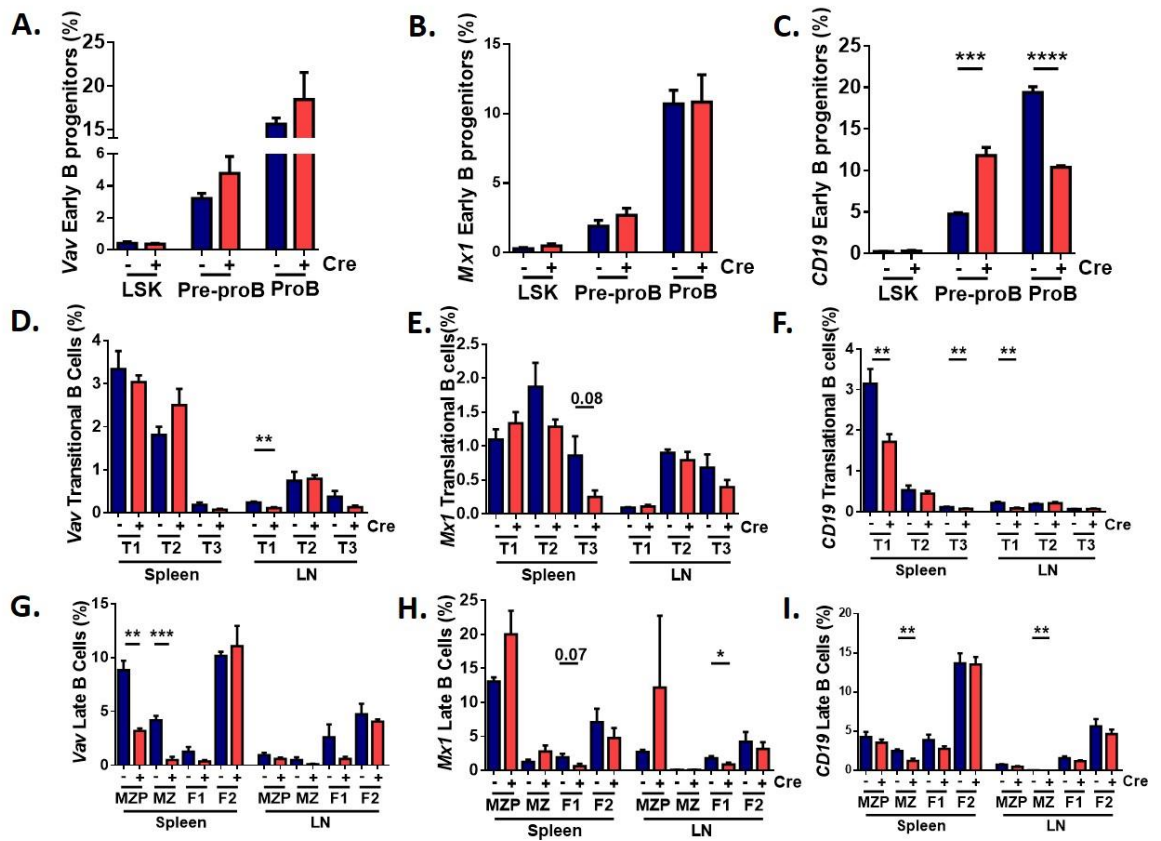
Figure 4.26: *Rictor*-deficiency at the HSC stage, in adult mice, and in B cells leads to aberrations in late B cells *in vivo.*

Bar graphs showing the percentage of LSK, pre-proB and proB cells in the BM of *Vav-Rictor* control and *Vav-Rictor* KO mice aged 8 wk (n=5) **(A)**, *Mx1-Rictor* control and *Mx1-Rictor* cKO mice assessed 5 wk post 4 poly(I:C) inoculation (n=6) **(B)**, and *CD19-Rictor* control and *CD19-Rictor* KO mice (n=6) **(C)**. Percentage of T1, T2 and T3 B cells in the spleen and LN of *Vav-Rictor* control and *Vav-Rictor* KO mice aged 8 wk (n=5) **(D)**, *Mx1-Rictor* control and *Mx1-Rictor* cKO mice assessed 5 wk post 4 poly(I:C) inoculation (n=6) **(E)**, and *CD19-Rictor* control and *CD19-Rictor* KO mice (n=6) **(F)**. Percentage of MZP, MZ, Fol1, and Fol2 cells in the spleen and LN of *Vav-Rictor* control and *Vav-Rictor* KO mice aged 8 wk (n=5) **(G)**, *Mx1-Rictor* control and *Mx1-Rictor* cKO mice assessed 5 wk post 4 poly(I:C) inoculation (n=6) **(H)**, and *CD19-Rictor* control and *CD19-Rictor* KO mice (n=6) **(I)**. Data are expressed as mean±SEM (p *≤0.05, p **≤0.001, p ***≤0.0001, p ****≤0.00001).

Chapter 5

Role of mTORC1 and mTORC2 in CLL

5 Role of mTORC1 and mTORC2 in CLL

5.1 Introduction

This chapter focusses on the role of mTORC1 and mTORC2 in leukaemia initiation and/or maintenance. As the *Vav*-cre⁺*Raptor^{fl/fl}* model is lethal at the perinatal stage, we did not use this model. As such, two mTORC1 KO models – *Mx1*-cre *Raptor^{fl/fl}* (*Mx1-Raptor*) and *CD19*-cre *Raptor^{fl/fl}* (*CD19-Raptor*) were used. To assess the role of mTORC2 in leukaemia initiation/development, the *CD19*-cre *Rictor^{fl/fl}* (*CD19-Rictor*), *Vav*-cre *Rictor^{fl/fl}* (*Vav-Rictor*) and *Mx1*-cre *Rictor^{fl/fl}* (*Mx1-Rictor*) mice models were used. Our lab has previously generated a murine CLL-like disease by retrovirally transducing lymphocyte-progenitors obtained from FLs of wildtype mice with a GFP-tagged kinase dead PKCα (PKCαKR) (229). We utilised a similar technique to generate a murine CLL-like disease from the BM of *Raptor* and *Rictor* KO mouse models to assess the role of mTORC1 and mTORC2 respectively in CLL initiation and/or development *in vitro* and *in vivo*.

5.2 Results

5.2.1 Ablation of mTORC1 blocks CLL initiation *in vitro.*

In order to assess the role of mTORC1 in CLL initiation/development *in vitro,* the *Mx1-Raptor* mouse model was used. To generate a CLL-like disease with *Raptor* cKO, mice were inoculated with either 3 or 4 rounds of poly(I:C) as indicated, and BM from either *Mx1-Raptor* control (cre^{-/-}) or *Mx1-Raptor* cKO (cre^{+/-}) mice was dissected. Purified CD117^{+} lymphoid progenitors from the BM were then retrovirally transduced with either GFP^{+}-MIEV (for generation into B cells as a control) or GFP^{+}-PKCαKR, to induce a murine CLL-like disease, in both *Mx1-Raptor* control or *Mx1-Raptor* cKO models, upon co-culture with OP9 cells (229,231).

Mx1-Raptor cKO MIEV and PKCαKR co-cultures (derived from mice dissected 3 wk post 3 poly(I:C) inoculation) failed to generate a CD19^{+}GFP^{+} population compared to *Mx1-Raptor* controls over D7, 11, 14 and 18 *in vitro* (Figure 5.1). Data demonstrated the inability of the PKCαKR construct to rescue the B cell lineage commitment block caused by *Raptor*-deficiency. Additionally, BM derived from *Mx1-Raptor* cKO mice with 4 poly(I:C) inoculation and dissected 5 wk post treatment, and then retrovirally transduced with MIEV or PKCαKR constructs showed a significant decrease in cellularity of GFP^{+}CD19^{+} MIEV cells over D3 and D7, coupled with a decrease in percentage of GFP^{+}CD19^{+} cells at D7, 11, and 14 as compared to *Mx1-Raptor* control MIEV cells (Figure 5.1A,B, Figure 5.2A,C). Similarly, *Mx1-Raptor* cKO PKCαKR cells had a significant decrease in cellularity of GFP^{+}CD19^{+} cells at D3 and D11 with a significant decrease in the percentage of GFP^{+}CD19^{+} PKCαKR cells over all culture days compared to *Mx1-Raptor* control PKCαKR cells (Figure 5.1C,D, Figure 5.2B,D). A significant increase in the percentage of GFP^{+}CD11b^{+} population in *Mx1-Raptor* cKO MIEV cells at D14 and in *Mx1-Raptor* cKO PKCαKR cells at D11 and D14 was observed compared to *Mx1-Raptor* control MIEV and PKCαKR cells (Figure 5.2E,F). These data suggest a lack in B cell lineage commitment with *Raptor*-deficiency regardless of the viral construct. In addition, there is an increase in GFP^{+}CD11b^{+} population over time suggesting a block in B cell differentiation compared to *Mx1-Raptor* control cells and block in CLL-like development with *Raptor*-deficiency compared to controls.

To further assess the role of mTORC1 in CLL cells, the *CD19-Raptor* KO model was used as it specifically excises *Raptor* in B-cells, as described previously (Section 1.7.1.3). Unlike, *Mx1-Raptor* cKO PKCαKR cells, *CD19-Raptor* KO PKCαKR cells developed a CLL-like phenotype. *CD19-Raptor* control and KO MIEV and PKCαKR cells were cultured until D18 to mimic later stages of disease development, then cell proliferation, viability and migration assays were carried out. No changes were observed in MIEV cells derived from CD19-cre$^-$ or CD19-cre$^{+/-}$ *Raptor* mice, but there was an increase in the cell trace violet (CTV) ratios comparing to D0, which was significant in D1/D0 ratio of *CD19-Raptor* KO PKCαKR cells compared to *CD19-Raptor* control PKCαKR cells (Figure 5.3A-C). This suggests a decrease in proliferation in PKCαKR cells with *Raptor*-deficiency as compared to controls. *CD19-Raptor* KO PKCαKR cells displayed a significant decrease in the percentage of early (AnnV$^+$) and late apoptosis (AnnV$^+$7AAD$^+$) with a significant increase in percentage of live cells (AnnV$^-$7AAD$^-$) compared to *CD19-Raptor* control PKCαKR cells (Figure 5.3D,E) suggesting *Raptor*-deficiency reduces apoptosis in CLL-like cells. To assess whether the *CD19-Raptor* KO PKCαKR cells migrate to the same extent as controls, a migration assay was performed where the cells were serum-starved for 2 hr and then allowed to migrate towards SDF-1 in transwell plates. There was a significant decrease in the cellularity and percentage of PKCαKR migrating cells in the absence of *Raptor*, with ~50% decrease in migration in *CD19-Raptor* KO PKCαKR cells compared to *CD19-Raptor* control PKCαKR cells (Figure 5.3F,G). Lastly, *Raptor*-deficient CLL-like cells displayed a trend in increase in G_0/G_1 phase with a decreasing trend in the G_2 phase compared to *CD19-Raptor* control PKCαKR cells (Figure 5.3H), further suggesting a block in proliferation with *Raptor*-deficiency.

As inducing *Raptor*-deficiency in all haemopoietic populations (*Mx1-Raptor* cKO model) leads to a block in B cell lineage commitment and a lack in CLL-like disease initiation, we assessed the role of mTORC1 in CLL maintenance. Therefore, GFP$^+$-PKCαKR cells were generated from BM of *Mx1-Raptor* control and cKO mice in the absence of poly(I:C) inoculation. There was no significant difference between the percentage of GFP$^+$CD19$^+$ cells generated from *Mx1-Raptor* cKO MIEV compared to control and *Mx1-Raptor* cKO PKCαKR cells compared to their respective control (Figure 5.4A,B). *Mx1-Raptor* control and cKO (no poly(I:C)) PKCαKR cells were cultured *in vitro* until D10 to mimic disease

development. To assess role of *Raptor* in disease maintenance, these cells were treated with 200 units (U) IFNβ for 24 hr, stimulating a TLR3 response and cre expression, to induce cKO *in vitro*. PCR analysis showed successful excision of *Raptor* in *Mx1-Raptor* cKO PKCαKR cells compared to controls (Figure 5.4C). Moreover, there was a decrease in the protein expression of RAPTOR in *Mx1-Raptor* cKO MIEV and PKCαKR cells compared to *Mx1-Raptor* controls with IFNβ treatment suggesting successful KO *in vitro* (Figure 5.4D,E). In addition, there were trends in decrease in $pS6^{S235/S236}$ expression with no changes in RICTOR and $pAKT^{S473}$ expression in *Mx1-Raptor* cKO PKCαKR cells treated with IFNβ compared to controls (Figure 5.4D,G,H) suggesting mTORC1 downstream targets were reduced upon *Raptor* excision with no effect on mTORC2 signalling.

To assess the effect of *Raptor*-deficiency in CLL maintenance *in vitro*, *Mx1-Raptor* cKO PKCαKR CLL-like cells treated with IFNβ were assessed for proliferation and cell cycling. There was a significant decrease in the cellularity, with a similar trend in the percentage, of GFP^+CD19^+ population in the co-cultures of *Mx1-Raptor* cKO PKCαKR cells treated with 50U IFNβ for 3 days and 200U for 24 hr, compared to *Mx1-Raptor* controls (Figure 5.5A,B). As 200U IFNβ treatment for 24 hr was more robust compared to other treatment arms, 200U IFNβ treatment was carried out on all future experiments. Interestingly, there was also a significant decrease in the cellularity of GFP^+CD19^+ *Mx1-Raptor* cKO PKCαKR cells receiving no IFNβ treatment (pink bars) (Figure 5.5A) compared to untreated *Mx1-Raptor* control PKCαKR cells (light blue bars). While this effect was significant, it did not occur to the same extent as with higher IFNβ treatments. Indeed, a significant decrease in the GFP^+CD19^+ cellularity was observed in *Mx1-Raptor* cKO PKCαKR cells with IFNβ treatment compared to untreated cells, with no reductions in cell populations in *Mx1-Raptor* control PKCαKR cells with or without IFNβ treatment (Figure 5.5C). IFNβ treatment of *Mx1-Raptor* cKO PKCαKR cells slightly increased G_0 phase, with a decreasing trend in S/G_2 phase compared to the untreated *Mx1-Raptor* cKO PKCαKR cells and *Mx1-Raptor* control PKCαKR cells treated and untreated with IFNβ (Figure 5.5D). Moreover, there is a significant increase in the CTV MFI of D2 in IFNβ treated *Mx1-Raptor* cKO PKCαKR cells compared to treated controls suggesting a block in proliferation due to an increase in CTV MFI (Figure 5.5E,F). These data suggest a similar role for *Raptor* in disease maintenance as in disease initiation,

whereby there is a block in proliferation with induced *Raptor*-deficiency after mimicking disease development *in vitro*.

5.2.2 mTORC2 plays a role in CLL-like phenotype maintenance at later stages *in vitro.*

To determine the role of mTORC2 in CLL initiation/development, the *Vav-Rictor, Mx1-Rictor* and *CD19-Rictor* mouse models were used. BM was derived from *Vav-, Mx1-* (dissected 5 wk post 4 poly(I:C) inoculation), and *CD19-Rictor* control or KO mice, and retrovirally transduced with either GFP⁺-MIEV or GFP⁺-PKCαKR constructs to induce a CLL-like phenotype. Unlike *Raptor*-deficient cells, PKCαKR cells derived from all the *Rictor* KO models developed a CLL-like phenotype *in vitro*. There was little difference in the cellularity of GFP⁺CD19⁺ population earlier in the co-cultures, with a slight decrease in cellularity of GFP⁺CD19⁺ population at D28 in *Vav-*, and *CD19-Rictor* KO MIEV and PKCαKR cells compared to their respective controls (Figure 5.6A-C,E,F,H). There was a trend in increase in the cellularity of GFP⁺CD19⁺ population of *Mx1-Rictor* cKO MIEV cells with decreasing trends in *Mx1-Rictor* cKO PKCαKR cells at D21 (Figure 5.6D,G). These data suggest *Rictor* is not fundamental for CLL-like disease initiation but may play a role in disease maintenance. Similarly, there was no difference in the percentage of GFP⁺CD19⁺ population, but a decreasing trend in the percentage of GFP⁺CD19⁺ population was observed at D21 and later days in *Vav-*, *Mx1-* and *CD19- Rictor* KO MIEV and PKCαKR cells, compared to their respective controls (Figure 5.7A-F). This suggests there may be a role of *Rictor* in CLL-like disease maintenance, similar to that played in late B cell maintenance (Chapter 4). Additionally, no changes were observed in GFP⁺CD11b⁺ population in *Vav-*, *Mx1-*, or *CD19-Rictor* KO MIEV and PKCαKR cells compared to their respective controls suggesting mTORC2 does not play a role in B cell lineage commitment, further reiterating the redundant role of mTORC2 in CLL-like phenotype initiation *in vitro* (Figure 5.7G-L).

As there was a decreasing trend in GFP⁺CD19⁺ cellularity and percentage in later stages of both MIEV and PKCαKR co-cultures with *Rictor*-deficiency, *Vav-* and *Mx1-Rictor* cKO and control PKCαKR cells at D21 were further assessed. Successful KO, confirmed by a significant decrease in *Rictor* expression, was associated with an increasing trend in *Ccnd1* expression and no changes in

Cdkn1a and *Cdkn1b* in *Vav-Rictor* KO PKCαKR cells compared to *Vav-Rictor* control PKCαKR cells, with no changes in *Ccnd1, Cdkn1a* and *Cdkn1b* expression in *Vav-Rictor* KO MIEV cells compared to *Vav-Rictor* control MIEV cells (Figure 5.8A). A similar trend was seen in *Mx1-Rictor* cKO PKCαKR cells (4 poly(I:C) inoculation), with a strong trend in increase in *Ccnd1* with a significant decrease in *Rictor* expression compared to *Mx1-Rictor* control PKCαKR cells cultured till D21 (Figure 5.8B) alluding to a potential role of mTORC2 in regulating cell cycling in CLL-maintenance *in vitro.* At the protein level, there was a significant decrease in RICTOR expression with a slight decrease in pAKT^{S473} expression in *Mx1-Rictor* cKO PKCαKR cells compared to *Mx1-Rictor* control PKCαKR cells at D21 of culture (Figure 5.8C-E). This confirmed a lack of *Rictor* at the later co-culture stages mimicking CLL-disease, suggesting that the *Mx1-Rictor* cKO model is not 'leaky'. To further assess the role of mTORC2 in CLL, migration, proliferation and cell cycle assays were carried out. An increasing trend in the cellularity and percentage of migrating cells towards SDF-1 was observed at D15 of *Vav-Rictor* KO PKCαKR cells (Figure 5.9A,B), which was significant at D21 of *Vav-Rictor* KO PKCαKR cells compared to controls (Figure 5.9C,D), alluding to a role at later stages of disease development. Nevertheless, there were no changes in the MFI ratios of CTV values in *Vav-Rictor* KO PKCαKR cells at D14 or at D21 compared to controls suggesting no changes in proliferation (Figure 5.9E,F). However, at both D14 and D21 of culture, there was an increasing trend in the percentage of *Mx1-Rictor* cKO (4 poly(I:C) inoculation) PKCαKR cells in S phase with a decreasing trend of cells in G_0/G_1 phase compared to *Mx1-Rictor* control PKCαKR cells (Figure 5.9G,H) suggesting a potential increase in cell cycling in PKCαKR cells with *Rictor*-deficiency.

5.2.3 mTORC1 affects CLL maintenance *in vivo.*

As mTORC1 plays a fundamental role in disease initiation and maintenance *in vitro,* the role of mTORC1 in disease maintenance was assessed *in vivo.* Immunocompromised NSG mice were transplanted with 5x10^5 *Mx1-Raptor* control or cKO (no poly(I:C) inoculation) PKCαKR cells co-cultured till D7-10. Upon disease development, classified as ≥ 10% GFP⁺CD19⁺ CLL-like disease assessed by weekly tail bleeds, half the cohort of mice were inoculated with poly(I:C) to induce *Raptor* cKO in the CLL-like cells transplanted into NSG mice. Screening for CLL-like disease in weekly blood samples of NSG mice showed a drastic

reduction, from ≥89.3% in an untreated mouse and other two mice transplanted with *Mx1-Raptor* control PKCαKR cells with or without poly(I:C) treatment to 3.45% in GFP+CD19+ CLL-like disease in a mouse transplanted with *Mx1-Raptor* cKO PKCαKR cells and poly(I:C) treated (Figure 5.10A-D). Although there were no changes in splenic weight (Figure 5.11A), there was a decreasing trend in splenic cellularity in mice transplanted with *Mx1-Raptor* cKO PKCαKR cells with poly(I:C) treatment compared to untreated and *Mx1-Raptor* control with or without poly(I:C) treatment *in vivo* (Figure 5.11B). There was also a decreasing trend in BM cellularity in mice transplanted with *Mx1-Raptor* cKO PKCαKR cells treated with poly(I:C) compared to mice treated with poly(I:C) and transplanted with *Mx1-Raptor* control PKCαKR cells (Figure 5.11C). Weekly bloods taken from mice to assess disease progression after inducing *Raptor*-deficiency showed a trend in increase in the percentage of GFP+CD19+ population in mice transplanted with *Mx1-Raptor* control and cKO PKCαKR cells (no poly(I:C)) (Figure 5.11D). Interestingly, there was a delay in increase in the percentage of GFP+CD19+ cells in mice transplanted with *Mx1-Raptor* control PKCαKR cells after treatment with poly(I:C) suggesting that poly(I:C) alters disease progression (Figure 5.11D). Mice transplanted with *Mx1-Raptor* cKO PKCαKR cells and then treated with poly(I:C) had a decreased percentage of disease load in the blood (GFP+CD19+ population) compared to the other arms (Figure 5.11E). Whilst assessing the organs, there was a significant decrease in GFP+CD19+ cellularity in the spleen, and a significant decrease in the percentage of GFP+CD19+ population in the BM and spleen of poly(I:C) treated mice transplanted with *Mx1-Raptor* cKO PKCαKR cells compared to those transplanted with *Mx1-Raptor* cKO PKCαKR cells (untreated) and *Mx1-Raptor* control PKCαKR cells respectively (Figure 5.11F,G). No significant difference was noted between the percentage of survival in poly(I:C) treated or untreated mice transplanted with *Mx1-Raptor* control PKCαKR cells (Figure 5.11H) suggesting poly(I:C) inoculation does not increase survival in mice with a CLL-like disease *in vivo*. However, there was a significant increase in survival of poly(I:C) treated mice transplanted with *Mx1-Raptor* cKO PKCαKR cells compared to untreated mice transplanted with *Mx1-Raptor* cKO or control PKCαKR cells (Figure 5.11I,J), which suggests that *Raptor*-deficiency increases survival in mice with a CLL-like disease *in vivo*.

Interestingly, there was no significant difference in pAKT^{S473} phosphorylation, but a significant increase in RAPTOR expression, together with a strong trend in increase downstream targets p4EBP1$^{T36/T47}$ expression in poly(I:C) treated mice transplanted with *Mx1-Raptor* cKO PKCαKR cells compared to *Mx1-Raptor* control PKCαKR cells (Figure 5.12A-D). Additionally, there was a trend in increase in pS6$^{S235/S236}$ expression with a significant decrease in the downstream expression of RICTOR (Figure 5.12E-F). These data suggest a possible re-population of a CLL-like disease clone with increased RAPTOR expression which escaped poly(I:C) dependent *Raptor*-excision. It is important to note here that all the transplanted mice were sacrificed at disease end and not after a single time point, therefore most of the mice transplanted with *Mx1-Raptor* cKO PKCαKR cells + poly(I:C) treated were sacrificed at a later time than the other arms due to a delay in disease (Figure 5.11I,J). We would have expected to see a decrease in RAPTOR if the mice would have been sacrificed at the same time point.

To further assess the role of mTORC1 in leukemogenesis, CD19-*Raptor* control or KO BM cells were transduced with GFP$^+$-PKCαKR and transplanted into NSG mice between D7-10 of culture. There was a decreasing trend of GFP$^+$CD19$^+$ CLL-like disease percentage in the bloods of NSG mice transplanted with *CD19-Raptor* KO cells as compared to controls (Figure 5.13) suggesting a non-redundant role of *Raptor* in CD19$^+$ cells in disease progression. Although there were no changes in the spleen weight, BM and spleen organ cellularity, there was a clear delay in disease onset, observed by a delay in GFP$^+$CD19$^+$ CLL-like cells in the bloods, along with a significant increase in survival of mice transplanted with *CD19-Raptor* KO PKCαKR cells compared to controls (Figure 5.14A-D). As all mice were sacrificed at disease end, most of the mice transplanted with *CD19-Raptor KO* PKCαKR cells survived longer than the controls allowing disease to accumulate eventually compromising the health of the mouse leading to end point. At end point, no change was observed in the cellularity of GFP$^+$CD19$^+$ CLL-like cells in the BM and spleen, but there was a significant decrease in percentage of GFP$^+$CD19$^+$ CLL-like cells in the BM with a similar trend in the LN of mice transplanted with *CD19-Raptor* KO PKCαKR cells compared to controls (Figure 5.14E,F). Moreover, there were no changes in RAPTOR, pAKT^{S473}, and pS6$^{S235/S236}$ expression in the spleens of mice transplanted with *CD19-Raptor* KO PKCαKR cells compared to controls (Figure 5.14G-J), suggesting a re-population of *Raptor*

in CD19$^+$ cells thereby leading to an increase in GFP$^+$CD19$^+$ cell population in mice treated with *CD19-Raptor* KO PKCαKR cells over time.

5.2.4 Using mTOR inhibitors and current clinical drugs to combat CLL *in vivo.*

To compare the effect of mTOR inhibitors and current clinical drugs for CLL in mice transplanted with a CLL-like disease, CD117$^+$ lymphocytes purified from BM of B6.SJL mice were retrovirally transduced with GFP$^+$-PKCαKR to generate a CLL-like disease and 5x10^5 cells were transplanted into NSG mice after D7-10 of co-culture. Once the mice had established disease (≥0.4% GFP$^+$CD19$^+$ CLL-like disease), the mice were treated with either vehicle control (captisol+0.5%methylcellulose), AZD2014 (dual mTOR complex inhibitor), ibrutinib (BTK inhibitor used in clinics), or a combination of AZD2014+Ibrutinib (combo). AZD2014 and ibrutinib were administered at 15 mg/kg and 12 mg/kg by OG daily for 2 wk, after which mice were sacrificed and analyzed for disease. A drastic reduction in the percentage of GFP$^+$CD19$^+$ CLL-like cells was observed in the bloods, from 93.6% in mice treated with vehicle control to 3.68% and 5.92% in mice treated with AZD2014 and ibrutinib respectively (Figure 5.15A-C). Additionally, mice treated with the combo showed a greater decrease in GFP$^+$CD19$^+$ percentage, from 3.68% in AZD2014 treated mice and 5.92% in ibrutinib treated mice to 0.57% in mice treated with combination (Figure 5.15B-D). These data suggest that mice treated with a combination therapy have a greater reduction in disease load in the blood compared to single agents. There was a clear reduction in the spleen size and a significant reduction in spleen/body weight ratio and spleen cellularity, with no changes in BM cellularity in mice treated with either AZD2014, ibrutinib, or combination compared to vehicle control (Figure 5.16A-C). These findings suggest a reversal of splenomegaly observed in CLL with no changes in BM cellularity with single agents or combination therapy. There was a clear decrease in percentage of GFP$^+$CD19$^+$ CLL-like disease in mice in weekly tail bleeds post treatment with AZD2014, ibrutinib or combination compared to vehicle controls (Figure 5.16D). Moreover, a significant decrease in cellularity and percentage of the GFP$^+$CD19$^+$ CLL-like population in the BM, together with a significant decrease in the cellularity and a similar decreasing trend in the percentage of GFP$^+$CD19$^+$ cells in the spleen were observed in mice treated with AZD2014, ibrutinib or

combination compared to controls (Figure 5.16E-H). GFP$^+$CD19$^+$ CLL-like cells were assessed for the expression of CD5$^+$ marker, which is a subset of CLL cells associated with increased migration as described in the Calissano model (156). A significant decrease in the cellularity of GFP$^+$CD19$^+$CD5$^+$ CLL-like cells was observed in the BM and spleen of mice treated with single agents or with combination compared to controls (Figure 5.16I). These data suggest a potent role of the dual mTOR complex inhibitor, AZD2014, as a promising therapeutic compound for CLL as it has similar results as ibrutinib, a drug currently used as first-line therapy for CLL patients with *TP53* mutation/17p deletion. However, combination of ibrutinib and AZD2014 did not have any additive effect with little evidence for synergy.

To assess the ability of mTOR inhibitors to treat advanced CLL-like disease, we performed secondary transplants, where 4×10^5 cells from the spleen of mice carrying a CLL-like disease (≥95%) was transplanted into NSG or NRG host mice. Once disease was established (≥10% GFP$^+$CD19$^+$ CLL-like disease), mice were treated with either rapamycin (administered by ip injection at 4 mg/kg) or AZD2014 (administered by OG at 15 mg/kg) once daily for 3 wk and disease progression was assessed. A reduction in the percentage of GFP$^+$CD19$^+$ CLL-like cells in the bloods of mice treated with AZD2014 and rapamycin was seen, from 90.1% to 77.9% and 0.69% respectively compared to vehicle control (Figure 5.17A-C). There was a clear reduction in the spleen size and a strong decreasing trend in spleen/body weight ratio, with no changes in BM and splenic cellularity in mice treated with rapamycin. These findings are coupled with no change in the spleen size and weight, or BM or spleen cellularity in mice treated with AZD2014 compared to vehicle controls, suggesting rapamycin is more potent at decreasing disease load in mice that have undergone secondary transplants (Figure 5.18A-C). In addition, there was a clear decrease in percentage of GFP$^+$CD19$^+$ CLL-like disease in the blood post rapamycin treatment, but not with AZD2014 compared to vehicle controls (Figure 5.18D). Moreover, there was a significant decrease in the percentage of GFP$^+$CD19$^+$ CLL-like cells in the BM and blood with a similar trend in the spleen and LN, and a decreasing trend in cellularity of GFP$^+$CD19$^+$ CLL-like cells in the BM and spleen in mice treated with rapamycin compared to AZD2014 or controls (Figure 5.18E-G). These data indicate a potential decrease in disease load with rapamycin and not with

AZD2014. As expected, no changes in RAPTOR and RICTOR expression was noted in spleens of mice treated with AZD2014 or rapamycin, despite the more potent effect of rapamycin in decreasing disease load, as this was not a KO model (Figure 5.19A-C). No significant changes in $pAKT^{S473}$ and $pS6^{S235/S236}$ levels were noted in drug treated spleens (Figure 5.19A,D,E). Furthermore, spleens of mice treated with AZD2014, and not with rapamycin, had an increasing trend in cyclin genes *Ccnd1, Ccnd2 and Ccnd3*, with trends in increase in the pro-apoptotic target *Bid* and no changes in *Prkcb* (Figure 5.19F,G), suggesting possible increase in cell cycling with AZD2014 treatment compared to vehicle controls. These data suggest that rapamycin is more potent in targeting a CLL-like disease in secondary transplants of mice than AZD2014, which could have a potential effect on cell cycling of CLL-like disease *in vivo*.

5.3 Discussion

To assess the role of the mTOR complexes in leukaemia initiation and/or development, cre-loxP models were used for both *in vitro* and *in vivo* studies. CLL is characterised by having increased BCR signalling where CLL is driven by antigen-independent autonomous signalling(308). Moreover, it is known that BCR signalling in CLL cells which are anergic internalise and accumulate ligand in exosomes more than in normal B cells. Additionally, ligation of CD79b or IgM has shown independent internalisation in CLL cells but not in healthy B cells. Ibrutinib, a BTK inhibitor has been shown to reduce BCR signalling capacity and induce efficient internalisation(309). Several other inhibitors have been tested to reduce this chronic BCR signalling. Once such drug, Fostamatinib, a partial spleen tyrosine kinase (SYK) inhibitor, although effective in causing CLL-apoptosis, was deemed toxic to certain cell lines and clinical development was discontinued(310). Dasatinib, a tyrosine kinase inhibitor, blocking LYN, BTK and other kinases inhibits BCR signalling and block BCR mediated survival of CLL cells, together with decreasing migration towards SDF-1(311). Although there are very efficient drugs in clinics for CLL, it currently remains incurable and therefore there is a need for curative therapy. The mTOR pathway has previously shown to be upregulated in CLL(312), and here we target this pathway downstream the BCR as a potential therapeutic strategy. We used cre-loxP mouse models to generate a CLL-like disease and assess the role of mTORC1 and mTORC2 in CLL *in vitro* and *in vivo*. Our laboratory has previously developed a CLL mouse model by the retroviral transduction of a kinase-dead PKCα (PKCαKR) into lymphocytes isolated from FL of mice(230). We used a similar technique, but we induced a CLL-like disease from the BM of mice enabling us to utilize the KO mouse models. For all the experiments, the BM was purified for CD117$^+$ lymphocytes and retrovirally transduced with either GFP tagged MIEV to assess B cell development, or PKCαKR to induce a CLL-like disease. These cells were cultured *in vitro* for experiments or were transplanted into NSG host mice after D7-10 of culture to introduce a CLL-like disease *in vivo*.

5.3.1 Role of mTORC1 and mTORC2 in leukaemia initiation and/or progression *in vitro*

CD117^{+} lymphocytes retrovirally transduced with GFP^{+}-PKCαKR from the BM of *Mx1-Raptor* cKO mice with 4 poly(I:C) inoculation failed to initiate a CLL-like disease as compared to *Mx1-Raptor* controls *in vitro*. *Mx1-Raptor* control MIEV and PKCαKR cells are driven to a B cell lineage in culture, however, *Mx1-Raptor* cKO MIEV cells failed to commit to a B cell lineage alluding to the role of mTORC1 not only in B cell development (Chapter 4), but also in CLL initiation. Our results highlight that the PKCαKR retroviral construct was unable to rescue the lineage commitment block caused due to *Raptor*-deficiency. The increased percentage of GFP^{+}CD11b^{+} cells with a concomitant decline in B cell/CLL-like cell population in *Mx1-Raptor* cKO MIEV and PKCαKR cells does not allude to an increase in myeloid population with *Raptor*-deficiency. As there is a block in B cell development, there is increased GFP^{+}CD11b^{+} population as myeloid lineage development is not completely compromised with *Raptor*-deficiency. Nevertheless, due to the OP9-system(231), there is a bias for B-cell development with the addition of Flt3 ligand and IL7 (33,313), and a lack of M-CSF, which hinders myeloid lineage development and proliferation. Therefore, there is an initial increase in CD11b^{+} population and subsequent decline in this population by D7 in *Mx1-Raptor* control MIEV and PKCαKR cells but this trend is compromised with *Raptor* deficiency leading to an increase in percentage of GFP^{+}CD11b^{+} population.

Whilst assessing the role of mTORC1 in CLL progression, the *CD19-Raptor* KO model was used. Unlike the *Mx1-Raptor* cKO model, there was successful CLL-like disease initiation with *Raptor*-deficiency in CD19^{+} cells. As CD19 is expressed at the preB cell stage (205), retroviral transduction is done at an earlier stage in CD117^{+} lymphocytes thereby leading to disease initiation. However, the model would KO *Raptor* in CLL-CD19 expressing cells thereby enabling the assessment of the role of *Raptor* in CLL *in vitro*. *CD19-Raptor* KO PKCαKR cells demonstrated a similar block in proliferation and migration with an increasing trend in G_0/G_1 phase. It was interesting to observe a maintenance of disease till later stages *in vitro* as opposed to a rapid decrease in disease, as *Raptor*-deficiency in B cells leads to a block in B cell development altogether (Chapter 4). One of the reasons for this could be due to the microenvironmental factors due to the co-

culture. Unlike the *Mx1-Raptor* cKO model, *Raptor*-deficiency is induced solely in CD19^{+} cells and not in other haemopoietic lineages in the *CD19-Raptor* KO model. To induce a CLL-like disease in *CD19-Raptor* KO model, CD117^{+} lymphocytes are retrovirally transduced with GFP^{+}-PKCαKR construct. These retrovirally cells are co-cultured with murine derived OP9 stromal cells to aid B-cell/PKCαKR cells generation(314). Additionally, other lymphocytes such as NK cells and a low percentage of macrophages could be present at early stages of culture. Besides the role of OP9 stromal cells in aiding B cell development, it is possible that these other cells release cytokines which aid disease progression till a later stage of disease progression after *Raptor* KO in B cells. Indeed, chemokines released by BMSCs and NLCs including SDF-1 lead to increased chemotaxis and decreased apoptosis in CLL(315). NLCs also activate the BCR through antigens such as vimentin and calreticulin(316). Although tumour associated macrophages (TAMs) and T cells play critical roles in CLL maintenance, BM cells which are retrovirally transduced do not have a high percentage of T cells. They contain macrophages but not TAMs. With the induction of a CLL-like disease there is a decrease in macrophages. However, it has previously been shown that secretion of CD14 by monocytes has shown to protect CLL by decreasing apoptosis and activating NFκB-mediated signals (317), which could potentially increase the disease progression in *CD19-Raptor* PKCαKR cells.

It was reassuring to see that BM of *Mx1-Raptor* cKO mice not treated with poly(I:C) developed a CLL-like disease, confirming that it is indeed *Raptor*-deficiency causing the block in disease initiation. Optimization of the dosage and time of IFNβ treatment, a TLR receptor agonist used to induce cKO *in vitro,* was carried out: 200U IFNβ for 24 hr was optimal and was used in all experiments *in vitro*. However, there was a significant decrease in cellularity in *Mx1-Raptor* cKO PKCαKR cells (without prior poly(I:C) treatment) without IFNβ treatment compared to *Mx1-Raptor* controls. This was interesting as no changes were observed in *Mx1-Raptor* cKO PKCαKR cells treated with 50U IFNβ suggesting this result is not due to cre toxicity(208). However, it suggests an activation of TLR signalling in *Mx1-Raptor* cKO PKCαKR cells with no prior drug treatment. The reason for this potential TLR activation is not known and requires further assessment. Indeed, it has been demonstrated that there can be spontaneous cre

expression prior to induction of cre expression(203). It is possible that such spontaneous cre expression caused the significant decrease in *Mx1-Raptor* PKCαKR cellularity with no prior drug treatment.

TLRs are present on innate cells and act a bridge between innate and adaptive immunity. In murine B cells, TLR4 and TLR10 have shown to be prevalently expressed(318). In humans, TLR expression in CLL is similar to that on normal B lymphocytes. However, Dadashian *et al.*, have recently demonstrated an increased cooperation of TLR signalling with BCR signalling leading to downstream NFκB signalling thereby increasing survival of CLL cells residing in LN of patients, which was partially inhibited with ibrutinib treatment(319). However, expression of various TLRs on the PKCαKR mouse model of CLL has not yet been assessed. Therefore, it is possible that there is an increase in stochastic TLR signalling with our murine CLL model leading to cre expression and subsequent *Raptor*-excision. Nevertheless, there was a clear excision of *Raptor* in *Mx1-Raptor* cKO (no poly(I:C) treatment) PKCαKR cells with IFNβ treatment which led to a decrease in CLL-disease load with an increasing trend in G_0/G_1 phase with a decrease in proliferation *in vitro*. These data suggest *Raptor*-deficiency in B cells and in haemopoietic cells affects CLL progression in a similar manner as its role in CLL initiation.

On the other hand, *Rictor*-deficiency at the HSC stage, in haemopoietic lineages in adult mice, and solely in CD19$^+$ cells in PKCαKR cells led to a CLL-like disease with a decline in GFP$^+$CD11b$^+$ myeloid cells *in vitro* suggesting a redundant role of mTORC2 in CLL initiation and lineage commitment. PKCαKR cells with *Rictor*-deficiency displayed an increase in migration, a trend in increased cell cycling (increased percentage of cells in the S phase), with an increasing trend in *Ccnd1* expression at later stages of disease progression (D21 of culture) compared to controls alluding to a role of mTORC2 in disease maintenance. A similar trend has been observed in previous studies where there was a decrease in Notch-driven T-acute lymphocytic leukaemia (T-ALL) progression with *Rictor*-deficiency, with an increase in CXCR4 expression causing increased migration and homing in the spleen and not the BM, together with an arrest in proliferation and cell cycling at the G_0 phase via *FoxO3* activation(123,320). As our data demonstrate an increasing trend in cell cycling and proliferation, this opposing trend could be due to the anti-proliferative role of mTORC2 in T cells as

compared to in B cells. As chronic BCR activation in CLL has been shown to increase RNA translation along with the upregulation of MYC(321), future directions of assessing *Rictor*-deficiency in CLL should include assessing MYC levels, a downstream target.

5.3.2 Role of mTORC1 and mTORC2 in leukaemia progression *in vivo*

As *Mx1-Raptor* cKO PKCαKR cells (with prior poly(I:C) inoculation) failed to develop disease *in vitro*, NSG mice were transplanted with *Mx1-Raptor* control or cKO PKCαKR cells (without poly(I:C) inoculation) cultured till D7-10. After disease was well established (≥10% disease), the mice were either left untreated or inoculated with poly(I:C) doses to induce *Raptor*-deficiency in the transplanted CLL-like disease to assess the role of mTORC1 in CLL progression *in vivo*. There was a significant decrease in disease percentage in the BM and spleen together with increased survival in diseased mice with *Raptor* cKO with poly(I:C) inoculation, compared to mice with *Mx1-Raptor* control PKCαKR cells (with no poly(I:C)) suggesting a decrease in disease maintenance with *Raptor*-deficiency. However, there was an observed delay in GFP$^+$CD19$^+$ disease progression with mice transplanted with *Mx1-Raptor* control PKCαKR cells treated with poly(I:C) suggesting a potential role of poly(I:C) in initiating TLR response. TLR in normal B lymphocytes are responsible for identifying virus, bacteria and other agents. Therefore, it is possible that TLR activation delays disease progression. As TLR signalling in CLL has shown to phosphorylate STAT1 and STAT3 and activate NFκB signalling and cause subsequent survival of CLL(319), it is also possible that poly(I:C) inoculation affects normal and leukaemic B cells thereby causing in initial delay in CLL progression, but also protecting the murine CLL disease *in vivo* to an extent. Nevertheless, it was reassuring to see no difference in survival between NSG mice transplanted with *Mx1-Raptor* control PKCαKR cells with and without poly(I:C) inoculation. Although host mice with *Mx1-Raptor* cKO PKCαKR cells (with poly(I:C)) had increased survival and decreased disease load, these mice did not have a complete abrogation in disease and eventually the mice succumbed to a CLL-like disease. All mice were sacrificed after their health was compromised due to disease progression, and not after a common time point thereby allowing us to determine the role of mTORC1 in disease maintenance. Analysis of spleens from

Mx1-Raptor cKO PKCαKR cells (with poly(I:C)) at disease end showed a significant increase in RAPTOR expression and an increase in p4EBP1$^{T36/T47}$, compared to *Mx1-Raptor* control PKCαKR cells (no poly(I:C)). This suggests 'escaped deletion'(208) of *Raptor* in *Mx1-Raptor* cKO PKCαKR cells by poly(I:C), leading to a repopulation of disease with *Raptor* and eventual death of host mice. Interestingly, there was a drastic decrease in RICTOR expression in *Mx1-Raptor* cKO PKCαKR cells with poly(I:C) inoculation compared to *Mx1-Raptor* cKO PKCαKR cells alluding to possible regulation of RICTOR by mTORC1. Brown *et al.*, have shown that mTORC2 negatively regulates TLR response as *Rictor*-excision induces a hyperinflammatory response via TLR activation through *FoxO1* modulation(71). However, it is not known whether TLR activation modulates *Rictor* function via *FoxO1* modulation thereby affecting RICTOR expression as observed in our results. A similar trend is observed in the *Mx1-Raptor* control PKCαKR cells with poly(I:C) where there is a significant decrease in RICTOR expression, suggesting TLR mediated modulation of mTORC2. However, as this experiment was performed once, it would be beneficial to perform this again to evaluate this further.

CD19-Raptor control or KO PKCαKR cells were transplanted into NSG mice to address the role of mTORC1 solely in CD19$^+$-CLL disease. As the *Mx1-Raptor* cKO PKCαKR cells with poly(I:C) treatment exhibit a decrease in disease load, we hypothesised a similar result would be seen in the *CD19-Raptor* KO PKCαKR transplanted mice *in vivo*. Indeed, we observed a more pronounced increase in survival in mice with *CD19-Raptor* KO PKCαKR cells compared to *CD19-Raptor* control PKCαKR cells. Although there was an increase in survival, these mice still died of disease at a later timepoint as seen with an increase in disease load in the blood of NSG mice with *CD19-Raptor* KO PKCαKR cells after 5 wk. When assessed further, this was due to re-emergence of RAPTOR expression. These data suggest that although *Raptor* excision can abrogate disease progression, the *CD19*-cre-loxP model was not very efficient in inducing a 100% knockout in CLL-like cells leading to 'escaped deletions' and subsequent re-population of disease. This also reiterates that the *CD19*-cre KO model is not as efficient as the *Vav*- and *Mb1*-cre models, where *CD19*-cre model has ≥75% KO efficiency compared to *Vav*- and *Mb1*- cre with 95% KO efficiency(208), thereby not being the ideal KO model for these experiments.

Previous studies have assessed the role of mTOR in leukaemic settings by inducing PTEN loss which leads to myeloproliferative neoplasms (MPN)(322). This could be a good model for CLL. Kalaitzidis *et al.*, have demonstrated that *Pten*-loss leads to MPN and inducing *Raptor* loss after MPN using the cre-loxP system leads to increased survival suggesting a fundamental role of mTORC1 in disease progression(91) as is also seen from our results. Additionally, *Rictor* deletion using the *Mx1*-cre system in PTEN loss evoked disease resulted in a disruption in disease maintenance and prevention of HSC exhaustion in adult, but not neonatal mice(93) suggesting a role of mTORC2 in later stages of normal haemopoiesis and in disease, similar to our data.

To determine the therapeutic potential of targeting mTOR complexes pharmacologically in CLL, we transplanted a CLL like disease into mice and then treated mice with clinically relevant inhibitors of the PI3K/mTOR pathway in mice with an established disease to assess leukaemia progression *in vivo*. Ibrutinib, a BTK inhibitor, has been approved as the current first line therapy for patients with 17p deletion or *TP53* mutation (patients displaying a more aggressive form of CLL) after the RESONATE-2 trial (323). AZD2014, the dual mTOR complex inhibitor is currently in phase II clinical trials for gastric carcinoma(324) and shown promise in other cancers such as breast cancer(325). AZD2014, in synergy with ibrutinib has been demonstrated to ablate diffuse large B-cell lymphoma (DLBL) cell lines (ABC subtype)(326) thereby making it an ideal drug for testing in our CLL model. Mice given combination therapy with AZD2014 and ibrutinib had a better overall decrease in disease load in the BM and spleen as compared to the vehicle controls or single agents, suggesting synergy between ibrutinib and AZD2014 in combating CLL(128). Additionally, there was a decrease in CD5$^+$ CLL-like cells with combination and with single agents in the BM and spleen of mice. CLL population with high levels of CD5 expression are classified as the migrating CLL population(156). A recent study has shown a population of CLL cells with high IgM expression residing in the LN as compared to those in the blood suggesting a functional difference between the two subtypes(309). Whether they correlate to the migrating subtype or are different to the Calissano model is unclear. However, our results highlight the importance of combination therapy in targeting different clonal subtypes of the heterogenous disease.

Although combination therapy was more efficient in decreasing disease load, secondary transplants were performed to assess the efficiency between rapamycin (mTORC1 inhibitor) or AZD2014 to assess whether combination therapy of ibrutinib with AZD2014 or rapamycin would yield a better outcome. We hypothesised that AZD2014, inhibiting both mTORC1 and mTORC2 would be a more potent inhibitor than rapamycin alone. However, secondary transplants showed a significant difference between the two agents where AZD2014 was inferior compared to rapamycin in decreasing disease load *in vivo*. Our results indicate a decreasing trend in splenic cellularity with rapamycin treatment compared to AZD2014 and controls. As there is a clear reduction in spleen size with rapamycin, it was surprising that this did not co-relate with a significant decrease in splenic cellularity. Splenomegaly in CLL is associated with an increase in red pulp(327) thereby increasing splenic cellularity. However, all total counts of the spleen were taken after enrichment of lymphocytes thereby depleting other cell types which could explain the lack of a significant decrease in the splenic cellularity of rapamycin treated mice compared to vehicle controls and those treated with AZD2014. The pharmacokinetics of both the drugs have shown fast absorption with the peak concentration in serum reaching between 0.5-1 hr when both drugs are given orally. Nevertheless, rapamycin yielded best results when the drug was given daily for 2 weeks, whereas AZD2014 inhibited phosphorylation of 4EBP1 by -45% and -41% and phosphorylation of $S6K^{S235/S236}$ by -62% and -37% at 2 and 6 to 8 hr after dose compared to baseline respectively. As rapamycin has a longer half-life compared to AZD2014 (30 hr compared to 3 hr)(328,329) , it would have been interesting to test downstream signalling after one dose (preferably after 2 hr) of AZD2014 and rapamycin to determine the downstream mechanisms. Our laboratory has recently shown that AZD8055 (a drug with the same pharmacophore as AZD2014) is superior to rapamycin at reducing CLL in primary transplants(128) thereby suggesting that the disease is more aggressive as a secondary transplant and potentially more dependent on mTORC1.

Spleens with a CLL-like disease treated with AZD2014 or rapamycin had no changes in RAPTOR or RICTOR expression. However, the phosphorylation of these proteins was not tested making it difficult to comment upon the functionality of the proteins. Nevertheless, there was a trend in decrease in $pAKT^{S473}$ with both

drugs compared to vehicle controls. It is known that continuous rapamycin treatment leads to mTORC2 inhibition in certain cells(330) suggesting that rapamycin inhibits mTORC2 as seen by the decrease in downstream AKT phosphorylation. Indeed, a phase II trial has shown similar results in patients with refractory renal cancer where patients given AZD2014 treatment had a shorter progression-free survival (PFS) with an increase in disease progression compared to patients given everolimus, a compound derived from rapamycin(331). Assessing the mechanism of action of the two drugs would allow a better understanding about these findings. Rapamycin binds to FKBP12 and this complex allosterically inhibits mTORC1. Rapamycin is known to be a potent immunosuppressant as it hinders T cell activity and proliferation along with inhibiting antibody production(332). As our host mice are immunocompromised, it is unlikely that rapamycin is compromising the microenvironment alluding to rapamycin inhibition of mTORC1 downstream the BCR in a CLL-like disease.

Moreover, we observed a trend in increase in cell cycling genes in the spleens of AZD2014 treated mice whereas those treated with rapamycin do not show similar trends suggesting that the classical cell cycle arrest mechanism was not engaged with rapamycin treatment in decreasing disease load *in vivo*. Faller *et al.*, have shown that in the murine intestinal cancer model, rapamycin treatment caused a decrease in cancer cell proliferation (not initiation) independent of the classical cell cycle arrest mechanism. They demonstrate a novel mechanism by which mTORC1 regulates translation elongation of malignant cells via the S6K-elongation factor 2 kinase (EF2K)-EF2 axis which, after *Raptor*-deletion or rapamycin treatment, was reversed(333). It would be of great benefit to assess this S6K mediated translational elongation in our CLL-secondary transplants to determine whether this more aggressive form of disease is increasingly mTORC1 dependent.

Taken together, mTORC1 plays a fundamental role in CLL initiation and progression *in vitro* and *in vivo* whereas mTORC2 has roles in CLL maintenance at a later stage *in vitro*. Although the dual mTOR complex inhibitor, AZD2014 significantly reduces disease load in mice in primary transplants, and is synergistic with ibrutinib in decreasing disease load, AZD2014 is inferior to rapamycin in decreasing disease load in secondary transplants. It will be

interesting to test whether rapamycin can also exhibit synergy with ibrutinib or other drugs in clinics to combat CLL.

5.4 Figures
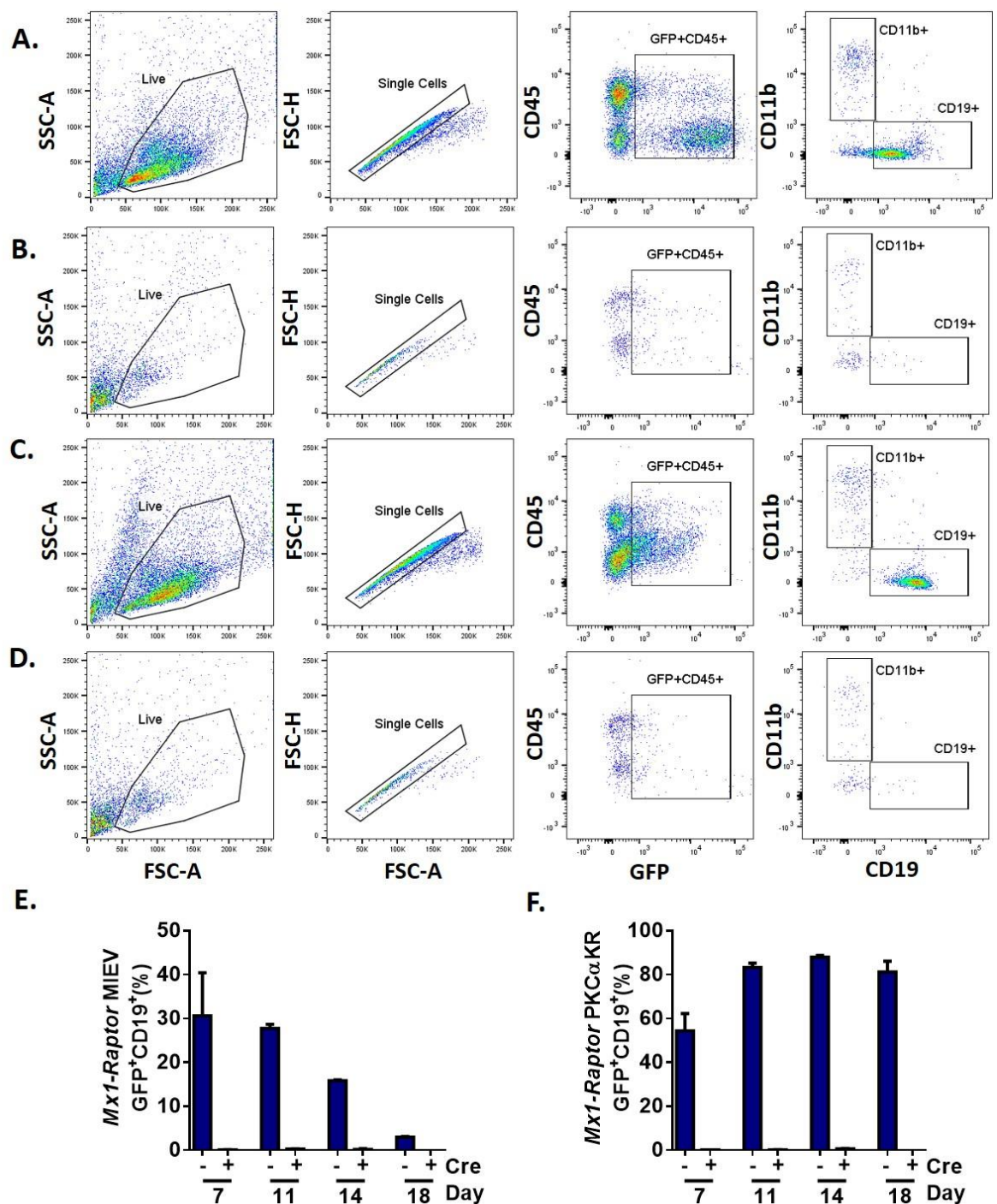
Figure 5.1 BM from adult mice with *Raptor*-deficiency does not develop into PKCαKR CLL-like cells *in vitro*.
Representative flow cytometry plots showing D7 post retroviral transduction of either GFP-tagged MIEV construct of purified CD117⁺ lymphocyte progenitors from the BM of *Mx1-Raptor* control **(A)** or cKO **(B)** mice, or GFP-tagged PKCαKR construct of purified CD117⁺ lymphocyte progenitors from the BM of *Mx1-Raptor* control **(C)** or cKO **(D)** mice dissected 5 wk post 4 poly(I:C) inoculation. Plots were live and size (FSC-A/SSC-A) gated, and doublet cells were excluded and were gated for GFP⁺CD45⁺ before assessing surface expression of CD19⁺ or CD11b⁺ populations. Percentage of GFP⁺CD45⁺CD19⁺ MIEV (n=2)**(E)** or PKCαKR CLL-like cells (n=2) **(F)** from *Mx1-Raptor* control (cre-, blue bars) or cKO (cre+, red bars) mice dissected 3 wk post 3 poly(I:C) inoculation and assessed D7, 11, 14, and 18 post retroviral transduction. Data are expressed as mean±SD.
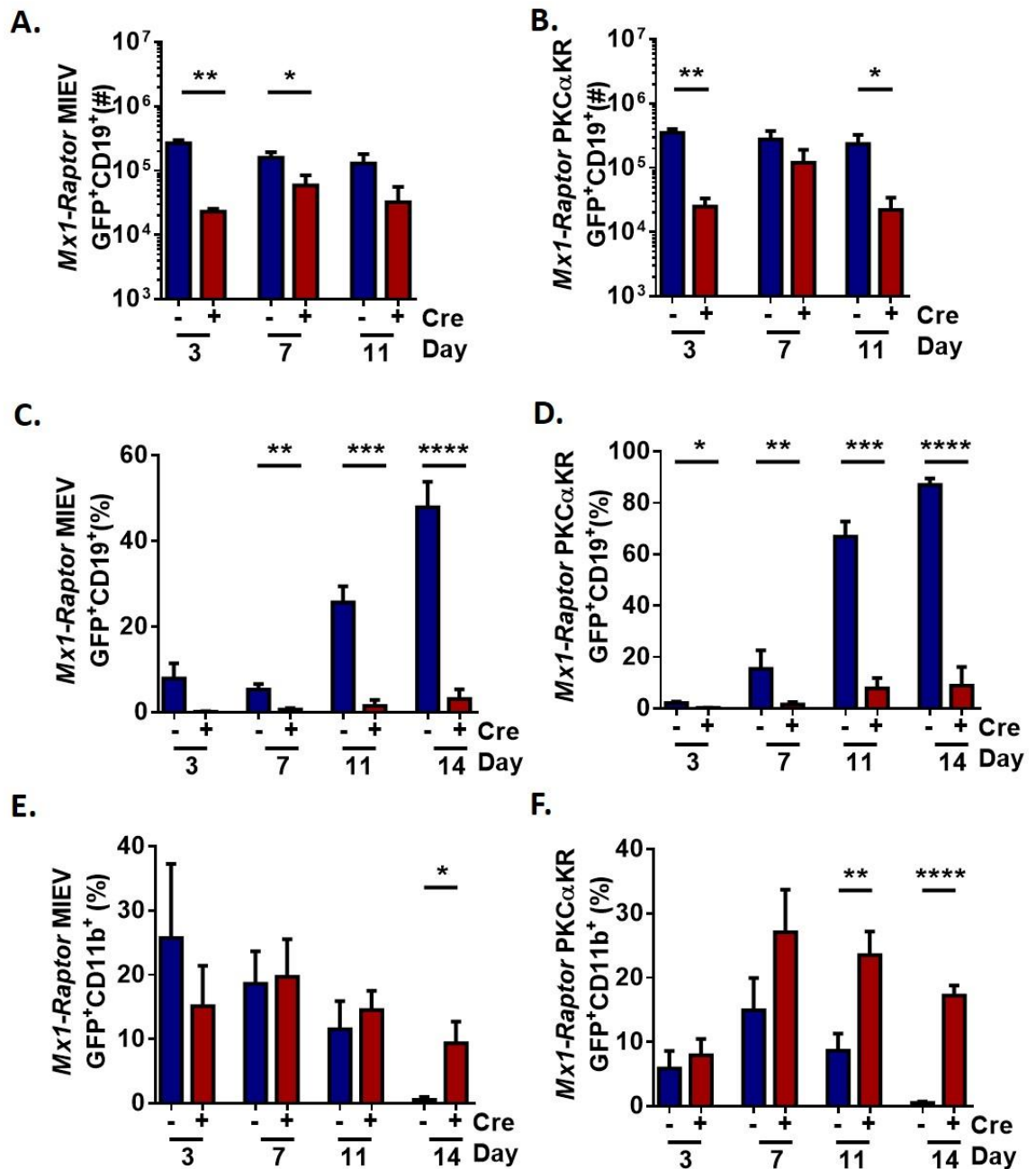
Figure 5.2 *Raptor*-deficiency abrogates B cell lineage commitment and leads to the absence of PKCαKR CLL-like cells *in vitro*.

Cellularity of GFP+CD19+ population of *Mx1-Raptor* control or cKO (4 poly(I:C)) MIEV **(A)** and *Mx1-Raptor* control or cKO (4 poly(I:C)) PKCαKR **(B)** cells over D3 (n=3), 7 (n=6) and 11 (n=6) of culture, together with percentage of GFP+CD19+ population of *Mx1-Raptor* control or cKO (4 poly(I:C)) MIEV **(C)** and *Mx1-Raptor* control or cKO (4 poly(I:C)) PKCαKR **(D)** cells over D3 (n=5), 7 (n=9), 11 (n=8) and 14 (n=8) of culture. Percentage of GFP+CD11b+ population of *Mx1-Raptor* control or cKO (4 poly(I:C)) MIEV **(E)** and *Mx1-Raptor* control or cKO (4 poly(I:C)) PKCαKR **(F)** cells over D3 (n=5), 7 (n=8), 11 (n=10) and 14 (n=6) of culture. Cre-: *Raptor*-control samples, cre+: *Raptor*-cKO samples. Data are expressed as mean±SEM (p *≤0.05, p **≤0.001, p ***≤0.0001, p ****≤0.00001).
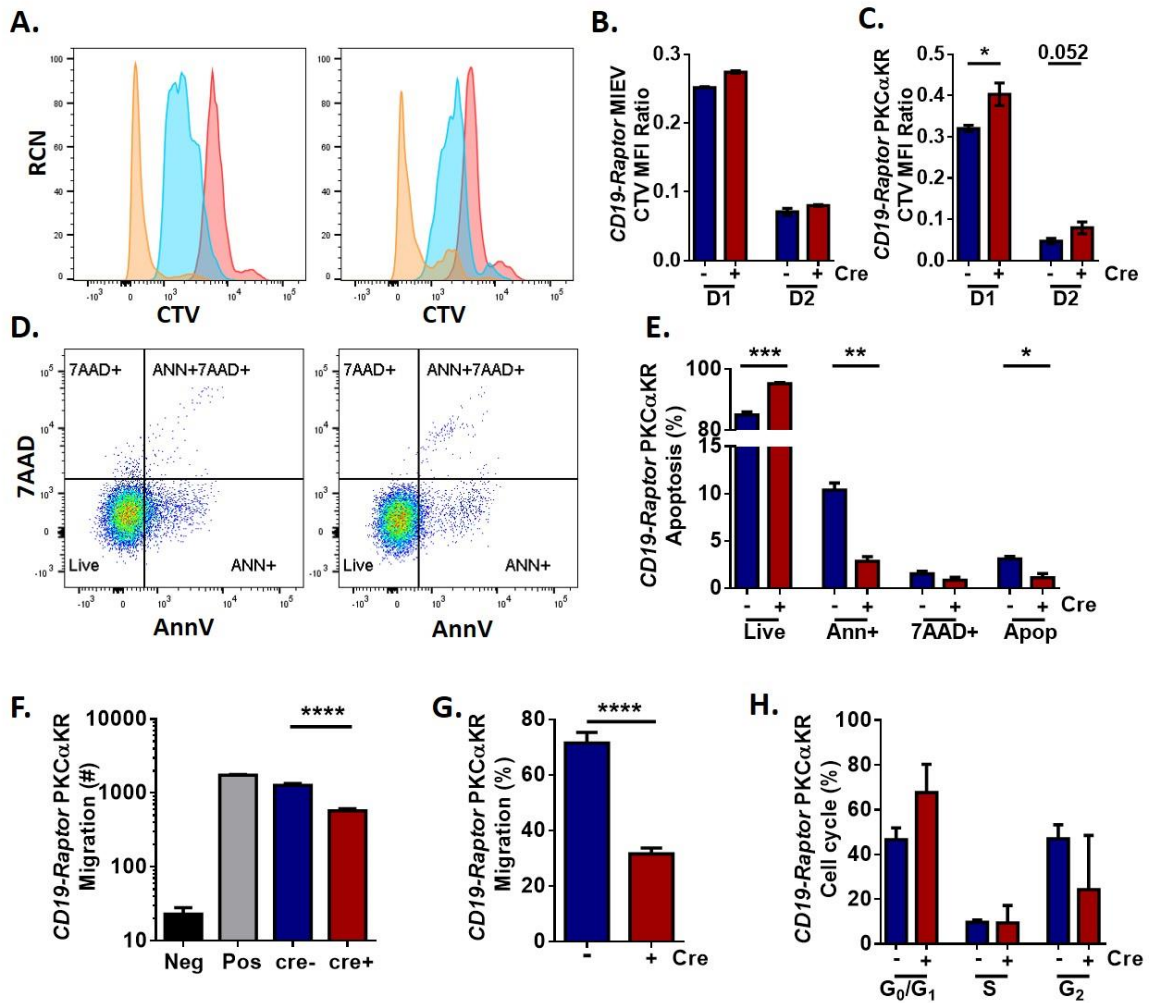
Figure 5.3 *Raptor-deficiency* in CD19⁺ cells leads to decreased proliferation, migration and cell cycle arrest of PKCaKR CLL-like cells *in vitro*.

A. Representative plot showing CTV proliferation assay performed every 24 hr for 72 hr on *CD19-Raptor* control (left) or KO (right) PKCαKR cells at D18 of culture. Bar graphs demonstrating CTV MFI ratios of D1/D0 and D2/D0 of *CD19-Raptor* control (n=2) and *CD19-Raptor* KO MIEV (n=2) cells **(B)** and *CD19-Raptor* control (n=5) and *CD19-Raptor* KO PKCαKR cells (n=3) **(C)**. Representative flow cytometry plots **(D)**, together with percentage **(E)** of AnnV⁻7AAD⁻ (Live), AnnV⁺ (early apoptotic), 7AAD⁺ (necrotic cells), and AnnV⁺7AAD⁺ (late apoptotic) populations of *CD19-Raptor* control (n=3) (left) and *CD19-Raptor* KO (n=3) PKCαKR cells (right) at D18 of culture. Cellularity **(F)** and percentage **(G)** of migration of *CD19-Raptor* control (n=3) and *CD19-Raptor* KO (n=3) PKCαKR cells towards SDF-1 after serum starvation. Negative and positive controls represent migration without SDF-1 and 100% migration respectively. **H.** Percentage of *CD19-Raptor* control (n=2) and *CD19-Raptor* KO (n=2) PKCαKR cells at D18 of culture in G_0/G_1, S, and G_2 phases of cell cycling. Cre-: *Raptor*-control samples, cre+: *Raptor*-KO samples. Data are expressed as mean±SD/SEM (p *≤0.05, p **≤0.001, p ***≤0.0001, p ****≤0.00001).
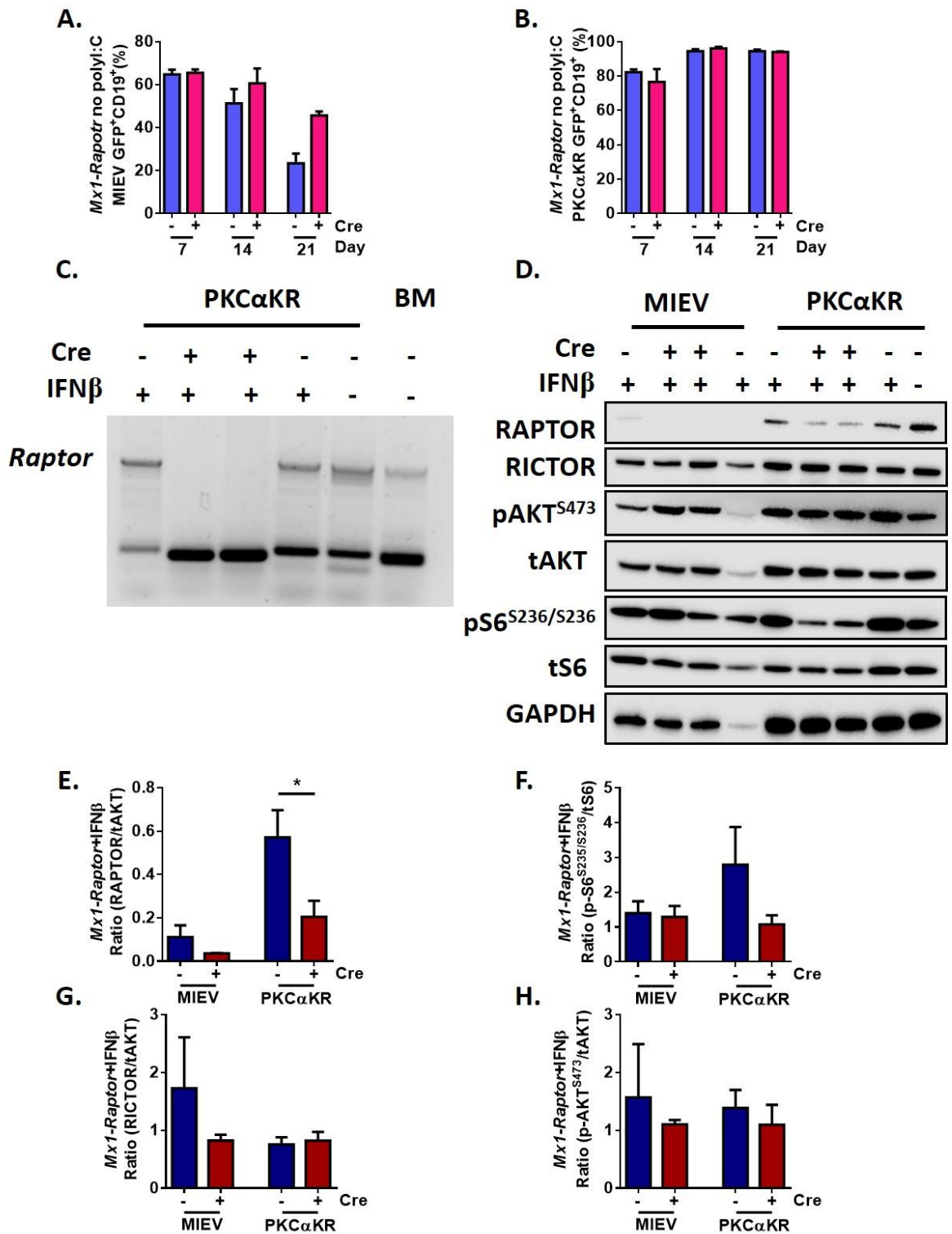
Figure 5.4 The generation of an inducible model of *Raptor*-deficiency *in vitro*.
Bar graphs showing percentage of CD19⁺GFP⁺ *Mx1-Raptor* control or *Mx1-Raptor* cKO MIEV **(A)** and *Mx1-Raptor* control or *Mx1-Raptor* cKO PKCαKR **(B)** cells at D7 (n=2), 14 (n=4), and 21 (n=3) with no poly(I:C) inoculation given to mice. **C.** DNA agarose gel of a PCR reaction showing expression of *Raptor* in *Mx1-Raptor* control or *Mx1-Raptor* cKO (no poly(I:C)) PKCαKR cells treated with or without 200U IFNβ for 24 hr and assessed 72 hr post treatment together with *Mx1-Raptor* control BM as a reference for *Raptor* expression. Representative western blot **(D)** and bar graphs showing expression of RAPTOR/tAKT **(E)**, pS6$^{S235/S236}$/tS6 **(F)**, RICTOR/tAKT **(G)**, pAKT^{S473}/tAKT **(H)** of *Mx1-Raptor* control or cKO MIEV (n=2) and *Mx1-Raptor* control or cKO PKCαKR (n=4) cells treated with IFNβ and assessed 72 hr post treatment. Cre-: *Raptor*-control samples, cre+: *Raptor*-cKO samples. Data are expressed as mean±SD/SEM (p *≤0.05).
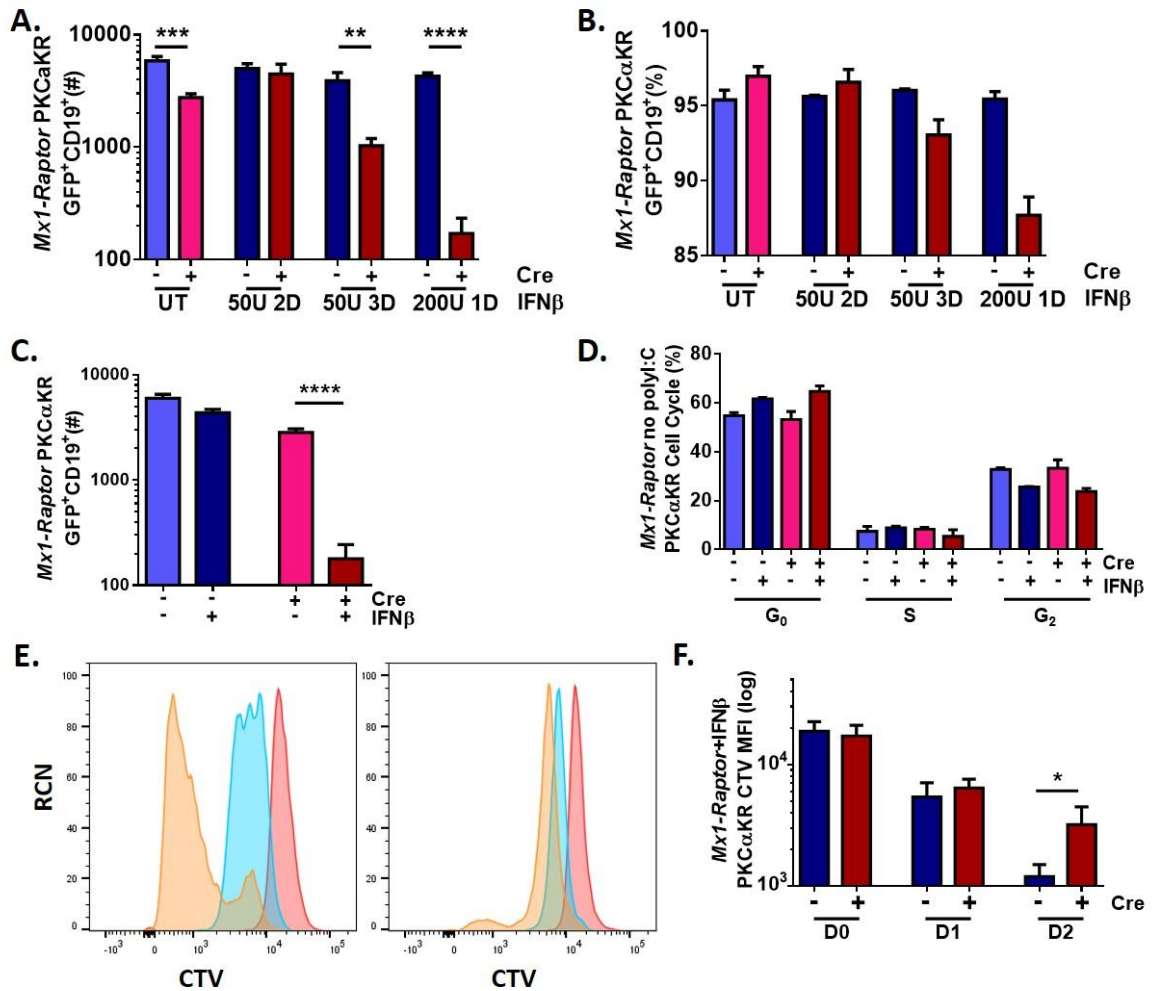
Figure 5.5 CLL-like cells with induced *Raptor*-deficiency exhibit a block in proliferation *in vitro*.

Cellularity (n=6) **(A)** and percentage (n=2) **(B)** of GFP+CD19+ *Mx1-Raptor* control or cKO (no poly(I:C)) PKCαKR cells, either untreated (UT, light blue and pink bars) or treated with 50U IFNβ for D2, D3 or 200U for 24 hr (blue and red bars) and assessed 72 hr post treatment. **C.** Cellularity (n=6) of *Mx1-Raptor* control or cKO (no poly(I:C)) PKCαKR cells either untreated or treated with 200U IFNβ for 24 hr and assessed 72 hr post treatment. **D.** PI staining showing percentage of *Mx1-Raptor* control and cKO (no poly(I:C)) PKCαKR cells (n=2), either untreated or treated with 200U IFNβ for 24 hr and assessed 72 hr post treatment, in G_0/G_1, S, and G_2 phases of cell cycling. Representative plot **(E)** and bar graphs **(F)** showing CTV MFI of D0, D1 and D2 performed every 24 hr for 3 days of *Mx1-Raptor* control (left) or cKO (no poly(I:C), right) PKCαKR cells (n=6) treated with 200U IFNβ for 24 hr (right) and assessed 72 hr post treatment. Cre-: *Raptor*-control samples, cre+: *Raptor*-cKO samples. Data are expressed as mean±SD/SEM (p *≤0.05, p **≤0.001, p ***≤0.0001, p ****≤0.00001).
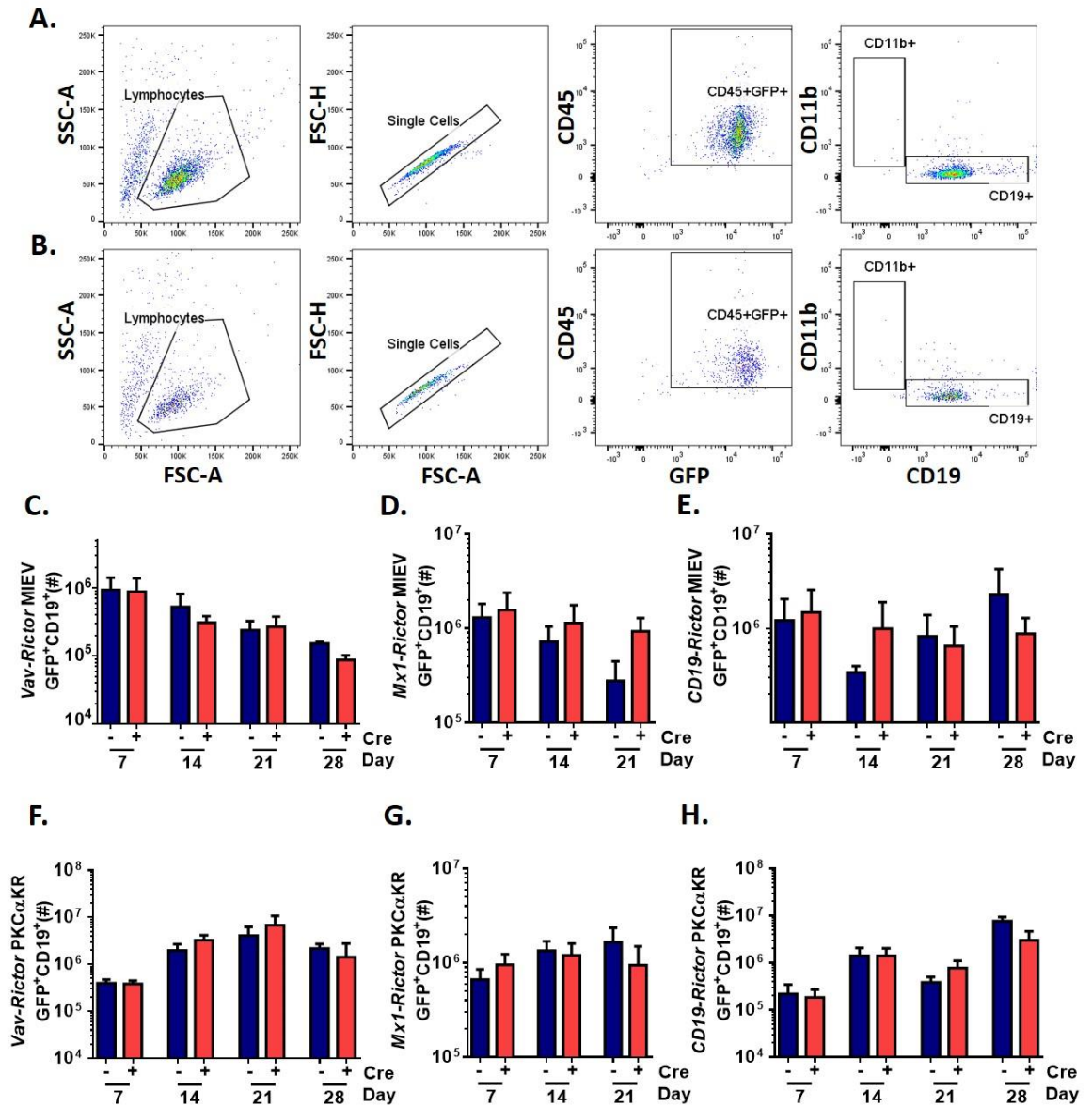
Figure 5.6 *Rictor*-deficiency does not abrogate CLL-initiation *in vitro*.
Representative graphs showing proportion of GFP⁺CD19⁺ cells of *Vav-Rictor* control **(A)** and *Vav-Rictor* KO **(B)** PKCαKR cells at D21 of culture. Plots were live and size (FSC-A/SSC-A) gated, and doublet cells were excluded and were gated for GFP⁺CD45⁺ before assessing surface expression of CD19⁺ or CD11b⁺ populations. Cellularity of GFP⁺CD19⁺ population of *Vav-Rictor* control or KO at D7 (n=6), 14 (n=3), 21 (n=5) and 28 (n=2) of culture **(C)**, *Mx1-Rictor* control or cKO (4 poly(I:C) inoculation) at D7 (n=6), 14 (n=5) and 21 (n=4) of culture **(D)**, and *CD19-Rictor* control (n=2) or KO (n=2) at D7, 14, 21 and 28 of culture **(E)** MIEV cells. Cellularity of GFP⁺CD19⁺ cells of *Vav-Rictor* control or KO at D7 (n=5), 14 (n=6), 21 (n=7) and 28 (n=3) of culture **(F)**, *Mx1-Rictor* control or cKO (4 poly(I:C) inoculation) at D7 (n=8), 14 (n=7), and 21 (n=7) of culture **(G)**, and *CD19-Rictor* control or KO at D7 (n=2), 14 (n=3), 21 (n=3) and 28 (n=3) of culture **(H)** PKCαKR cells. Cre-: *Rictor*-control samples, cre+: *Rictor*-cKO/KO samples. Data are expressed as mean±SD/SEM.
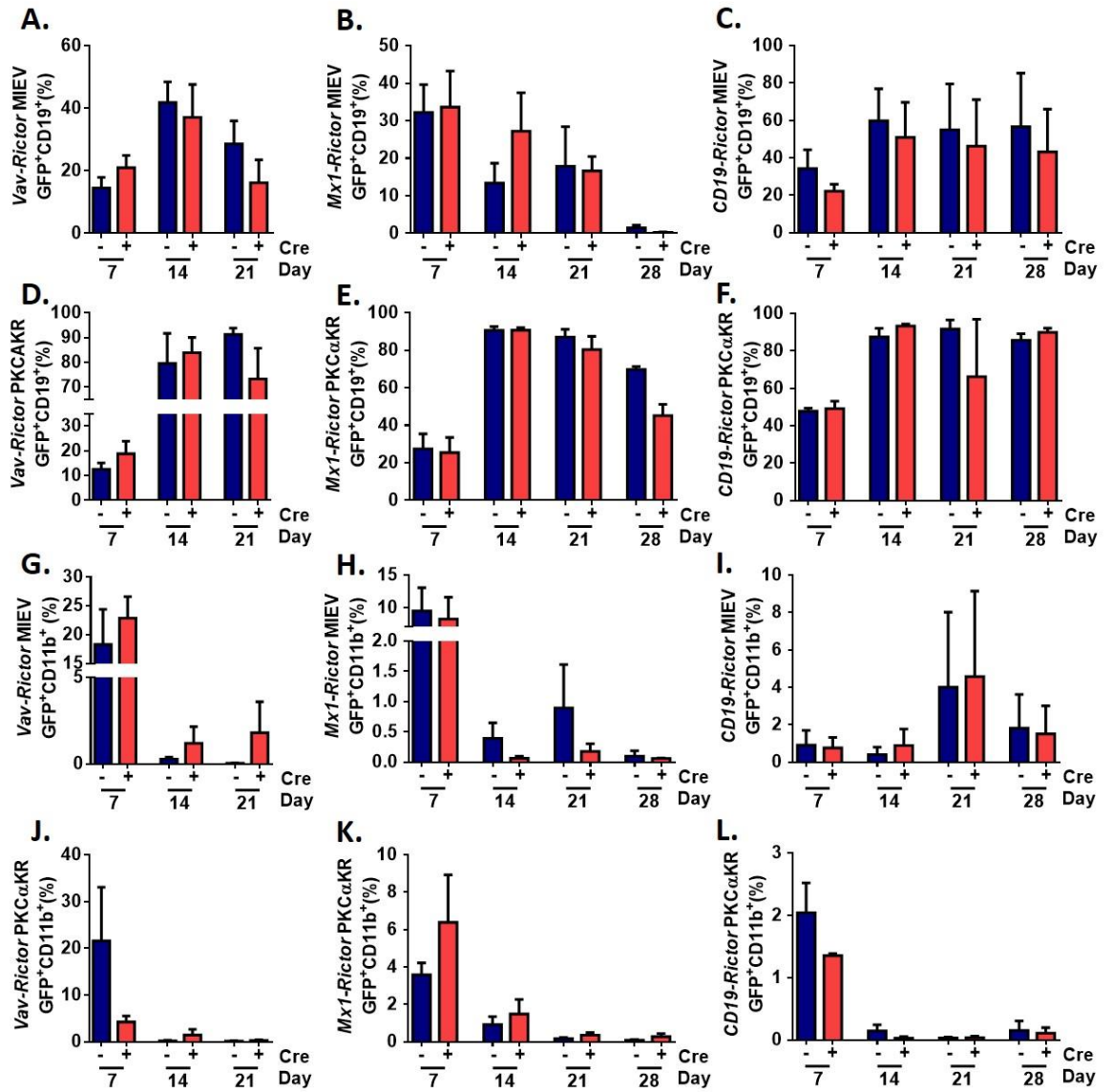
**Figure 5.7 CLL-like cells with *Rictor*-deficiency exhibit a decreasing trend in cell count and percentage at later stages of culture *in vitro*.**
Percentage of GFP+CD19+ cells of *Vav-Rictor* control or KO at D7 (n=7), 14 (n=7), and 21 (n=6) of culture **(A)**, *Mx1-Rictor* control or cKO (4 poly(I:C) inoculation) at D7 (n=9), 14 (n=9), 21 (n=5) and 28 (n=3) of culture **(B)**, and *CD19-Rictor* control (n=3) or KO (n=3) at D7, 14, 21 and 28 of culture **(C)** of MIEV cells. Percentage of GFP+CD19+ cells of *Vav-Rictor* control (n=7) or KO (n=7) at D7, 14, and 21 of culture **(D)**, *Mx1-Rictor* control or cKO (4 poly(I:C) inoculation) at D7 (n=8), 14 (n=8), 21 (n=6) and 28 (n=2) of culture **(E)**, and *CD19-Rictor* control (n=3) or KO (n=3) at D7, 14, 21 and 28 of culture **(F)** PKCαKR cells. Bar graphs showing percentage of GFP+CD11b+ cells of *Vav-Rictor* control (n=6) or KO (n=6) at D7, 14, and 21 of culture **(G)**, *Mx1-Rictor* control or cKO (4 poly(I:C) inoculation) at D7 (n=9), 14 (n=9), 21 (n=5) and 28 (n=3) of culture **(H)**, and *CD19-Rictor* control (n=3) or KO (n=3) at D7, 14, 21 and 28 of culture **(I)** MIEV cells. Percentage of GFP+CD11b+ cells of *Vav-Rictor* control (n=6) or KO (n=6) at D7, 14, and 21 of culture **(J)**, *Mx1-Rictor* control or cKO (4 poly(I:C) inoculation) at D7 (n=9), 14 (n=11), 21 (n=7) and 28 (n=5) of culture **(K)**, and *CD19-Rictor* control (n=3) or KO (n=3) at D7, 14, 21 and 28 of culture **(L)** PKCαKR cells. Cre-: *Rictor*-control samples, cre+: *Rictor*-cKO/KO samples. Data are expressed as mean±SD/SEM.
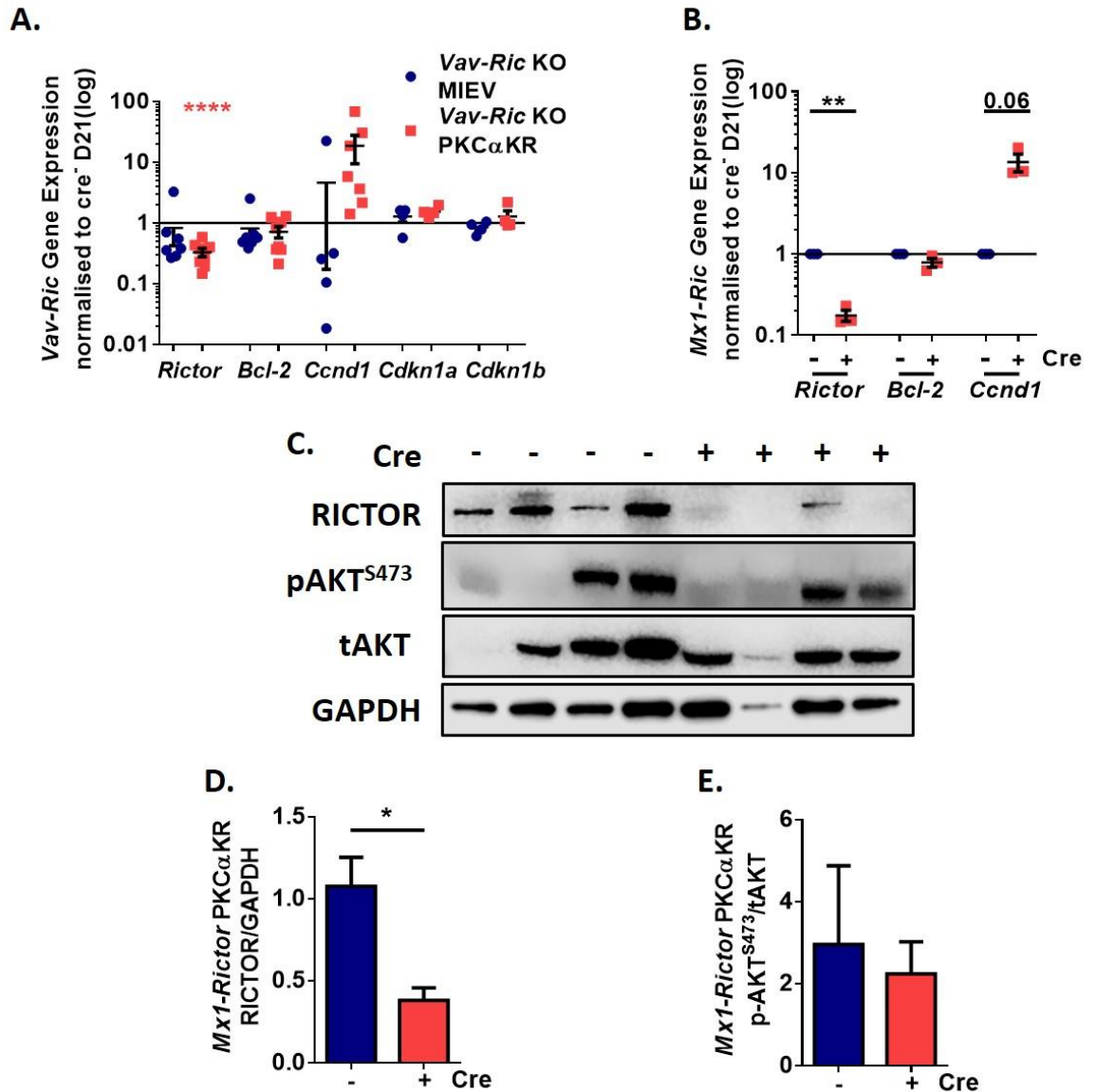
Figure 5.8 *Rictor*-deficiency at the HSC stage and in adult mice plays a role at later stages of CLL *in vitro*.
Gene expression of *Rictor* (n=7), *Bcl-2* (n=7), *Ccnd1* (n=5), *Cdkn1a* (n=4), *Cdkn1b* (n=4) in *Vav-Rictor* KO MIEV (blue) and *Vav-Rictor* KO PKCαKR (pink) cells **(A)**, along with gene expression of *Rictor, Bcl-2* and *Ccnd1* in *Mx1-Rictor* control (blue, n=3) and KO (pink, n=3) PKCαKR cells **(B)**. ΔΔCT calculated by taking *Tbp* as a reference gene and *Vav/Mx1-Rictor* control MIEV/PKCαKR samples as reference where all samples were cultured till D21 *in vitro*. Representative western blot **(C)** along with bar graphs demonstrating protein expression ratio of RICTOR/GAPDH **(D)** and pAKT[S473]/tAKT **(E)** in *Mx1-Rictor* control (n=4) and cKO (n=4) PKCαKR cells cultured till D21. Cre-: *Rictor*-control samples, cre+: *Rictor*-cKO samples. Data are expressed as mean±SEM (p *≤0.05, p **≤0.001, p ***≤0.0001, p ****≤0.00001).
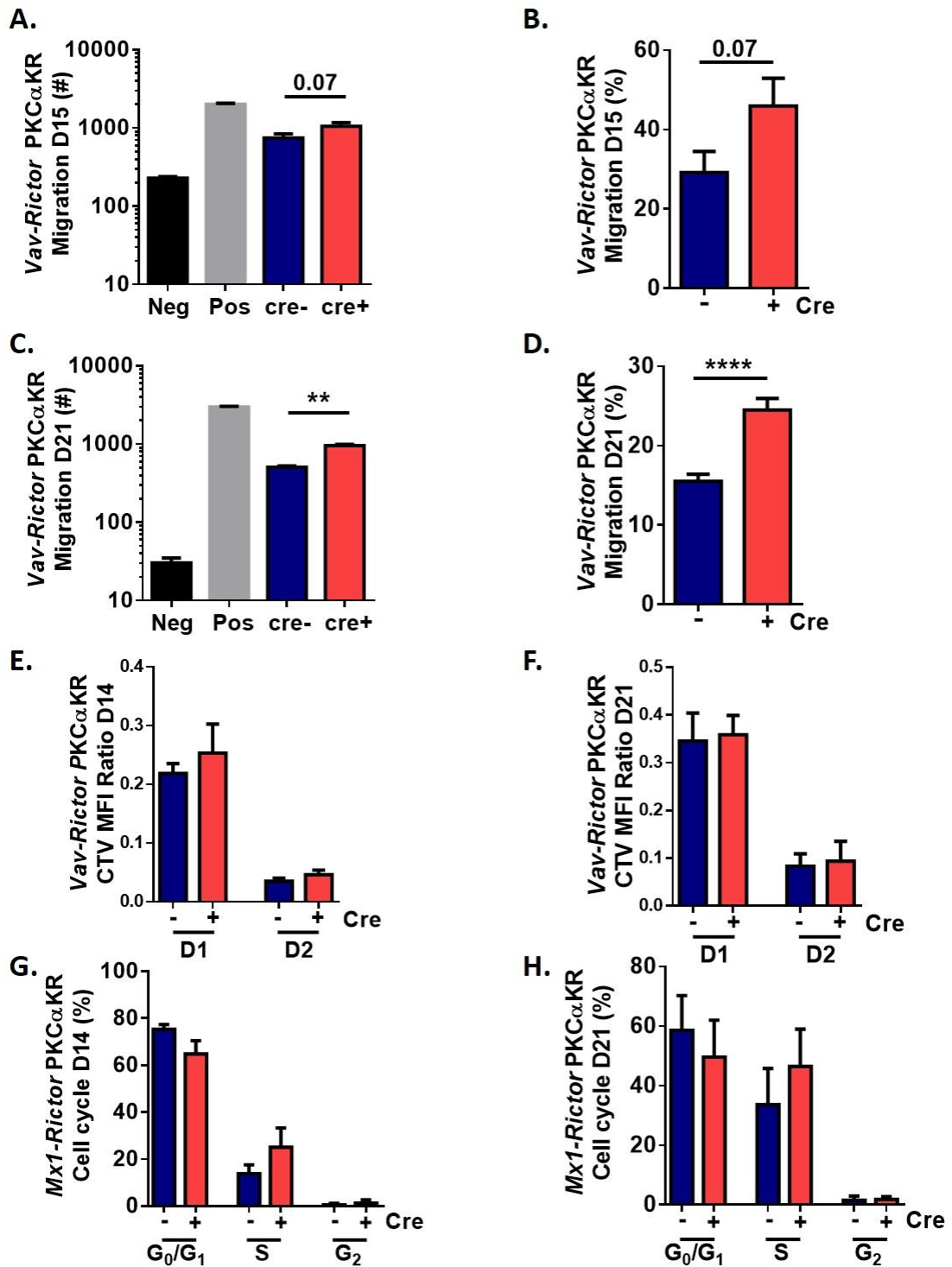
Figure 5.9 CLL cells with *Rictor*-deficiency at the HSC stage exhibit increased migration at later stages of culture.
Cellularity **(A)** and percentage **(B)** of migration of *Vav-Rictor* control (cre-, n=2) and *Vav-Rictor* KO (cre+, n=2) PKCαKR cells at D15 together with the cellularity **(C)** and percentage **(D)** of migration of *Vav-Rictor* control (n=4) and *Vav-Rictor* KO (n=4) PKCαKR cells towards SDF-1 after serum starvation when cultured for D21 *in vitro*. Negative and positive controls represent migration without SDF-1 and 100% migration respectively. Bar graphs of *Vav-Rictor* control (n=4) and KO PKCαKR cells cultured up to D14 (n=3 *Vav-Rictor* KO) **(E)** and D21 (n=2 *Vav-Rictor* KO) **(F)** showing CTV MFI ratios of D0/D1 and D2/D0 performed every 24 hr for 3 days. Bar graphs of *Mx1-Rictor* control (n=4) and cKO (n=5) (4 poly(I:C) inoculation) PKCαKR cells cultured to D14 **(G)** and D21 *in vitro* **(H)** demonstrating percentage of G_0/G_1, S, and G_2 phases of cell cycling. Cre-: *Rictor*-control samples, cre+: *Rictor*-cKO samples. Data are expressed as mean±SD/SEM (p *≤0.05, p **≤0.001, p ***≤0.0001, p ****≤0.00001).
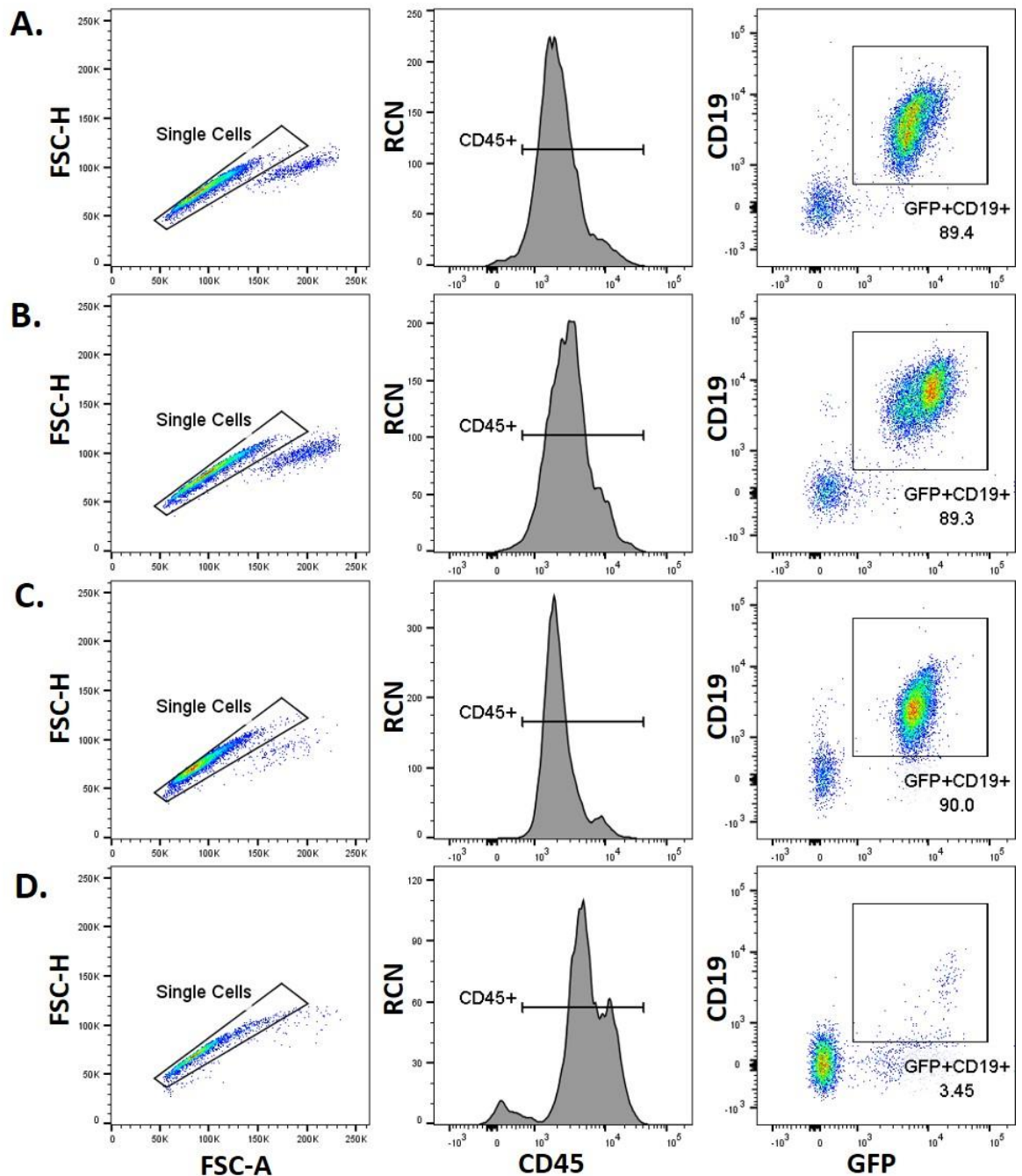
Figure 5.10 *Raptor*-deficiency induced after disease development abrogates CLL-like disease *in vivo.*
Immunocompromised NSG mice were transplanted with PKCαKR cells and developed disease. Representative flow cytometry plots showing proportion of GFP+CD45+CD19+ CLL-like PKCαKR cells in the blood of NSG mice which were transplanted with 5x10⁵ *Mx1-Raptor* control PKCαKR cells **(A)**, *Mx1-Raptor* control PKCαKR cells and given 4 inoculation of poly(I:C) after disease development **(B)**, *Mx1-Raptor* cKO PKCαKR cells **(C)** and *Mx1-Raptor* cKO PKCαKR cells and given 4 inoculation of poly(I:C) after disease development **(D)**. Plots are live and size (FSC-A/SSC-A) gated prior to the gating shown. Doublet cells were excluded (FSC-A/FSC-H) and positively selected for CD45 before assessing surface expression of GFP+CD19+ population.
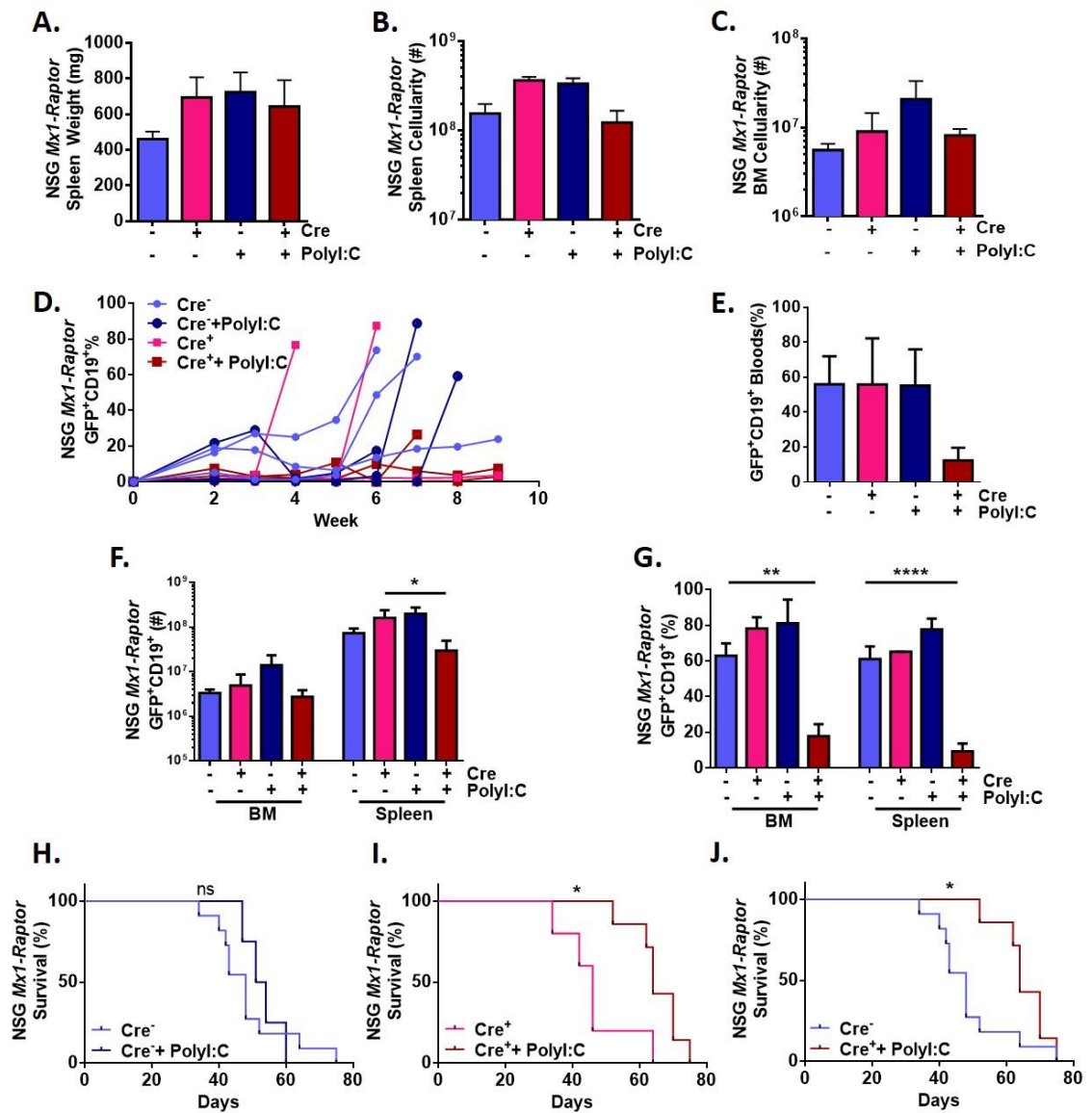
Figure 5.11 Mice with an established CLL-like disease exhibit a decrease in disease load with induced *Raptor*-deficiency *in vivo*.

Data represents transplanted NSG mice with an established CLL-like disease. Spleen weight (mg) **(A)** and spleen **(B)** and BM **(C)** organ cellularity of mice transplanted with either $5x10^5$ *Mx1-Raptor* control PKCαKR cells (light blue bar, n=11), *Mx1-Raptor* cKO PKCαKR cells (pink bar, n=2), *Mx1-Raptor* control PKCαKR cells and given 4 inoculation of poly(I:C) after disease development (blue bar, n=3), or *Mx1-Raptor* cKO PKCαKR cells and given 4 inoculation of poly(I:C) after disease development (red bar, n=5). Percentage of GFP+CD19+ CLL-like disease (representative, n=3/arm) in bloods from weekly tail bleeds **(D)** and from bloods of sacrificed mice **(E)** which were transplanted with *Mx1-Raptor* control PKCαKR cells, *Mx1-Raptor* cKO PKCαKR cells, *Mx1-Raptor* control PKCαKR cells and given 4 inoculation of poly(I:C), or *Mx1-Raptor* cKO PKCαKR cells and given 4 inoculation of poly(I:C). Cellularity **(F)** and percentage **(G)** of GFP+CD19+ cells in BM and spleen of NSG mice transplanted with either *Mx1-Raptor* control PKCαKR cells (n=8), *Mx1-Raptor* cKO PKCαKR cells (n=3), *Mx1-Raptor* control PKCαKR cells + poly(I:C) (n=4) or *Mx1-Raptor* cKO PKCαKR cells + poly(I:C) (n=5). Kaplan-meier survival graphs comparing the percentage survival between NSG mice transplanted with *Mx1-Raptor* control PKCαKR cells with (n=4) or without (n=11) poly(I:C) inoculation **(H)**, *Mx1-Raptor* cKO PKCαKR cells with (n=5) or without (n=7) poly(I:C) inoculation **(I)**, and *Mx1-Raptor* control (no poly(I:C), n=11) and cKO PKCαKR cells given poly(I:C) (n=7) after disease development **(J)**. Data are expressed as mean±SD/SEM (p *≤0.05, p **≤0.001, p ***≤0.0001, p ****≤0.00001).
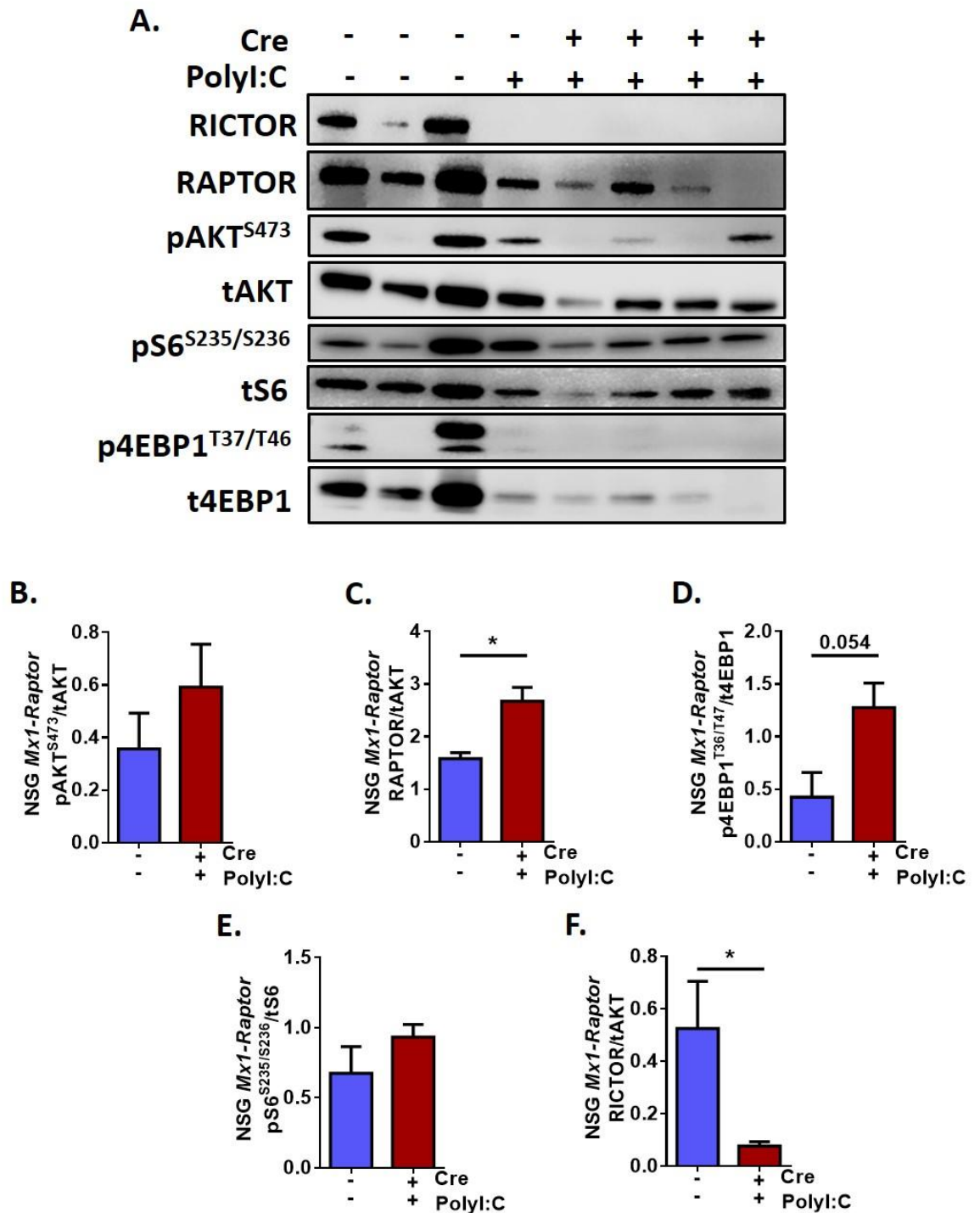
Figure 5.12 *Mx1-Raptor* cKO model is not completely efficient and causes disease relapse due to increased *Raptor* expression.
Representative western blot **(A)** and densitometry showing protein expression ratios of pAKT^{S473}/tAKT **(B)**, RAPTOR/tAKT **(C)**, p4EBP1$^{T36/T47}$/t4EBP1 **(D)**, pS6$^{S235/S236}$/tS6 **(E)**, and RICTOR/tAKT **(F)** in the spleen taken from host mice transplanted with 5x10^5 *Mx1-Raptor* control PKCαKR cells (n=3) and *Mx1-Raptor* cKO PKCαKR cells with 4 inoculation of poly(I:C) after disease development (n=4). Mice were sacrificed once health of the mice has been compromised due to disease. Cre-: *Raptor*-control, Cre+: *Raptor*-cKO. Data are expressed as mean±SEM (p *≤0.05).
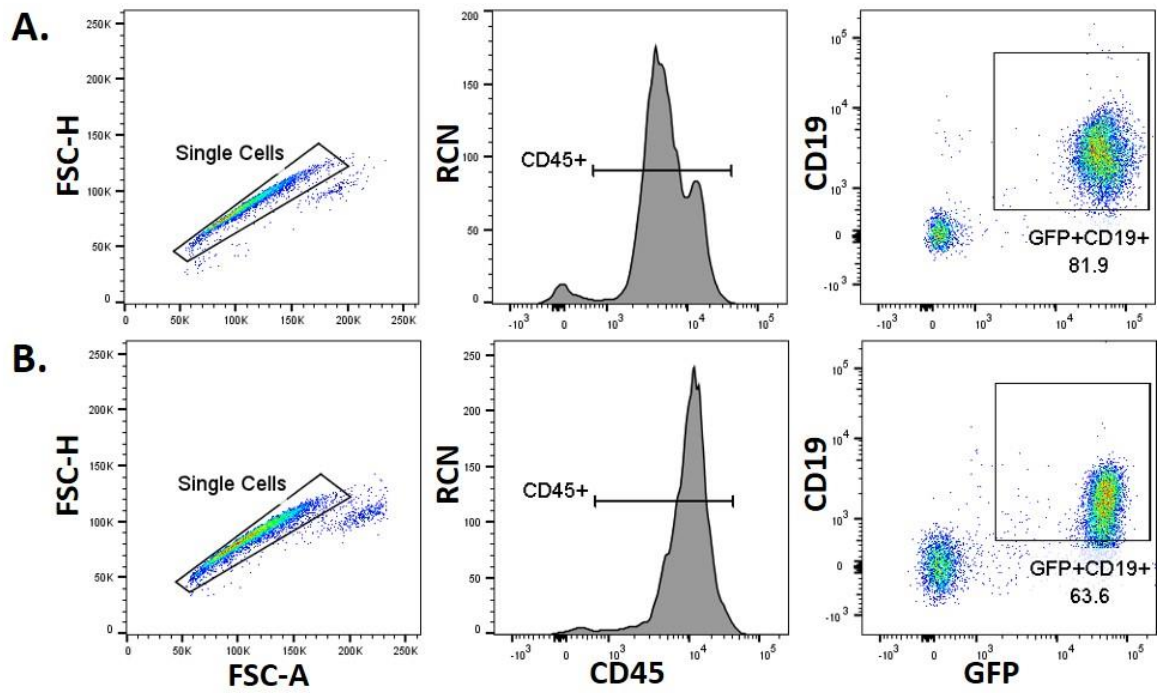
Figure 5.13 *Raptor*-deficiency solely in CD19+ CLL-like cells does not affect CLL-like disease initiation *in vivo.*
All NSG mice were transplanted with PKCαKR cells and developed disease. Representative flow cytometry plots showing proportion of GFP+CD45+CD19+ CLL-like PKCαKR cells in the blood of NSG mice transplanted with 5x10^5 *CD19-Raptor* control **(A)** or *CD19-Raptor* KO **(B)** PKCαKR cells. Plots are live and size (FSC-A/SSC-A) gated prior to the gating shown. Doublet cells were excluded (FSC-A/FSC-H) and positively selected for CD45 before assessing surface expression of GFP+CD19+ population.
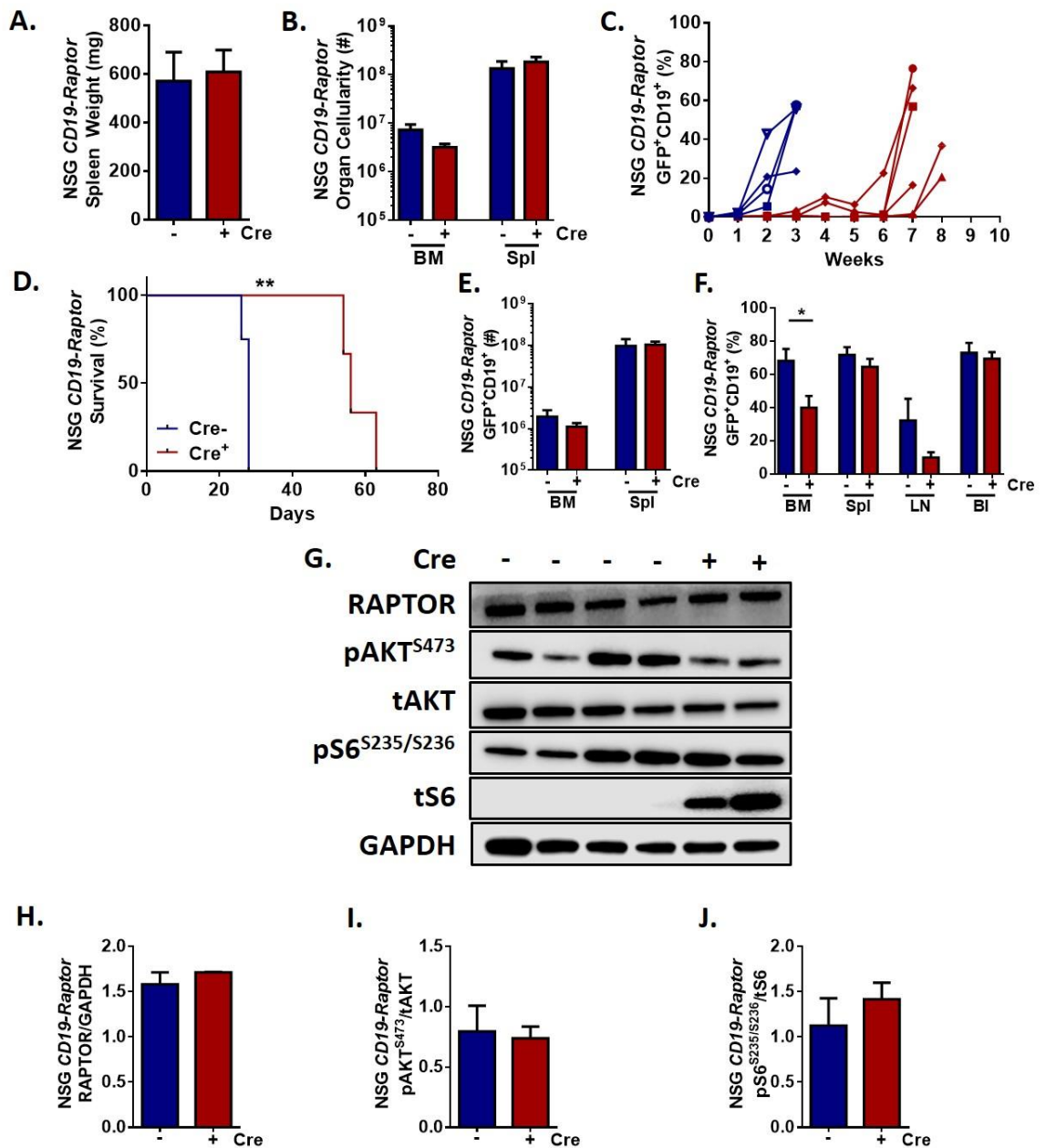
Figure 5.14 *Raptor*-deficiency solely in CD19⁺ CLL-like cells increases survival in CLL-like disease *in vivo*.

All NSG mice were transplanted with PKCαKR cells and developed disease. Spleen weight (mg) **(A)** and BM and spleen **(B)** organ cellularity of NSG mice transplanted with 5x10^5 *CD19-Raptor* control (n=6) or KO PKCαKR cells (n=6). **C.** Weekly blood samples were taken and assessed for percentage of GFP⁺CD19⁺ CLL-like disease in mice transplanted with *CD19-Raptor* control or KO PKCαKR cells. **D.** Kaplan-meier survival graph comparing the percentage of survival between NSG mice transplanted with *CD19-Raptor* control (n=4) or KO (n=7) PKCαKR cells. Cellularity of GFP⁺CD19⁺ cells in the BM and spleen **(E)** and percentage of GFP⁺CD19⁺ cells in BM, spleen, LN and blood **(F)** of mice transplanted with *CD19-Raptor* control (n=6) or KO PKCαKR (n=6) cells. Representative western blot **(G)** and protein expression ratio of RAPTOR/GAPDH **(H)**, pAKT^{S473}/tAKT **(I)**, and pS6$^{S235/S236}$/tS6 **(J)** in the spleen of mice transplanted with *CD19-Raptor* control (n=4) or KO PKCαKR cells (n=2). Data are expressed as mean±SD/SEM (p *≤0.05, p **≤0.001).
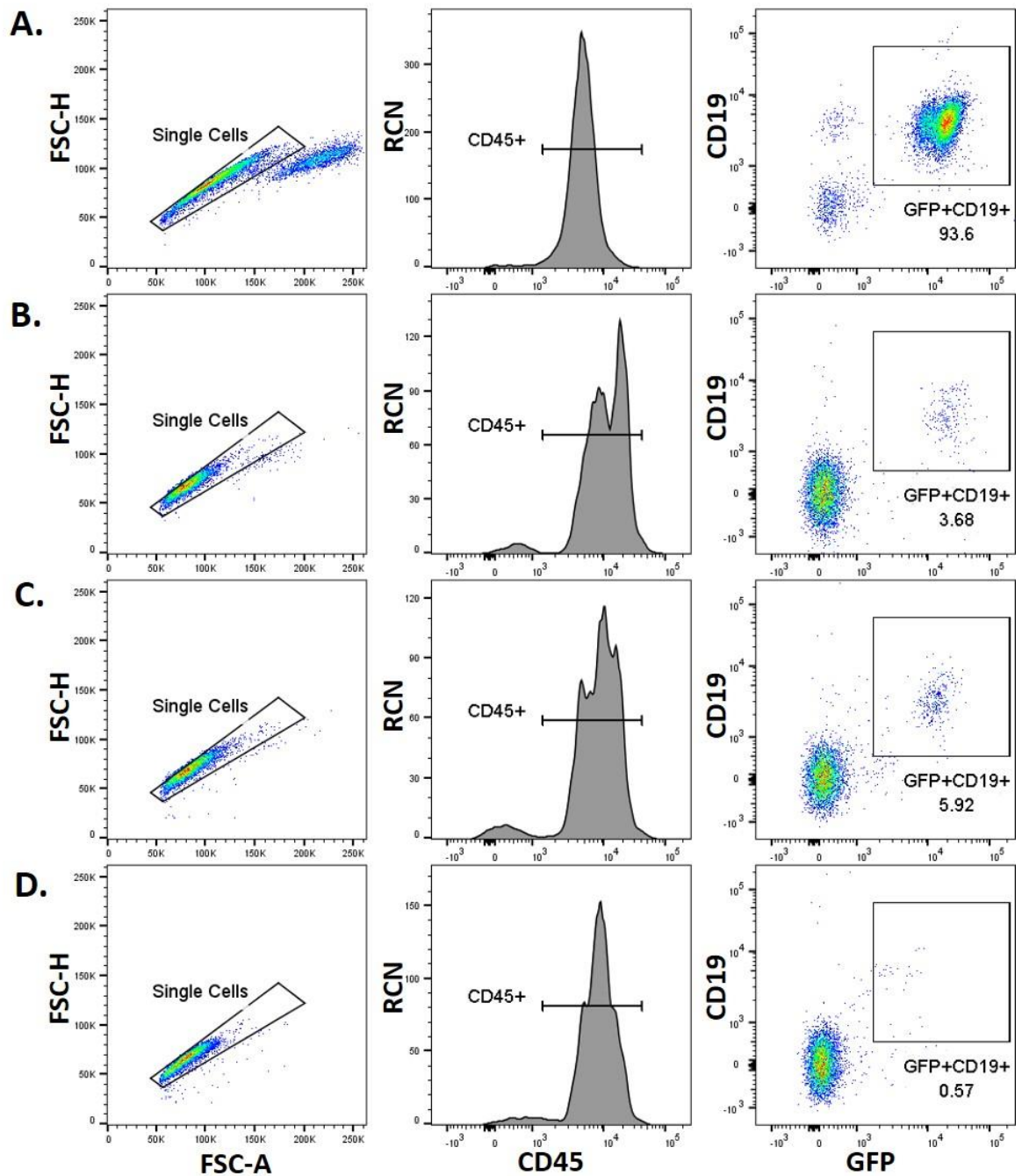
Figure 5.15 CLL-like disease is reduced with a combination treatment of AZD2014 and ibrutinib *in vivo*.
NSG mice were transplanted with PKCαKR cells and established disease. Representative flow cytometry plots showing proportion of GFP+CD45+CD19+ CLL-like PKCαKR cells in the blood of mice which were transplanted with 5x10^5 PKCαKR cells derived from B6.SJL BM and were treated with either the vehicle control (captisol+0.5%methylcellulose) **(A)**, AZD2014 (15 mg/kg) **(B)**, Ibrutinib (12 mg/kg) **(C)** or a combination of AZD2014+Ibrutinib **(D)** once daily for 14 days by oral gavage. Plots are live and size (FSC-A/SSC-A) gated prior to the gating shown. Doublet cells were excluded (FSC-A/FSC-H) and positively selected for CD45 before assessing surface expression of GFP+CD19+ population.
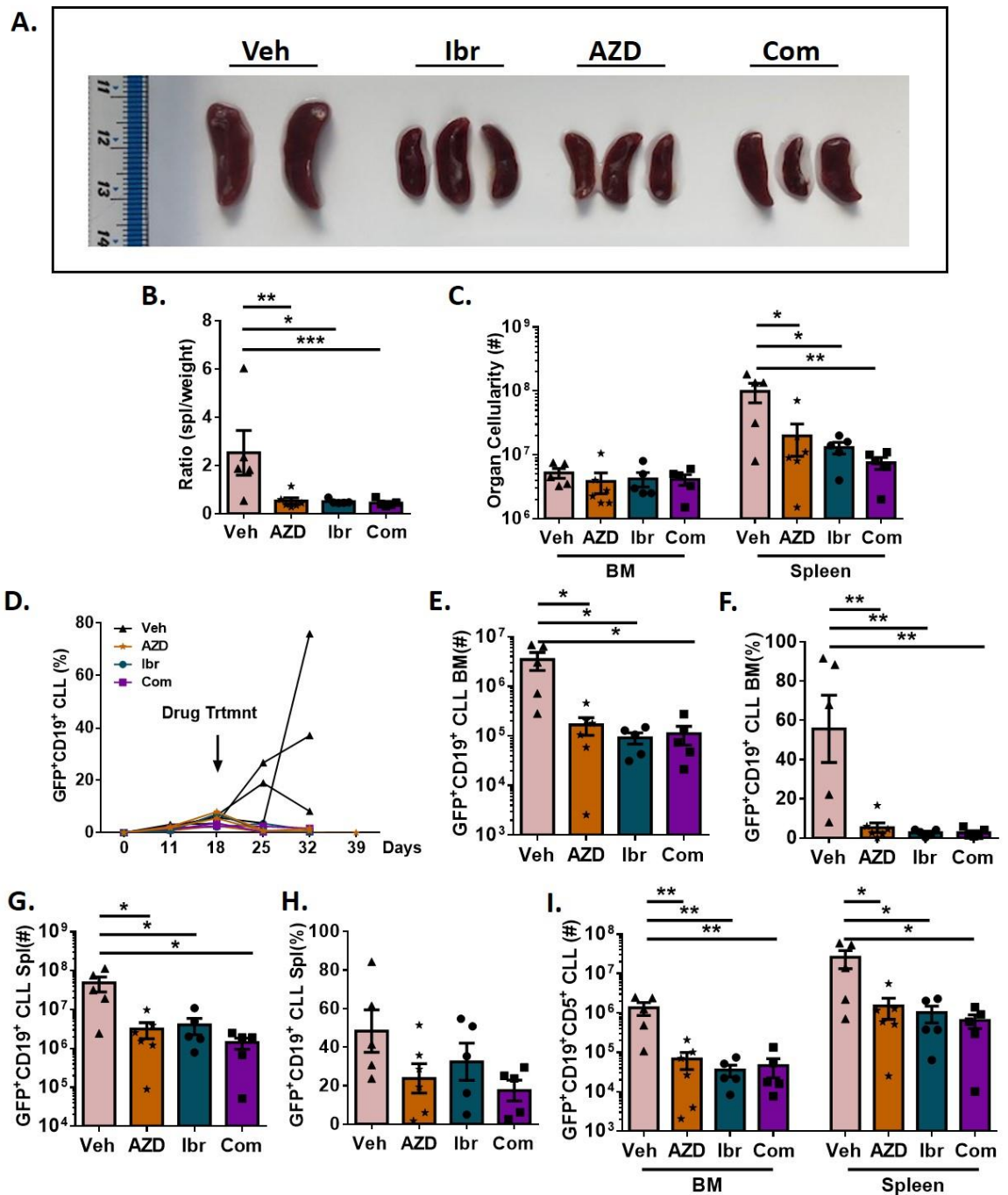
Figure 5.16 Combination therapy does not reduce CLL-disease load more efficiently than single agents *in vivo*.
NSG mice were transplanted with $5x10^5$ PKCαKR cells and disease was established prior to commencement of drug therapy. **A.** Representative picture of spleens from NSG mice with established CLL-like disease and treated with either vehicle control (Veh; captisol+0.5% methylcellulose, n=5), ibrutinib (Ibr, 12 mg/kg n=6), AZD2014 (AZD, 15 mg/kg, n=5) or a combination of AZD2014+ Ibrutinib (Com, n=5). Ratio of spleen weight/total body weight **(B)** and cellularity of BM and spleen **(C)** in mice with established disease and treated with either the Veh (light pink bar), AZD (orange bar), Ibr (turquoise bar) or Com (purple bar). **D.** Weekly blood samples (representative n=3) were taken and were assessed for percentage of GFP+CD19+ CLL-like disease in mice, treated with Veh, AZD, Ibr or Com. Cellularity **(E)** and percentage **(F)** of GFP+CD19+ CLL-like cells in the BM, and cellularity **(G)** and percentage **(H)** of GFP+CD19+ CLL-like cells in the spleen of mice treated with either Veh, AZD, Ibr or Com. **I.** Cellularity of GFP+CD19+CD5+ cells in the BM and spleen of mice treated with either Veh, AZD, Ibr or Com. Data are expressed as mean±SEM (p *≤0.05, p **≤0.001, p ***≤0.0001).
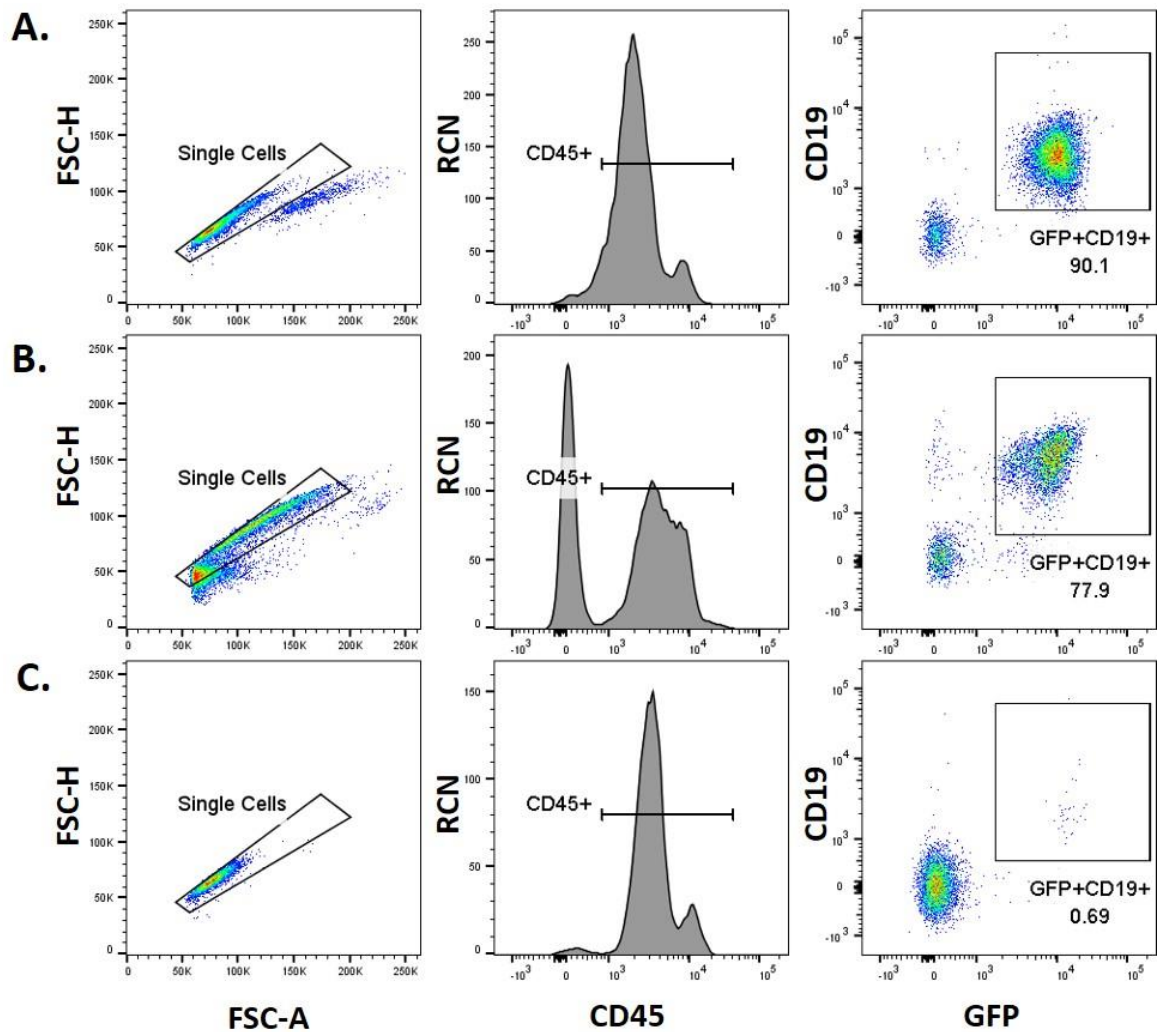
Figure 5.17 Secondary transplants of CLL-like disease are responsive to rapamycin treatment *in vivo*.
Secondary transplants were carried out with NSG or NRG mice transplanted with PKCαKR cells isolated from the spleen of mice with ≥95% CLL-like disease. Representative flow cytometry plots showing the proportion of GFP+CD45+CD19+ CLL-like PKCαKR cells in the blood of mice treated with either vehicle control (captisol) **(A)**, AZD2014 (15 mg/kg delivered by OG) **(B)**, or rapamycin (4mg/kg, delivered intraperitoneally) **(C)** given once daily for 3 wk. Plots are live and size (FSC-A/SSC-A) gated prior to the gating shown. Doublet cells were excluded (FSC-A/FSC-H) and positively selected for CD45 before assessing surface expression of GFP+CD19+ population.
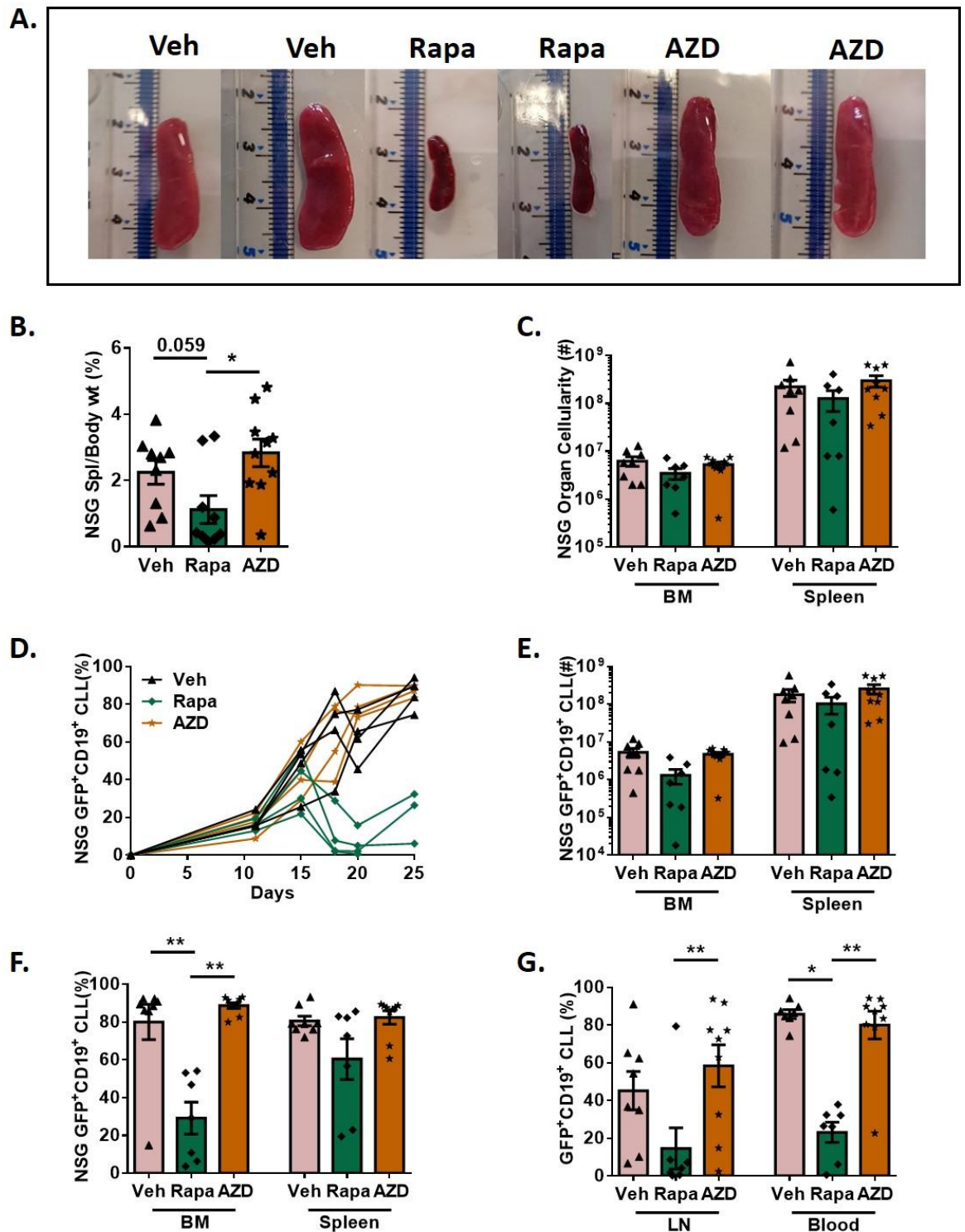
Figure 5.18 Rapamycin is a more potent agent for decreasing CLL-disease load *in vivo*. Secondary transplants were carried out with NSG and NRG mice transplanted with PKCαKR cells from the spleen of mice with ≥95% CLL-like disease. **A.** Picture of spleens from mice with established disease and treated with either vehicle control (Veh; captisol, n=8), rapamycin (Rapa, 4 mg/kg delivered intraperitoneally, n=7) or AZD2014 (AZD, 15 mg/kg, n=9) given once daily for 3 wk. Percentage of spleen/body weight **(B)** and total cellularity of BM and spleen **(C)** in mice with a CLL-like disease and treated with either Veh (light pink bar), Rapa (green bar) or AZD (orange bar). **D.** Weekly blood samples (representative, n=3) were assessed for percentage of GFP+CD19+ CLL-like disease in Veh, Rapa or AZD treated mice. Cellularity **(E)** and percentage **(F)** of GFP+CD19+ CLL-like cells in the BM and spleen together with the percentage **(G)** of GFP+CD19+ CLL-like cells in the LN and blood of mice treated with either Veh, Rapa or AZD. Data are expressed as mean±SEM (p *≤0.05, p **≤0.001).
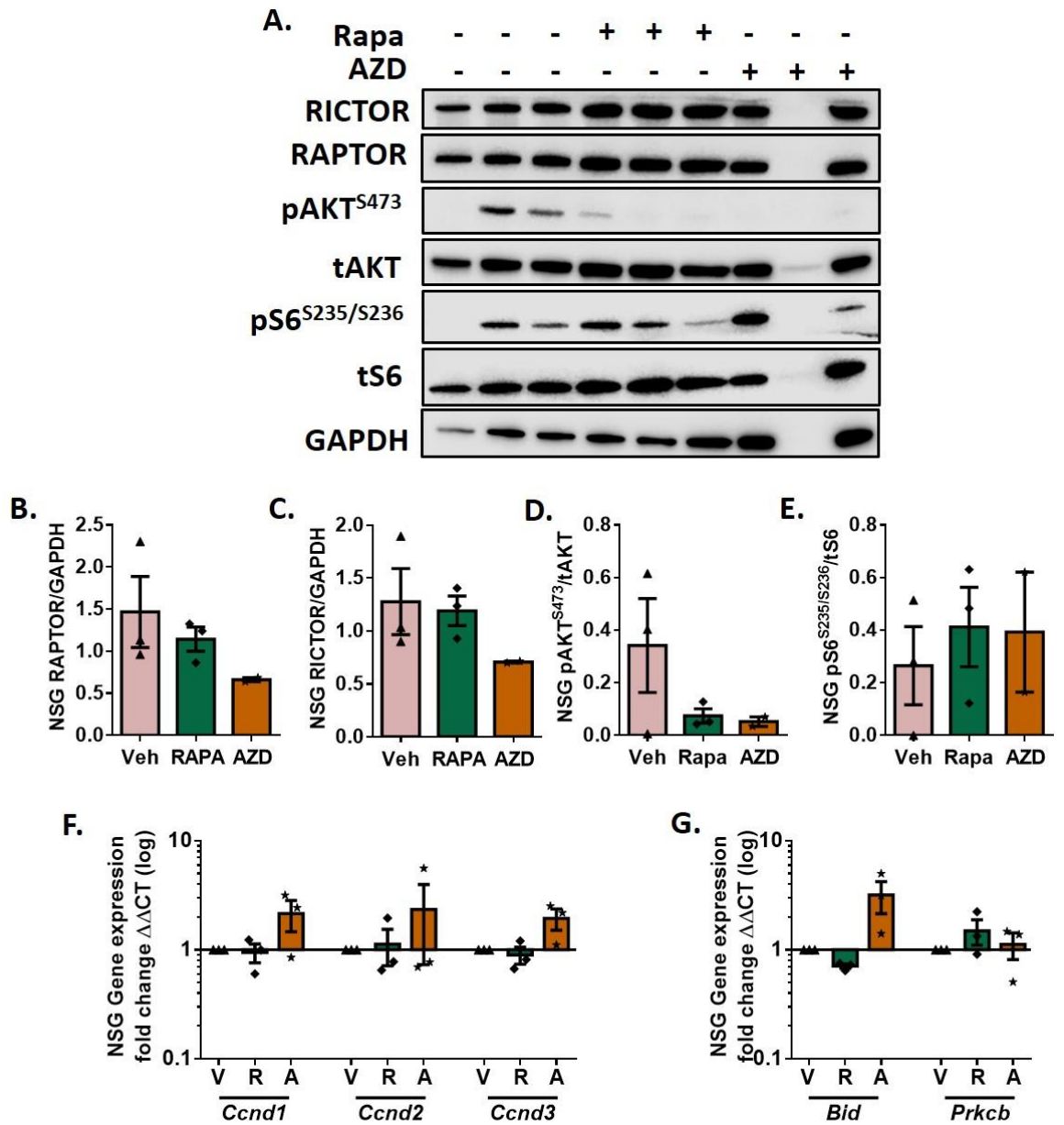
Figure 5.19 A potentially different mechanism of rapamycin in decreasing CLL-like disease load compared to AZD2014 *in vivo.*
Secondary transplants were carried out where all NSG and NRG mice were transplanted with PKCαKR cells from the spleen of NSG mice with ≥95% CLL-like disease. Representative western blot **(A)** and densitometry of protein expression of ratio of RAPTOR/GAPDH **(B)**, RICTOR/GAPDH **(C)**, pAKT^{S473}/tAKT **(D)**, and pS6$^{S235/S236}$/tS6 **(E)** of the spleens of mice treated with either Veh (n=3), Rapa (4 mg/kg delivered intraperitoneally, n=3) or AZD (15 mg/kg delivered by OG, n=2) given once daily for 3 wk. Gene expression (log fold change) of *Ccnd1, Ccnd2, Ccnd3* **(F)** and *Bid* and *Prkcb* **(G)** in the spleen of mice treated with either Veh (n=3), Rapa (n=3) or AZD (n=2). All gene expression data is relative to the vehicle control with *Actb* as the endogenous reference gene. Data are expressed as mean±SEM (p *≤0.05).

General Discussion and Conclusions

Although much is known about the mTOR signalling pathway and its role in metabolism and diseases such as diabetes, the exact role of the individual complexes, mTORC1 and mTORC2 in normal B cell development and in B cell malignancies was not well known. Therefore, my thesis addressed the individual roles of mTORC1 and mTORC2 in normal haemopoiesis and in CLL initiation/maintenance and the potential for mTOR as a valid therapeutic target in CLL.

Using the well-developed cre-loxP KO systems, KO mouse models were generated for mTORC1 and mTORC2 excising either *Raptor* or *Rictor* respectively at different haemopoietic stages giving rise to *Vav-* (KO at HSC stage), *Mx1-* (cKO in haemopoietic organs) or *CD19*-cre (KO in B cells) mouse models. Furthermore, utilising the PKCαKR retroviral construct which enables the generation of a murine CLL-like disease(230), combined analysis of the role of the individual mTOR complexes was carried out during leukaemogenesis *in vitro* and *in vivo*.

Generation of mTORC1 KO mouse model confirmed the previous findings that mTORC1-deficiency at the HSC stage is lethal at the perinatal stage due to its fundamental role in regulating erythropoiesis (97). mTORC1-deficiency leads to a block in erythropoiesis at the MEP stage. In agreement with previous literature, the results demonstrate the potent role of mTORC1 in B cell development(109), as deficiency of mTORC1 (in *Vav-* or *Mx1-* mice) leads to a block in B cell development at the LSK stage (Chapter 3). While mTORC1 plays a role early in development, mTORC2 plays a subtle opposite yet complementary role to mTORC1 regulation in haemopoiesis giving both the complexes a yin-yang undertone. mTORC2-deficiency leads to aberrations in late B cell populations. Where mTORC1 plays a positive role in erythropoiesis, our results suggest a suppressive role of mTORC2 as *Rictor*-deficiency leads to an increase in RBC colony capacity. mTORC2 has also shown to play an important role in T cell development, as our results demonstrate a drastic decrease in DP T cells and an increase in DN T cells suggesting a block in T cell development, which is in agreement with previously published data (115)(Chapter 4).

Whilst assessing the role of mTORC1 and mTORC2 in CLL-like disease initiation and/or maintenance, the PKCαKR retroviral construct was used to induce a CLL-

like disease in the BM of the KO models and their respective controls. Our results showed that although mTORC1 and mTORC2 have distinct roles in haemopoiesis and leukaemogenesis, both the complexes regulate CLL and normal haemopoiesis in a similar manner: mTORC1 plays a fundamental role in CLL initiation (due to its role in B cell lineage commitment) *in vitro* and *in vivo*, whereas mTORC2 plays a role at later stages of B cell development and leukaemia alluding to a role in B cell and leukaemia maintenance *in vitro*. Induced *Raptor*-deficiency in established CLL-like disease led to a decrease in migration, proliferation and trends towards decreased cell cycling *in vitro* with an abrogation or a delay in disease maintenance *in vivo*. While the results showing an extension in survival in the PKCαKR *CD19*-cre mouse model *in vivo* was interesting, we concluded that the *CD19*-cre mouse models are not ideal as a KO model due to the reduced efficiency of cre-recombinase excision in this model(208). Therefore, it would be interesting to assess leukaemia maintenance *in vivo* using other efficient KO models such as *Mb1*-cre KO model (Chapter 5).

CLL-like disease with *Rictor*-deficiency led to an increase in migration and trends in increase in cell cycling. Although there were trends showing a decrease in disease load at later stages of disease *in vitro,* we did not look into this in great detail due to time restrictions of this project. Additionally, the role of mTORC2 in disease maintenance was not assessed *in vivo* also due to time restrictions. These experiments would be very beneficial in further assessing the exact mechanisms by which mTORC2 plays a role in disease maintenance. These processes allude to a role of mTORC2 in enhancing microenvironmental signals. However, as this cannot be assessed *in vivo* in NSG mice (highly immunocompromised), it would be of great interest to assess whether mTORC2 maintains CLL by modulating the microenvironment *in vitro*.

The opposing trends observed in a leukaemic setting between *Rictor*- and *Raptor*-deficient PKCαKR cells *in vitro* was interesting as there are other functions that have been assessed that the mTOR pathway regulates such as B cell development and erythropoiesis which are also differentially regulated by the two complexes where mTORC1 is fundamental for haemopoiesis and mTORC2 either regulates haemopoiesis at a later stage (B cells) or dampens the generation of haemocytes (erythropoiesis) (Chapter 3)(282). These trends

between the two complexes in disease initiation/maintenance, disease migration and trends in cell cycling alludes to the feedback loop in the mTOR pathway between mTORC1 and mTORC2(66) thereby highlighting the importance of both the complexes in the maintenance of both normal haemopoiesis and leukaemogenesis.

Lastly, to test CLL-disease maintenance by using clinically relevant compounds targeting the mTOR signalling pathway, we transplanted NSG mice with the PKCαKR CLL-like disease to induce a CLL-like disease *in vivo*. Subsequent treatments with AZD2014, ibrutinib, or a combination resulted in a potent reduction of disease maintenance with both ibrutinib and AZD2014 suggesting dual mTOR inhibition could prove a valid therapeutic target for CLL. Moreover, combination therapy on CLL was not additive and did not confer synergy suggesting dual mTOR inhibition to be as potent as combination therapy (Chapter 5).

As mTORC1 has shown to play a fundamental role in disease initiation and maintenance, it was important to address the role of rapamycin in disease maintenance. To test this, secondary transplants were carried out to generate a more aggressive CLL-like disease in host mice which were subsequently treated with either rapamycin or AZD2014, to test whether only mTORC1 inhibition is sufficient for disease attenuation as opposed to using the dual mTOR complex inhibitor AZD2014. Despite the known role of rapamycin in partially inhibiting mTORC1 (partially inhibits 4EBP1 activity, but a potent inhibitor of S6K), rapamycin was superior to AZD2014 in reducing disease load in host mice (Chapter 5). This suggests that an aggressive disease is more mTORC1 dependent, as our previous studies comparing rapamycin and AZD8055 (dual mTOR complex inhibitor with the same pharmacophore as AZD2014) in disease maintenance resulted in a superior effect of AZD8055 in primary transplants(128). This has led us to consider that another target of rapamycin in the mTOR pathway could potentially regulate disease: S6K. Previous research has shown the role of S6K in driving colorectal cancer through the mTOR-S6K-EF2K axis in regulating translational elongation and thus disease maintenance(333). It would be interesting to test the mTORC1-substrate profile

in this aggressive CLL-like disease and compare the sensitivity of rapamycin and AZD2014/AZD8055 on these targets.

Therefore, future directions would be to re-examine the role of mTORC1 in CLL-like disease initiation/maintenance by using an alternative B cell promoter for the cre-LoxP mouse model. Instead of utilising the *CD19-Raptor* KO model, assessing another promoter which is more effieinct at Raptor deletion such as the *Mb1-Raptor* KO model would give a clearer insight into the role of mTORC1 in disease progression. Moreover, perfoming secondary transplants of a WT CLL-like disease led to the finding that Rapamycin is more superior than AZD2014 in decreasing disease load in NSG mice suggesting a more aggressive CLL-like disease is mTORC1 dependent. Therefore, re-performing this experiment to assess further downstream mTORC1 targets such as EF2 and EF2K by IHC on spleen and assessing the expression levels of these targets at the protein and message level on the haemopoietic organs (BM and spleen) of these mice would help answer whether translation events are attenuated in this more aggressive CLL-like disease.

Future directions further assessing the role of mTORC2 in CLL would include performing transplants of PKCαKR CLL-like cells transformed from *Vav-Rictor* KO BM into NSG mice and assessing disease maintenance by evaluating survival and assessing downstream mTOR targets by IHC on the spleens which include $pAKT^{S473}$, $pS6^{S235/S236}$. Additionally, at the end of the project, RNA-sequencing of MIEV and PKCαKR cells (transformed from *Vav-Rictor* control or KO BM) was performed after co-culturing these cells till D21 (mimicking later stages of disease progression). Initial sequencing results showed the intriguing downregulation of Proopiomelanocortin (POMC) in *Vav-Rictor* KO PKCαKR datasets compared to controls. Therefore, future directions would include further assessing these results by qPCR via assessing various *POMC* variants in PKCαKR cells, and with dual mTORC inhibition. This could also be assessed in human CLL patient sample cells treated with AZD8055/AZD2014. It has recently been known that POMC is expressed in B lymphocytes(334), and therefore would be an interesting experiment to further determine the exact role of mTORC2 in the maintenance of late stages of CLL.

Taken together, we highlight the opposite and complementary roles of mTORC1 and mTORC2 in haemopoiesis and in leukaemogenesis where mTORC1 playing a fundamental developmental role and mTORC2 regulating later stages of B cell lineages and leukaemia. Additionally, we demonstrate a synergistic effect of the dual mTOR inhibitor AZD2014 and ibrutinib in decreasing CLL-like disease *in vivo*. Lastly, although dual mTOR inhibition has previously shown to be more potent at reducing disease load compared to rapamycin *in vivo*, our results showed a significant superior role of rapamycin in reducing disease load in a more aggressive form of leukaemia suggesting that the disease becomes more dependent on mTORC1 for the maintenance on disease.

Bibliography

1. de Bruijn MF, Speck NA, Peeters MC, Dzierzak E. Definitive hematopoietic stem cells first develop within the major arterial regions of the mouse embryo. EMBO J. 2000 Jun 1;19(11):2465–74.

2. Orkin SH, Zon LI. Hematopoiesis: An Evolving Paradigm for Stem Cell Biology. Cell. 2008 Feb 22;132(4):631–44.

3. Palis J, Robertson S, Kennedy M, Wall C, Keller G. Development of erythroid and myeloid progenitors in the yolk sac and embryo proper of the mouse. Development. 1999 Nov 15;126(22):5073–84.

4. Notta F, Zandi S, Takayama N, Dobson S, Gan OI, Wilson G, et al. Distinct routes of lineage development reshape the human blood hierarchy across ontogeny. Science. 2016 Jan 8;351(6269):aab2116.

5. Hussen KA, Manh T-PV, Guimiot F, Nelson E, Chabaane E, Delord M, et al. Molecular and Functional Characterization of Lymphoid Progenitor Subsets Reveals a Bipartite Architecture of Human Lymphopoiesis. Immunity. 2017 Oct 17;47(4):680–96.

6. Zhang Q, Iida R, Yokota T, Kincade PW. Early Events in Lymphopoiesis, an Update. Curr Opin Hematol. 2013 Jul;20(4):265–72.

7. Adolfsson J, Månsson R, Buza-Vidas N, Hultquist A, Liuba K, Jensen CT, et al. Identification of Flt3+ Lympho-Myeloid Stem Cells Lacking Erythro-Megakaryocytic Potential: A Revised Road Map for Adult Blood Lineage Commitment. Cell. 2005 Apr 22;121(2):295–306.

8. Stoilova B, Karamitros D, Aboukhalil Z, Hamey F, Reinisch A, Samitsch M, et al. A Novel Model of Human Hemopoiesis Based on Single Cell Functional and Transcriptional Analysis of Lympho-Myeloid Progenitors. Blood. 2017 Dec 7;130:2413–2413.

9. Murre C. Developmental trajectories in early hematopoiesis. Genes Dev. 2009 Oct 15;23(20):2366–70.

10. Suzuki M, Kobayashi-Osaki M, Tsutsumi S, Pan X, Ohmori S, Takai J, et al. GATA factor switching from GATA2 to GATA1 contributes to erythroid differentiation. Genes to Cells. 2013 Nov 1;18(11):921–33.

11. McIver SC, Kang Y-A, DeVilbiss AW, O'Driscoll CA, Ouellette JN, Pope NJ, et al. The exosome complex establishes a barricade to erythroid maturation. Blood. 2014 Oct 2;124(14):2285–97.

12. Dijon M, Bardin F, Murati A, Batoz M, Chabannon C, Tonnelle C. The role of Ikaros in human erythroid differentiation. Blood. 2008 Feb 1;111(3):1138–46.

13. Kueh HY, Champhekhar A, Nutt SL, Elowitz MB, Rothenberg EV. Positive feedback between PU.1 and the cell cycle controls myeloid differentiation. Science. 2013 Aug 9;341(6146):670–3.

14. Nerlov C, Graf T. PU.1 induces myeloid lineage commitment in multipotent hematopoietic progenitors. Genes Dev. 1998 Aug 1;12(15):2403–12.

15. Suh HC, Gooya J, Renn K, Friedman AD, Johnson PF, Keller JR. C/EBPα determines hematopoietic cell fate in multipotential progenitor cells by inhibiting erythroid differentiation and inducing myeloid differentiation. Blood. 2006 Jun 1;107(11):4308–16.

16. Avellino R, Delwel R. Expression and regulation of C/EBPα in normal myelopoiesis and in malignant transformation. Blood. 2017 13;129(15):2083–91.

17. Zhang P, Behre G, Pan J, Iwama A, Wara-aswapati N, Radomska HS, et al. Negative cross-talk between hematopoietic regulators: GATA proteins repress PU.1. Proc Natl Acad Sci USA. 1999 Jul 20;96(15):8705–10.

18. Zhang P, Zhang X, Iwama A, Yu C, Smith KA, Mueller BU, et al. PU.1 inhibits GATA-1 function and erythroid differentiation by blocking GATA-1 DNA binding. Blood. 2000 Oct 15;96(8):2641–8.

19. Anderson KP, Crable SC, Lingrel JB. The GATA-E box-GATA motif in the EKLF promoter is required for in vivo expression. Blood. 2000 Mar 1;95(5):1652–5.

20. Levy JE, Jin O, Fujiwara Y, Kuo F, Andrews N. Transferrin receptor is necessary for development of erythrocytes and the nervous system. Nature Genetics. 1999 Apr;21(4):396–9.

21. Kina T, Ikuta K, Takayama E, Wada K, Majumdar AS, Weissman IL, et al. The monoclonal antibody TER-119 recognizes a molecule associated with glycophorin A and specifically marks the late stages of murine erythroid lineage. Br J Haematol. 2000 May;109(2):280–7.

22. Koulnis M, Pop R, Porpiglia E, Shearstone JR, Hidalgo D, Socolovsky M. Identification and Analysis of Mouse Erythroid Progenitors using the CD71/TER119 Flow-cytometric Assay. J Vis Exp. 2011 Aug 5;(54).

23. Siatecka M, Bieker JJ. The multifunctional role of EKLF/KLF1 during erythropoiesis. Blood. 2011 Aug 25;118(8):2044–54.

24. Asano H, Stamatoyannopoulos G. Activation of ß-Globin Promoter by Erythroid Krüppel-Like Factor. Mol Cell Biol. 1998 Jan;18(1):102–9.

25. Novodvorsky P, Chico TJA. The role of the transcription factor KLF2 in vascular development and disease. Prog Mol Biol Transl Sci. 2014;124:155–88.

26. Berland R, Wortis HH. Origins and Functions of B-1 Cells with Notes on the Role of CD5. Annual Review of Immunology. 2002;20(1):253–300.

27. Haas KM, Poe JC, Steeber DA, Tedder TF. B-1a and B-1b Cells Exhibit Distinct Developmental Requirements and Have Unique Functional Roles in Innate and Adaptive Immunity to S. pneumoniae. Immunity. 2005 Jul 1;23(1):7–18.

28. Lalor PA, Stall AM, Adams S, Herzenberg LA. Permanent alteration of the murine Ly-1 B repertoire due to selective depletion of Ly-1 B cells in neonatal animals. Eur J Immunol. 1989 Mar;19(3):501–6.

29. DeKoter RP, Singh H. Regulation of B Lymphocyte and Macrophage Development by Graded Expression of PU.1. Science. 2000 May 26;288(5470):1439–41.

30. Fuxa M, Skok JA. Transcriptional regulation in early B cell development. Current Opinion in Immunology. 2007 Apr 1;19(2):129–36.

31. Ogawa M, ten Boekel E, Melchers F. Identification of CD19(-)B220(+)c-Kit(+)Flt3/Flk-2(+)cells as early B lymphoid precursors before pre-B-I cells in juvenile mouse bone marrow. Int Immunol. 2000 Mar;12(3):313–24.

32. Nutt SL, Kee BL. The transcriptional regulation of B cell lineage commitment. Immunity. 2007 Jun;26(6):715–25.

33. Sitnicka E, Brakebusch C, Martensson I-L, Svensson M, Agace WW, Sigvardsson M, et al. Complementary Signaling through flt3 and Interleukin-7 Receptor α Is Indispensable for Fetal and Adult B Cell Genesis. Journal of Experimental Medicine. 2003 Nov 17;198(10):1495–506.

34. Sellars M, Kastner P, Chan S. Ikaros in B cell development and function. World J Biol Chem. 2011 Jun 26;2(6):132–9.

35. Lin H, Grosschedl R. Failure of B-cell differentiation in mice lacking the transcription factor EBF. Nature. 1995 Jul;376(6537):263.

36. Lin YC, Jhunjhunwala S, Benner C, Heinz S, Welinder E, Mansson R, et al. A global network of transcription factors, involving E2A, EBF1 and Foxo1, that orchestrates B cell fate. Nat Immunol. 2010 Jul;11(7):635–43.

37. Holmes ML, Carotta S, Corcoran LM, Nutt SL. Repression of Flt3 by Pax5 is crucial for B-cell lineage commitment. Genes Dev. 2006 Apr 15;20(8):933–8.

38. Amin RH, Schlissel MS. Foxo1 directly regulates the transcription of recombination-activating genes during B cell development. Nat Immunol. 2008 Jun;9(6):613–22.

39. Escribano L, Ocqueteaub M, Almeida J, Orfao A, Migue JFS. Expression of the c-kit (CD117) Molecule in Normal and Malignant Hematopoiesis. Leukemia & Lymphoma. 1998 Jan 1;30(5–6):459–66.

40. Allman D, Li J, Hardy RR. Commitment to the B Lymphoid Lineage Occurs before DH-JH Recombination. J Exp Med. 1999 Feb 15;189(4):735–40.

41. Hobeika E, Thiemann S, Storch B, Jumaa H, Nielsen PJ, Pelanda R, et al. Testing gene function early in the B cell lineage in mb1-cre mice. Proc Natl Acad Sci U S A. 2006 Sep 12;103(37):13789–94.

42. Pieper K, Grimbacher B, Eibel H. B-cell biology and development. Journal of Allergy and Clinical Immunology. 2013 Apr;131(4):959–71.

43. Hardy RR, Hayakawa K. B cell development pathways. Annu Rev Immunol. 2001;19:595–621.

44. Cariappa A, Boboila C, Moran ST, Liu H, Shi HN, Pillai S. The Recirculating B Cell Pool Contains Two Functionally Distinct, Long-Lived, Posttransitional, Follicular B Cell Populations. The Journal of Immunology. 2007 Aug 15;179(4):2270–81.

45. Eibel H, Kraus H, Sic H, Kienzler A-K, Rizzi M. B cell Biology: An Overview. Curr Allergy Asthma Rep. 2014 Mar 16;14(5):434.

46. Del Nagro CJ, Otero DC, Anzelon AN, Omori SA, Kolla RV, Rickert RC. CD 19 function in central and peripheral B-cell development. Immunol Res. 2005 Mar 1;31(2):119-31.

47. Jellusova J, Rickert RC. The PI3K Pathway in B Cell Metabolism. Crit Rev Biochem Mol Biol. 2016 Sep;51(5):359–78.

48. Abdelrasoul H, Werner M, Setz CS, Okkenhaug K, Jumaa H. PI3K induces B-cell development and regulates B cell identity. Scientific Reports. 2018 Jan 22;8(1):1327.

49. Jou S-T, Carpino N, Takahashi Y, Piekorz R, Chao J-R, Carpino N, et al. Essential, nonredundant role for the phosphoinositide 3-kinase p110delta in signaling by the B-cell receptor complex. Mol Cell Biol. 2002 Dec;22(24):8580–91.

50. Durand CA, Hartvigsen K, Fogelstrand L, Kim S, Iritani S, Vanhaesebroeck B, et al. Phosphoinositide 3-Kinase p110δ Regulates Natural Antibody Production, Marginal Zone and B-1 B Cell Function, and Autoantibody Responses. The Journal of Immunology. 2009 Nov 1;183(9):5673–84.

51. Aiba Y, Kameyama M, Yamazaki T, Tedder TF, Kurosaki T. Regulation of B-cell development by BCAP and CD19 through their binding to phosphoinositide 3-kinase. Blood. 2008 Feb 1;111(3):1497–503.

52. He X, Dai H, Wang X, Skidmore D, Kurosaki T, Jensen PE. BCAP (B-cell adaptor for phosphoinositide 3-kinase) plays a role in development of Marginal Zone B cells in mice. The Journal of Immunology. 2016 May 1;196:122.9-122.9.

53. Xu Y, Fairfax K, Light A, Huntington ND, Tarlinton DM. CD19 differentially regulates BCR signalling through the recruitment of PI3K. Autoimmunity. 2014 Nov 1;47(7):430–7.

54. Laplante M, Sabatini DM. mTOR Signaling. Cold Spring Harb Perspect Biol. 2012 Feb;4(2).

55. Laplante M, Sabatini DM. mTOR signaling in growth control and disease. Cell. 2012 Apr 13;149(2):274–93.

56. Wullschleger S, Loewith R, Hall MN. TOR Signaling in Growth and Metabolism. Cell. 2006 Feb 10;124(3):471–84.

57. Yang H, Rudge DG, Koos JD, Vaidialingam B, Yang HJ, Pavletich NP. mTOR kinase structure, mechanism and regulation by the rapamycin-binding domain. Nature. 2013 May 9;497(7448):217–23.

58. Hay N, Sonenberg N. Upstream and downstream of mTOR. Genes Dev. 2004 Aug 15;18(16):1926–45.

59. Hara K, Maruki Y, Long X, Yoshino K, Oshiro N, Hidayat S, et al. Raptor, a Binding Partner of Target of Rapamycin (TOR), Mediates TOR Action. Cell. 2002 Jul 26;110(2):177–89.

60. Gwinn DM, Shackelford DB, Egan DF, Mihaylova MM, Mery A, Vasquez DS, et al. AMPK phosphorylation of raptor mediates a metabolic checkpoint. Mol Cell. 2008 Apr 25;30(2):214-26.

61. Siddiqui N, Sonenberg N. Signalling to eIF4E in cancer. Biochem Soc Trans. 2015 Oct 1;43(5):763–72.

62. Tavares MR, Pavan ICB, Amaral CL, Meneguello L, Luchessi AD, Simabuco FM. The S6K protein family in health and disease. Life Sciences. 2015 Jun 15;131:1–10.

63. Dorrello NV, Peschiaroli A, Guardavaccaro D, Colburn NH, Sherman NE, Pagano M. S6K1- and ßTRCP-Mediated Degradation of PDCD4 Promotes Protein Translation and Cell Growth. Science. 2006 Oct 20;314(5798):467–71.

64. Ip CKM, Cheung ANY, Ngan HYS, Wong AST. p70 S6 kinase in the control of actin cytoskeleton dynamics and directed migration of ovarian cancer cells. Oncogene. 2011 May;30(21):2420-32.

65. Julien L-A, Carriere A, Moreau J, Roux PP. mTORC1-activated S6K1 phosphorylates Rictor on threonine 1135 and regulates mTORC2 signaling. Mol Cell Biol. 2010 Feb;30(4):908–21.

66. Treins C, Warne PH, Magnuson MA, Pende M, Downward J. Rictor is a novel target of p70 S6 kinase-1. Oncogene. 2009 Nov 23;29(7):1003–16.

67. Vadlakonda L, Dash A, Pasupuleti M, Anil Kumar K, Reddanna P. The Paradox of Akt-mTOR Interactions. Front Oncol. 2013 Jun 20;3.

68. Gao M, Kong Q, Hua H, Yin Y, Wang J, Luo T, et al. AMPK-mediated up-regulation of mTORC2 and MCL-1 compromises the anti-cancer effects of aspirin. Oncotarget. 2016 Feb 23;7(13):16349–61.

69. Lam EW-F, Brosens JJ, Gomes AR, Koo C-Y. Forkhead box proteins: tuning forks for transcriptional harmony. Nat Rev Cancer. 2013 Jul;13(7):482–95.

70. Brunet A, Bonni A, Zigmond MJ, Lin MZ, Juo P, Hu LS, et al. Akt promotes cell survival by phosphorylating and inhibiting a Forkhead transcription factor. Cell. 1999 Mar 19;96(6):857–68.

71. Brown J, Wang H, Suttles J, Graves DT, Martin M. Mammalian Target of Rapamycin Complex 2 (mTORC2) Negatively Regulates Toll-like Receptor 4-

mediated Inflammatory Response via FoxO1. J Biol Chem. 2011 Dec 30;286(52):44295–305.

72. Yao C-A, Ortiz-Vega S, Sun Y-Y, Chien C-T, Chuang J-H, Lin Y. Association of mSin1 with mTORC2 Ras and Akt reveals a crucial domain on mSin1 involved in Akt phosphorylation. Oncotarget. 2017 Jun 28;8(38):63392–404.

73. Jacinto E, Facchinetti V, Liu D, Soto N, Wei S, Jung SY, et al. SIN1/MIP1 maintains rictor-mTOR complex integrity and regulates Akt phosphorylation and substrate specificity. Cell. 2006 Oct 6;127(1):125–37.

74. Ikenoue T, Inoki K, Yang Q, Zhou X, Guan K-L. Essential function of TORC2 in PKC and Akt turn motif phosphorylation, maturation and signalling. EMBO J. 2008 Jul 23;27(14):1919–31.

75. Nakashima S. Protein kinase C alpha (PKC alpha): regulation and biological function. J Biochem. 2002 Nov;132(5):669–75.

76. García-Martínez JM, Alessi DR. mTOR complex 2 (mTORC2) controls hydrophobic motif phosphorylation and activation of serum- and glucocorticoid-induced protein kinase 1 (SGK1). Biochem J. 2008 Dec 15;416(3):375–85.

77. Heikamp EB, Patel CH, Collins S, Waickman A, Oh M-H, Sun I-H, et al. The AGC kinase serum- and glucocorticoid-regulated kinase 1 (SGK1) regulates TH1 and TH2 differentiation downstream of mTORC2. Nat Immunol. 2014 May;15(5):457–64.

78. Goncharova EA, Goncharov DA, Li H, Pimtong W, Lu S, Khavin I, et al. mTORC2 is required for proliferation and survival of TSC2-null cells. Mol Cell Biol. 2011 Jun;31(12):2484–98.

79. Gangloff Y-G, Mueller M, Dann SG, Svoboda P, Sticker M, Spetz J-F, et al. Disruption of the Mouse mTOR Gene Leads to Early Postimplantation Lethality and Prohibits Embryonic Stem Cell Development. Mol Cell Biol. 2004 Nov;24(21):9508–16.

80. Guertin DA, Stevens DM, Thoreen CC, Burds AA, Kalaany NY, Moffat J, et al. Ablation in Mice of the mTORC Components raptor, rictor, or mLST8 Reveals that mTORC2 Is Required for Signaling to Akt-FOXO and PKCα, but Not S6K1. Developmental Cell. 2006 Dec;11(6):859–71.

81. Yilmaz ÖH, Valdez R, Theisen BK, Guo W, Ferguson DO, Wu H, et al. Pten dependence distinguishes haematopoietic stem cells from leukaemia-initiating cells. Nature. 2006 May 25;441(7092):475–82.

82. Gan B, Sahin E, Jiang S, Sanchez-Aguilera A, Scott KL, Chin L, et al. mTORC1-dependent and -independent regulation of stem cell renewal, differentiation, and mobilization. PNAS. 2008 Dec 9;105(49):19384–9.

83. Chen C, Liu Y, Liu R, Ikenoue T, Guan K-L, Liu Y, et al. TSC-mTOR maintains quiescence and function of hematopoietic stem cells by repressing mitochondrial biogenesis and reactive oxygen species. J Exp Med. 2008 Sep 29;205(10):2397–408.

84. Guo F, Zhang S, Grogg M, Cancelas JA, Varney ME, Starczynowski DT, et al. Mouse gene targeting reveals an essential role of mTOR in hematopoietic stem cell engraftment and hematopoiesis. Haematologica. 2013 Sep;98(9):1353–8.

85. Baumgartner C, Toifl S, Farlik M, Halbritter F, Scheicher R, Fischer I, et al. An ERK-Dependent Feedback Mechanism Prevents Hematopoietic Stem Cell Exhaustion. Cell Stem Cell. 2018 Jun 1;22(6):879–92.

86. Inoki K, Ouyang H, Zhu T, Lindvall C, Wang Y, Zhang X, et al. TSC2 integrates Wnt and energy signals via a coordinated phosphorylation by AMPK and GSK3 to regulate cell growth. Cell. 2006 Sep 8;126(5):955–68.

87. Huang J, Zhang Y, Bersenev A, O'Brien WT, Tong W, Emerson SG, et al. Pivotal role for glycogen synthase kinase–3 in hematopoietic stem cell homeostasis in mice. J Clin Invest. 2009 Dec 1;119(12):3519–29.

88. Huang J, Nguyen-McCarty M, Hexner EO, Danet-Desnoyers G, Klein PS. Maintenance of Hematopoietic Stem Cells through Regulation of Wnt and mTOR Pathways. Nat Med. 2012 Dec;18(12):1778–85.

89. Selman C, Sinclair A, Pedroni SMA, Irvine EE, Michie AM, Withers DJ. Evidence that hematopoietic stem cell function is preserved during aging in long-lived S6K1 mutant mice. Oncotarget. 2016 Apr 13;7(21):29937–43.

90. Luo Y, Li L, Zou P, Wang J, Shao L, Zhou D, et al. Rapamycin enhances long-term hematopoietic reconstitution of ex vivo expanded mouse hematopoietic stem cells by inhibiting senescence. Transplantation. 2014 Jan 15;97(1):20–9.

91. Kalaitzidis D, Sykes SM, Wang Z, Punt N, Tang Y, Ragu C, et al. mTOR Complex 1 Plays Critical Roles in Hematopoiesis and Pten-Loss-Evoked Leukemogenesis. Cell Stem Cell. 2012 Sep 7;11(3):429–39.

92. Zhang Y, Hu T, Hua C, Gu J, Zhang L, Hao S, et al. Rictor Is Required for Early B Cell Development in Bone Marrow. PLoS One. 2014 Aug 1;9(8).

93. Magee JA, Ikenoue T, Nakada D, Lee JY, Guan K-L, Morrison SJ. Temporal Changes in PTEN and mTORC2 Regulation of Hematopoietic Stem Cell Self-Renewal and Leukemia Suppression. Cell Stem Cell. 2012 Sep 7;11(3):415–28.

94. Zhang X, Campreciós G, Rimmelé P, Liang R, Yalcin S, Mungamuri SK, et al. FOXO3-mTOR metabolic cooperation in the regulation of erythroid cell maturation and homeostasis. Am J Hematol. 2014 Oct;89(10):954-63.

95. Zhang J, Wu K, Xiao X, Liao J, Hu Q, Chen H, et al. Autophagy as a Regulatory Component of Erythropoiesis. Int J Mol Sci. 2015 Feb 13;16(2):4083-94.

96. Zhang Y, Li L, Yu C, Senyuk V, Li F, Quigley JG, et al. miR-9 upregulation leads to inhibition of erythropoiesis by repressing FoxO3. Scientific Reports. 2018 Apr 25;8(1):6519.

97. Knight ZA, Schmidt SF, Birsoy K, Tan K, Friedman JM. A critical role for mTORC1 in erythropoiesis and anemia. eLife. 2014 Sep 8;3.

98. Zhang S, Macias-Garcia A, Velazquez J, Paltrinieri E, Kaufman RJ, Chen J-J. HRI coordinates translation by eIF2αP and mTORC1 to mitigate ineffective erythropoiesis in mice during iron deficiency. Blood. 2017 Jan 1;131(4):450–61.

99. Chung J, Bauer DE, Ghamari A, Nizzi CP, Deck KM, Kingsley PD, et al. The mTORC1/4E-BP pathway coordinates hemoglobin production with L-leucine availability. Sci Signal. 2015 Apr 14;8(372).

100. Hoshii T, Tadokoro Y, Naka K, Ooshio T, Muraguchi T, Sugiyama N, et al. mTORC1 is essential for leukemia propagation but not stem cell self-renewal. J Clin Invest. 2012 Jun;122(6):2114–29.

101. Zhao Y, Shen X, Na N, Chu Z, Su H, Chao S, et al. mTOR masters monocyte development in bone marrow by decreasing the inhibition of STAT5 on IRF8. Blood. 2018 Apr 5;131(14):1587–99.

102. Karmaus PWF, Herrada AA, Guy C, Neale G, Dhungana Y, Long L, et al. Critical roles of mTORC1 signaling and metabolic reprogramming for M-CSF–mediated myelopoiesis. Journal of Experimental Medicine. 2017 Aug 7;

103. Byles V, Covarrubias AJ, Ben-Sahra I, Lamming DW, Sabatini DM, Manning BD, et al. The TSC-mTOR pathway regulates macrophage polarization. Nat Commun. 2013;4:2834.

104. Tang F, Zhang P, Ye P, Lazarski CA, Wu Q, Bergin IL, et al. A population of innate myelolymphoblastoid effector cell expanded by inactivation of mTOR complex 1 in mice. eLife Sciences. 2017 Dec 5;6.

105. Babaev VR, Huang J, Ding L, Zhang Y, May JM, Linton MF. Loss ofRictorin Monocyte/Macrophages Suppresses Their Proliferation and Viability Reducing Atherosclerosis in LDLR Null Mice. Front Immunol. 2018;9:215.

106. Festuccia WT, Pouliot P, Bakan I, Sabatini DM, Laplante M. Myeloid-specific Rictor deletion induces M1 macrophage polarization and potentiates in vivo pro-inflammatory response to lipopolysaccharide. PLoS ONE. 2014;9(4).

107. Zhang S, Readinger JA, DuBois W, Janka-Junttila M, Robinson R, Pruitt M, et al. Constitutive reductions in mTOR alter cell size, immune cell development, and antibody production. Blood. 2011 Jan 27;117(4):1228–38.

108. Benhamron S, Tirosh B. Direct activation of mTOR in B lymphocytes confers impairment in B-cell maturation andloss of marginal zone B cells. Eur J Immunol. 2011 Aug;41(8):2390–6.

109. Iwata TN, Ramírez JA, Tsang M, Park H, Margineantu DH, Hockenbery DM, et al. Conditional Disruption of Raptor Reveals an Essential Role for mTORC1 in B Cell Development, Survival, and Metabolism. J Immunol. 2016 15;197(6):2250–60.

110. Jones DD, Gaudette BT, Wilmore JR, Chernova I, Bortnick A, Weiss BM, et al. mTOR has distinct functions in generating versus sustaining humoral immunity. J Clin Invest. 2016 Nov 1;126(11):4250–61.

111. Lee K, Heffington L, Jellusova J, Nam KT, Raybuck A, Cho SH, et al. Requirement for Rictor in homeostasis and function of mature B lymphoid cells. Blood. 2013 Oct 3;122(14):2369–79.

112. Lazorchak AS, Liu D, Facchinetti V, Di Lorenzo A, Sessa WC, Schatz DG, et al. Sin1-mTORC2 suppresses rag and il7r gene expression through Akt2 in B cells. Mol Cell. 2010 Aug 13;39(3):433–43.

113. Zou Z, Chen J, Liu A, Zhou X, Song Q, Jia C, et al. mTORC2 promotes cell survival through c-Myc-dependent up-regulation of E2F1. J Cell Biol. 2015 Oct 12;211(1):105–22.

114. Hoshii T, Kasada A, Hatakeyama T, Ohtani M, Tadokoro Y, Naka K, et al. Loss of mTOR complex 1 induces developmental blockage in early T-lymphopoiesis and eradicates T-cell acute lymphoblastic leukemia cells. Proc Natl Acad Sci USA. 2014 Mar 11;111(10):3805–10.

115. Tang F, Wu Q, Ikenoue T, Guan K-L, Liu Y, Zheng P. A Critical Role for Rictor in T Lymphopoiesis. The Journal of Immunology. 2012 Aug 15;189(4):1850–7.

116. Lee K, Nam KT, Cho SH, Gudapati P, Hwang Y, Park D-S, et al. Vital roles of mTOR complex 2 in Notch-driven thymocyte differentiation and leukemia. J Exp Med. 2012 Apr 9;209(4):713–28.

117. Prevot N, Pyaram K, Bischoff E, Sen JM, Powell JD, Chang C-H. Mammalian Target of Rapamycin Complex 2 Regulates Invariant NKT Cell Development and Function Independent of Promyelocytic Leukemia Zinc-Finger. The Journal of Immunology. 2015 Jan 1;194(1):223–30.

118. Wang H-X, Cheng JS, Chu S, Qiu Y-R, Zhong X-P. mTORC2 in Thymic Epithelial Cells Controls Thymopoiesis and T Cell Development. The Journal of Immunology. 2016 Jul 1;197(1):141–50.

119. Yang K, Neale G, Green DR, He W, Chi H. Tuberous sclerosis complex 1 (Tsc1) enforces quiescence of naive T cells to promote immune homeostasis and function. Nat Immunol. 2011 Jul 17;12(9):888–97.

120. Pollizzi KN, Patel CH, Sun I-H, Oh M-H, Waickman AT, Wen J, et al. mTORC1 and mTORC2 selectively regulate CD8^{+} T cell differentiation. J Clin Invest. 2015 May;125(5):2090–108.

121. Waickman AT, Powell JD. mTOR, metabolism, and the regulation of T-cell differentiation and function. Immunol Rev. 2012 Sep;249(1):43–58.

122. Angela M, Endo Y, Asou HK, Yamamoto T, Tumes DJ, Tokuyama H, et al. Fatty acid metabolic reprogramming via mTOR-mediated inductions of PPARγ directs early activation of T cells. Nature Communications. 2016 Nov 30;7:13683.

123. Lee K, Gudapati P, Dragovic S, Spencer C, Joyce S, Killeen N, et al. Mammalian target of rapamycin protein complex 2 regulates differentiation of Th1 and Th2 cell subsets via distinct signaling pathways. Immunity. 2010 Jun 25;32(6):743–53.

124. Delgoffe GM, Pollizzi KN, Waickman AT, Heikamp E, Meyers DJ, Horton MR, et al. The kinase mTOR regulates the differentiation of helper T cells through the selective activation of signaling by mTORC1 and mTORC2. Nat Immunol. 2011 Apr;12(4):295–303.

125. Zhang L, Tschumi BO, Lopez-Mejia IC, Oberle SG, Meyer M, Samson G, et al. Mammalian Target of Rapamycin Complex 2 Controls CD8 T Cell Memory Differentiation in a Foxo1-Dependent Manner. Cell Rep. 2016 Feb 9;14(5):1206–17.

126. Velde L-AV de, Murray PJ. Proliferating Helper T Cells Require Rictor/mTORC2 Complex to Integrate Signals from Limiting Environmental Amino Acids. J Biol Chem. 2016 Dec 9;291(50):25815–22.

127. Kim A, Seong KM, Kang HJ, Park S, Lee S-S. Inhibition of Lyn is a promising treatment for mantle cell lymphoma with bortezomib resistance. Oncotarget. 2015 Nov 10;6(35):38225–38.

128. Cosimo E, Tarafdar A, Moles MW, Holroyd AK, Malik N, Catherwood MA, et al. AKT/mTORC2 Inhibition Activates FOXO1 Function in CLL Cells Reducing B-Cell Receptor-Mediated Survival. Clinical cancer research : an official journal of the American Association for Cancer Research. 2019 Mar;25(5):1574–87.

129. Ringshausen I, Peschel C, Decker T. Mammalian target of rapamycin (mTOR) inhibition in chronic lymphocytic B-cell leukemia: a new therapeutic option. Leuk Lymphoma. 2005 Jan;46(1):11–9.

130. Dumont FJ, Su Q. Mechanism of action of the immunosuppressant rapamycin. Life Sci. 1996;58(5):373–95.

131. Decker T, Hipp S, Ringshausen I, Bogner C, Oelsner M, Schneller F, et al. Rapamycin-induced G1 arrest in cycling B-CLL cells is associated with reduced expression of cyclin D3, cyclin E, cyclin A, and survivin. Blood. 2003 Jan 1;101(1):278–85.

132. Darwiche W, Gubler B, Marolleau J-P, Ghamlouch H. Chronic Lymphocytic Leukemia B-Cell Normal Cellular Counterpart: Clues From a Functional Perspective. Front Immunol. 2018;9.

133. Chronic lymphocytic leukaemia (CLL) incidence statistics [Internet]. Cancer Research UK. [cited 2015 Nov 22]. Available from: http://www.cancerresearchuk.org/health-professional/cancer-statistics/statistics-by-cancer-type/leukaemia-cll/incidence

134. Schuh AH, Parry-Jones N, Appleby N, Bloor A, Dearden CE, Fegan C, et al. Guideline for the treatment of chronic lymphocytic leukaemia. British Journal of Haematology. 2018 Aug 1;182(3):344–59.

135. Leach, Mike, Drummond, Mark, Doig, Allyson. Chronic Lymphoid Leukaemias and Exfoliating Lymphoma. In: Practical Flow Cytometry in Haematology Diagnosis [Internet]. John Wiley & Sons, Ltd; [cited 2019 Jul 26]. p. 100–51. Available from: https://onlinelibrary.wiley.com/doi/book/10.1002/9781118487969

136. Leukemia - Chronic Lymphocytic - CLL - Stages [Internet]. Cancer.Net. 2012 [cited 2019 Jul 27]. Available from: https://www.cancer.net/cancer-types/leukemia-chronic-lymphocytic-cll/stages

137. Rai KR, Sawitsky A, Cronkite EP, Chanana AD, Levy RN, Pasternack BS. Clinical staging of chronic lymphocytic leukemia. Blood. 1975 Aug 1;46(2):219–34.

138. Binet JL, Auquier A, Dighiero G, Chastang C, Piguet H, Goasguen J, et al. A new prognostic classification of chronic lymphocytic leukemia derived from a multivariate survival analysis. Cancer. 1981 Jul 1;48(1):198–206.

139. Hamblin TJ, Davis Z, Gardiner A, Oscier DG, Stevenson FK. Unmutated Ig V(H) genes are associated with a more aggressive form of chronic lymphocytic leukemia. Blood. 1999 Sep 15;94(6):1848–54.

140. Dürig J, Naschar M, Schmücker U, Renzing-Köhler K, Hölter T, Hüttmann A, et al. CD38 expression is an important prognostic marker in chronic lymphocytic leukaemia. Leukemia. 2002 Jan 24;16(1):30–5.

141. Fortunato Morabito GC. Surrogate molecular markers for IGHV mutational status in chronic lymphocytic leukemia for predicting time to first treatment. Leukemia research. 2015;39(8).

142. Hallek M. Chronic lymphocytic leukemia: 2015 Update on diagnosis, risk stratification, and treatment. Am J Hematol. 2015 May 1;90(5):446–60.

143. Dameshek W. Chronic lymphocytic leukemia--an accumulative disease of immunolgically incompetent lymphocytes. Blood. 1967 Apr;29(4):566–84.

144. Messmer BT, Messmer D, Allen SL, Kolitz JE, Kudalkar P, Cesar D, et al. In vivo measurements document the dynamic cellular kinetics of chronic lymphocytic leukemia B cells. J Clin Invest. 2005 Mar;115(3):755–64.

145. Kater AP, Evers LM, Remmerswaal EBM, Jaspers A, Oosterwijk MF, van Lier RAW, et al. CD40 stimulation of B-cell chronic lymphocytic leukaemia cells enhances the anti-apoptotic profile, but also Bid expression and cells remain susceptible to autologous cytotoxic T-lymphocyte attack. Br J Haematol. 2004 Nov;127(4):404–15.

146. Petlickovski A, Laurenti L, Li X, Marietti S, Chiusolo P, Sica S, et al. Sustained signaling through the B-cell receptor induces Mcl-1 and promotes survival of chronic lymphocytic leukemia B cells. Blood. 2005 Jun 15;105(12):4820–7.

147. Riches JC, Davies JK, McClanahan F, Fatah R, Iqbal S, Agrawal S, et al. T cells from CLL patients exhibit features of T-cell exhaustion but retain capacity for cytokine production. Blood. 2013 Feb 28;121(9):1612–21.

148. Xerri L, Chetaille B, Serriari N, Seriari N, Attias C, Guillaume Y, et al. Programmed death 1 is a marker of angioimmunoblastic T-cell lymphoma and B-cell small lymphocytic lymphoma/chronic lymphocytic leukemia. Hum Pathol. 2008 Jul;39(7):1050–8.

149. Ansell SM, Lesokhin AM, Borrello I, Halwani A, Scott EC, Gutierrez M, et al. PD-1 blockade with nivolumab in relapsed or refractory Hodgkin's lymphoma. N Engl J Med. 2015 Jan 22;372(4):311–9.

150. Bachy E, Coiffier B. Anti-PD1 antibody: a new approach to treatment of lymphomas. Lancet Oncol. 2014 Jan;15(1):7–8.

151. Burger JA, Quiroga MP, Hartmann E, Bürkle A, Wierda WG, Keating MJ, et al. High-level expression of the T-cell chemokines CCL3 and CCL4 by chronic lymphocytic leukemia B cells in nurselike cell cocultures and after BCR stimulation. Blood. 2009 Mar 26;113(13):3050–8.

152. Kurtova AV, Balakrishnan K, Chen R, Ding W, Schnabl S, Quiroga MP, et al. Diverse marrow stromal cells protect CLL cells from spontaneous and drug-induced apoptosis: development of a reliable and reproducible system to assess stromal cell adhesion-mediated drug resistance. Blood. 2009 Nov 12;114(20):4441–50.

153. Burger JA, Burger M, Kipps TJ. Chronic Lymphocytic Leukemia B Cells Express Functional CXCR4 Chemokine Receptors That Mediate Spontaneous Migration Beneath Bone Marrow Stromal Cells. Blood. 1999 Dec 1;94(11):3658–67.

154. Bürkle A, Niedermeier M, Schmitt-Gräff A, Wierda WG, Keating MJ, Burger JA. Overexpression of the CXCR5 chemokine receptor, and its ligand, CXCL13 in B-cell chronic lymphocytic leukemia. Blood. 2007 Nov 1;110(9):3316–25.

155. Endo T, Nishio M, Enzler T, Cottam HB, Fukuda T, James DF, et al. BAFF and APRIL support chronic lymphocytic leukemia B-cell survival through activation of the canonical NF-κB pathway. Blood. 2007 Jan 15;109(2):703–10.

156. Calissano C, Damle RN, Marsilio S, Yan X-J, Yancopoulos S, Hayes G, et al. Intraclonal Complexity in Chronic Lymphocytic Leukemia: Fractions Enriched in Recently Born/Divided and Older/Quiescent Cells. Mol Med. 2011;17(11–12):1374–82.

157. Chen S-S, Chang BY, Chang S, Tong T, Ham S, Sherry B, et al. BTK inhibition results in impaired CXCR4 chemokine receptor surface expression, signaling and function in chronic lymphocytic leukemia. Leukemia. 2016 Apr;30(4):833–43.

158. Brown JR, Cheson BD, Furman RR, Ghia P, Hallek M, Hillmen P, et al. Patterns of Lymphocytosis in Patients with Chronic Lymphocytic Leukemia (CLL) or Small Lymphocytic Lymphoma (SLL) Treated with Idelalisib. Blood. 2015 Dec 3;126(23):2952–2952.

159. Landau DA, Tausch E, Taylor-Weiner AN, Stewart C, Reiter JG, Bahlo J, et al. Mutations driving CLL and their evolution in progression and relapse. Nature. 2015 Oct 22;526(7574):525–30.

160. Hallek M, Fischer K, Fingerle-Rowson G, Fink AM, Busch R, Mayer J, et al. Addition of rituximab to fludarabine and cyclophosphamide in patients with chronic lymphocytic leukaemia: a randomised, open-label, phase 3 trial. Lancet. 2010 Oct 2;376(9747):1164–74.

161. Turgut B, Vural O, Pala FS, Pamuk GE, TabakcioǦlu K, Demir M, et al. 17p Deletion is associated with resistance of B-cell chronic lymphocytic leukemia cells to in vitro fludarabine-induced apoptosis. Leukemia & Lymphoma. 2007 Jan 1;48(2):311–20.

162. Goede V, Fischer K, Busch R, Engelke A, Eichhorst B, Wendtner CM, et al. Obinutuzumab plus chlorambucil in patients with CLL and coexisting conditions. N Engl J Med. 2014 Mar 20;370(12):1101–10.

163. Hillmen P, Robak T, Janssens A, Babu KG, Kloczko J, Grosicki S, et al. Chlorambucil plus ofatumumab versus chlorambucil alone in previously untreated patients with chronic lymphocytic leukaemia (COMPLEMENT 1): a randomised, multicentre, open-label phase 3 trial. Lancet. 2015 May 9;385(9980):1873–83.

164. Burger JA, Tedeschi A, Barr PM, Robak T, Owen C, Ghia P, et al. Ibrutinib as Initial Therapy for Patients with Chronic Lymphocytic Leukemia. N Engl J Med. 2015 Dec 17;373(25):2425–37.

165. Rickert RC. New insights into pre-BCR and BCR signalling with relevance to B cell malignancies. Nat Rev Immunol. 2013 Aug;13(8):578–91.

166. Minden MD, Übelhart R, Schneider D, Wossning T, Bach MP, Buchner M, et al. Chronic lymphocytic leukaemia is driven by antigen-independent cell-autonomous signalling. Nature. 2012 Sep 13;489(7415):309–12.

167. Fruman DA, Snapper SB, Yballe CM, Davidson L, Yu JY, Alt FW, et al. Impaired B cell development and proliferation in absence of phosphoinositide 3-kinase p85alpha. Science. 1999 Jan 15;283(5400):393–7.

168. Chellappa S, Kushekhar K, Munthe LA, Tjønnfjord GE, Aandahl EM, Okkenhaug K, et al. The PI3K p110δ Isoform Inhibitor Idelalisib Preferentially Inhibits Human Regulatory T Cell Function. The Journal of Immunology. 2019 Jan 28;

169. Hoellenriegel J, Meadows SA, Sivina M, Wierda WG, Kantarjian H, Keating MJ, et al. The phosphoinositide 3'-kinase delta inhibitor, CAL-101, inhibits B-cell receptor signaling and chemokine networks in chronic lymphocytic leukemia. Blood. 2011 Sep 29;118(13):3603–12.

170. Coutré SE, Barrientos JC, Brown JR, de Vos S, Furman RR, Keating MJ, et al. Management of adverse events associated with idelalisib treatment: expert panel opinion. Leuk Lymphoma. 2015;56(10):2779–86.

171. Okkenhaug K, Bilancio A, Farjot G, Priddle H, Sancho S, Peskett E, et al. Impaired B and T Cell Antigen Receptor Signaling in p110δ PI 3-Kinase Mutant Mice. Science. 2002 Aug 9;297(5583):1031–4.

172. Furman RR, Sharman JP, Coutre SE, Cheson BD, Pagel JM, Hillmen P, et al. Idelalisib and rituximab in relapsed chronic lymphocytic leukemia. N Engl J Med. 2014 Mar 13;370(11):997–1007.

173. Herman SEM, Gordon AL, Hertlein E, Ramanunni A, Zhang X, Jaglowski S, et al. Bruton tyrosine kinase represents a promising therapeutic target for treatment of chronic lymphocytic leukemia and is effectively targeted by PCI-32765. Blood. 2011 Jun 9;117(23):6287–96.

174. Woyach JA, Bojnik E, Ruppert AS, Stefanovski MR, Goettl VM, Smucker KA, et al. Bruton's tyrosine kinase (BTK) function is important to the development and expansion of chronic lymphocytic leukemia (CLL). Blood. 2014 Feb 20;123(8):1207–13.

175. O'Brien S, Jones JA, Coutre SE, Mato AR, Hillmen P, Tam C, et al. Ibrutinib for patients with relapsed or refractory chronic lymphocytic leukaemia with 17p deletion (RESONATE-17): a phase 2, open-label, multicentre study. Lancet Oncol. 2016 Oct;17(10):1409–18.

176. Burger JA, Landau DA, Taylor-Weiner A, Bozic I, Zhang H, Sarosiek K, et al. Clonal evolution in patients with chronic lymphocytic leukaemia developing resistance to BTK inhibition. Nat Commun. 2016 20;7:11589.

177. Stilgenbauer S, Eichhorst B, Schetelig J, Coutre S, Seymour JF, Munir T, et al. Venetoclax in relapsed or refractory chronic lymphocytic leukaemia with 17p deletion: a multicentre, open-label, phase 2 study. Lancet Oncol. 2016 Jun;17(6):768–78.

178. Thompson PA, Burger JA. Bruton's tyrosine kinase inhibitors: first and second generation agents for patients with Chronic Lymphocytic Leukemia (CLL). Expert Opin Investig Drugs. 2018;27(1):31–42.

179. Reiff SD, Mantel R, Smith LL, Greene JT, Muhowski EM, Fabian CA, et al. The BTK Inhibitor ARQ 531 Targets Ibrutinib-Resistant CLL and Richter Transformation. Cancer Discov. 2018 Oct;8(10):1300–15.

180. Jones J, Choi MY, Mato AR, Furman RR, Davids MS, Heffner LT, et al. Venetoclax (VEN) Monotherapy for Patients with Chronic Lymphocytic Leukemia (CLL) Who Relapsed after or Were Refractory to Ibrutinib or Idelalisib. Blood. 2016 Dec 2;128(22):637–637.

181. Cramer P, Langerbeins P, Eichhorst B, Hallek M. Advances in first-line treatment of chronic lymphocytic leukemia: current recommendations on management and first-line treatment by the German CLL Study Group (GCLLSG). Eur J Haematol. 2015 Nov 1;n/a-n/a.

182. Blombery P, Anderson MA, Gong J, Thijssen R, Birkinshaw RW, Thompson ER, et al. Acquisition of the recurrent Gly101Val mutation in BCL2 confers resistance to venetoclax in patients with progressive chronic lymphocytic leukemia. Cancer Discov. 2018 Jan 1;1118–9.

183. Mewawalla P, Nathan S. Role of allogeneic transplantation in patients with chronic lymphocytic leukemia in the era of novel therapies: a review. Ther Adv Hematol. 2014 Oct;5(5):139-52.

184. Gribben JG. Stem cell transplantation in chronic lymphocytic leukemia. Biol Blood Marrow Transplant. 2008 Jan;15(1 Suppl):53-8.

185. Brudno JN, Kochenderfer JN. Chimeric antigen receptor T-cell therapies for lymphoma. Nature Reviews Clinical Oncology. 2018 Jan;15(1):31.

186. Turtle CJ, Hanafi L-A, Li D, Chaney C, Heimfeld S, Riddell SR, et al. CD19 CAR-T Cells Are Highly Effective in Ibrutinib-Refractory Chronic Lymphocytic Leukemia. Blood. 2016 Dec 2;128(22):56–56.

187. Kos CH. Methods in Nutrition Science: Cre/loxP System for Generating Tissue-specific Knockout Mouse Models. Nutr Rev. 2004 Jun 1;62(6):243-6.

188. Kühn R, Torres RM. Cre/loxP recombination system and gene targeting. Methods Mol Biol. 2002;180:175–204.

189. Cai Y, Xue F, Qin H, Chen X, Liu N, Fleming C, et al. Differential Roles of the mTOR-STAT3 Signaling in Dermal γδ T Cell Effector Function in Skin Inflammation. Cell Reports. 2019 Jun 4;27(10):3034-3048.e5.

190. Zhang S, Pruitt M, Tran D, Bois WD, Zhang K, Patel R, et al. B Cell-specific Deficiencies in mTOR Limit Humoral Immune Responses. J Immunol. 2013 Aug 15;191(4):1692–703.

191. Li B, Li Z, Wang P, Huang Q, Xu L, He R, et al. Mammalian target of rapamycin complex 1 signalling is essential for germinal centre reaction. Immunology. 2017 Oct;152(2):276–86.

192. Ogilvy S, Elefanty AG, Visvader J, Bath ML, Harris AW, Adams JM. Transcriptional Regulation of vav, a Gene Expressed Throughout the Hematopoietic Compartment. Blood. 1998 Jan 15;91(2):419–30.

193. Bustelo XR. Vav family exchange factors: an integrated regulatory and functional view. Small GTPases. 2014 Nov 17;5(2).

194. Tarakhovsky A, Turner M, Schaal S, Mee PJ, Duddy LP, Rajewsky K, et al. Defective antigen receptor-mediated proliferation of B and T cells in the absence of Vav. Nature. 1995 Mar 30;374(6521):467–70.

195. Crespo P, Schuebel KE, Ostrom AA, Gutkind JS, Bustelo XR. Phosphotyrosine-dependent activation of Rac-1 GDP/GTP exchange by the vav proto-oncogene product. Nature. 1997 Jan 9;385(6612):169-72.

196. de Boer J, Williams A, Skavdis G, Harker N, Coles M, Tolaini M, et al. Transgenic mice with hematopoietic and lymphoid specific expression of Cre. Eur J Immunol. 2003 Feb 1;33(2):314–25.

197. Georgiades P, Ogilvy S, Duval H, Licence DR, Charnock-Jones DS, Smith SK, et al. VavCre transgenic mice: a tool for mutagenesis in hematopoietic and endothelial lineages. Genesis. 2002 Dec;34(4):251-6.

198. Siegemund S, Shepherd J, Xiao C, Sauer K. hCD2-iCre and Vav-iCre Mediated Gene Recombination Patterns in Murine Hematopoietic Cells. PLOS ONE. 2015 Apr 17;10(4).

199. Tissue expression of MX1 - Summary - The Human Protein Atlas [Internet]. [cited 2019 Jan 31]. Available from: https://www.proteinatlas.org/ENSG00000157601-MX1/tissue

200. Verhelst J, Parthoens E, Schepens B, Fiers W, Saelens X. Interferon-Inducible Protein Mx1 Inhibits Influenza Virus by Interfering with Functional Viral Ribonucleoprotein Complex Assembly. Journal of Virology. 2012 Dec 15;86(24):13445–55.

201. Rasschaert J, Ladrière L, Urbain M, Dogusan Z, Katabua B, Sato S, et al. Toll-like Receptor 3 and STAT-1 Contribute to Double-stranded RNA+ Interferon-γ-induced Apoptosis in Primary Pancreatic β-Cells. J Biol Chem. 2005 Oct 7;280(40):33984–91.

202. Alexopoulou L, Holt AC, Medzhitov R, Flavell RA. Recognition of double-stranded RNA and activation of NF-κB by Toll-like receptor 3. Nature. 2001 Oct 18;413(6857):732–8.

203. Mupo A, Celani L, Dovey O, Cooper JL, Grove C, Rad R, et al. A powerful molecular synergy between mutant Nucleophosmin and Flt3-ITD drives acute myeloid leukemia in mice. Leukemia. 2013 Sep;27(9):1917–20.

204. Velasco-Hernandez T, Säwén P, Bryder D, Cammenga J. Potential Pitfalls of the Mx1-Cre System: Implications for Experimental Modeling of Normal and Malignant Hematopoiesis. Stem Cell Reports. 2016 Jun 30;7(1):11–8.

205. Wang K, Wei G, Liu D. CD19: a biomarker for B cell development, lymphoma diagnosis and therapy. Exp Hematol Oncol. 2012 Nov 29;1:36.

206. Rickert RC, Roes J, Rajewsky K. B lymphocyte-specific, Cre-mediated mutagenesis in mice. Nucleic Acids Res. 1997 Mar 15;25(6):1317–8.

207. Thyagarajan B, Guimarães MJ, Groth AC, Calos MP. Mammalian genomes contain active recombinase recognition sites. Gene. 2000 Feb 22;244(1):47–54.

208. Sharma S, Zhu J. Immunologic Applications of Conditional Gene Modification Technology in the Mouse. Curr Protoc Immunol. 2014 Apr 2;105:1–13.

209. Loonstra A, Vooijs M, Beverloo HB, Allak BA, Drunen E van, Kanaar R, et al. Growth inhibition and DNA damage induced by Cre recombinase in mammalian cells. PNAS. 2001 Jul 31;98(16):9209–14.

210. Li Y, Choi PS, Casey SC, Felsher DW. Activation of Cre Recombinase Alone Can Induce Complete Tumor Regression. PLOS ONE. 2014 Sep 10;9(9).

211. McLellan MA, Rosenthal NA, Pinto AR. Cre-loxP-Mediated Recombination: General Principles and Experimental Considerations. Curr Protoc Mouse Biol. 2017 Mar 2;7(1):1–12.

212. Bosma GC, Custer RP, Bosma MJ. A severe combined immunodeficiency mutation in the mouse. Nature. 1983 Feb 10;301(5900):527–30.

213. Yamauchi T, Takenaka K, Urata S, Shima T, Kikushige Y, Tokuyama T, et al. Polymorphic Sirpa is the genetic determinant for NOD-based mouse lines to achieve efficient human cell engraftment. Blood. 2013 Feb 21;121(8):1316–25.

214. Greiner DL, Shultz LD, Yates J, Appel MC, Perdrizet G, Hesselton RM, et al. Improved engraftment of human spleen cells in NOD/LtSz-scid/scid mice as compared with C.B-17-scid/scid mice. Am J Pathol. 1995 Apr;146(4):888–902.

215. Yoshino H, Ueda T, Kawahata M, Kobayashi K, Ebihara Y, Manabe A, et al. Natural killer cell depletion by anti-asialo GM1 antiserum treatment enhances human hematopoietic stem cell engraftment in NOD/Shi-scid mice. Bone Marrow Transplant. 2000 Dec;26(11):1211–6.

216. Ohbo K, Suda T, Hashiyama M, Mantani A, Ikebe M, Miyakawa K, et al. Modulation of hematopoiesis in mice with a truncated mutant of the interleukin-2 receptor gamma chain. Blood. 1996 Feb 1;87(3):956–67.

217. Ito M, Hiramatsu H, Kobayashi K, Suzue K, Kawahata M, Hioki K, et al. NOD/SCID/γ mouse: an excellent recipient mouse model for engraftment of human cells. Blood. 2002 Nov 1;100(9):3175–82.

218. Brehm MA, Cuthbert A, Yang C, Miller DM, Dilorio P, Laning J, et al. Parameters for Establishing Humanized Mouse Models to Study Human Immunity: Analysis of Human Hematopoietic Stem Cell Engraftment in Three Immunodeficient Strains of Mice Bearing the IL2rγnull Mutation. Clin Immunol. 2010 Apr;135(1):84–98.

219. Bresin A, D'Abundo L, Narducci MG, Fiorenza MT, Croce CM, Negrini M, et al. TCL1 transgenic mouse model as a tool for the study of therapeutic targets and microenvironment in human B-cell chronic lymphocytic leukemia. Cell Death Dis. 2016 Jan 28;7(1):e2071.

220. Virgilio L, Lazzeri C, Bichi R, Nibu K, Narducci MG, Russo G, et al. Deregulated expression of TCL1 causes T cell leukemia in mice. Proc Natl Acad Sci USA. 1998 Mar 31;95(7):3885–9.

221. Bichi R, Shinton SA, Martin ES, Koval A, Calin GA, Cesari R, et al. Human chronic lymphocytic leukemia modeled in mouse by targeted TCL1 expression. Proc Natl Acad Sci USA. 2002 May 14;99(10):6955–60.

222. Hamblin TJ. The TCL1 mouse as a model for chronic lymphocytic leukemia. Leukemia Research. 2010 Feb 1;34(2):135–6.

223. Ghia P, Chiorazzi N, Stamatopoulos K. Microenvironmental influences in chronic lymphocytic leukaemia: the role of antigen stimulation. Journal of Internal Medicine. 2008 Dec 1;264(6):549–62.

224. Hayakawa K, Formica AM, Brill-Dashoff J, Shinton SA, Ichikawa D, Zhou Y, et al. Early generated B1 B cells with restricted BCRs become chronic

lymphocytic leukemia with continued c-Myc and low Bmf expression. J Exp Med. 2016 Dec 12;213(13):3007-24.

225. Nishizuka Y. Protein kinase C and lipid signaling for sustained cellular responses. The FASEB Journal. 1995 Apr 1;9(7):484–96.

226. Ruland J, Duncan GS, Elia A, Barrantes I del B, Nguyen L, Plyte S, et al. Bcl10 Is a Positive Regulator of Antigen Receptor–Induced Activation of NF-κ B and Neural Tube Closure. Cell. 2001 Jan 12;104(1):33–42.

227. Dutil EM, Toker A, Newton AC. Regulation of conventional protein kinase C isozymes by phosphoinositide-dependent kinase 1 (PDK-1). Curr Biol. 1998 Dec 17;8(25):1366–75.

228. Michie AM, Nakagawa R. Elucidating the role of protein kinase C in chronic lymphocytic leukaemia. Hematol Oncol. 2006 Sep;24(3):134-8.

229. Nakagawa R, Soh JW, Michie AM. Subversion of Protein Kinase Cα Signaling in Hematopoietic Progenitor Cells Results in the Generation of a B-Cell Chronic Lymphocytic Leukemia–Like Population In vivo. Cancer Res. 2006 Jan 1;66(1):527–34.

230. Nakagawa R, Vukovic M, Tarafdar A, Cosimo E, Dunn K, McCaig AM, et al. Generation of a poor prognostic chronic lymphocytic leukemia-like disease model: PKCα subversion induces up-regulation of PKCβII expression in B lymphocytes. Haematologica. 2015 Apr;100(4):499–510.

231. Nakano T, Kodama H, Honjo T. Generation of lymphohematopoietic cells from embryonic stem cells in culture. Science. 1994 Aug 19;265(5175):1098–101.

232. Gao J, Yan X-L, Li R, Liu Y, He W, Sun S, et al. Characterization of OP9 as authentic mesenchymal stem cell line. Journal of Genetics and Genomics. 2010 Jul 1;37(7):475–82.

233. Bentzinger CF, Romanino K, Cloëtta D, Lin S, Mascarenhas JB, Oliveri F, et al. Skeletal Muscle-Specific Ablation of raptor, but Not of rictor, Causes Metabolic Changes and Results in Muscle Dystrophy. Cell Metabolism. 2008 Nov 5;8(5):411–24.

234. Kuhn R, Schwenk F, Aguet M, Rajewsky K. Inducible gene targeting in mice. Science. 1995 Sep 8;269(5229):1427–9.

235. Georgiades P, Ogilvy S, Duval H, Licence DR, Charnock-Jones DS, Smith SK, et al. vavCre Transgenic mice: A tool for mutagenesis in hematopoietic and endothelial lineages. genesis. 2002 Dec 1;34(4):251–6.

236. Nakano T. Lymphohematopoietic development from embryonic stem cells in vitro. Seminars in Immunology. 1995 Jun 1;7(3):197–203.

237. Markowitz D, Hesdorffer C, Ward M, Goff S, Bank A. Retroviral Gene Transfer Using Safe and Efficient Packaging Cell Lines. Annals of the New York Academy of Sciences. 612(1):407–14.

238. Nakagawa R, Mason SM, Michie AM. Determining the role of specific signaling molecules during lymphocyte development in vivo: instant transgenesis. Nat Protocols. 2006 Sep;1(3):1185–93.

239. Lozzio CB, Lozzio BB. Human chronic myelogenous leukemia cell-line with positive Philadelphia chromosome. Blood. 1975 Mar;45(3):321–34.

240. Bianchi N, Ongaro F, Chiarabelli C, Gualandi L, Mischiati C, Bergamini P, et al. Induction of erythroid differentiation of human K562 cells by cisplatin analogs. Biochemical Pharmacology. 2000 Jul 1;60(1):31–40.

241. Karvela M, Baquero P, Kuntz EM, Mukhopadhyay A, Mitchell R, Allan EK, et al. ATG7 regulates energy metabolism, differentiation and survival of Philadelphia-chromosome-positive cells. Autophagy. 2016 May 11;12(6):936–48.

242. Schmittgen TD, Livak KJ. Analyzing real-time PCR data by the comparative C_T method. Nature Protocols. 2008 Jun;3(6):1101–8.

243. Bradford MM. A rapid and sensitive method for the quantitation of microgram quantities of protein utilizing the principle of protein-dye binding. Analytical Biochemistry. 1976 May 7;72(1):248–54.

244. Li Y-G, Siripanyaphinyo U, Tumkosit U, Noranate N, A-Nuegoonpipat A, Pan Y, et al. Poly (I:C), an agonist of toll-like receptor-3, inhibits replication of the Chikungunya virus in BEAS-2B cells. Virol J. 2012 Jun 14;9:114.

245. Jagannathan-Bogdan M, Zon LI. Hematopoiesis. Development. 2013 Jun 15;140(12):2463–7.

246. Knutson M, Wessling-Resnick M. Iron Metabolism in the Reticuloendothelial System. Critical Reviews in Biochemistry and Molecular Biology. 2003 Jan 1;38(1):61–88.

247. Isoda H, Motojima H, Onaga S, Samet I, Villareal MO, Han J. Analysis of the erythroid differentiation effect of flavonoid apigenin on K562 human chronic leukemia cells. Chemico-Biological Interactions. 2014 Sep 5;220:269-77.

248. Ida C, Ogata S, Okumura K, Taguchi H. Induction of Differentiation in K562 Cell Line by Nicotinic Acid-Related Compounds. Bioscience, Biotechnology, and Biochemistry. 2009;73(1):79–84.

249. Furusawa M, Onishi T, Taira T, Iguchi-Ariga SM, Ariga H. AMY-1 is a trigger for the erythrocyte differentiation of K562 cells. International Journal of Oncology. 2000 Feb 1;16(2):339-84.

250. Carayol N, Vakana E, Sassano A, Kaur S, Goussetis DJ, Glaser H, et al. Critical roles for mTORC2- and rapamycin-insensitive mTORC1-complexes in growth and survival of BCR-ABL-expressing leukemic cells. PNAS. 2010 Jul 13;107(28):12469–74.

251. Choo AY, Yoon S-O, Kim SG, Roux PP, Blenis J. Rapamycin differentially inhibits S6Ks and 4E-BP1 to mediate cell-type-specific repression of mRNA translation. PNAS. 2008 Nov 11;105(45):17414-9.

252. Bayeva M, Khechaduri A, Puig S, Chang H-C, Patial S, Blackshear PJ, et al. mTOR Regulates Cellular Iron Homeostasis through Tristetraprolin. Cell Metabolism. 2012 Nov 7;16(5):645–57.

253. Diekmann F, Rovira J, Diaz-Ricart M, Arellano EM, Vodenik B, Jou JM, et al. mTOR inhibition and erythropoiesis: microcytosis or anaemia? Nephrol Dial Transplant. 2012 Feb;27(2):537–41.

254. Wang J, Tran J, Wang H, Guo C, Harro D, Campbell AD, et al. mTOR Inhibition Improves Anaemia and Reduces Organ Damage in a Murine Model of Sickle Cell Disease. Br J Haematol. 2016 Aug;174(3):461–9.

255. Raz T, Avni R, Addadi Y, Cohen Y, Jaffa AJ, Hemmings B, et al. The Hemodynamic Basis for Positional- and Inter-Fetal Dependent Effects in Dual Arterial Supply of Mouse Pregnancies. PLOS ONE. 2012 Dec 20;7(12):e52273.

256. McGrath KE, Koniski AD, Malik J, Palis J. Circulation is established in a stepwise pattern in the mammalian embryo. Blood. 2003 Mar 1;101(5):1669-76.

257. Zhang P, Behre G, Pan J, Iwama A, Wara-Aswapati N, Radomska HS, et al. Negative cross-talk between hematopoietic regulators: GATA proteins repress PU.1. Proc Natl Acad Sci USA. 1999 Jul 20;96(15):8705–10.

258. Stamatoyannopoulos G. Control of globin gene expression during development and erythroid differentiation. Exp Hematol. 2005 Mar;33(3):259.

259. Xiong Q, Zhang Z, Chang K-H, Qu H, Wang H, Qi H, et al. Comprehensive characterization of erythroid-specific enhancers in the genomic regions of human Krüppel-like factors. BMC Genomics. 2013 Aug 28;14:587.

260. Wu J, Bohanan CS, Neumann JC, Lingrel JB. KLF2 Transcription Factor Modulates Blood Vessel Maturation through Smooth Muscle Cell Migration. J Biol Chem. 2008 Feb 15;283(7):3942–50.

261. Manesia JK, Xu Z, Broekaert D, Boon R, van Vliet A, Eelen G, et al. Highly proliferative primitive fetal liver hematopoietic stem cells are fueled by oxidative metabolic pathways. Stem Cell Research. 2015 Nov 1;15(3):715–21.

262. Kalaitzidis D, Sykes SM, Wang Z, Punt N, Tang Y, Ragu C, et al. mTOR complex 1 plays critical roles in hematopoiesis and Pten-loss-evoked leukemogenesis. Cell Stem Cell. 2012 Sep 7;11(3):429-39.

263. Guo F, Zhang S, Grogg M, Cancelas JA, Varney ME, Starczynowski DT, et al. Mouse gene targeting reveals an essential role of mTOR in hematopoietic stem cell engraftment and hematopoiesis. Haematologica. 2013 Sep;98(9):1353–8.

264. Liu TX, Rhodes J, Deng M, Hsu K, Radomska HS, Kanki JP, et al. Dominant-interfering C/EBPα stimulates primitive erythropoiesis in zebrafish. Experimental Hematology. 2007 Feb 1;35(2):230–9.

265. Hagman J, Lukin K. Transcription factors drive B cell development. Current Opinion in Immunology. 2006 Apr 1;18(2):127–34.

266. Osti F, Corradini FG, Hanau S, Matteuzzi M, Gambari R. Human leukemia K562 cells: induction to erythroid differentiation by guanine, guanosine and guanine nucleotides. Haematologica. 1997 Jan 1;82(4):395–401.

267. Luo S-T, Zhang D-M, Qin Q, Lu L, Luo M, Guo F-C, et al. The Promotion of Erythropoiesis via the Regulation of Reactive Oxygen Species by Lactic Acid. Sci Rep. 2017 Feb 6;7.

268. Nakajima O, Iwasaki S, Hashimoto Y. Hemin-induced erythroid differentiation of human myeloleukemia K562 cell line and its modification by bioresponse modifiers. Cell Mol Biol. 1997 Feb;43(1):115-34.

269. Osmulski PA, Gaczynska M. Rapamycin allosterically inhibits the proteasome. Mol Pharmacol. 2013 Jul;84(1):104–13.

270. Thoreen CC, Sabatini DM. Rapamycin inhibits mTORC1, but not completely. Autophagy. 2009 Jul;5(5):725-6.

271. Chresta CM, Davies BR, Hickson I, Harding T, Cosulich S, Critchlow SE, et al. AZD8055 is a potent, selective, and orally bioavailable ATP-competitive mammalian target of rapamycin kinase inhibitor with in vitro and in vivo antitumor activity. Cancer Res. 2010 Jan 1;70(1):288–98.

272. Fingar DC, Salama S, Tsou C, Harlow E, Blenis J. Mammalian cell size is controlled by mTOR and its downstream targets S6K1 and 4EBP1/eIF4E. Genes Dev. 2002 Jun 15;16(12):1472–87.

273. Marinkovic D, Zhang X, Yalcin S, Luciano JP, Brugnara C, Huber T, et al. Foxo3 is required for the regulation of oxidative stress in erythropoiesis. J Clin Invest. 2007 Aug 1;117(8):2133-44.

274. Zhang X, D'Escamard V, Rimmele P, Ghaffari S. Regulation of Erythroid Cell Maturation Is Mediated by a Foxo3-mTOR Cross Talk: Outcome for Beta-Thalassemic Erythropoiesis. Blood. 2011 Nov 18;118(21):176–176.

275. Fraser CS. The molecular basis of translational control. Prog Mol Biol Transl Sci. 2009;90:1–51.

276. Gingras A-C, Kennedy SG, O'Leary MA, Sonenberg N, Hay N. 4E-BP1, a repressor of mRNA translation, is phosphorylated and inactivated by the Akt(PKB) signaling pathway. Genes Dev. 1998 Feb 15;12(4):502-13.

277. Peterson RT, Desai BN, Hardwick JS, Schreiber SL. Protein phosphatase 2A interacts with the 70-kDa S6 kinase and is activated by inhibition of FKBP12–rapamycinassociated protein. PNAS. 1999 Apr 13;96(8):4438-42.

278. Liu J, Stevens P, Eshleman N, Gao T. Protein Phosphatase PPM1G Regulates Protein Translation and Cell Growth by Dephosphorylating 4E Binding Protein 1 (4E-BP1). The Journal of biological chemistry. 2013 Jun 28;288.

279. Zhang W, Tamura J, Sakuraya M, Naruse T, Kubota K. Effect of inhibitors of protein phosphatase 1 and 2A on erythroid colony formation: an investigation of the specificities of inhibitors. J Int Med Res. 2001 Apr;29(2):114-8.

280. Chen W, Gu P, Jiang X, Ruan H-B, Li C, Gao X. Protein phosphatase 2A catalytic subunit α (PP2Acα) maintains survival of committed erythroid cells in fetal liver erythropoiesis through the STAT5 pathway. Am J Pathol. 2011 May;178(5):2333–43.

281. Trakarnsanga K, Griffiths RE, Wilson MC, Blair A, Satchwell TJ, Meinders M, et al. An immortalized adult human erythroid line facilitates sustainable and scalable generation of functional red cells. Nature Communications. 2017 Mar 14;8:14750.

282. Malik N, Sansom OJ, Michie AM. The role of mTOR-mediated signals during haemopoiesis and lineage commitment. Biochem Soc Trans. 2018 Oct 19;46(5):1313-24.

283. Mouse Strain Datasheet - 006785 [Internet]. The Jackson Laboratory. [cited 2019 Feb 27]. Available from: https://www.jax.org/strain/006785

284. Lee K, Cho SH, Potter RM, Gudapati P, Park D-S, Magnuson MA, et al. mTORC2 in T Lymphocyte Development and Proliferation. <I>The FASEB Journal</I>. 2008 Mar 1;22(1_MeetingAbstracts):661.13.

285. Hu T, Li C, Wang L, Zhang Y, Peng L, Cheng H, et al. PDK1 plays a vital role on hematopoietic stem cell function. Scientific Reports. 2017 Jul 10;7(1):4943.

286. Ruvinsky I, Meyuhas O. Ribosomal protein S6 phosphorylation: from protein synthesis to cell size. Trends in Biochemical Sciences. 2006 Jun 1;31(6):342–8.

287. Pende M, Um SH, Mieulet V, Sticker M, Goss VL, Mestan J, et al. S6K1−/−/S6K2−/− Mice Exhibit Perinatal Lethality and Rapamycin-Sensitive 5′-Terminal Oligopyrimidine mRNA Translation and Reveal a Mitogen-Activated Protein Kinase-Dependent S6 Kinase Pathway. Molecular and Cellular Biology. 2004 Apr 15;24(8):3112–24.

288. Pullen N, Dennis PB, Andjelkovic M, Dufner A, Kozma SC, Hemmings BA, et al. Phosphorylation and Activation of p70s6k by PDK1. Science. 1998 Jan 30;279(5351):707–10.

289. Sturgill TW, Jie Wu. Recent progress in characterization of protein kinase cascades for phosphorylation of ribosomal protein S6. Biochimica et Biophysica Acta (BBA) - Molecular Cell Research. 1991 May 17;1092(3):350–7.

290. Sturgill TW, Ray LB, Erikson E, Maller JL. Insulin-stimulated MAP-2 kinase phosphorylates and activates ribosomal protein S6 kinase II. Nature. 1988 Aug;334(6184):715.

291. Scheid MP, Marignani PA, Woodgett JR. Multiple Phosphoinositide 3-Kinase-Dependent Steps in Activation of Protein Kinase B. Molecular and Cellular Biology. 2002 Sep 1;22(17):6247–60.

292. Casola S. Mouse Models for miRNA Expression: The ROSA26 Locus. In: Monticelli S, editor. MicroRNAs and the Immune System: Methods and Protocols. Totowa, NJ: Humana Press; 2010. p. 145–63.

293. Asano A, Jin HK, Watanabe T. Mouse Mx2 gene: organization, mRNA expression and the role of the interferon-response promoter in its regulation. Gene. 2003 Mar 13;306:105–13.

294. Liu L, Luo Y, Chen L, Shen T, Xu B, Chen W, et al. Rapamycin Inhibits Cytoskeleton Reorganization and Cell Motility by Suppressing RhoA Expression and Activity. Journal of Biological Chemistry. 2010 Dec 3;285(49):38362–73.

295. Jacinto E, Loewith R, Schmidt A, Lin S, Rüegg MA, Hall A, et al. Mammalian TOR complex 2 controls the actin cytoskeleton and is rapamycin insensitive. Nature Cell Biology. 2004 Nov;6(11):1122–8.

296. Dos D. Sarbassov, Ali SM, Kim D-H, Guertin DA, Latek RR, Erdjument-Bromage H, et al. Rictor, a Novel Binding Partner of mTOR, Defines a Rapamycin-Insensitive and Raptor-Independent Pathway that Regulates the Cytoskeleton. Current Biology. 2004 Jul 27;14(14):1296–302.

297. Huang L, Zhang Y, Xu C, Gu X, Niu L, Wang J, et al. Rictor positively regulates B cell receptor signaling by modulating actin reorganization via ezrin. PLOS Biology. 2017 Aug 18;15(8):e2001750.

298. Scholzen T, Gerdes J. The Ki-67 protein: from the known and the unknown. J Cell Physiol. 2000 Mar;182(3):311–22.

299. Dowling RJO, Topisirovic I, Alain T, Bidinosti M, Fonseca BD, Petroulakis E, et al. mTORC1-mediated cell proliferation, but not cell growth, controlled by the 4E-BPs. Science. 2010 May 28;328(5982):1172–6.

300. Wang S, Amato KR, Song W, Youngblood V, Lee K, Boothby M, et al. Regulation of Endothelial Cell Proliferation and Vascular Assembly through Distinct mTORC2 Signaling Pathways. Mol Cell Biol. 2015 Apr;35(7):1299–313.

301. Knutson M, Wessling-Resnick M. Iron Metabolism in the Reticuloendothelial System. Critical Reviews in Biochemistry and Molecular Biology. 2003 Jan;38(1):61–88.

302. Rosario FJ, Gupta MB, Myatt L, Powell TL, Glenn JP, Cox L, et al. Mechanistic Target of Rapamycin Complex 1 Promotes the Expression of Genes Encoding Electron Transport Chain Proteins and Stimulates Oxidative

Phosphorylation in Primary Human Trophoblast Cells by Regulating Mitochondrial Biogenesis. Sci Rep. 2019 Jan 22;9.

303. Tze LE, Schram BR, Lam K-P, Hogquist KA, Hippen KL, Liu J, et al. Basal Immunoglobulin Signaling Actively Maintains Developmental Stage in Immature B Cells. PLoS Biol. 2005 Mar;3(3).

304. Babaev VR, Huang J, Ding L, Zhang Y, May JM, Linton MF. Loss of Rictor in Monocyte/Macrophages Suppresses Their Proliferation and Viability Reducing Atherosclerosis in LDLR Null Mice. Front Immunol. 2018 Feb 13;9:215.

305. Shah DK. T-cell development in thymus [Internet]. British Society for Immunology. [cited 2019 Feb 27]. Available from: https://www.immunology.org/public-information/bitesized-immunology/immune-development/t-cell-development-in-thymus

306. Araki K, Turner AP, Shaffer VO, Gangappa S, Keller SA, Bachmann MF, et al. mTOR regulates memory CD8 T-cell differentiation. Nature. 2009 Jul 2;460(7251):108–12.

307. Delgoffe GM, Kole TP, Zheng Y, Zarek PE, Matthews KL, Xiao B, et al. mTOR differentially regulates effector and regulatory T cell lineage commitment. Immunity. 2009 Jun 19;30(6):832–44.

308. Minden MD, Übelhart R, Schneider D, Wossning T, Bach MP, Buchner M, et al. Chronic lymphocytic leukaemia is driven by antigen-independent cell-autonomous signalling. Nature. 2012 Sep;489(7415):309–12.

309. Coulter EM, Pepper A, Mele S, Folarin N, Townsend W, Cuthill K, et al. In vitro and in vivo evidence for uncoupling of B-cell receptor internalization and signaling in chronic lymphocytic leukemia. Haematologica. 2018 Mar 1;103(3):497–505.

310. Young RM, Staudt LM. Targeting pathological B cell receptor signalling in lymphoid malignancies. Nature Reviews Drug Discovery. 2013 Mar;12(3):229–43.

311. McCaig AM, Cosimo E, Leach MT, Michie AM. Dasatinib Inhibits CXCR4 Signaling in Chronic Lymphocytic Leukaemia Cells and Impairs Migration Towards CXCL12. PLOS ONE. 2012 Nov 2;7(11):e48929.

312. Schrader A, Popal W, Lilienthal N, Crispatzu G, Mayer P, Jones D, et al. AKT-pathway inhibition in chronic lymphocytic leukemia reveals response relationships defined by TCL1. Curr Cancer Drug Targets. 2014;14(8):700–12.

313. Miller JP, Izon D, DeMuth W, Gerstein R, Bhandoola A, Allman D. The Earliest Step in B Lineage Differentiation from Common Lymphoid Progenitors Is Critically Dependent upon Interleukin 7. Journal of Experimental Medicine. 2002 Sep 2;196(5):705–11.

314. Cho SK, Webber TD, Carlyle JR, Nakano T, Lewis SM, Zúñiga-Pflücker JC. Functional characterization of B lymphocytes generated in vitro from

embryonic stem cells. Proc Natl Acad Sci U S A. 1999 Aug 17;96(17):9797–802.

315. Burger JA, Tsukada N, Burger M, Zvaifler NJ, Dell'Aquila M, Kipps TJ. Blood-derived nurse-like cells protect chronic lymphocytic leukemia B cells from spontaneous apoptosis through stromal cell–derived factor-1. Blood. 2000 Oct 15;96(8):2655–63.

316. Binder M, Léchenne B, Ummanni R, Scharf C, Balabanov S, Trusch M, et al. Stereotypical Chronic Lymphocytic Leukemia B-Cell Receptors Recognize Survival Promoting Antigens on Stromal Cells. PLOS ONE. 2010 Dec 30;5(12):e15992.

317. Seiffert M, Schulz A, Ohl S, Döhner H, Stilgenbauer S, Lichter P. Soluble CD14 is a novel monocyte-derived survival factor for chronic lymphocytic leukemia cells, which is induced by CLL cells in vitro and present at abnormally high levels in vivo. Blood. 2010 Nov 18;116(20):4223–30.

318. Muzio M, Fonte E, Caligaris-Cappio F. Toll-like Receptors in Chronic Lymphocytic Leukemia. Mediterr J Hematol Infect Dis. 2012 Aug 9;4(1):e2012055.

319. Dadashian EL, McAuley EM, Liu D, Shaffer AL, Young RM, Iyer JR, et al. TLR Signaling Is Activated in Lymph Node-Resident CLL Cells and Is Only Partially Inhibited by Ibrutinib. Cancer Res. 2019 Jan 15;79(2):360–71.

320. Hua C, Guo H, Bu J, Zhou M, Cheng H, He F, et al. Rictor/mammalian target of rapamycin 2 regulates the development of Notch1 induced murine T-cell acute lymphoblastic leukemia via forkhead box O3. Exp Hematol. 2014 Dec;42(12):1031-1040.e1-4.

321. Yeomans A, Thirdborough SM, Valle-Argos B, Linley A, Krysov S, Hidalgo MS, et al. Engagement of the B-cell receptor of chronic lymphocytic leukemia cells drives global and MYC-specific mRNA translation. Blood. 2016 Jan 28;127(4):449–57.

322. Zhang J, Grindley JC, Yin T, Jayasinghe S, He XC, Ross JT, et al. PTEN maintains haematopoietic stem cells and acts in lineage choice and leukaemia prevention. Nature. 2006 May 25;441(7092):518–22.

323. Lymphoid leukaemia - NICE Pathways [Internet]. [cited 2019 Feb 21]. Available from: https://pathways.nice.org.uk/pathways/blood-and-bone-marrow-cancers/leukaemia#path=view%3A/pathways/blood-and-bone-marrow-cancers/lymphoid-leukaemia.xml&content=view-node%3Anodes-first-line-treatment-for-chronic-lymphocytic-leukaemia

324. Phase II Trial of AZD2014 in TSC1/2 Mutated or TSC1/2 Null GC Patients as Second-line Chemotherapy - Full Text View - ClinicalTrials.gov [Internet]. [cited 2019 Mar 8]. Available from: https://clinicaltrials.gov/ct2/show/NCT03082833

325. Guichard SM, Curwen J, Bihani T, D'Cruz CM, Yates JWT, Grondine M, et al. AZD2014, an Inhibitor of mTORC1 and mTORC2, Is Highly Effective in

ER+ Breast Cancer When Administered Using Intermittent or Continuous Schedules. Mol Cancer Ther. 2015 Nov;14(11):2508–18.

326. Ezell SA, Mayo M, Bihani T, Tepsuporn S, Wang S, Passino M, et al. Synergistic induction of apoptosis by combination of BTK and dual mTORC1/2 inhibitors in diffuse large B cell lymphoma. Oncotarget. 2014 Jul 15;5(13):4990–5001.

327. Ma S, Shukla V, Fang L, Gould KA, Joshi SS, Lu R. Accelerated Development of Chronic Lymphocytic Leukemia in New Zealand Black Mice Expressing a Low Level of Interferon Regulatory Factor 4. J Biol Chem. 2013 Sep 13;288(37):26430–40.

328. O'Donnell A, Faivre S, Burris HA, Rea D, Papadimitrakopoulou V, Shand N, et al. Phase I pharmacokinetic and pharmacodynamic study of the oral mammalian target of rapamycin inhibitor everolimus in patients with advanced solid tumors. J Clin Oncol. 2008 Apr 1;26(10):1588–95.

329. Basu B, Dean E, Puglisi M, Greystoke A, Ong M, Burke W, et al. First-in-human pharmacokinetic and pharmacodynamic study of the dual m-TORC 1/2 inhibitor, AZD2014. Clin Cancer Res. 2015 Aug 1;21(15):3412–9.

330. Zeng Z, Sarbassov DD, Samudio IJ, Yee KWL, Munsell MF, Ellen Jackson C, et al. Rapamycin derivatives reduce mTORC2 signaling and inhibit AKT activation in AML. Blood. 2007 Apr 15;109(8):3509–12.

331. Powles T, Wheater MJ, Din O, Geldart TR, Boleti E, Stockdale A, et al. A randomized phase II study of AZ2014 versus everolimus in patients with VEGF refractory metastatic clear cell renal cancer (mRCC). JCO. 2015 Mar 1;33:409–409.

332. Sehgal SN. Sirolimus: its discovery, biological properties, and mechanism of action. Transplant Proc. 2003 May;35:7S-14S.

333. Faller WJ, Jackson TJ, Knight JRP, Ridgway RA, Jamieson T, Karim SA, et al. mTORC1-mediated translational elongation limits intestinal tumour initiation and growth. Nature. 2015 Jan 22;517(7535):497–500.

334. Maddila SC, Busch-Dienstfertig M, Stein C. B Lymphocytes Express Pomc mRNA, Processing Enzymes and β-Endorphin in Painful Inflammation. J Neuroimmune Pharmacol. 2017;12(1):180–6.

Related Publications

1. **Malik N**, Sansom OJ, Michie AM. The role of mTOR-mediated signals during haemopoiesis and lineage commitment. Biochem Soc Trans. 2018 Oct 19;46(5):1313–24.

2. Cosimo E, Tarafdar A, Moles MW, Holroyd AK, Malik N, Catherwood MA, et al. AKT/mTORC2 Inhibition Activates FOXO1 Function in CLL Cells Reducing B-Cell Receptor-Mediated Survival. Clinical cancer research : an official journal of the American Association for Cancer Research. 2019 Mar;25(5):1574–87.